

**Chromium amino-bis(phenolate) complexes for CO₂ and cyclohexene
oxide copolymerization**

By

Kaijie Ni

A Thesis submitted to the School of Graduate Studies

in partial fulfillment of the requirements for the degree of

Doctor of Philosophy

Department of Chemistry

Memorial University of Newfoundland

September 2017

St. John's

Newfoundland

Abstract

Utilization of CO₂ as a C1 feedstock for polycarbonate production has received considerable attention in the past decades. One of the promising methods is the catalytic copolymerization of CO₂ and epoxides to afford polycarbonates. In this thesis, Cr(III) amino-bis(phenolate) complexes were synthesized and investigated as catalysts for the copolymerization of CO₂ and cyclohexene oxide (CHO). These Cr(III) complexes were characterized by MALDI-TOF mass spectrometry, single crystal X-ray diffraction, UV-Vis spectroscopy and elemental analysis. In the presence of cocatalysts such as 4-(dimethylamino)pyridine (DMAP), bis(triphenylphosphoranylidene) iminium chloride or azide (PPNCl or PPN₃), these Cr(III) complexes showed efficient activities to selectively produce polycarbonate from CO₂ and CHO with moderate molecular weights and narrow dispersities. End-group analysis of the resulting polymers by MALDI-TOF mass spectrometry suggested both the nucleophiles from cocatalyst and the Cr(III) complex could initiate the reaction. However, DMAP was found to be a better initiator to ring-open the epoxide than the chloride from the Cr(III) complex. Monitoring the copolymerization reaction via in situ attenuated total reflectance infrared spectroscopy (ATR-IR), combined with the studies of binding of azide to Cr(III) complexes via mass spectrometry showed that the steric effect of the pendant donor group of amino-bis(phenolate) Cr(III) complex played an important role in increasing the

copolymerization rate. Furthermore, polycarbonate diol from CO₂ and CHO was synthesized by a modified Cr(III) complex. The resulting polycarbonate diol was used to afford tri-block copolymers via its use as a macroinitiator in the subsequent base-catalysed ring-opening polymerization of *rac*-lactide. The resulting copolymers showed a decreased glass transition temperature and an increased decomposition temperature compared to the original polycarbonates.

Acknowledgements

Firstly I want to thank my supervisor Dr. Christopher M. Kozak for giving me this opportunity to work on this exciting research project. His patient supervision and humor helped me complete this thesis and enjoy my four years of research life. He also provided a free environment for us to conduct research and encouraged us to be bold to try although we often made mistakes. Because of his training, I have learned not only various proficient research skills, but also thinking independently, team work, leadership, communication skill and the ability to troubleshoot. He was generous with his time in that every week we had one-on-one meetings in his office where he patiently directed me to solve the problems faced in my research. I will never forget him patiently teaching me how to write better and explaining to me in detail, since English is my second language. I also want to express my most sincere thanks to Dr. Francesca Kerton for her valuable advice and criticism throughout the period of my studies. Without her help and influence, completion of this research work on time is impossible. In addition, I learned a lot from her passion for chemistry.

I also would like to thank my committee member, Dr. Christina Bottaro for providing suggestions on my research, Dr. Louise N. Dawe and Julie Collins for solving my crystal structures, Dr. Celine Schneider and Dr. Dave Davidson for the help with NMR, Linda Winsor for the training on MALDI-TOF and ESI mass spectrometries and Adam Gerald

Beaton for the training on DSC and TGA.

I thank NSERC (Dr. Christopher M. Kozak's research grant), Department of Chemistry, School of Graduate Studies, Graduate Students' Union and Memorial University for financial support, which contributed to the successful completion of my research program.

I am also thankful to the members of the Green Chemistry and Catalysis Group, especially Katalin Devaine-Pressing, Hua Chen, Ali Elkurtehi and Hart Plommer, who helped me in the lab. Special thanks to Yi Liu, George Margoutidis, Kenson Ambrose, Jennifer Murphy, Erika Butler, Tim Anderson and Kori Andrea for their friendship. We really had a good time together. Because of these friends' help and encouragement, my research life became colorful.

Last but not least, I want to thank my parents Yonggen Ni and Huifang Zhang for their support, love and encouragements. They always support me with any decisions I made. Without their support I will not be where I am today. Special thanks go to my wife Yanyang Chen. Without her love, patience and understanding, this thesis work would not be completed.

Table of Contents

Abstract	ii
Acknowledgements	iv
List of Tables	xii
List of Figures	xiii
List of Schemes	xxiii
List of Abbreviations and Symbols	xxv
List of Appendices	xxix
Chapter 1. Introduction	1
1.1 CO ₂ as a carbon feedstock	1
1.2 Overview of polycarbonate	2
1.3 Copolymerization of CO ₂ and epoxide	5
1.3.1 Background	5
1.3.2 Early catalyst developments	8
1.3.3 Binary chromium salen catalyst system	12
1.3.4 Mechanistic studies of binary chromium salen catalysts	15
1.3.5 Recent catalyst developments	24
1.4 Strategies of modifying properties of CO ₂ -based polycarbonate	29
1.4.1 Motivation	29

1.4.2 Synthesis of regio- and stereoregular polycarbonate	29
1.4.3 Copolymerization of CO ₂ with new epoxides.....	31
1.4.4 Terpolymerization and block copolymerization	33
1.5 Objectives	36
1.6 References	39
Chapter 2. Kinetic studies of copolymerization of cyclohexene oxide with CO ₂ by a monometallic amino-bis(phenolate) chromium(III) complex.....	48
2.1 Introduction.....	48
2.2 Results and discussion	52
2.2.1 Synthesis and characterization of Cr(III) complex	52
2.2.2 Crystal structure determination	56
2.2.3 Copolymerization of CHO and CO ₂	58
2.2.4 Kinetic studies	65
2.2.5 End-group analysis	71
2.3 Conclusions.....	76
2.4 Experimental	76
2.4.1 General materials.....	76
2.4.2 Instrumentation.....	77
2.4.3 Synthesis of the amino-bis(phenolate) chromium complex	79

2.4.4 Copolymerization conditions	80
2.5 References	81
Chapter 3. Chromium(III) amino-bis(phenolate) complex as the catalyst for CO ₂ and cyclohexene oxide copolymerization and initiation mechanism studies	89
3.1 Introduction	89
3.2 Results and discussion	92
3.2.1 Synthesis and characterization of Cr(III) complex 3.1	92
3.2.2 Crystal structure determination	95
3.2.3 UV-Vis titration	97
3.2.4 Copolymerization of CHO and CO ₂	102
3.2.5 End-group analysis	108
3.2.6 Mechanistic considerations	116
3.3 Conclusions	119
3.4 Experimental	119
3.4.1 General materials	119
3.4.2 Instrumentation	120
3.4.3 Synthesis of complex 3.1	122
3.4.4 Copolymerization conditions	123
3.5 References	125

Chapter 4. MALDI-TOF and ESI MS analysis studies of the binding of azide to amino-bis(phenolate) Cr(III) chloride complexes: Mechanistic understanding of catalytic CO ₂ /cyclohexene oxide copolymerization.....	128
4.1 Introduction.....	128
4.2 Results and discussion	132
4.2.1 Binding of azide to amino-bis(phenolate) Cr(III) chloride complexes	132
4.2.2 Ring-opening steps examined by ESI-MS	140
4.2.3 Propagating species observed by MALDI-TOF MS.....	143
4.2.4 Mechanistic understanding.....	147
4.3 Conclusions.....	152
4.4 Experimental	153
4.4.1 General materials.....	153
4.4.2 MALDI-TOF MS experimental	153
4.4.3 ESI-MS experimental	154
4.5 References.....	156
Chapter 5. Synthesis of polycarbonate diols and their polylactide tri-block copolymers	160
5.1 Introduction.....	160
5.2 Results and discussion	162
5.2.1 Synthesis and characterization	162

5.2.2 Single crystal structure determination.....	164
5.2.3 Copolymerization of CHO and CO ₂	171
5.2.4 Block copolymerization of PCHC and lactide	183
5.3 Conclusions.....	190
5.4 Experimental	191
5.4.1 General materials.....	191
5.4.2 Instrumentation.....	192
5.4.3 Synthesis of complex 5.1 and Ph ₂ P(O)NPPH ₃	194
5.4.4 Copolymerization conditions.	195
5.4.5 Block copolymerization conditions.....	195
5.5 References.....	197
Chapter 6. Attempted synthesis of derivatives of Cr(III) amino-bis(phenolate) complexes	200
6.1 Introduction.....	200
6.2 Preparation and characterization of new Cr(III) complexes 6.1 and 6.2	200
6.3 Experimental	203
6.3.1 General experimental conditions.....	203
6.3.2 MALDI-TOF MS	204
6.3.3 Preparation of complex 6.1	204

6.3.4 Preparation of complex 6.2	205
Chapter 7. Future work and conclusions.....	206
7.1 Ideas for the future work.....	206
7.2 Conclusions.....	209
7.3 References	214

List of Tables

Table 2-1. Selected bond distances (Å) and angles (°) of complex 2.1	58
Table 2-2. Results of copolymerization of CHO and CO ₂ by complex 2.1 ^a	62
Table 2-3. Effect of CO ₂ pressure on the copolymerization of CHO and CO ₂ ^a	65
Table 3-1. Selected bond distances (Å) and angles (°) for complex 3.1	97
Table 3-2. Results of the copolymerization of CO ₂ and CHO by 3.1	104
Table 5-1. Selected bond distances (Å) and angles (°) of 5.3	168
Table 5-2. Selected bond distances (Å) and angles (°) of complex 2.6	171
Table 5-3. Copolymerization of CHO and CO ₂ catalyzed by 5.1 ^a	172
Table 5-4. The result of tri-block copolymerization from PCHC and <i>rac</i> -lactide	184

List of Figures

Figure 1-1. The number of publications per year concerning CO ₂ /epoxide copolymerization from 1969 to 2016 (Note: the search was conducted by SciFinder using key words of CO ₂ , epoxide and copolymerization).	6
Figure 1-2. Representative homogeneous catalyst systems for the copolymerization of CO ₂ and epoxide.	11
Figure 1-3. Salen Cr(III) complexes and commonly used cocatalysts.	13
Figure 1-4. General structure of salen Cr(III) catalysts used in CO ₂ /epoxide copolymerization.....	14
Figure 1-5. Structures of salen and salan chromium complexes used in Lu's ESI-MS study. ⁵³	19
Figure 1-6. ESI mass spectra of the reaction mixtures resulting from the catalyst system 1.7c /DMAP (1:1, molar ratio) during CO ₂ /PO copolymerization at 25 °C and 6 bar CO ₂ pressure. Time: (A) 2 h, (B) 4 h, (C) 6 h, (D) 8 h. Reprinted with permission from Rao, D.-Y.; Li, B.; Zhang, R.; Wang, H.; Lu, X.-B. <i>Inorg. Chem.</i> 2009 , 48, 2830. Copyright (2009) American Chemical Society.	20
Figure 1-7. The structures of salen-based bifunctional catalysts.	25
Figure 1-8. Structures of bimetallic catalysts.....	27
Figure 1-9. Recent catalysts reported for CO ₂ /epoxide copolymerization.	28

Figure 1-10. Regio- and stereochemical forms of PPC.	31
Figure 1-11. Chiral Co(III) salen complexes.	31
Figure 1-12. Representative other epoxides used for CO ₂ /epoxide copolymerization.	32
Figure 1-13. Catalysts used for the synthesis of polycarbonate diols.	36
Figure 2-1. The investigated Cr(III) amino-bis(phenolate) complexes in the Kozak group.	51
Figure 2-2. MALDI-TOF mass spectrum of complex 2.1 with the experimental and theoretical isotopic distribution patterns.	54
Figure 2-3. MALDI-TOF mass spectrum of 2.6 with the experimental and theoretical isotopic distribution patterns.	55
Figure 2-4. UV-Vis absorption spectra of complex 2.1 (black) and complex recovered from 2.6 by dissolution in THF (pink) at a concentration of 10 ⁻³ mol L ⁻¹ in dichloromethane.	56
Figure 2-5. Molecular structure (ORTEP) and partial numbering scheme of 2.1 . Ellipsoids are drawn at 50% probability. Hydrogen atoms omitted for clarity.	57
Figure 2-6. Representative ¹ H NMR spectrum in CDCl ₃ of the purified polycarbonate using PPNCl as cocatalyst (Table 2-2, entry 5).	59
Figure 2-7. Representative carbonyl region of the ¹³ C NMR spectrum in CDCl ₃ of PCHC (Table 2-2, entry 1).	60

Figure 2-8. Time profiles of the absorbance at 1750 cm^{-1} corresponding to the PCHC production by **2.1** and different cocatalysts (Table 2-2, entries 4-7): [Cr]:[CHO]:DMAP = 1:500:1, ●; [Cr]:[CHO]:PPNCl = 1:500:1, ▲; or [Cr]:[CHO]:PPNN₃ = 1:500:1, ■; [Cr]:[CHO]:PPNCl = 1:1000:1, ◆63

Figure 2-9. Plots of absorbance vs. time for the linear portion of polycarbonate formation for the data presented in Figure 2-8. Straight lines represent best fits of the data for [Cr]:[CHO]:DMAP = 1:500:1, ●, $y = 0.0355x$, $R^2 = 0.9909$; [Cr]:[CHO]:PPNCl = 1:500:1, ▲, $y = 0.0566x$, $R^2 = 0.9964$; [Cr]:[CHO]:PPNN₃ = 1:500:1, ■, $y = 0.0702x$, $R^2 = 0.9928$; [Cr]:[CHO]:PPNCl = 1:1000:1, ◆, $y = 0.0201x$, $R^2 = 0.9954$64

Figure 2-10. (A) Three-dimensional stack plot of IR spectra collected every 60 s during the reaction of CHO and CO₂ by the binary system of **2.1** and DMAP with a **2.1**:CHO:DMAP molar ratio of 1:500:1. (B) Time profile of the absorbance at 1750 cm^{-1} at different temperatures.67

Figure 2-11. (A) Time profiles of the absorbance at 1750 cm^{-1} corresponding to the PCHC using DMAP as cocatalysts at 60 °C and 85 °C. (B) Three-dimensional stack plots of the IR spectra.68

Figure 2-12. ¹H NMR spectrum in CDCl₃ of PCHC using DMAP as cocatalyst at 85 °C.69

Figure 2-13. (A) Plots of absorbance vs. time for the linear portion of polycarbonate

formation at various temperatures. 30 °C: $y = 0.0076x$, $R^2 = 0.9942$, 40 °C: $y = 0.0105x$, $R^2 = 0.9975$, 60 °C: $y = 0.0526x$, $R^2 = 0.9969$, 70 °C: $y = 0.0777x$, $R^2 = 0.9928$, 80 °C: $y = 0.1558x$, $R^2 = 0.9947$. (B) Arrhenius plot for the formation of PCHC. Straight line represents best fit with $y = -6503.5x + 16.4557$, $R^2 = 0.9858$	70
Figure 2-14. Series of chain end-groups observed in MALDI-TOF MS of the polymers produced by complex 2.1 with different cocatalysts.....	71
Figure 2-15. (A) MALDI-TOF mass spectrum of PCHC obtained using 2.1 and DMAP (Table 2-2, entry 4). (B) Higher mass region of the spectrum ($n = 44 - 47$) with the modeled polymer chain (b) illustrated in Figure 2-14.	73
Figure 2-16. Lower mass region ($2750 - 3350 m/z$, $n = 19 - 22$) of the MALDI-TOF mass spectrum obtained using DMAP as cocatalyst.....	73
Figure 2-17. High mass region ($m/z 6500 - 11100$, $n = 45 - 77$) of the MALDI-TOF mass spectrum obtained using PPNCI as cocatalyst.	74
Figure 2-18. High mass region ($m/z 5500 - 10000$, $n = 41 - 67$) of the MALDI-TOF mass spectrum obtained using PPNN ₃ as cocatalyst.....	75
Figure 3-1. Possible initiation pathways for the salen complex and cocatalyst.....	90
Figure 3-2. The dimeric structure of the Cr(III) amino-bis(phenolate) complex with a methoxy pendant donor group.	91
Figure 3-3. MALDI-TOF mass spectrum of complex 3.1 with isotopic patterns.....	94

Figure 3-4. Molecular structure (ORTEP) and partial numbering scheme of complex 3.1 . Ellipsoids are drawn at 50% probability. Hydrogen atoms omitted for clarity. Symmetry operations used to generate equivalent atoms (*): -x,-y,-y+1.	96
Figure 3-5. MALDI-TOF mass spectrum of the sample of complex 3.1 with PPnCl in negative mode.	99
Figure 3-6. UV-Vis spectra of complex 3.1 with different ratios of PPnCl added.	100
Figure 3-7. UV-Vis spectra of complex 3.1 with different amounts of CHO.	101
Figure 3-8. Time profiles of the absorbance at 1750 cm ⁻¹ corresponding to the PCHC obtained using different PPnCl to Cr ratios (Table 3-2, entries 1-3).	106
Figure 3-9. Time profiles of the absorbance at 1750 cm ⁻¹ corresponding to the PCHC obtained using different cocatalysts (Table 3-2, entries 1, 7 and 8).	107
Figure 3-10. MALDI-TOF mass spectrum of the sample of complex 3.1 with PPnN ₃ in negative mode.	108
Figure 3-11. Higher mass region (<i>m/z</i> 7111 – 10809, <i>n</i> = 49 – 75) of the MALDI-TOF mass spectrum obtained using PPnCl as cocatalyst (Table 3-2, entry 1).	109
Figure 3-12. Lower mass region (<i>m/z</i> 3403 – 5682, <i>n</i> = 23 – 39) of the MALDI-TOF mass spectrum obtained using PPnCl as cocatalyst (Table 3-2, entry 1).	110
Figure 3-13. Low mass region (<i>m/z</i> 1879 – 2405, <i>n</i> = 12 – 15) of the MALDI-TOF mass spectrum obtained using PPnN ₃ as cocatalyst (Table 3-2, entry 7).	111

Figure 3-14. MALDI-TOF mass spectra of aliquots obtained at the specified times from the copolymerization of CHO and CO ₂ by 3.1 and DMAP.	113
Figure 3-15. MALDI-TOF mass spectrum of the polymer produced using DMAP as cocatalyst (Table 3-2, entry 8).....	115
Figure 3-16. MALDI-TOF mass spectrum in the low molecular weight region of the polymer produced using DMAP as cocatalyst (Table 2, entry 8).	115
Figure 3-17. MALDI-TOF mass spectrum in the high molecular weight region of the polymer produced using DMAP as cocatalyst (Table 2, entry 8) and the modeled isotopic masses: C ₇ H ₁₀ N ₂ (DMAP) + (C ₇ H ₁₀ O ₃) _n (repeating unit) + C ₆ H ₉ (cyclohexenyl), n = 80 – 95.	116
Figure 3-18. The special cuvette used for UV-Vis titration under inert atmosphere.	122
Figure 4-1. Chromium(III) complexes with different pendant donor groups.	131
Figure 4-2. Amino-bis(phenolate) Cr(III) chloride complexes 2.1 and 3.1	132
Figure 4-3. Anions and radical anions observed in the MALDI-TOF mass spectra of 2.1 with added PPNN ₃ . The corresponding ions of 3.1 are represented by the analogous structures shown for F1–F6.	134
Figure 4-4. MALDI-TOF mass spectra of different molar ratios of 3.1 /PPNN ₃ and 2.1 /PPNN ₃ . (A) 1:0, (B) 1:0.5, (C) 1:1, (D) 1:2, (E) 1:4, and (F) 1:10.....	135
Figure 4-5. Comparison of relative abundance of ions observed by MALDI-TOF MS for	

complexes 3.1 (top) and 2.1 (bottom) with varying amounts of PPNN ₃ as shown. Relative abundance is given in % and structure numbers F1–F6 correspond to ions shown in Figure 4-3.	136
Figure 4-6. Negative mode ESI mass spectra of mixtures of 3.1 /PPNN ₃ (left) and 2.1 /PPNN ₃ (right) in the following molar ratios: (A) 1:0, (B) 1:0.5, (C) 1:1, (D) 1:2, (E) 1:4, and (F) 1:10.	138
Figure 4-7. Comparison of relative abundance of ions observed by ESI-MS for complexes 3.1 (top) and 2.1 (bottom) with varying amounts of PPNN ₃ as shown. Relative abundance is given in % and structure numbers F1–F6 correspond to ions shown in Figure 4-3.	139
Figure 4-8. ESI mass spectra of the mixture of 2.1 /PPNN ₃ /CHO in a ratio of 1:1:20. ...	141
Figure 4-9. Magnified sections of MALDI-TOF mass spectrum for the polymer by 2.1 and PPNN ₃ . (A) Low mass (n = 21 – 24) and (B) high mass regions (n = 41 – 67).	142
Figure 4-10. MALDI-TOF mass spectra of aliquots obtained at the specified times from the copolymerization of CHO and CO ₂ by 2.1 and DMAP.	144
Figure 4-11. MALDI-TOF mass spectrum in the low mass region of aliquot obtained after 60 min shown in Figure 4-10. Modeled isotopic masses for polymers (a and b) are shown below the experimental spectrum.	145
Figure 4-12. MALDI-TOF mass spectra of the aliquots obtained from the copolymerization of CHO and CO ₂ by complex 2.1 and PPNN ₃ at various intervals.	146

Figure 4-13. Time profiles of the absorbance at 1750 cm^{-1} corresponding to PCHC obtained using complexes 3.1 (solid blue line) and 2.1 (dashed pink line) in the presence of 1 equivalent of PPNN ₃	148
Figure 5-1. MALDI-TOF mass spectra of 2.1 (blue, bottom) and 5.1 (green, top).	164
Figure 5-2. The structure of 5.2	165
Figure 5-3. Molecular structure (ORTEP) and partial numbering scheme of complex 5.3 . Ellipsoids are drawn at 50% probability. Hydrogen atoms omitted for clarity.	167
Figure 5-4. Molecular structure (ORTEP) and partial numbering scheme of 2.2 . Ellipsoids are drawn at 50% probability. Hydrogen atoms other than H(1) and H(3A) are omitted for clarity.	170
Figure 5-5. Magnified section of MALDI-TOF mass spectrum of PCHC ($n = 13-16$) obtained using 5.1 and PPNNCl (Table 5-3, entry 2). Modeled isotopic masses for polymers (a-d) containing different end-groups are shown below the experimental spectrum.	174
Figure 5-6. ^{31}P NMR spectra in CDCl_3 of commercial $\text{Ph}_2\text{P}(\text{O})\text{NPPH}_3$ (red, bottom) and $\text{Ph}_2\text{P}(\text{O})\text{NPPH}_3$ obtained from the reaction of PPNNCl and NaOH (blue, top).	175
Figure 5-7. Magnified section of MALDI-TOF mass spectrum of PCHC obtained using 5.1 and $\text{Ph}_2\text{P}(\text{O})\text{NPPH}_3$ (Table 5-3, entry 3). Modeled isotopic masses for polymers (a-c) containing different end-groups are shown below the experimental spectrum.	176
Figure 5-8. GPC traces determined by triple detection of the polymers obtained from	

CHO/CO ₂ copolymerization by 5.1 and Ph ₂ P(O)NPPPh ₃ with different reaction times (a)	
24 h (b) 2 h.....	178
Figure 5-9. ³¹ P { ¹ H} NMR spectrum of Ph ₂ P(O)NPPPh ₃ in CDCl ₃	179
Figure 5-10. ³¹ P { ¹ H} NMR spectrum in CDCl ₃ of the purified polymer obtained from	
CHO/CO ₂ copolymerization by 5.1 and Ph ₂ P(O)NPPPh ₃ for 2 h.....	180
Figure 5-11. MALDI-TOF mass spectrum of polycarbonate diol produced using Bu ₄ NOH	
as cocatalyst according to the conditions in Table 5-3, entry 4.	181
Figure 5-12. ¹ H NMR spectrum of the polymer produced using Bu ₄ NOH as cocatalyst	
according to the conditions in Table 5-3, entry 4.....	182
Figure 5-13. ¹ H NMR spectrum in CDCl ₃ of PLA-PCHC-PLA (Table 5-4, entry 1).	
Resonances at 3.4 ppm and 5.3 ppm in spectrum correspond to ether linkages (omitted in	
the above structure for clarify) and CH ₂ Cl ₂ , respectively.....	186
Figure 5-14. GPC traces of PCHC and PLA-PCHC-PLA from RI detector using THF as	
eluent (Table 5-4, entries 1 and 2).	188
Figure 5-15. DSC second heating curves of PCHC and PLA-PCHC-PLA (Table 5-4,	
entries 1 and 2).....	189
Figure 5-16. TGA curves of PCHC and PLA-PCHC-PLA (Table 5-4, entries 1 and 2).	189
Figure 5-17. (A) Reaction profile and (B) resulting three-dimensional plot of IR spectra.	
The absorptions at 1772 and 1757 cm ⁻¹ arise from the carbonyl groups from <i>rac</i> -lactide and	

the resulting PLA of the tri-block copolymer, respectively. DBU added at $t = 10$ min...	190
Figure 6-1. MALDI-TOF mass spectrum of 6.1 and the isotopic distributions of the model peaks.	202
Figure 6-2. MALDI-TOF mass spectrum of 6.2 and the isotopic distribution of the model peaks.	203
Figure 7-1. The new amino-bis(phenol) ligands worth being synthesized for the future work.	206
Figure 7-2. Bun Yeoul Lee's salen ligand ³ and the proposed amino-bis(phenol) ligand.	208

List of Schemes

Scheme 1-1. Utilization of CO ₂ as a carbon feedstock for industrial chemical production.	2
Scheme 1-2. Industrial routes to the synthesis of polycarbonate. ¹²	4
Scheme 1-3. Typical copolymerization of epoxide and CO ₂ to produce polycarbonate (and ether linkages) and cyclic carbonate byproduct (PO = propylene oxide, CHO = cyclohexene oxide).	7
Scheme 1-4. A general catalytic cycle for the catalytic copolymerization of CO ₂ and epoxide (P = polymer chain, X = halide).	8
Scheme 1-5. Initiation mechanism for the catalyst system of the planar salen based metal complex containing X initiator (typically chloride or azide) and added nucleophile (Nu).	16
Scheme 1-6. Monometallic intramolecular ring-opening of epoxide by salen chromium complex and anionic cocatalyst.	17
Scheme 1-7. Catalytic cycle for the activation of DMAP.	18
Scheme 1-8. Proposed mechanism of initiation with salenCr(III)X and DMAP (X = Cl or NO ₃).	21
Scheme 1-9. Proposed bimetallic pathway followed by zinc β-diiminate complex (P = polymer).	23
Scheme 1-10. Alternating structure of the PO/CHO/CO ₂ terpolymer.	34

Scheme 2-1. Synthetic route to complexes 2.1 and 2.6 .	52
Scheme 3-1. Synthetic route to complex 3.1 .	92
Scheme 3-2. Equilibrium reactions of 3.1 with PPnCl and CHO	102
Scheme 3-3. Proposed initiation mechanism in the presence of PPnCl as cocatalyst. (A) Major initiation pathway (B) Minor initiation pathway.	117
Scheme 4-1. Proposed initiation pathways for the copolymerization of CHO and CO ₂ by 2.1 and PPNN ₃ .	150
Scheme 5-1. Synthetic route to complex 5.1 .	163
Scheme 5-2. The proposed mechanism of the reaction of HMDSO with a hydroxide ion.	165
Scheme 5-3. Copolymerization of CHO and CO ₂ and subsequent block copolymerization with <i>rac</i> -lactide.	184
Scheme 6-1. Preparation of derivatives of Cr(III) amino-bis(phenolate) complexes 6.1 and 6.2	201

List of Abbreviations and Symbols

E_a: activation energy

Å: Ångstrom (10^{-10} m)

ATR: attenuated total reflectance (spectroscopy)

BPA: bisphenol A

Acacen: *N,N'*-bis(*t*-butylacetylacetone)-1,2-ethylenediamine

Salan: *N,N'*-bis(phenolato)-1,2-diaminoethane

Salen: *N,N'*-bis(salicylidene-ethylenediamine)

PPNN₃: bis(triphenylphosphoranylidene)iminium azide

PPNCl: bis(triphenylphosphoranylidene)iminium chloride

CO₂: carbon dioxide

Co-cat.: cocatalyst

CDCl₃: deuterated chloroform

CCS: carbon capture and storage

CHO: cyclohexene oxide

Conv.: conversion

(°): degree

CDCl₃: deuterated chloroform

Đ: dispersity (M_w/M_n)

DCM: dichloromethane

DFT: density functional theory

DSC: differential scanning calorimetry

BDI: β -diiminate

DMAP: 4-(dimethylamino)pyridine

DBU: 1,8-diazabicyclo(5.4.0)undec-7-ene

DHBA: 2,5-dihydroxybenzoic acid

ESI: electrospray ionization

GPC: gel permeation chromatography

T_g: glass transition temperature

Hz: hertz

h: hour

HMDS: hexamethyldisilazane

HMDSO: hexamethyldisiloxane

IR: infrared

K: Kelvin

LA: lactide

M: mol L⁻¹

MS: mass spectrometry

m/z: mass to charge ratio

MALDI-TOF: matrix assisted laser desorption/ionization time of flight

mL: milliliter (10^{-3} L)

min: minute

NMR: nuclear magnetic resonance

ND: not determined

Nu: nucleophile

M_n : number average molecular weight

M_w : weight average molecular weight

ORTEP: Oak Ridge thermal-ellipsoid plot program

PC: propylene carbonate

PLA: polylactide

PCHC: poly(cyclohexene carbonate)

PPC: poly(propylene carbonate)

PEC: poly(ethylene carbonate)

PO: propylene oxide

rac: racemic

THF: tetrahydrofuran

TGA: thermal gravimetric analysis

TOF: turnover frequency

TON: turnover number

TFA: trifluoroacetate

UV-Vis: ultraviolet-visible

vs.: versus

List of Appendices

Figure A-1. Molecular structure (ORTEP) and partial numbering scheme of 5.2 (single crystals obtained from a solution of 5.1 in hexamethyldisiloxane (HMDSO) and toluene). Ellipsoids are drawn at 50% probability. Hydrogen atoms omitted for clarity.	219
Figure A-2. Molecular structure (ORTEP) and partial numbering scheme of 7 (single crystals obtained from a solution of 2.1 in hexamethyldisilazane (HMDS) and toluene). Ellipsoids are drawn at 50% probability. Hydrogen atoms omitted for clarity.	221
Figure B-1. MALDI-TOF mass spectrum of complex 2.1	223
Figure B-2. (A) MALDI-TOF mass spectrum of PCHC obtained using 2.1 and PPNCI. (B) Magnified low mass region of the spectrum ($n = 23 - 26$) with modeled polymer chains.	224
Figure B-3. (A) MALDI-TOF mass spectrum of PCHC obtained using 2.1 and PPNN ₃ . (B) Magnified low mass region of the spectrum ($n = 23 - 26$) with modeled polymer chains.	225
Figure B-4. MALDI-TOF mass spectrum of complex 3.1 with isotopic patterns.	226
Figure B-5. The MALDI-TOF mass spectrum of polymer obtained using 3.1 and PPNCI (Table 3-2, entry 1).	227
Figure B-6. MALDI-TOF mass spectrum of PCHC using Ph ₂ P(O)NPPh ₃ as cocatalyst precipitated from methanol (Table 5-3, entry 3).	227

Figure B-7. MALDI-TOF mass spectrum of PCHC using Bu ₄ NOH as cocatalyst precipitated from methanol (Table 5-3, entry 4).	228
Figure C-1. Representative ¹ H NMR spectrum in CDCl ₃ of the aliquot taken right after polymerization (Table 2-2, entry 5). % Conversion calculation = polymer peak integration (10.06 at 4.65 ppm) divided by the sum of the polymer (10.06 at 4.65 ppm) and monomer (1.00 at 3.12 ppm) peak integrations.....	229
Figure C-2. ¹ H NMR spectrum in CDCl ₃ of PCHC (Table 2-2, entry 1) in the solution layer.....	230
Figure C-3. ¹ H NMR spectrum of raw polycarbonate obtained by 3.1 and PPNCI (Table 3-2, entry 1). The conversion % = polycarbonate peak intergration (6.66 at 4.65 ppm) divided by the sum of the polycarbonate intergration (6.66 at 4.65 ppm) and CHO peak intergration (1.00 at 3.12 ppm).	231
Figure C-4. ¹³ C{ ¹ H} NMR spectrum of a representative polycarbonate obtained by 3.1 and PPNCI (Table 3-2, entry 1) showing the presence of both isotactic and syndiotactic isomers.	231
Figure C-5. ¹ H NMR spectrum in CDCl ₃ of polycarbonate obtained by 5.1 and Ph ₂ P(O)NPPPh ₃ (Table 5-3, entry 3).....	232
Figure C-6. ³¹ P NMR spectrum in acetone-d ₆ of polycarbonate obtained by 5.1 and Ph ₂ P(O)NPPPh ₃ (Table 5-3, entry 3).....	233

Figure C-7. ^{31}P NMR spectrum in solid state of polycarbonate obtained by 5.1 and $\text{Ph}_2\text{P}(\text{O})\text{NPPH}_3$ (Table 5-3, entry 3).....	233
Figure C-8. $^{31}\text{P}\{^1\text{H}\}$ NMR of commercial $\text{Ph}_2\text{P}(\text{O})\text{NPPH}_3$	234
Figure C-9. $^{31}\text{P}\{^1\text{H}\}$ NMR spectrum in deuterated acetone of the purified polymer obtained from CHO/CO ₂ copolymerization by 5.1 and $\text{Ph}_2\text{P}(\text{O})\text{NPPH}_3$ for 2 h.	235
Figure C-10. $^{31}\text{P}\{^1\text{H}\}$ NMR spectrum in dichloromethane-d of the mixture of 5.1 and $\text{Ph}_2\text{P}(\text{O})\text{NPPH}_3$	236
Figure D-1. UV-Vis absorption spectrum of complex 2.1 at concentration of 10^{-4} mol L ⁻¹ in dichloromethane.....	237
Figure D-2. Photos of (a) complex 2.1 (b) complex 2.2 (c) recovered complex 2.1	237
Figure D-3. (a) Complex 2.1 dissolved in THF, MeCN and CH ₂ Cl ₂ . (b) The solution of 2.1 was exposed to air for 1 h, 3 h, 1 day and 3 days.	238
Figure E-1. Representative DSC second heating curve of polymer produced using DMAP as cocatalyst.	239
Figure E-2. Representative DSC second heating curve of polymer produced using PPNN ₃ as cocatalyst.	240
Figure E-3. Representative TGA curve of polymer produced using PPNN ₃ as cocatalyst at a heating rate of 10 °C min ⁻¹	241
Figure E-4. DSC second heating curves of polycarbonate obtained by 5.1 and PPNCI	

(Table 5-3, entry 2).....	242
Figure E-5. DSC second heating curves of polycarbonate obtained by 5.1 and Ph ₂ P(O)NPPPh ₃ (Table 5-3, entry 3).....	243
Figure E-6. TGA curve of PCHC at a heating rate of 10 °C min ⁻¹ (Table 5-3, entry 2). .	244
Figure E-7. TGA curve of PCHC at a heating rate of 10 °C min ⁻¹ (Table 5-3, entry 3). .	245

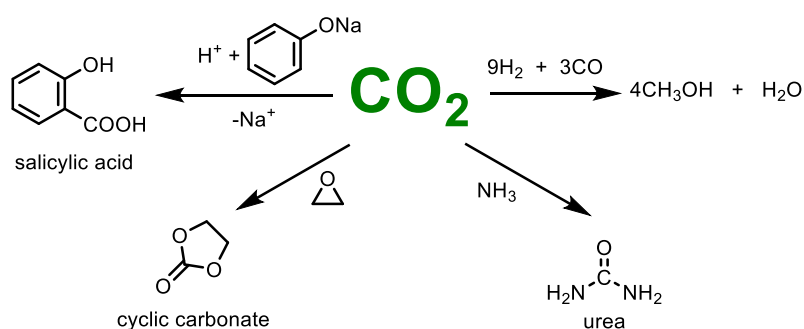
Chapter 1. Introduction

1.1 CO₂ as a carbon feedstock

CO₂ is the most abundant renewable carbon resource and a well-known greenhouse gas. Since the industrial revolution, the level of CO₂ in the atmosphere has significantly increased due to the extensive use of fossil fuels. There is an urgent need to reduce CO₂ emissions, which are associated with detrimental environmental effects such as global warming and ocean acidification. One efficient strategy to reduce CO₂ emissions is carbon dioxide capture and storage (CCS).¹⁻³ However, this technology has limitations including high energy requirements, high cost and uncertain permanence time of the stored CO₂.⁴ Utilization of CO₂ as a carbon feedstock is now receiving much attention as it is not only a form of CO₂ storage but also provides access to high value products from an abundant, non-toxic, inexpensive and renewable resource.⁵⁻⁸

There are only few examples of industrial applications of CO₂ as a starting material for chemical production.⁵ This is because CO₂ has a relatively high thermodynamic stability and therefore a large input of energy is required to convert CO₂ into other chemicals. Most of the research on CO₂ activation uses energy-rich substrates, thus providing a direct thermodynamic driving force. Impressive progress has been made on a range of reactions with industrial potential, such as coupling of CO₂ with epoxides or

aziridines, formylation and methylation of amines, and reduction of CO₂ in the presence of hydrogen.⁹ Currently, CO₂ has been commercially converted to salicylic acid, urea, cyclic carbonates and used as an additive in the synthesis of methanol (Scheme 1-1).¹⁰ Although the amount of CO₂ consumed in these processes (*ca.* 120 Mt) only makes up a very small fraction of the total CO₂ generated from human activities (*ca.* 37 Gt), these processes provide more environmentally friendly routes to produce valuable chemicals otherwise made from reagents that may be detrimental to the environment.⁸



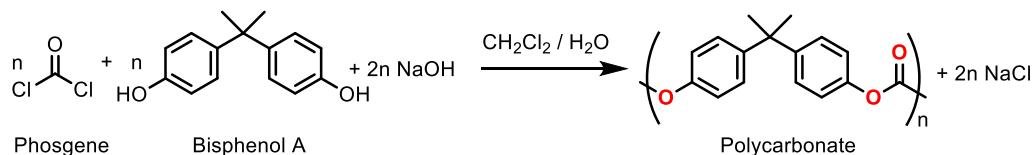
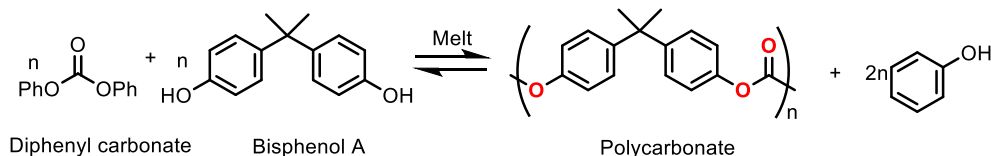
Scheme 1-1. Utilization of CO₂ as a carbon feedstock for industrial chemical production.

1.2 Overview of polycarbonate

Polycarbonates are a class of thermoplastic polymers containing carbonate groups. In particular, aromatic polycarbonates made from bisphenol A are the most commonly used and possess outstanding physical properties including lightness, strength, durability, high transparency, good electrical insulation and heat resistance.¹¹ By virtue of these properties

they have been widely used in construction materials, data storage devices, optical media, office equipment, electronic components, packaging and automotive industry.

Industrially, the conventional production of polycarbonate involves the reaction of bisphenol A with phosgene (Scheme 1-2, A), which generates a number of environmental and safety issues.¹² First, phosgene is a highly toxic gas that can be used as a chemical weapon, thus its production and utilization have been severely controlled worldwide. Second, a great amount of dichloromethane (a suspected human carcinogen), typically more than ten times by weight of the produced polycarbonate, is used as a polymerization solvent. Due to the low boiling point of dichloromethane, it is very difficult to completely avoid the release of dichloromethane into the atmosphere. In addition, a large amount of waste water containing organic compounds and dichloromethane require treatment to meet environmentally acceptable levels before discharged. Although this conventional process has a lot of disadvantages, it is still used by industry to annually produce approximately 2.7 Mt of polycarbonate globally.¹²

Phosgene Process A**Non-Phosgene Process B**

Scheme 1-2. Industrial routes to the synthesis of polycarbonate.¹²

Another industrial route to polycarbonate involves the reaction of bisphenol A with diphenyl carbonate, avoiding the use of phosgene (Scheme 1-2, B).¹³ However, the equilibrium of this transesterification reaction favors the reactants. The phenol byproduct, therefore, must be efficiently removed from the produced polycarbonate to drive the reaction forward. To meet this requirement, high reaction temperature (to reduce the viscosity of the produced polycarbonate) and high vacuum are typically applied in this reaction, which result in a high energy consumption and more side reactions. In addition, the commercial diphenyl carbonate is typically produced from phenol and toxic phosgene. Therefore, the use of diphenyl carbonate monomer for the polycarbonate production does not completely solve the issue of using toxic phosgene.

Another important consideration of traditional polycarbonate synthesis is that

bisphenol A is now recognized as an endocrine disruptor.¹⁴ The extensive use of bisphenol A based polycarbonate in food and beverage containers has raised health concerns since traces of bisphenol A were found to leach out of the product and into the food.¹⁵ Therefore, there is a great interest to develop new technologies to substitute these current industrial routes for polycarbonate production.

1.3 Copolymerization of CO₂ and epoxide

1.3.1 Background

Copolymerization of CO₂ and epoxide to produce polycarbonate was first identified by Inoue over 40 years ago.¹⁶ This process not only uses CO₂ as a carbon feedstock but also provides a potentially sustainable route to produce valuable cyclic and polycarbonates. It was not until 2000 that the number of publications in this research field started to increase significantly (Figure 1-1). A discussion of the evolution of this discovery will be given in the next section.

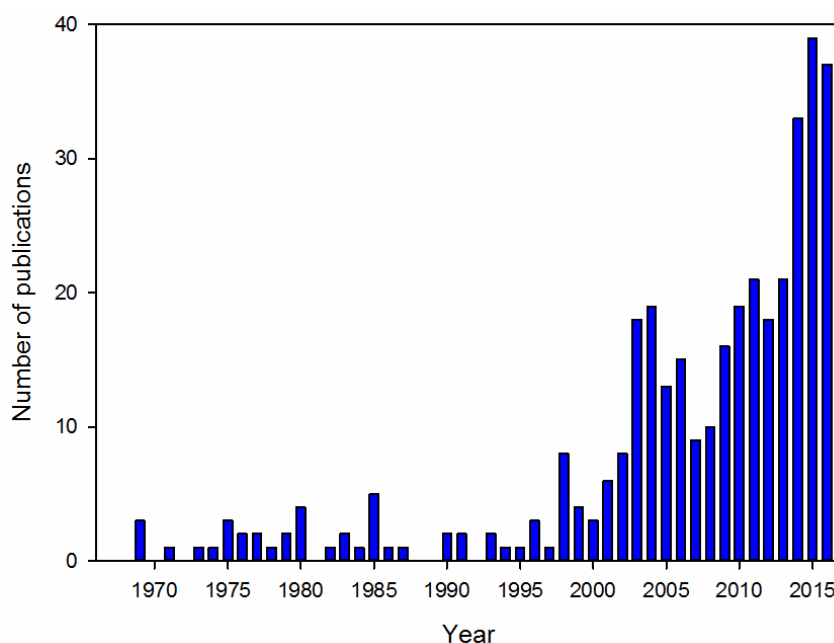
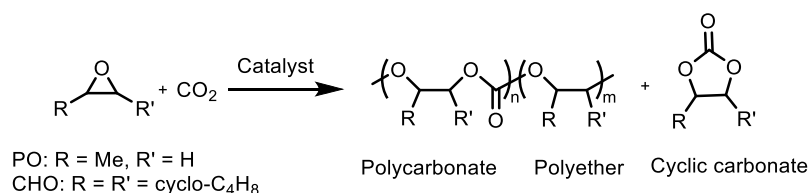


Figure 1-1. The number of publications concerning CO₂/epoxide copolymerization per year from 1969 to 2016 (Note: the search was conducted by SciFinder using key words of CO₂, epoxide and copolymerization).

In general, this reaction is accompanied by the formation of cyclic carbonate byproduct and varying quantities of ether linkages (Scheme 1-3). Two general observations are also found for this catalytic reaction regardless of the catalyst.⁸ First, aliphatic epoxides more easily form cyclic carbonates than alicyclic epoxides. Second, an increase in temperature leads to an increase in the formation of cyclic carbonate. Among the investigated epoxides, propylene oxide (PO) and cyclohexene oxide (CHO) are the most commonly used epoxides, of which PO and CO₂ provide the corresponding polycarbonate that has been industrially most developed; CHO, on the other hand, affords a polycarbonate that exhibits poor mechanical properties for current industrial needs.¹⁷

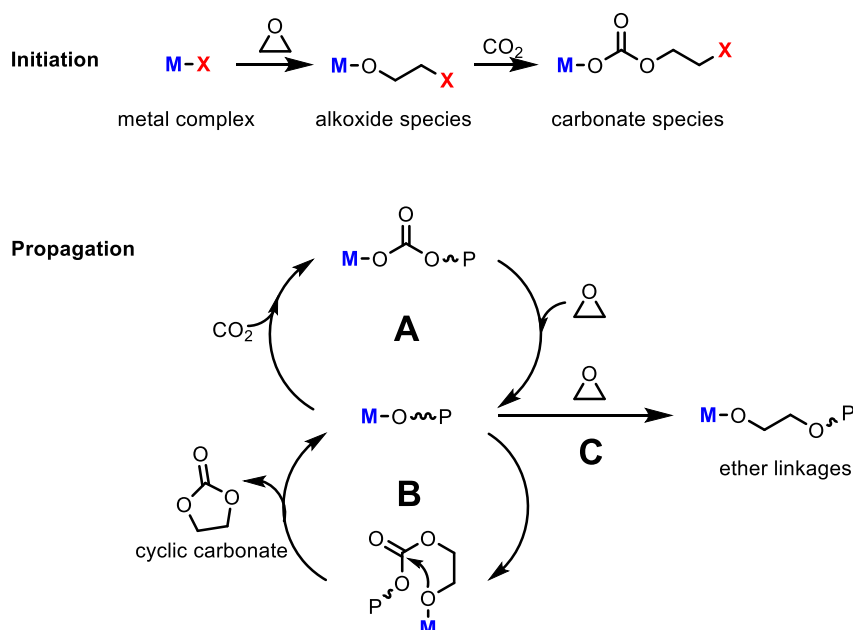
However, CHO exhibits low propensity to form cyclic carbonate byproduct in the copolymerization process making it useful for academic studies.



Scheme 1-3. Typical copolymerization of epoxide and CO₂ to produce polycarbonate (and ether linkages) and cyclic carbonate byproduct (PO = propylene oxide, CHO = cyclohexene oxide).

A general catalytic cycle of CO₂/epoxide copolymerization is shown in Scheme 1-4.¹⁸

The reaction begins with a ring-opening of the metal-activated epoxide by the initiator X (halide) to generate an alkoxide. The metal alkoxide species subsequently undergoes CO₂ insertion to afford the metal carbonate. The resulting carbonate serves as an initiator to ring-open another coordinated epoxide, followed by CO₂ insertion to generate carbonate which continues the polymerization process (Scheme 1-4, A). During this process, the metal bound polymer chain may backbite to afford cyclic carbonate byproduct (Scheme 1-4, B). For some catalysts, the resulting metal alkoxide can also ring-open epoxide, leading to ether linkages in the copolymer backbone (Scheme 1-4, C).



Scheme 1-4. A general catalytic cycle for the catalytic copolymerization of CO_2 and epoxide (P = polymer chain, X = halide).

1.3.2 Early catalyst developments

The first metal-catalyzed CO_2 /epoxide copolymerization reaction can be traced back to 1969 when Inoue and co-workers discovered the heterogeneous catalyst system containing a 1:1 mixture of diethyl zinc and water could catalyze PO/ CO_2 copolymerization to afford poly(propylene carbonate) (PPC) with a turnover frequency (TOF) of $0.12\ h^{-1}$.¹⁶ Subsequently, various heterogeneous catalyst systems such as diethylzinc/dihydric phenols¹⁹ and dialkylzinc/carboxylic acid²⁰ were developed for this copolymerization process. However, these heterogeneous catalysts were generally plagued by low turnover frequencies, low reproducibility and broad molecular weight

distributions due to lack of the controlled active species.

Inoue and co-workers reported the aluminum porphyrin complex (Figure 1-2, **1.1a**) as the first homogeneous catalyst for the copolymerization of CO₂ and epoxide.²¹ In the presence of quaternary organic salts or triphenylphosphine in dichloromethane at ambient temperature and 49 bar CO₂, this catalyst produced polycarbonates with a narrow dispersity below 1.10 and a molecular weight ranging between 3500 g mol⁻¹ and 6200 g mol⁻¹. However, this reaction took over 12 days to reach completion (TOF < 1 h⁻¹). A significant increase in activity of porphyrin catalysts was achieved by Holmes, who developed a fluorinated Cr(III) porphyrin complex (Figure 1-2, **1.1b**), which was soluble in supercritical CO₂.²² In supercritical CO₂, this catalyst combined with 4-(dimethylamino)pyridine (DMAP) could produce polycarbonate from CO₂ and CHO with a TOF of *ca.* 170 h⁻¹. The resulting polycarbonate showed a dispersity of less than 1.4 and high carbonate content ranging from 90 to 97%; however, it exhibited a low molecular weight of *ca.* 3000 g mol⁻¹.

The development of well characterized Zn-phenoxide complexes (Figure 1-2, **1.2a-e**) was a breakthrough for the exploration of homogeneous Zn catalysts. The first zinc bisphenoxide catalyst (Figure 1-2, **1.2a**) showed a low TOF of 2.6 h⁻¹ for polycarbonate formation from CHO and CO₂ at 80 °C and 55 bar CO₂.²³ The produced polymer exhibited a high molecular weight of 38000 g mol⁻¹ and a broad dispersity of 4.5. Subsequent

investigations of zinc bisphenoxide complexes found that their activities toward CO₂/CHO copolymerization were affected by the steric hindrance of *ortho* substituents on the phenolate ligand. Their catalytic activities increased in the order of isopropyl (**1.2b**) < phenyl (**1.2a**) < *t*-butyl (**1.2c**) < methyl substituents (**1.2d**).²⁴ Introducing more electron-withdrawing and less sterically demanding fluorine substituents in the *ortho* positions of the phenolate ring provided a dimeric zinc bisphenoxide complex (Figure 1-2. **1.2e**).²⁵ This complex showed improved catalytic activity with a TOF of 16 h⁻¹. However, these zinc-phenoxide catalysts generally produced polycarbonates exhibiting broad dispersities varying from 2.5 to 4.5, most likely due to catalyst aggregation phenomena.

A breakthrough in the catalyst system design was the development of zinc β-diiminate (BDI) complexes (Figure 1-2, **1.3a-e**, **1.4a-d**) by Coates and co-workers in 1998.²⁶ These zinc β-diiminate derivatives were observed to be more efficient for CO₂/epoxide copolymerization compared to previously developed catalysts.²⁷ Copolymerization of CO₂ with CHO catalyzed by **1.3a** gave a high TOF of 135 h⁻¹ even at 20 °C and 7 bar CO₂. The resultant polycarbonates exhibited high molecular weight with a narrow dispersity of 1.07 and over 95% carbonate content.²⁶ **1.3a** and **1.4a** showed nearly identical TOFs of 247 h⁻¹ and 224 h⁻¹ at 50 °C and 7 bar CO₂, which supported the formation of metal carbonate and alkoxide intermediates in CO₂/epoxide copolymerization. One of the most active catalysts reported to date for CO₂/CHO copolymerization is a zinc β-diiminate complex containing

the electron-withdrawing cyano substituent (**1.4d**).²⁸ At 50 °C and 7 bar CO₂, **1.4c** and **1.4d** were found to exhibit extremely high activity with TOFs of 2170 and 2290 h⁻¹, respectively. However, sterically unencumbered methyl substituents on the *N*-aryl *ortho* positions gave no copolymerization activity, which was attributed to the tightly bound dimeric state of the resulting complex. On the other hand, these zinc β-diiminate complexes were found to be less active for PO and led to the formation of cyclic carbonate byproduct.²⁹ For instance, the copolymerization of PO and CO₂ by the unsymmetrical **1.3e** produced PPC and PC (85:15) with a TOF of 47 h⁻¹ at 25 °C and 20 bar CO₂.

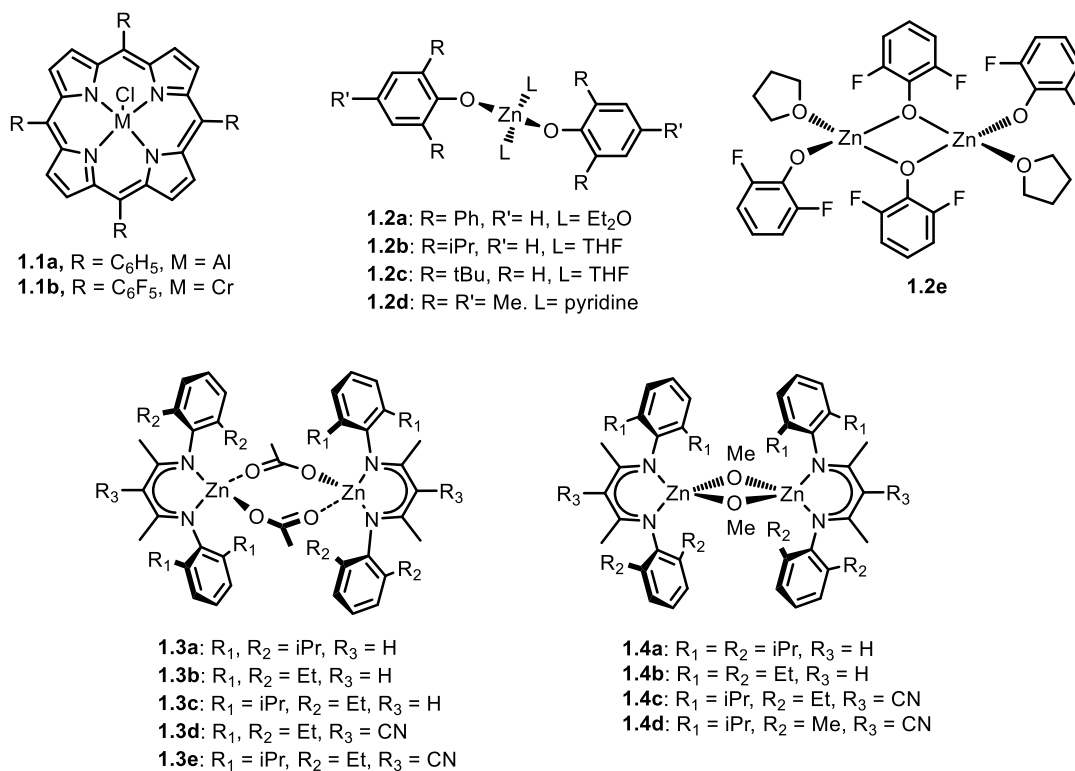


Figure 1-2. Representative homogeneous catalyst systems for the copolymerization of CO₂ and epoxide.

1.3.3 Binary chromium salen catalyst system

The development of a salen chromium catalyst (Figure 1-3, **1.5a**) by Darensbourg and co-workers was a landmark for CO₂/epoxide copolymerization.³⁰ Their work was inspired by Jacobsen and co-workers who found salen Cr(III) complexes (Figure 1-3, **1.5a-b**) showed high activity towards the asymmetric ring-opening of epoxides.³¹ Salen ligands are easily synthesized by the condensation between aldehydes and amines; additionally, the steric and electronic properties around the metal center can be readily modified by introducing different substituents.³² Therefore, in the literature salen complexes are one of the most studied catalysts for CO₂/epoxide copolymerization. Many researchers including Darensbourg,³³⁻³⁶ Lu,³⁷⁻³⁹ Coates,^{40,41} Nozaki,⁴² Rieger^{43,44} and others have contributed to the development of highly active salen metal complexes, particularly with Cr or Co. They found nucleophilic cocatalysts are typically required for these salen complexes to obtain efficient activities. The most commonly used cocatalysts including *N*-methylimidazole, 4-(dimethylamino)pyridine (DMAP) and bis(triphenylphosphine)iminium chloride or azide (PPNCl or PPNN₃) are shown in Figure 1-3.

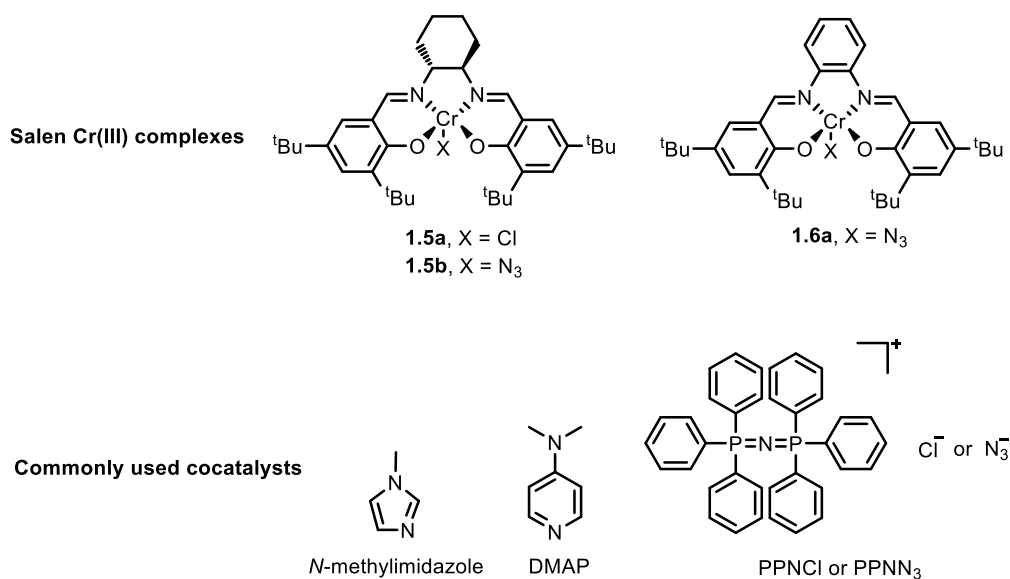


Figure 1-3. Salen Cr(III) complexes and commonly used cocatalysts.

Darensbourg and co-workers conducted detailed investigations into a variety of ligand substitutions on salen Cr(III) complexes (Figure 1-4), leading to increased catalytic activity for CO₂/CHO copolymerization.^{45,46} The steric effect on the diimine backbone was found to have a dramatic impact on catalyst activity, likely due to the hindered approach of the epoxide to the metal center. For example, when R₁ and R₂ were sterically bulky *t*-butyl groups, this complex (R₃ = R₄ = *t*-butyl) at 55 bar CO₂ and 80 °C could produce polycarbonate with a TOF of 0.8 h⁻¹ compared to 36 h⁻¹ for the analogue with R₁ = R₂ = H.⁴⁵ The decreased activity was believed to be caused by the bulky substituents, which sterically hinder the approach of the epoxide to the metal center. In addition, stronger electron donating substituents on the phenolate rings were found to enhance the catalytic activity.

For instance, in the presence of *N*-methylimidazole the salen Cr(III) complex with $R_3 = \text{OMe}$ and $R_4 = t\text{-butyl}$ was more active than the $R_3 = R_4 = t\text{-butyl}$ analogue, with a TOF of 57 h^{-1} and 36 h^{-1} , respectively. Furthermore, changing the ancillary ligand (X) of the salenCr(III)X ($R_1 = R_2 = \text{H}$, $R_3 = \text{OMe}$, $R_4 = t\text{-butyl}$) from chloride to azide increased TOF from 36 to 47 h^{-1} .

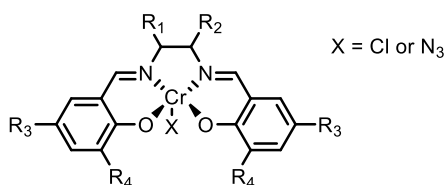


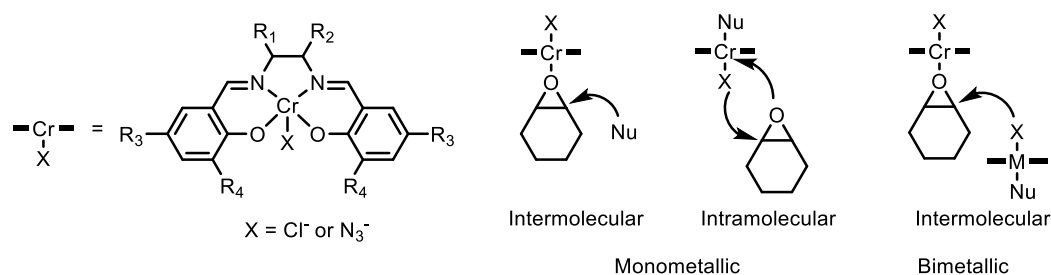
Figure 1-4. General structure of salen Cr(III) catalysts used in CO₂/epoxide copolymerization.

Despite the benefits of the modifiable electronic and steric properties around the chromium center, the most important aspect affecting the copolymerization rate is the cocatalyst.^{36,47} A TOF of 608 h^{-1} for CO₂/CHO copolymerization at 80 °C and 55 bar CO₂ can be achieved using the salenCr(III)X with $R_1 = R_2 = \text{H}$, $R_3 = R_4 = t\text{-butyl}$ and $X = \text{N}_3$ in combination with PPNN₃.⁴⁷ The salen Cr(III) complex (Figure 1-3, **1.5b**) in combination with PPNN₃ at 80 °C and 35 bar CO₂ further increased the catalytic activity, giving a TOF of 1153 h^{-1} .⁴⁸ The produced polycarbonate showed a negligible amount of ether linkages with a high molecular weight of $50\,000 \text{ g mol}^{-1}$ and a narrow dispersity of 1.13. These

complexes also showed activities for CO₂/PO copolymerization, but various amounts of cyclic carbonate byproduct were produced. The most active variant towards the PO copolymerization contained a phenylene group on the diimine backbone (Figure 1-3, **1.6a**) and in the presence of PPNCI at 60 °C and 34 bar CO₂ selectively generated PPC with 93% copolymer selectivity and 99% carbonate linkages (TOF of 192 h⁻¹).⁴⁹ Further investigations of salen ligands coupled with cobalt increased both the copolymerization rate and selectivity for polycarbonate, particularly for CO₂/PO copolymerization.^{40,50}

1.3.4 Mechanistic studies of binary chromium salen catalysts

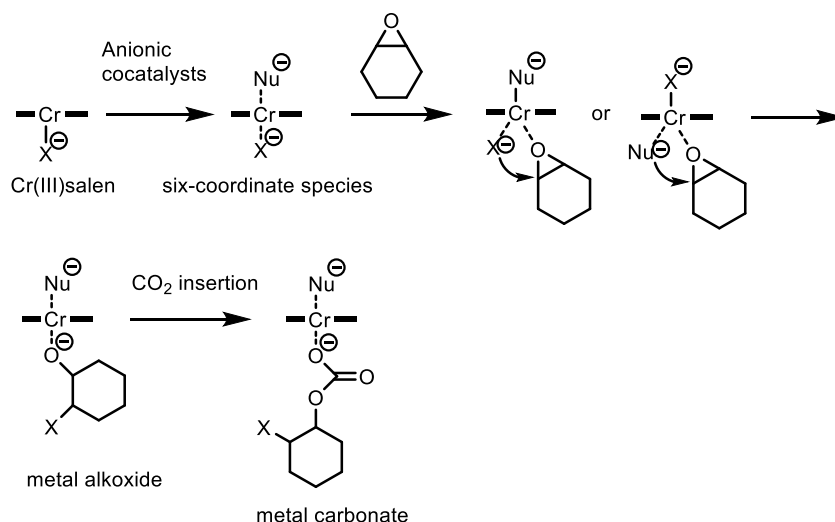
Despite the intense studies of catalyst systems consisting of salen complexes and cocatalysts in CO₂/epoxide copolymerization, the precise mechanisms are complex and not unequivocally defined. Initiation mechanism including bimetallic and monometallic pathways have been proposed, with the latter following either an intermolecular or intramolecular pathway (Scheme 1-5).⁵¹



Scheme 1-5. Initiation mechanism for the catalyst system of the planar salen based metal complex containing X initiator (typically chloride or azide) and added nucleophile (Nu).

The Darensbourg group proposed an intramolecular (monometallic) ring-opening of epoxide when an ionic cocatalyst was used (Scheme 1-6).⁴⁷ The ionic cocatalyst (Nu) binds to the chromium center, weakening the Cr-X bond and allowing the incoming epoxide to coordinate to the chromium center. As the epoxide coordinates, the adjacent metal ion bond becomes weaker while the other chromium ion bond is strengthened, which improves the concerted epoxide ring-opening. After the ring is opened, a dianion species is regenerated, weakening the chromium ion bonds again and allowing CO₂ insertion to generate the active metal carbonate. The produced carbonate can ring-open another coordinated epoxide and continues the polymerization process. Formation of the active species of the six-coordinate anion was proposed to be fast, which rationalizes the observation that ionic cocatalyst systems such as these typically show no induction period. Relevant to this proposed mechanism, the anionic six-coordinate complexes composed of *trans*-salenCr(III)X₂ species (X = Cl, N₃, CN) have been isolated and characterized by X-ray crystallography.⁵²

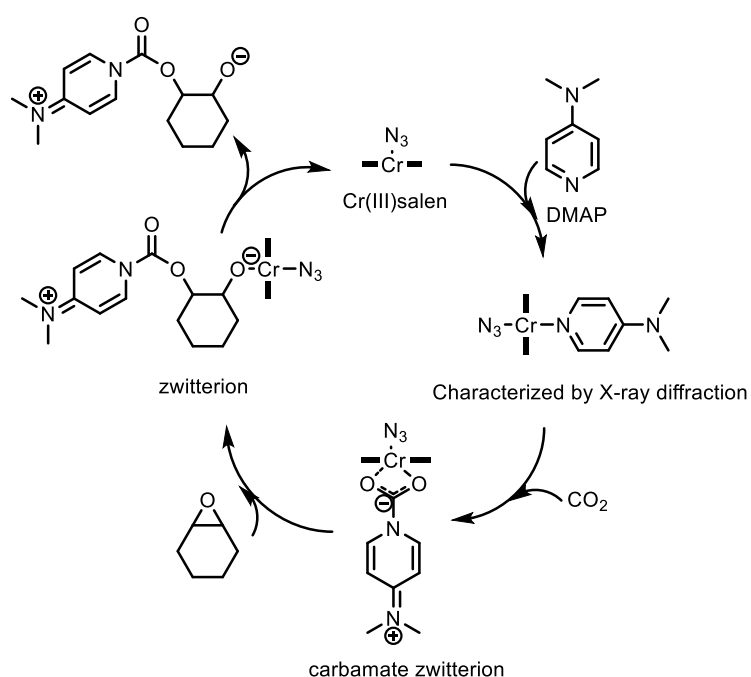
However, since both initiators X and nucleophile derived from cocatalyst were observed as polymer end-groups by MALDI-TOF MS, it is still unclear which initiator favors epoxide ring-opening. Moreover, the presence of excess ionic cocatalyst was found to lead to a rapid displacement of growing polymer chain and resulted in increased amounts of cyclic carbonate forming.⁴⁹



Scheme 1-6. Monometallic intramolecular ring-opening of epoxide by salen chromium complex and anionic cocatalyst.

The commonly used neutral cocatalyst DMAP was studied in detail for CO_2 /epoxide copolymerization by salen chromium complex in Darensbourg's group.⁴⁷ They proposed a catalytic cycle for activating DMAP, in which DMAP binds to the metal center of a salen chromium complex and interacts with CO_2 to generate a carbamate zwitterion, followed by

a reaction with epoxide to form another zwitterion, which dissociates to regenerate the salen chromium complex (Scheme 1-7). The six-coordinate $[\text{salenCr(III)N}_3]\cdot\text{DMAP}$ complex was characterized by X-ray diffraction and the carbamate zwitterion was identified by $\nu(\text{CO}_2)$ bands at 2097 and 2017 cm^{-1} . This carbamate zwitterion is proposed to serve as an analogue to the anion derived from ionic cocatalyst and it was demonstrated that the initiation period for polycarbonate formation ended with the disappearance of “free” DMAP IR band.



Scheme 1-7. Catalytic cycle for the activation of DMAP.

Lu and co-workers also investigated the role of DMAP in CO_2/PO copolymerization

by salen and salan chromium complexes (Figure 1-5, **1.7c** and **1.8c**).⁵³ The reaction mixtures examined by ESI-MS (Figure 1-6) showed a peak at m/z 181 corresponding to $[-OCH(CH_3)CH_2\text{-DMAP} + H^+]$, indicating that DMAP ring-opened PO. Moreover, peaks were observed to shift to higher molecular weight regions over time corresponding to addition of $[PO + CO_2]$ units to $[-OCH(CH_3)CH_2\text{-DMAP} + H^+]$ (Figure 1-6), providing evidence that the formation of a carbamate zwitterion is not required for initiation.

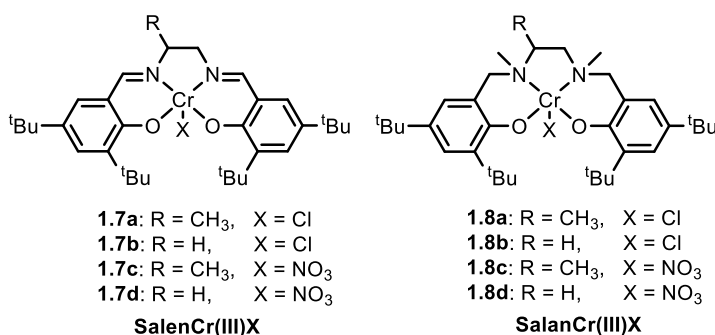


Figure 1-5. Structures of salen and salan chromium complexes used in Lu's ESI-MS study.⁵³

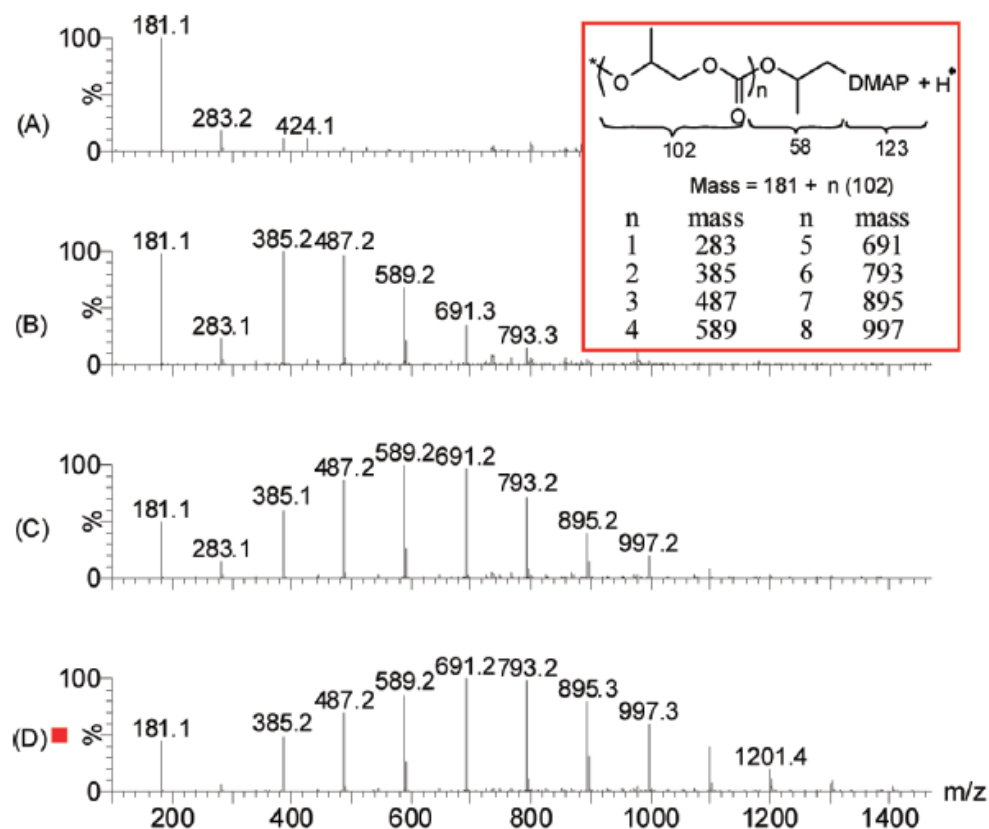
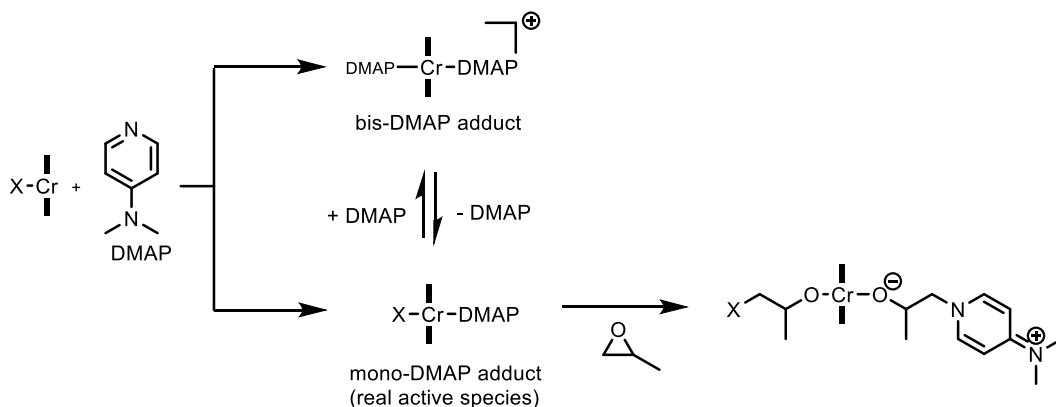


Figure 1-6. ESI mass spectra of the reaction mixtures resulting from the catalyst system **1.7c**/DMAP (1:1, molar ratio) during CO₂/PO copolymerization at 25 °C and 6 bar CO₂ pressure. Time: (A) 2 h, (B) 4 h, (C) 6 h, (D) 8 h. Reprinted with permission from Rao, D.-Y.; Li, B.; Zhang, R.; Wang, H.; Lu, X.-B. *Inorg. Chem.* **2009**, *48*, 2830. Copyright (2009) American Chemical Society.

Lu and co-workers also observed the salenCr(III)X complexes, containing two sp^3 hybridized amino donors (Figure 1-5, **1.8a-d**), combined with DMAP showed no or short (*ca.* 10 min) induction periods and significantly higher copolymerization rates than the salen counterparts (Figure 1-5, **1.7a-d**). Additionally, salenCr(III)X complexes also showed a long induction period up to 2 h. They proposed that salenCr(III)X complexes in

the presence of DMAP predominantly produce bis-DMAP adduct.⁵³ The bis-DMAP adduct does not easily dissociate one DMAP to generate the true active species, the mono-DMAP adduct, which leads to the observed long induction period (Scheme 1-8). This proposal was supported by the investigation of binding of DMAP to salenCr(III)X and salanCr(III)X complexes by ESI-MS, where [salenCr(III)(DMAP)₂]⁺ was predominantly observed upon combination of salenCr(III)X complexes with DMAP.⁵³ On the other hand, salanCr(III)X complexes predominantly showed [salanCr(III)(DMAP)]⁺ cations even in the presence of 10 equivalents of DMAP. This suggests that quite subtle changes in the salen vs. salan ligand structure can lead to different reactivities in these reactions. However, whether the major initiator is DMAP or the axial anion (X) is still debatable.



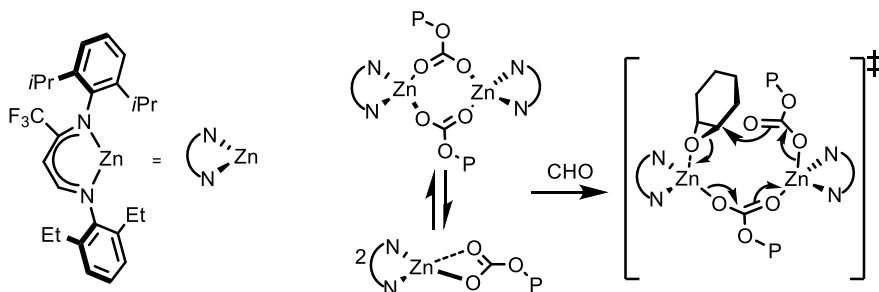
Scheme 1-8. Proposed mechanism of initiation with salenCr(III)X and DMAP (X = Cl or NO₃)

Relevant to Lu's proposal where formation of a bis-DMAP adduct is detrimental to the

copolymerization rate, Rieger and co-workers found that in the presence of two equivalents of DMAP the salen chromium complex (Figure 1-3, **1.6a**) showed no PPC formation from CO₂ and PO, but produced cyclic carbonate with a TOF of 602 h⁻¹.⁴⁴ However, 0.5 equivalents of DMAP gave a TOF of 154 h⁻¹ for PPC formation versus cyclic carbonate formation with a TOF of 34 h⁻¹. They proposed DMAP can compete with the growing polymer chain on the chromium center to form a bis-DMAP adduct and the dissociated polymer chain then readily forms cyclic carbonate through backbiting.

For the chain propagation process, a generally agreed mechanism involves the nucleophilic attack of the carbonate ion on the metal-activated epoxide to generate an alkoxide ion, followed by CO₂ insertion to produce the active carbonate anion again. However, whether the carbonate ion ring-opening of the activated epoxide always follows a monometallic or bimetallic pathway with a specific catalyst is still not known. The Darensbourg group conducted detailed kinetic studies on CO₂/epoxide copolymerization by salen chromium complexes in the presence of amine or phosphine cocatalysts and concluded a bimetallic initiation pathway was occurring followed by monometallic propagation for this system.^{30,35,49,54} On the other hand, DFT studies on salen complexes (containing Cr, Al, Ti, Fe or Al) and cocatalysts by Rieger support a bimetallic propagation process in which a metal-bound carbonate nucleophile attacks a second metal-bound epoxide.⁵⁵ Recent kinetic studies on salenCo(III)Cl/PPNCl and salenCo(III)X/Bu₄NX (X =

2, 4-dinitrophenoxide) catalyst systems showed the reaction order dependence on catalyst concentration is 1.57 and 1.61, respectively.^{42,56} These fractional orders indicate the carbonate chain growth pathway involves two metal complexes working cooperatively. Coates and co-workers have proposed that the highly active zinc β -diiminate complexes that catalyze CO₂/CHO copolymerization follow a bimetallic pathway in which the growing polymer chain on one zinc center ring-opens the epoxide coordinated to a second zinc center (i.e. the other half of the dimeric complex) (Scheme 1-9).⁵⁷ Within the Kozak group, it was recently discovered that a single component catalyst, where DMAP is coordinated to the amino-bis(phenolate) Cr(III) chloride complex to provide a stable octahedral Cr(III) complex, did not appear to follow this same sort of bimetallic mechanism.⁵⁸ The kinetic studies on this single component catalyst support a first-order dependence of the polymerization rate on the catalyst concentration,⁵⁹ hence the need for further mechanistic studies as described in part of this thesis.



Scheme 1-9. Proposed bimetallic pathway followed by zinc β -diiminate complex (P = polymer).

1.3.5 Recent catalyst developments

Recent improvements in catalyst design for CO₂/epoxide copolymerizations are the development of bifunctional and bimetallic catalysts. In the bifunctional catalysts, the cocatalyst is incorporated into the ligand, thus removing the need for an external cocatalyst. Nozaki and co-workers first reported a bifunctional Co(III) salen complex containing piperidinyl arms in the 3-position of the phenyl rings (Figure 1-7, **1.9**).⁶⁰ This new catalyst system showed 90% selectivity towards polycarbonate production using CO₂ and PO at 60 °C and 14 bar CO₂, whereas this reaction condition typically provides only cyclic propylene carbonate using traditional binary catalyst systems. The high selectivity of polymer formation at high temperature was attributed to a proton shuffling between the amine and free polymer chain, preventing the dissociated polymer chain from backbiting to form cyclic carbonate. Lee and co-workers subsequently reported various Co(III) bifunctional salen catalysts where the quaternary ammonium cations in the phenyl rings are balanced by cocatalytic anions (Figure 1-7, **1.10**).^{61,62} An important feature of this type of bifunctional catalyst is that the dissociated chain-growing carbonate unit can always remain close to the metal center by the electrostatic attraction of quaternary ammonium cations, which allows for a very low catalyst loading and reduces backbiting at high reaction temperatures. As a result, this new generation of Co(III) salen complexes showed one of the highest activities for PO/CO₂ copolymerization reported to date, with a TOF of

26000 h⁻¹ at 80 °C and 20 bar CO₂.⁶² Similarly, Lu and co-workers also developed the asymmetric Co(III) bifunctional salen catalyst (Figure 1-7, **1.11**), which showed a high TOF of 6105 h⁻¹ and > 99% selectivity for polycarbonate formation from CO₂ and CHO even at a high temperatures up to 120 °C. Notably, under even 1 bar CO₂ and ambient temperature, this Co(III) bifunctional catalyst **1.11** still showed excellent activity (TOF = 68 h⁻¹) and selectivity (> 99%) for polymer formation.⁶³

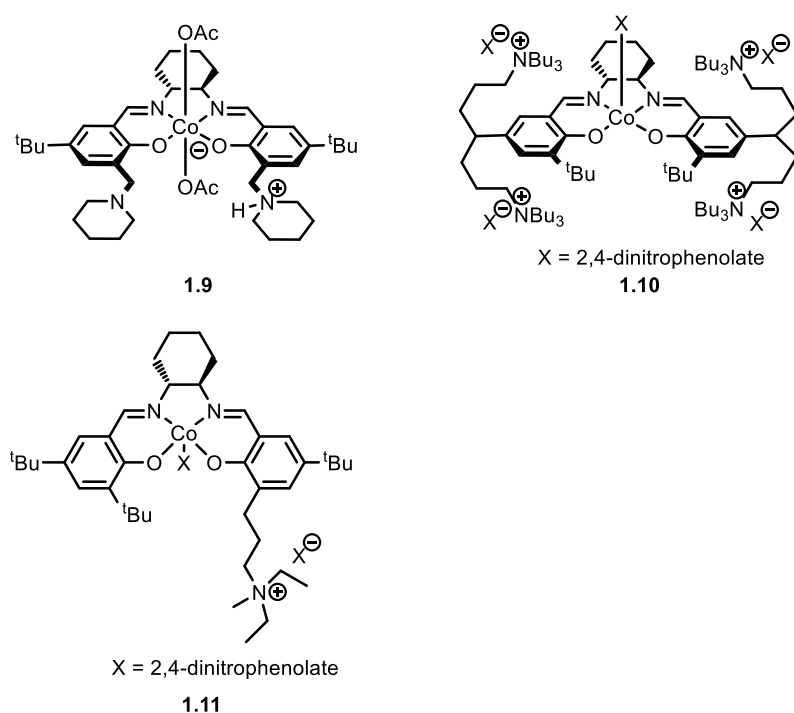


Figure 1-7. The structures of salen-based bifunctional catalysts.

The development of various bimetallic catalysts was inspired by the proposed

bimetallic pathway seen for Coates' zinc β -diiminate complexes.⁵⁷ For example, Nozaki and co-workers investigated Co(III) salen complexes with two salen ligands linked by the various numbers of methylene units (Figure 1-8, **1.12**).⁶⁴ These bimetallic complexes (in the absence of cocatalyst) showed 2 to 9 fold higher activities than the monometallic counterparts. The four-methylene linker variant showed the highest activity for CO₂/PO copolymerization with a TOF of 180 h⁻¹ at ambient temperature and 53 bar CO₂. Notably, this bimetallic catalyst maintained high activity even at very low catalyst loading (0.01%). This tendency is contrary to the monometallic counterpart that showed significantly reduced activity, which suggested a bimetallic mechanism in the copolymerization process. Rieger and co-workers also reported Cr(III) salen complexes with two salen ligands linked together (Figure 1-8, **1.13**).⁶⁵ These corresponding complexes also showed improved activity over the monometallic counterparts and maintained high activity under dilute conditions. In 2009, Williams and co-workers reported a novel di-Zn(II) acetate complex containing a macrocyclic ancillary ligand (Figure 1-8, **1.14**), which showed excellent activity for CO₂/CHO copolymerization at one atmosphere of CO₂.⁶⁶ Based on this novel ligand system, di-Co(III)⁶⁷, di-Mg(II)⁶⁸ and di-Fe(III)⁶⁹ catalysts were developed in the Williams' group and all showed remarkable activities for CO₂/CHO copolymerization. Kinetic studies on the di-Zn(II) acetate complex (Figure 1-8, **1.14**) showed a first-order dependence on catalyst concentration, which supported the proposed bimetallic

mechanism, and a zero-order dependence on the CO₂ pressure, which indicated that the ring-opening of epoxide was the rate determining step.⁷⁰

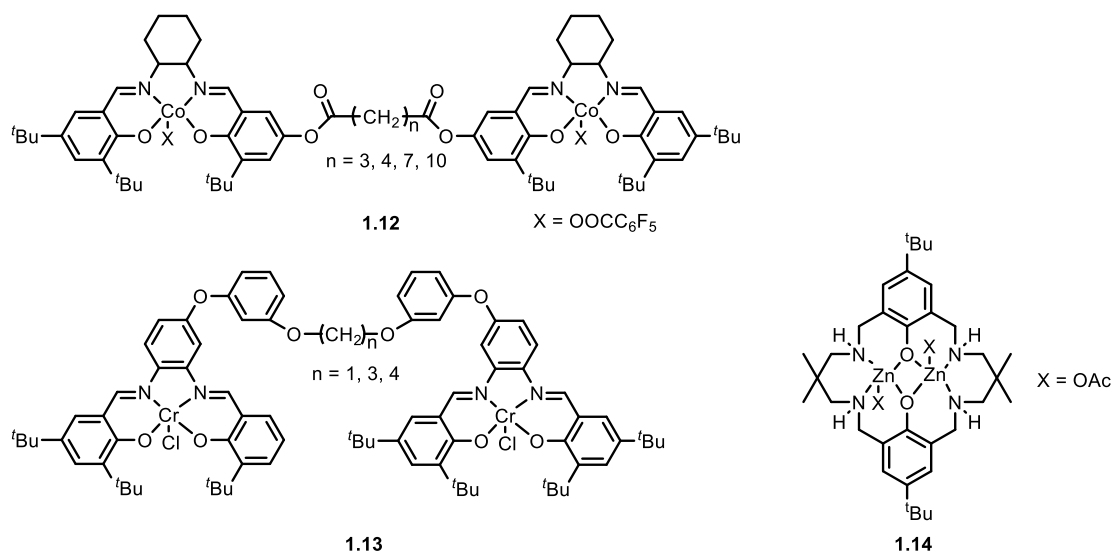


Figure 1-8. Structures of bimetallic catalysts.

In the 2010s, researchers began to explore amino-phenolate ligands as scaffolds for preparing catalysts for these reactions. It is worth noting that in 2011 Nozaki and co-workers also introduced tetravalent metal complexes comprised of a trianionic ligand and an ancillary chloride ligand (Figure 1-9, **1.15**), which exhibit a similar structure to metal salen complexes.⁷¹ These new tetravalent metal complexes showed lower catalytic activities for CO₂/epoxide copolymerization compared to the previously reported metal-salen catalysts. However, these tetravalent metal complexes introduce less toxic

metals such as titanium and germanium, thus providing attractive alternatives to these most active metal-salen catalysts containing cobalt or chromium. Recently, the Kozak group developed amino-bis(phenolate) Cr(III) chloride complexes (Figure 1-9, **1.16**, **1.17**), which exhibit different electronic and geometric properties compared to the Cr(III) salen complexes.^{58,72} Specifically, the amino-bis(phenolate) ligands have stronger electron donating abilities and the potential vacant site is *cis* to the ancillary ligand while planar salen complexes show a *trans* oriented potential vacant site. Moreover, amino-bis(phenol) ligands are readily synthesized and their electronic and steric properties around the metal center can also be readily modified by changing the substituents on the phenol rings and the pendant donor group.⁷³ Therefore, amino-bis(phenolate) Cr(III) chloride complexes provide a new avenue for developing active catalysts.

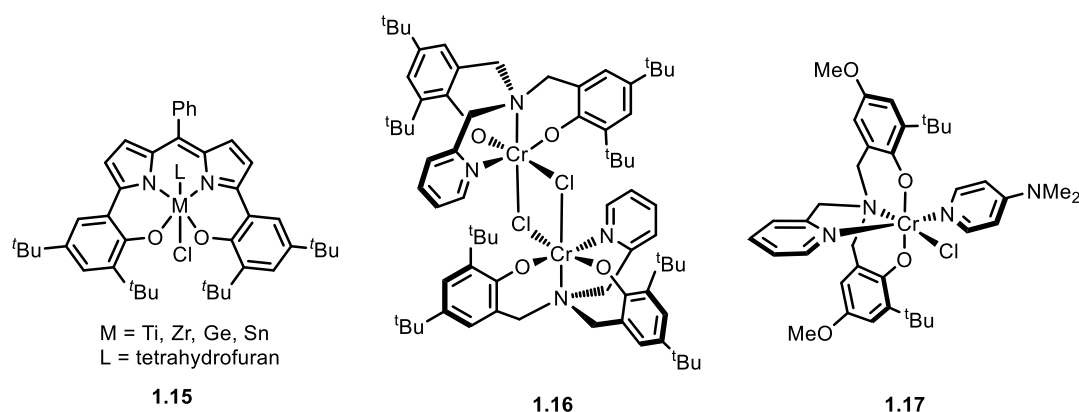


Figure 1-9. Recent catalysts reported for CO₂/epoxide copolymerization.

1.4 Strategies of modifying properties of CO₂-based polycarbonate

1.4.1 Motivation

Excellent progress in CO₂/epoxide copolymerization reactions has been achieved in terms of selectivity for polycarbonate products (in the case of CHO), molecular weight control, suppression of ether linkages, and mild reaction conditions. Industrial application of this method is limited to PO and ethylene oxide to produce poly(propylenecarbonate) (PPC) and poly(ethylene carbonate) (PEC), respectively, because of their superior polymer properties compared with PCHC.⁷⁴ The low glass transition temperatures of PPC and PEC, typically less than 35 °C, limit their utilization as commercial thermoplastics. Although PCHC shows a high glass transition temperature, its tensile properties are inferior to bisphenol A-based polycarbonate. Further advances in the thermo-mechanical properties of these CO₂-based polymers are required. This can potentially be achieved by controlling the regio- and stereochemistry of the resulting polymer, using new epoxides or introducing another monomer into the CO₂-based copolymer.

1.4.2 Synthesis of regio- and stereoregular polycarbonate

Preparation of regio- and stereoregular copolymers is desirable as regio- and stereoregularity can increase crystallinity, thus having the potential to affect copolymer properties. Specifically, PO can be copolymerized with CO₂ to provide different

regiochemical outcomes, including head to tail, head to head and tail to tail. The resulting copolymer can also be isotactic, syndiotactic or atactic (Figure 1-10). Significant effort has been made to prepare high regio- and stereoregular copolymers.⁷⁵⁻⁷⁷ Coates and co-workers first used chiral salen-based Co(III) complex (Figure 1-11, **1.18a**) for CO₂/PO copolymerization, affording PPC with 80% head to tail linkages with a TOF of 71 h⁻¹ at 55 bar CO₂ and 25 °C.⁴¹ Moreover, the use of (*S*)-PO led to an isotactic polycarbonate with a head to tail content of 93%. Subsequently, Lu and co-workers found that in the presence of quaternary ammonium salts (e.g. *n*Bu₄NCl) the chiral Co(III) salen complexes (Figure 1-11, **1.18a-c**) showed more efficient activity for regioselective polymer formation, affording PPC with head-to-tail content of >95% at 2 bar CO₂ and 25 °C.⁷⁸ However, the physical properties of these PPCs with high regioselectivities are not reported. Recently, Lu and co-workers reported synthesis of highly isotactic PCHC from *meso*-CHO and CO₂ using (*S,S*)-salenCo(III) complex (Figure 1-11, **1.19**) with PPNCl as a cocatalyst.⁷⁹ The presence of (*S*)-2-methyltetrahydrofuran further increased the enantioselectivity of the resultant PCHC up to 98:2 (*RR:SS*). It is worth noting that the previously reported non-enantioselective PCHC typically are amorphous and the reported decomposition temperatures of PCHC are between 253 °C and 275 °C. This new PCHC (*RR:SS* = 98:2) was found to possess a melting point of 216 °C and a high decomposition temperature of 310 °C.

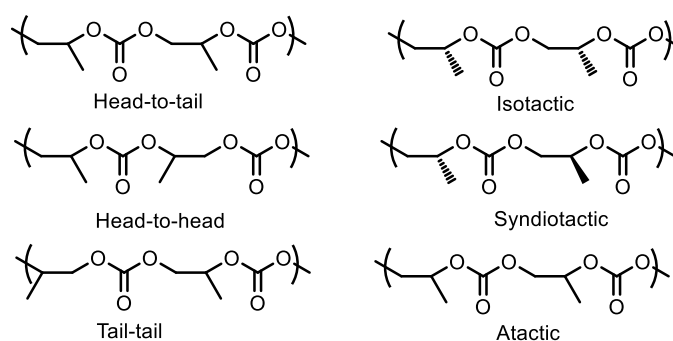


Figure 1-10. Regio- and stereochemical forms of PPC.

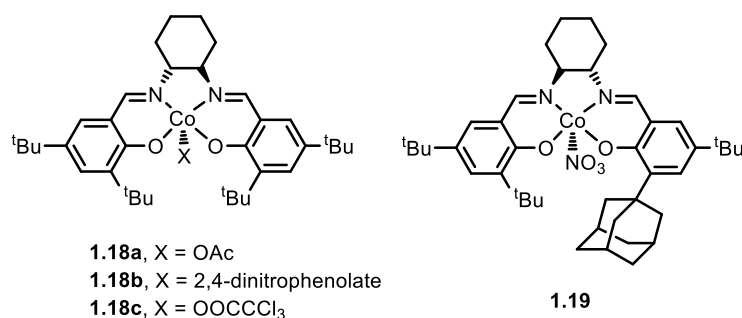


Figure 1-11. Chiral Co(III) salen complexes.

1.4.3 Copolymerization of CO₂ with new epoxides

Copolymerization of CO₂ with other epoxides is another method to change the copolymer thermomechanical properties, especially epoxides with groups that allow for further functionalization. Some of representative epoxides, which have been tested for copolymerization with CO₂ are shown in Figure 1-12. The general limitation of using other epoxides compared to the most commonly used CHO and PO is the lack of high catalytic activity for selective polycarbonate formation.⁸⁰⁻⁸⁵ For example, styrene oxide (Figure 1-12,

1.20) has an electron-withdrawing group and copolymerization with CO₂ typically generates cyclic carbonate.⁸⁵ Recently, Lu and Darensbourg reported the cobalt salen complex (Figure 1-11, **1.18b**) in the presence of PPNX (X = 2,4-dinitrophenoxide) could copolymerize CO₂ with styrene oxide, selectively affording polycarbonate with a TOF of 75 h⁻¹ at 20 bar CO₂ and ambient temperature. The resulting polycarbonate exhibited excellent thermal stability with a relatively high glass transition temperature of 80 °C. Limonene oxide (Figure 1-12, **1.21**), an attractive epoxide for copolymerization due to its bio-renewability, was copolymerized with CO₂ using zinc β-diiminate catalysts by Coates and co-workers.⁸⁶ By optimizing the reaction conditions and electron density around the metal center, a maximum TOF of 37 h⁻¹ for polycarbonate formation was achieved and the resulting polycarbonate exhibited a high glass transition temperature of 111 °C.

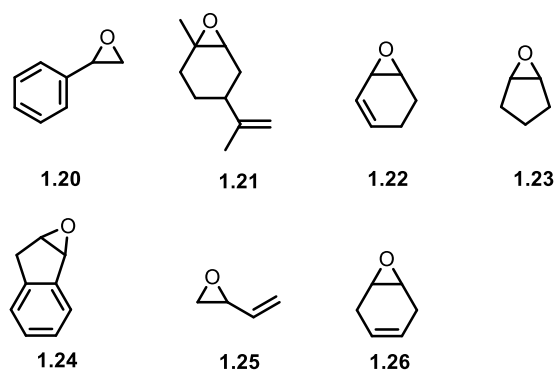
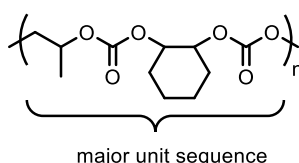


Figure 1-12. Representative other epoxides used for CO₂/epoxide copolymerization.

1.4.4 Terpolymerization and block copolymerization

Incorporation of another monomer into the copolymerization of CO₂ and epoxide is an important way to generate more diverse CO₂-based polymers, thus potentially improving their material performances. The binary catalyst system of cobalt salen complex (Figure 1-11, **1.18c**) and PPNCl has shown efficient activity (TOF = 129 h⁻¹) for the terpolymerization of CO₂ with equimolar quantities of CHO and PO at ambient temperature and 15 bar CO₂.⁸⁷ The resulting terpolymer exhibited a molecular weight of 24400 g mol⁻¹ with a narrow dispersity of 1.24 and more than 99% carbonate linkages. The Lu group proposed that an alternating nature of the two different carbonate units predominantly exists in the resulting terpolymer backbone (Scheme 1-10), which was supported by the observation of a single glass transition temperature of 69 °C and one thermolysis peak. In addition, the glass transition temperature of the resulting terpolymer could be readily adjusted between 50 and 100 °C by controlling the CHO/PO ratios. Subsequently, Lu and co-workers showed that the bifunctional cobalt salen complex (Figure 1-7, **1.11**) was a highly efficient catalyst for the terpolymerization of CO₂, CHO and PO and selectively afforded terpolymer with a TOF up to 3590 h⁻¹ at 90 °C and 25 bar CO₂.⁶³ Furthermore, direct terpolymerizations of CO₂, CHO and a third monomer other than epoxide, such as cyclic acid anhydrides, has generated controlled polyester-b-polycarbonate polymers.⁸⁸⁻⁹⁰ This process is successful as the cyclic anhydride

monomer copolymerizes with CHO at a much faster rate than CHO does with CO₂. On the other hand, direct terpolymerization of CO₂, epoxide and other monomers such as lactone,⁹¹ lactide⁹² and maleic anhydride⁹³ by various metal catalysts afforded polymers with random structures due to the difference in reactivity of the epoxide and the monomer.



Scheme 1-10. Alternating structure of the PO/CHO/CO₂ terpolymer.

Compared to direct terpolymerization, a better way of introducing another monomer into CO₂-based polymer is the use of polycarbonate diol, which can act as a macroinitiator for the ring-opening polymerization of a third monomer such as lactide to afford block polymers.^{74,94,95} A further application of polycarbonate diols is in the production of polyurethane foams.⁹⁶ Industrially, Bayer MaterialScience has developed polyurethanes that utilize polycarbonate polyols from PO and CO₂.⁹⁷ Therefore, developing catalysts that permit the controlled and selective formation of polycarbonate diol from CO₂ and epoxide is attractive. Williams and co-workers showed that the di-zinc catalyst bearing trifluoroacetate ancillary ligand (Figure 1-13, **1.27a**) could catalyze CO₂/CHO copolymerization under one atmosphere CO₂ pressure and 80 °C to selectively afford

polycarbonate diol exhibiting a molecular weight of 9200 g mol^{-1} and dispersity of 1.38 ($\text{TOF} = 20 \text{ h}^{-1}$).⁹⁴ The polycarbonate diol formation was attributed to the hydrolysis of the initiating trifluoroacetate group by trace water during the copolymerization process or upon work-up. Subsequently, Williams and co-workers demonstrated the use of the di-magnesium bis(trifluoroacetate) catalyst (Figure 1-13, **1.27b**) with water as a chain transfer reagent, which could efficiently produce polycarbonate diol from CO_2 and CHO.⁶⁸ Most recently, they reported that these di-Zn(II) and di-Mg(II) catalysts (Figure 1-13, **1.27a-c**), especially **1.27c**, are highly tolerant to water and can produce PCHC diols with different molecular weights in the range of 600 to 9000 g mol^{-1} and narrow dispersities (less than 1.10) by adding various amounts of water.⁹⁸ Similarly, Darensbourg and co-workers demonstrated that the use of the binary chromium salen system bearing a trifluoroacetate ligand (Figure 1-13, **1.28**) and PPNX (X = trifluoroacetate) cocatalyst, which copolymerized CO_2 and PO in the presence of various amounts of water to selectively afford PPC diols with different molecular weights.⁷⁴ These PPC diols were subsequently used for the ring-opening polymerization of lactide in the presence of 1,8-diazabicyclo(5.4.0)undec-7-ene (DBU), an organic base, to yield tri-block copolymers.

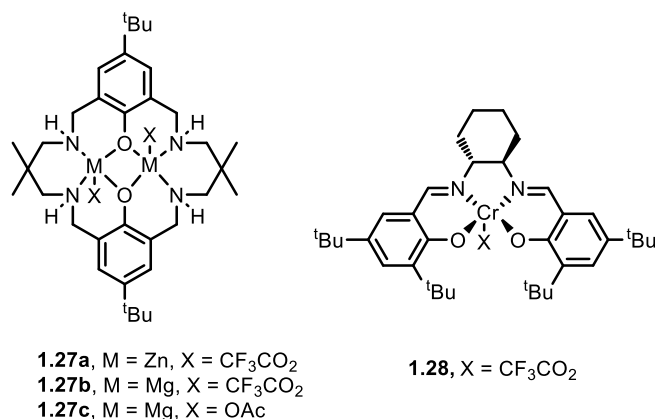


Figure 1-13. Catalysts used for the synthesis of polycarbonate diols.

More recently, Darensbourg and co-workers investigated the role of water in the copolymerization of CO₂ and epoxide by the salenCo(III) trifluoroacetate/PPNX (X = trifluoroacetate) binary system using IR and NMR spectroscopies.⁹⁹ They proposed that water is not the true chain-transfer reagent, but instead that it reacts initially with the epoxide to produce the corresponding diol that serves as the chain-transfer reagent.

1.5 Objectives

Previous research in the Kozak group developed Cr(III) amino-bis(phenolate) complexes which showed promising activities for CO₂/epoxide copolymerization in the presence of cocatalysts. The goal of this thesis was to synthesize new Cr(III) amino-bis(phenolate) complexes that can serve as catalysts for CO₂/CHO copolymerization. The interaction of the metal complex and cocatalyst was investigated

to elucidate the mechanism of the catalytic reaction. Another research goal was to modify the thermodynamic properties (i.e. decomposition and glass transition temperatures) of polycarbonate obtained from CO₂ and CHO through end-group functionalization and the incorporation of polylactide. These objectives resulted in the following discoveries: (1) a new Cr(III) amino-bis(phenolate) complex was synthesized and characterized, and which showed excellent catalytic activity and selectivity for CO₂/CHO copolymerization; (2) a mechanism was proposed for CO₂/CHO copolymerization catalyzed by this Cr(III) amino-bis(phenolate) and related complexes with DMAP, PPNCI or PPNN₃; (3) key factors for the design of highly active Cr(III) amino-bis(phenolate) catalysts were discovered; and (4) lactide ring-opening polymerization by PCHC polyol as a macroinitiator was performed, resulting in a tri-block copolymer, whose physical properties were characterized. As expected, the new copolymer possessed significantly different thermodynamic properties to the polycarbonate itself.

In Chapter 2, the kinetic studies of copolymerization of CHO and CO₂ by a new Cr(III) amino-bis(phenolate) complex were performed. In the presence of DMAP, PPNCI or PPNN₃, this new catalyst showed higher catalytic activities than the previously reported Cr(III) amino-bis(phenolate) complexes. In order to understand the mechanism of CO₂/epoxide copolymerization by this binary catalyst system, the study of the reaction of Cr(III) amino-bis(phenolate) complexes with cocatalyst was performed by

spectrophotometric titrations in Chapter 3. The equilibrium constants obtained explained why some catalyst derivatives were much more active than others in that strong metal-cocatalyst binding, as expected, hindered copolymerization. Chapter 4 presented mass spectrometric studies of PPNN₃ binding with Cr(III) amino-bis(phenolate) complexes and provided further mechanistic understanding. In Chapter 5, the synthesis of a new Cr(III) complex and cocatalyst were attempted in an effort to produce well-defined polycarbonate diols without relying on a hydrolysable site on the polymer. The resulting polycarbonate diol was used as a macroinitiator to ring-open *rac*-lactide to produce tri-block copolymer. Lastly, Chapter 6 included additional experiments of synthesizing derivatives of Cr(III) amino-bis(phenolate) complex to explore more active Cr(III) complexes. Some suggestions for future work and overall conclusions of this thesis were presented in Chapter 7.

1.6 References

- (1) Goeppert, A.; Czaun, M.; Surya Prakash, G. K.; Olah, G. A. *Energy Environ. Sci.* **2012**, *5*, 7833.
- (2) Orr, F. M., Jr. *Energy Environ. Sci.* **2009**, *2*, 449.
- (3) Wang, S.; Yan, S.; Ma, X.; Gong, J. *Energy Environ. Sci.* **2011**, *4*, 3805.
- (4) Aresta, M.; Dibenedetto, A.; Angelini, A. *Chem. Rev.* **2014**, *114*, 1709.
- (5) Sakakura, T.; Choi, J.-C.; Yasuda, H. *Chem. Rev.* **2007**, *107*, 2365.
- (6) Maeda, C.; Miyazaki, Y.; Ema, T. *Catal. Sci. Technol.* **2014**, *4*, 1482.
- (7) Markewitz, P.; Kuckshinrichs, W.; Leitner, W.; Linssen, J.; Zapp, P.; Bongartz, R.; Schreiber, A.; Müller, T. E. *Energy Environ. Sci.* **2012**, *5*, 7281.
- (8) Aresta, M. (Ed.), *Carbon dioxide as chemical feedstock*; Wiley-VCH Verlag GmbH & Co. KGaA, 2010.
- (9) Liu, Q.; Wu, L.; Jackstell, R.; Beller, M. *Nat. Commun.* **2015**, *6*, 5933.
- (10) Mikkelsen, M.; Jørgensen, M.; Krebs, F. C. *Energy Environ. Sci.* **2010**, *3*, 43.
- (11) Brunelle, D. J. In *Advances in Polycarbonates*; American Chemical Society: 2005; Vol. 898, p 1.
- (12) Fukuoka, S.; Tojo, M.; Hachiya, H.; Aminaka, M.; Hasegawa, K. *Polym. J. (Tokyo, Jpn.)* **2007**, *39*, 91.
- (13) Fukuoka, S.; Kawamura, M.; Komiya, K.; Tojo, M.; Hachiya, H.; Hasegawa, K.;

- Aminaka, M.; Okamoto, H.; Fukawa, I.; Konno, S. *Green Chem.* **2003**, *5*, 497.
- (14) Gibert, Y.; Sassi-Messai, S.; Fini, J.-B.; Bernard, L.; Zalko, D.; Cravedi, J.-P.; Balaguer, P.; Andersson-Lendahl, M.; Demeneix, B.; Laudet, V. *BMC Dev. Biol.* **2011**, *11*, 4.
- (15) Vom Saal, F. S.; Hughes, C. *Environ. Health Perspect.* **2005**, *113*, 926.
- (16) Inoue, S.; Koinuma, H.; Tsuruta, T. *J. Polym. Sci., Part B* **1969**, *7*, 287.
- (17) Darensbourg, D. J.; Wilson, S. J. *Green Chem.* **2012**, *14*, 2665.
- (18) Kember, M. R.; Buchard, A.; Williams, C. K. *Chem. Commun.* **2011**, *47*, 141.
- (19) Kobayashi, M.; Inoue, S.; Tsuruta, T. *Macromolecules* **1971**, *4*, 658.
- (20) Kobayashi, M.; Inoue, S.; Tsuruta, T. *J. Polym. Sci., Polym. Chem. Ed.* **1973**, *11*, 2383.
- (21) Aida, T.; Ishikawa, M.; Inoue, S. *Macromolecules* **1986**, *19*, 8.
- (22) Mang, S.; Cooper, A. I.; Colclough, M. E.; Chauhan, N.; Holmes, A. B. *Macromolecules* **2000**, *33*, 303.
- (23) Darensbourg, D. J.; Holtcamp, M. W. *Macromolecules* **1995**, *28*, 7577.
- (24) Darensbourg, D. J.; Holtcamp, M. W.; Struck, G. E.; Zimmer, M. S.; Niezgoda, S. A.; Rainey, P.; Robertson, J. B.; Draper, J. D.; Reibenspies, J. H. *J. Am. Chem. Soc.* **1999**, *121*, 107.
- (25) Darensbourg, D. J.; Wildeson, J. R.; Yarbrough, J. C.; Reibenspies, J. H. *J. Am.*

Chem. Soc. **2000**, *122*, 12487.

(26) Cheng, M.; Lobkovsky, E. B.; Coates, G. W. *J. Am. Chem. Soc.* **1998**, *120*, 11018.

(27) Coates, G. W.; Moore, D. R. *Angew. Chem., Int. Ed.* **2004**, *43*, 6618.

(28) Moore, D. R.; Cheng, M.; Lobkovsky, E. B.; Coates, G. W. *Angew. Chem., Int. Ed.* **2002**, *41*, 2599.

(29) Allen, S. D.; Moore, D. R.; Lobkovsky, E. B.; Coates, G. W. *J. Am. Chem. Soc.* **2002**, *124*, 14284.

(30) Darensbourg, D. J.; Yarbrough, J. C. *J. Am. Chem. Soc.* **2002**, *124*, 6335.

(31) Hansen, K. B.; Leighton, J. L.; Jacobsen, E. N. *J. Am. Chem. Soc.* **1996**, *118*, 10924.

(32) Cozzi, P. G. *Chem. Soc. Rev.* **2004**, *33*, 410.

(33) Darensbourg, D. J.; Chung, W.-C. *Polyhedron* **2013**, *58*, 139.

(34) Darensbourg, D. J.; Moncada, A. I.; Choi, W.; Reibenspies, J. H. *J. Am. Chem. Soc.* **2008**, *130*, 6523.

(35) Darensbourg, D. J.; Yeung, A. D. *Polym. Chem.* **2015**, *6*, 1103.

(36) Darensbourg, D. J. *Chem. Rev.* **2007**, *107*, 2388.

(37) Liu, Y.; Ren, W.-M.; He, K.-K.; Lu, X.-B. *Nat. Commun.* **2014**, *5*, 5687.

(38) Wu, G.-P.; Xu, P.-X.; Zu, Y.-P.; Ren, W.-M.; Lu, X.-B. *J. Polym. Sci., Part A: Polym. Chem.* **2013**, *51*, 874.

(39) Wu, G.-P.; Xu, P.-X.; Lu, X.-B.; Zu, Y.-P.; Wei, S.-H.; Ren, W.-M.; Darensbourg, D. J.

Macromolecules **2013**, *46*, 2128.

(40) Cohen, C. T.; Chu, T.; Coates, G. W. *J. Am. Chem. Soc.* **2005**, *127*, 10869.

(41) Qin, Z.; Thomas, C. M.; Lee, S.; Coates, G. W. *Angew. Chem., Int. Ed.* **2003**, *42*, 5484.

(42) Ohkawara, T.; Suzuki, K.; Nakano, K.; Mori, S.; Nozaki, K. *J. Am. Chem. Soc.* **2014**, *136*, 10728.

(43) Xia, W.; Salmeia, K. A.; Vagin, S. I.; Rieger, B. *Chem. - Eur. J.* **2015**, *21*, 4384.

(44) Eberhardt, R.; Allmendinger, M.; Rieger, B. *Macromol. Rapid Commun.* **2003**, *24*, 194.

(45) Darensbourg, D. J.; Mackiewicz, R. M.; Rodgers, J. L.; Fang, C. C.; Billodeaux, D. R.; Reibenspies, J. H. *Inorg. Chem.* **2004**, *43*, 6024.

(46) Darensbourg, D. J.; Mackiewicz, R. M.; Rodgers, J. L.; Phelps, A. L. *Inorg. Chem.* **2004**, *43*, 1831.

(47) Darensbourg, D. J.; Mackiewicz, R. M. *J. Am. Chem. Soc.* **2005**, *127*, 14026.

(48) Darensbourg, D. J.; Mackiewicz, R. M.; Billodeaux, D. R. *Organometallics* **2005**, *24*, 144.

(49) Darensbourg, D. J.; Phelps, A. L. *Inorg. Chem.* **2005**, *44*, 4622.

(50) Lu, X.-B.; Shi, L.; Wang, Y.-M.; Zhang, R.; Zhang, Y.-J.; Peng, X.-J.; Zhang, Z.-C.; Li, B. *J. Am. Chem. Soc.* **2006**, *128*, 1664.

- (51) Klaus, S.; Lehenmeier, M. W.; Anderson, C. E.; Rieger, B. *Coord. Chem. Rev.* **2011**, 255, 1460.
- (52) Darensbourg, D. J.; Moncada, A. I. *Inorg. Chem.* **2008**, 47, 10000.
- (53) Rao, D.-Y.; Li, B.; Zhang, R.; Wang, H.; Lu, X.-B. *Inorg. Chem.* **2009**, 48, 2830.
- (54) Darensbourg, D. J.; Yarbrough, J. C.; Ortiz, C.; Fang, C. C. *J. Am. Chem. Soc.* **2003**, 125, 7586.
- (55) Luinstra, G. A.; Haas, G. R.; Molnar, F.; Bernhart, V.; Eberhardt, R.; Rieger, B. *Chem. Eur. J.* **2005**, 11, 6298.
- (56) Liu, J.; Ren, W.-M.; Liu, Y.; Lu, X.-B. *Macromolecules* **2013**, 46, 1343.
- (57) Moore, D. R.; Cheng, M.; Lobkovsky, E. B.; Coates, G. W. *J. Am. Chem. Soc.* **2003**, 125, 11911.
- (58) Devaine-Pressing, K.; Dawe, L. N.; Kozak, C. M. *Polym. Chem.* **2015**, 6, 6305.
- (59) Devaine-Pressing, K.; Kozak, C. M. *ChemSusChem* **2017**, 10, 1266.
- (60) Nakano, K.; Kamada, T.; Nozaki, K. *Angew. Chem., Int. Ed.* **2006**, 45, 7274.
- (61) Noh, E. K.; Na, S. J.; S, S.; Kim, S.-W.; Lee, B. Y. *J. Am. Chem. Soc.* **2007**, 129, 8082.
- (62) Min, S. S. J. K.; Seong, J. E.; Na, S. J.; Lee, B. Y. *Angew. Chem., Int. Ed.* **2008**, 47, 7306.
- (63) Ren, W.-M.; Zhang, X.; Liu, Y.; Li, J.-F.; Wang, H.; Lu, X.-B. *Macromolecules* **2010**,

43, 1396.

(64) Nakano, K.; Hashimoto, S.; Nozaki, K. *Chem. Sci.* **2010**, *1*, 369.

(65) Vagin, S. I.; Reichardt, R.; Klaus, S.; Rieger, B. *J. Am. Chem. Soc.* **2010**, *132*, 14367.

(66) Kember, M. R.; Knight, P. D.; Reung, P. T. R.; Williams, C. K. *Angew. Chem., Int. Ed.* **2009**, *48*, 931.

(67) Kember, M. R.; Jutz, F.; Buchard, A.; White, A. J. P.; Williams, C. K. *Chem. Sci.* **2012**, *3*, 1245.

(68) Kember, M. R.; Williams, C. K. *J. Am. Chem. Soc.* **2012**, *134*, 15676.

(69) Buchard, A.; Kember, M. R.; Sandeman, K. G.; Williams, C. K. *Chem. Commun.* **2011**, *47*, 212.

(70) Jutz, F.; Buchard, A.; Kember, M. R.; Fredriksen, S. B.; Williams, C. K. *J. Am. Chem. Soc.* **2011**, *133*, 17395.

(71) Nakano, K.; Kobayashi, K.; Nozaki, K. *J. Am. Chem. Soc.* **2011**, *133*, 10720.

(72) Dean, R. K.; Dawe, L. N.; Kozak, C. M. *Inorg. Chem.* **2012**, *51*, 9095.

(73) Kerton, F. M.; Holloway, S.; Power, A.; Soper, R. G.; Sheridan, K.; Lynam, J. M.; Whitwood, A. C.; Willans, C. E. *Can. J. Chem.* **2008**, *86*, 435.

(74) Darensbourg, D. J.; Wu, G.-P. *Angew. Chem., Int. Ed.* **2013**, *52*, 10602.

(75) Nozaki, K.; Nakano, K.; Hiyama, T. *J. Am. Chem. Soc.* **1999**, *121*, 11008.

(76) Nakano, K.; Hiyama, T.; Nozaki, K. *Chem. Commun.* **2005**, 1871.

- (77) Cheng, M.; Darling, N. A.; Lobkovsky, E. B.; Coates, G. W. *Chem. Commun.* **2000**, 2007.
- (78) Lu, X.-B.; Wang, Y. *Angew. Chem., Int. Ed.* **2004**, *43*, 3574.
- (79) Wu, G.-P.; Ren, W.-M.; Luo, Y.; Li, B.; Zhang, W.-Z.; Lu, X.-B. *J. Am. Chem. Soc.* **2012**, *134*, 5682.
- (80) Darensbourg, D. J.; Chung, W.-C.; Wilson, S. J. *ACS Catal.* **2013**, *3*, 3050.
- (81) Darensbourg, D. J.; Wilson, S. J. *Macromolecules* **2013**, *46*, 5929.
- (82) Darensbourg, D. J.; Tsai, F.-T. *Macromolecules* **2014**, *47*, 3806.
- (83) Darensbourg, D. J.; Chung, W.-C.; Arp, C. J.; Tsai, F.-T.; Kyran, S. J. *Macromolecules* **2014**, *47*, 7347.
- (84) Winkler, M.; Romain, C.; Meier, M. A. R.; Williams, C. K. *Green Chem.* **2015**, *17*, 300.
- (85) Lu, X.-B.; Darensbourg, D. J. *Chem. Soc. Rev.* **2012**, *41*, 1462.
- (86) Byrne, C. M.; Allen, S. D.; Lobkovsky, E. B.; Coates, G. W. *J. Am. Chem. Soc.* **2004**, *126*, 11404.
- (87) Shi, L.; Lu, X.-B.; Zhang, R.; Peng, X.-J.; Zhang, C.-Q.; Li, J.-F.; Peng, X.-M. *Macromolecules* **2006**, *39*, 5679.
- (88) Jeske, R. C.; Rowley, J. M.; Coates, G. W. *Angew. Chem., Int. Ed.* **2008**, *47*, 6041.
- (89) Huijser, S.; HosseiniNejad, E.; Sablong, R.; de Jong, C.; Koning, C. E.; Duchateau,

R. *Macromolecules* **2011**, *44*, 1132.

(90) Darensbourg, D. J.; Poland, R. R.; Escobedo, C. *Macromolecules* **2012**, *45*, 2242.

(91) Hwang, Y.; Jung, J.; Ree, M.; Kim, H. *Macromolecules* **2003**, *36*, 8210.

(92) Kroeger, M.; Folli, C.; Walter, O.; Doering, M. *Adv. Synth. Catal.* **2006**, *348*, 1908.

(93) Liu, Y.; Huang, K.; Peng, D.; Wu, H. *Polymer* **2006**, *47*, 8453.

(94) Kember, M. R.; Copley, J.; Buchard, A.; Williams, C. K. *Polym. Chem.* **2012**, *3*, 1196.

(95) Wu, G.-P.; Darensbourg, D. J.; Lu, X.-B. *J. Am. Chem. Soc.* **2012**, *134*, 17739.

(96) Langanke, J.; Wolf, A.; Hofmann, J.; Boehm, K.; Subhani, M. A.; Mueller, T. E.; Leitner, W.; Guertler, C. *Green Chem.* **2014**, *16*, 1865.

(97) "CO₂: a convincing new building block for polyurethanes", *Covestro*, accessed date: 2017, <http://press.covestro.com/news.nsf/id/co2-a-convincing-new-building-block-for-polyurethanes>

(98) Chapman, A. M.; Keyworth, C.; Kember, M. R.; Lennox, A. J. J.; Williams, C. K. *ACS Catal.* **2015**, *5*, 1581.

(99) Wu, G.-P.; Darensbourg, D. J. *Macromolecules* **2016**, *49*, 807.

Co-authorship statement

Chapter 2: Kinetic studies of copolymerization of cyclohexene oxide with CO₂ by a monometallic amino-bis(phenolate) chromium(III) complex

This chapter is currently in the preparation for publication.

Authors: Kaijie Ni and Christopher M. Kozak

The first author (Kaijie Ni) contributed 90% of the content of the article as the main researcher including: performing the experiments, analyzing and collecting data, and writing the paper.

The corresponding author (Christopher M. Kozak), my supervisor, was the principal investigator of this research work. He suggested initial experiments, assisted with analyzing data and revised this manuscript.

Chapter 2. Kinetic studies of copolymerization of cyclohexene oxide with CO₂ by a monometallic amino-bis(phenolate) chromium(III) complex

2.1 Introduction

Carbon dioxide (CO₂) is an attractive raw material for the preparation of useful chemicals as it is widely available, non-toxic, cheap and bio-renewable.¹ The thermodynamic stability of CO₂, however, has made its utilization as a reagent for chemical synthesis very limited. Recently the development of catalysts for copolymerization of CO₂ with high free energy epoxides to yield polycarbonates has drawn considerable attention.²⁻⁸ This reaction is interesting as it not only uses CO₂ as a C1 feedstock but also provides an attractive alternative to the traditional synthesis of polycarbonates involving the use of toxic phosgene.

A variety of metal complexes typically containing metals such as magnesium,^{9,10} aluminum,¹¹⁻¹³ zinc,¹⁴⁻²⁶ cobalt,²⁷⁻³⁹ chromium,⁴⁰⁻⁵⁶ iron⁵⁷⁻⁵⁹ and ytterbium⁶⁰ have shown activity for coupling or copolymerization of CO₂ and epoxides. Well-defined homogeneous metal complexes such as chromium porphyrin compounds,^{40,56} zinc phenoxides²¹⁻²⁴ and β -diiminate zinc alkoxides^{25,26} have proven highly active. Tetravalent group 4 (Ti and Zr) and 14 (Ge and Sn) metals supported by planar trianionic bis(phenolate) ligands also have shown promising activity.⁶¹ By far the most widely

studied catalysts for epoxide/CO₂ copolymerization have been the Cr(III)^{41-47,50,52,53} or Co(III)^{27,35-39} salen complexes and more recently salan complexes.^{50,51,55,62} These complexes typically require an appropriate nucleophile as cocatalyst to achieve high activities. The most commonly used cocatalysts include chloride, bromide or azide paired with bulky cations such as bis(triphenylphosphoranylidene)iminium (PPN⁺) or tetrabutylammonium, or neutral bases such as *N*-methylimidazole or 4-(dimethylamino)pyridine (DMAP).

The mechanism of epoxide/CO₂ copolymerization, particularly the role of these cocatalysts, has been widely studied.⁶²⁻⁶⁷ ESI-MS studies of the binding affinity of neutral cocatalyst to Cr(III) salen or salan complexes by Lu have found Cr(III) salen complexes easily bind two DMAP molecules forming a [Cr(III)salen(DMAP)₂]⁺ cation; however, Cr(III) salan complexes tend to bind only one DMAP molecule even in the presence of excess of DMAP.⁶² As a result, significantly different activities and induction period towards PO/CO₂ copolymerization were observed, with the salan/DMAP system having a much shorter (or no) induction period and a 30-fold increase in reaction rate compared to the salen/DMAP system. This observation indicates that the bis-DMAP adduct species is inactive and it is difficult to dissociate one DMAP molecule to generate the active mono-DMAP species that initiates copolymerization, which resulted in a long induction period.

Kozak's group have synthesized and characterized Cr(III) amino-bis(phenolate) complexes (Figure 2-1, **2.2** – **2.5**) which showed good to excellent activity towards the copolymerization of epoxide and CO₂.⁶⁸⁻⁷² They previously also used MALDI-TOF MS to study the binding affinity of DMAP to a series of amino-bis(phenolate)Cr(III) complexes with different pendant donor groups such as nitrogen-containing *N,N*-dimethylaminoethyl (**2.1**) and 2-pyridyl moieties (**2.2** and **2.3**) or oxygen-containing tetrahydrofuran moiety (**2.4**).⁷³ Amino-bis(phenolate)Cr(III) complexes **2.2** – **2.4** showed the ability to bind two DMAP molecules to form a six-coordinate complex ion [LCr(DMAP)₂]⁺, with the exception of the *N,N*-dimethylaminoethyl complex **2.1** even when a 4:1 ratio of DMAP to Cr was used. Furthermore, this complex **2.1**, unlike the other derivatives **2.2** – **2.4**, showed no evidence of dimer formation via MALDI-TOF MS, likely due to the larger steric effect exhibited by the *N,N*-dimethylaminoethyl pendant donor group. As a result the preliminary copolymerization rate of the complex **2.1** in the presence of one equivalent of DMAP was found to be faster than the previously reported amino-bis(phenolate)Cr(III) complexes.^{68,70,71,73}

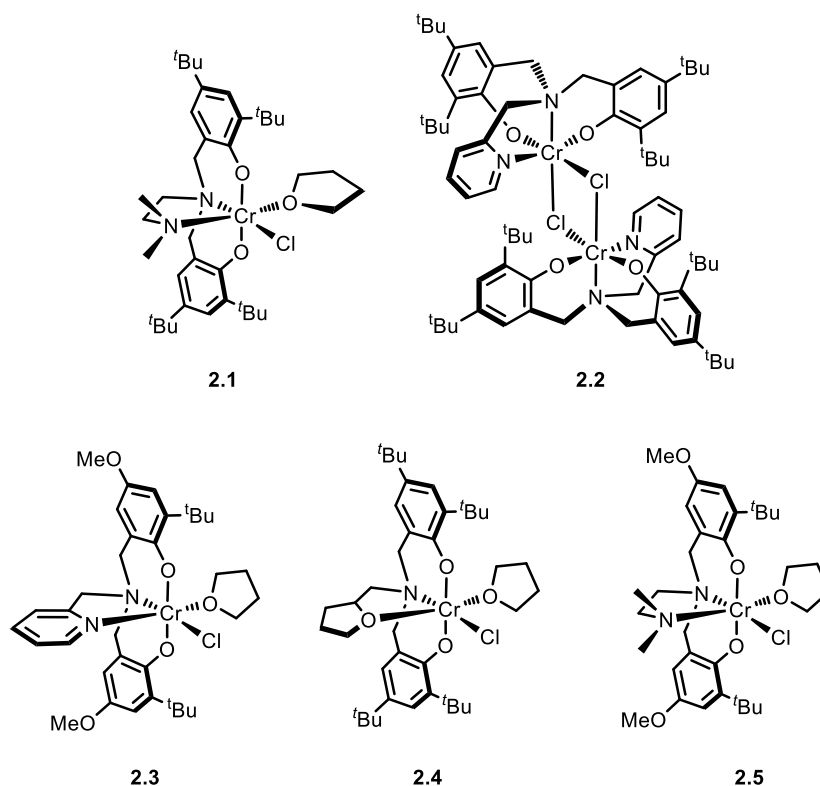


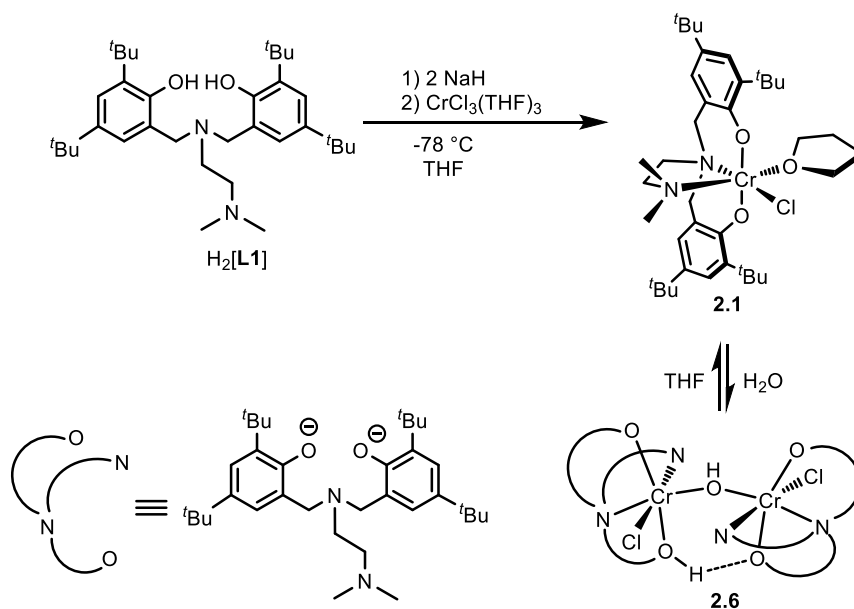
Figure 2-1. Cr(III) amino-bis(phenolate) complexes investigated in the Kozak group.

In this chapter, the detailed synthesis and structure of this Cr(III) complex **2.1** containing *N,N*-dimethylaminoethyl pendant donor group, and its utilization as a catalyst for CHO/CO₂ copolymerization were presented. The influence of varying reaction surface area, the effect of cocatalyst selections, CO₂ pressures and reaction temperatures were discussed. End-group analysis of the resulting polymer by MALDI-TOF MS revealed possible initiation pathways.

2.2 Results and discussion

2.2.1 Synthesis and characterization of Cr(III) complex

Cr(III) complex **2.1** was synthesized via deprotonation of the proligand with sodium hydride in THF at $-78\text{ }^{\circ}\text{C}$, followed by treatment with $\text{CrCl}_3(\text{THF})_3$ in THF at $-78\text{ }^{\circ}\text{C}$ to afford a purple/pink solid in a 95% yield (Scheme 2-1). The complex was characterized by MALDI-TOF mass spectrometry, elemental analysis, UV-Vis spectroscopy and X-ray diffraction.



Scheme 2-1. Synthetic route to complexes **2.1** and **2.6**.

The MALDI-TOF mass spectrum (Figure 2-2) of complex **2.1** showed peaks at m/z

609 and 574, which correspond to the radical cation of $[\text{CrCl}[\text{L1}]]^{+\bullet}$ and the fragment of $[\text{Cr}[\text{L1}]]^+$ resulting from a loss of a chloride ion. The isotopic distribution patterns of these experimental ions were in good agreement with the theoretical representations. Its composition as the monomer of $\text{CrCl}(\text{THF})[\text{L1}]$ in the solid state was also confirmed by elemental analysis. **2.1** was observed to proceed to react with moisture present in air to undergo a color change from purple in the solid state to light green when exposed to air for 4 day (see Appendix, Figure D-2). Green single crystals suitable for X-ray diffraction were obtained from a toluene solution of **2.1** exposed to air. The structure of the crystal was found to be a hydroxide-bridged dimer (**2.6**), which will be discussed in Chapter 5. The MALDI-TOF mass spectrum of **2.6** also showed peaks at m/z 574 and 609 corresponding to $[\text{Cr}[\text{L1}]]^+$ and $[\text{CrCl}[\text{L1}]]^{+\bullet}$ ions (Figure 2-3). The peak at m/z 1238 corresponding to $[\text{CrCl}[\text{L1}](\mu\text{-OH})\text{CrCl}[\text{HL1}]]^+$ was not observed, indicating the hydroxide-bridged structure is not stable under MS conditions. When the light green complex **2.6** was dissolved in THF, a pink solution was produced. UV-visible spectroscopic analysis of the resulting pink/purple solid after removed of THF showed an identical spectrum to that of complex **2.1** (Figure 2-4), which suggests **2.6** can revert to **2.1** in THF (Scheme 2-1).

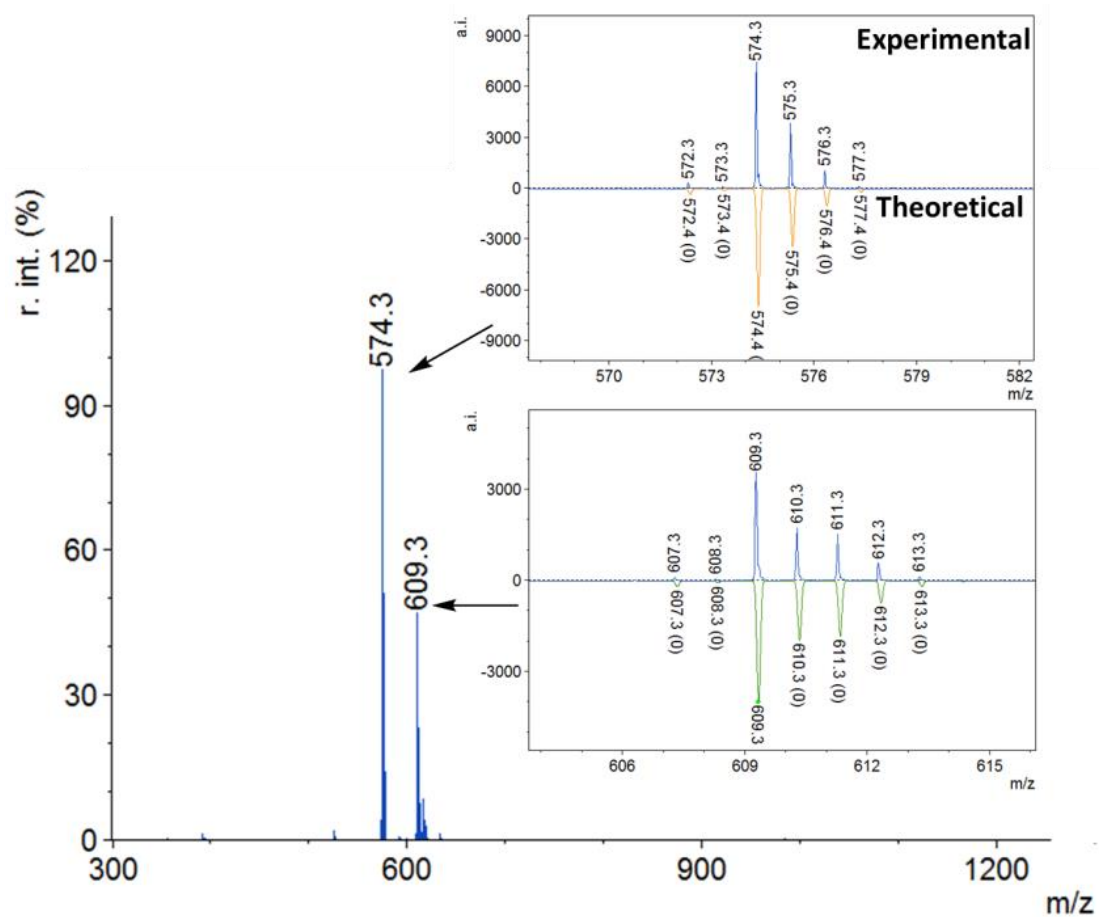


Figure 2-2. MALDI-TOF mass spectrum of complex **2.1** with the experimental and theoretical isotopic distribution patterns.

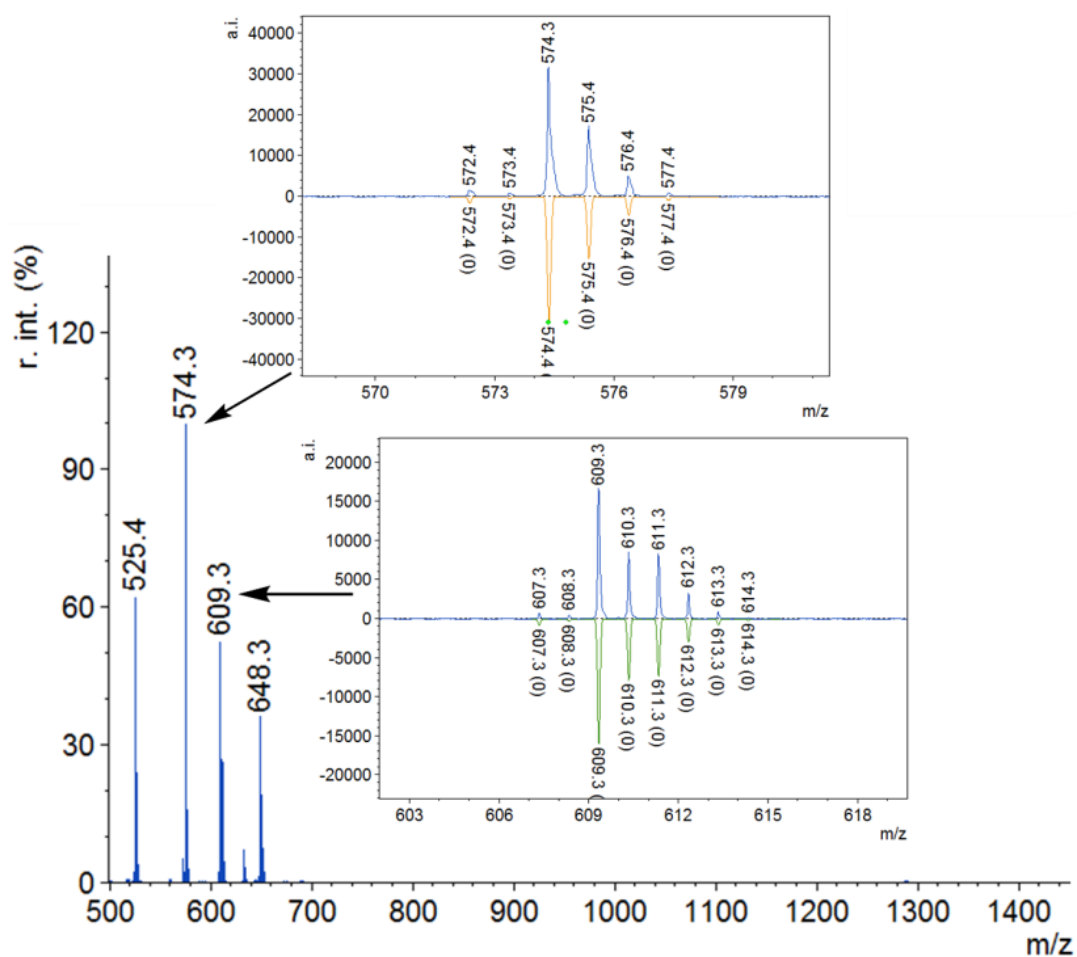


Figure 2-3. MALDI-TOF mass spectrum of **2.6** with the experimental and theoretical isotopic distribution patterns.

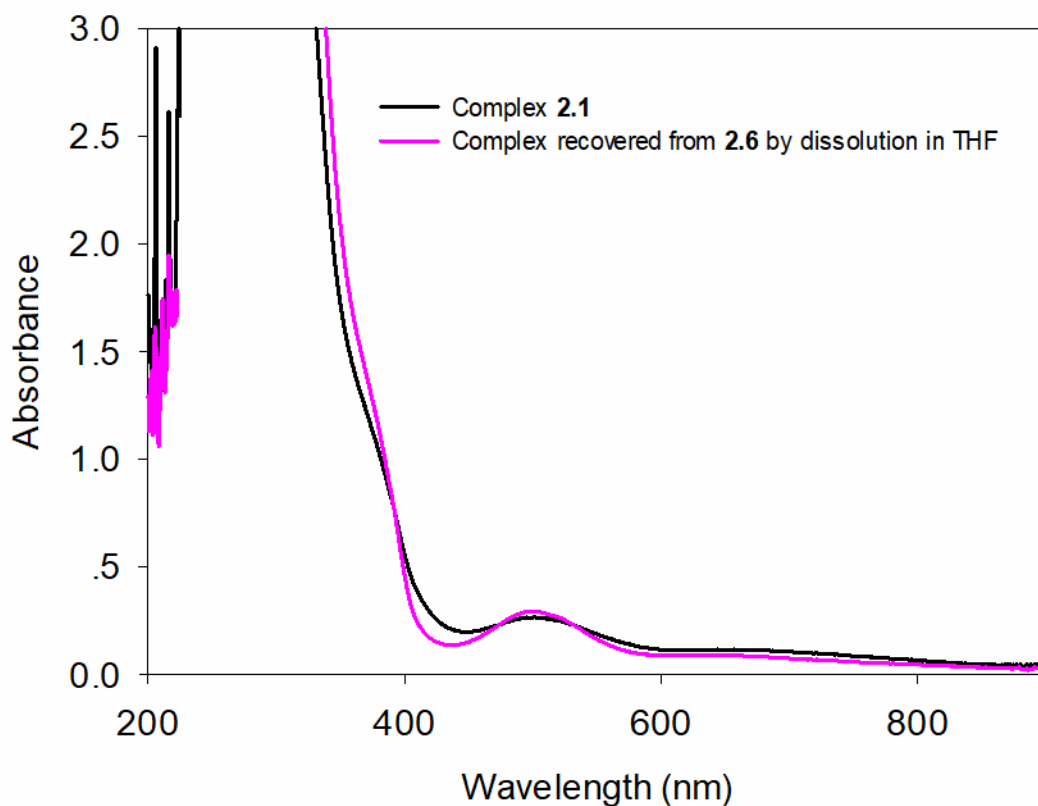


Figure 2-4. UV-Vis absorption spectra of complex **2.1** (black) and complex recovered from **2.6** by dissolution in THF (pink) at a concentration of 10^{-3} mol L⁻¹ in dichloromethane.

2.2.2 Crystal structure determination

Single crystals of **2.1** suitable for X-ray diffraction were obtained by slow evaporation of a solution of THF and hexamethyldisiloxane (HMDSO) under nitrogen in the glovebox. The X-ray structure and selected bond lengths and angles are shown in Figure 2-5 and Table 2-1. The structure of complex **2.1** shows a distorted octahedral geometry at the Cr(III) center. Four coordination sites are occupied by the ligand system where the two phenolate-oxygen atoms are oriented *trans* to each other. The other two

coordination sites are occupied by the chloride ancillary ligand *trans* to the central amino donor and a neutral molecule of THF which resides *trans* to the pendant dimethylaminoethyl group. This ligand arrangement and metric parameters are similar to those found in the previously reported X-ray structures of similar Cr(III) amino-bisphenolate complexes, but with very slightly longer bond distances between the Cr center and the amino-bis(phenolate) ligand when compared to that of a complex bearing methoxyl groups (instead of *t*-butyl groups) para to the phenolate O-donor.^{71,74}

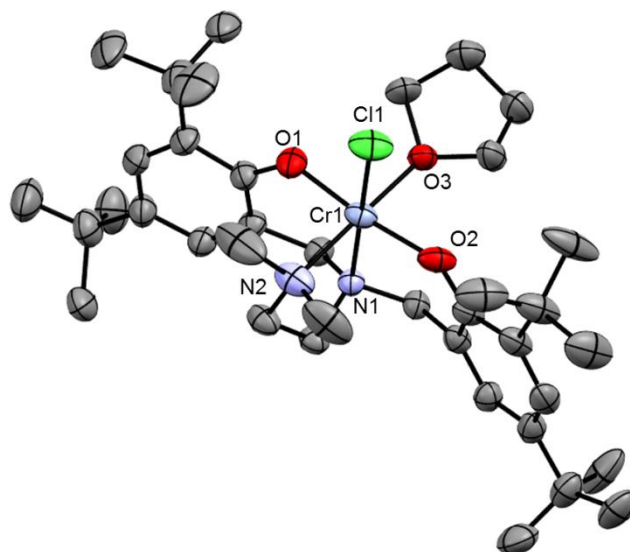


Figure 2-5. Molecular structure (ORTEP) and partial numbering scheme of **2.1**. Ellipsoids are drawn at 50% probability. Hydrogen atoms omitted for clarity.

Table 2-1. Selected bond distances (Å) and angles (°) of complex **2.1**

Bond lengths (Å)			
Cr(1) – Cl(1)	2.4783(8)	Cr(1) – O(3)	2.0862(17)
Cr(1) – O(2)	1.9241(19)	Cr(1) – N(1)	2.1025(19)
Cr(1) – O(1)	1.9305(19)	Cr(1) – N(2)	2.147(2)
Bond angles (°)			
O(3) – Cr(1) – Cl(1)	91.01(5)	O(3) – Cr(1) – N(1)	91.88(7)
O(3) – Cr(1) – N(2)	174.49(8)	O(2) – Cr(1) – Cl(1)	88.08(6)
O(2) – Cr(1) – O(3)	87.23(7)	O(2) – Cr(1) – N(1)	90.35(7)
O(2) – Cr(1) – O(1)	173.09(8)	O(2) – Cr(1) – N(2)	94.34(10)
N(1) – Cr(1) – Cl(1)	176.63(6)	N(1) – Cr(1) – N(2)	82.83(8)
O(1) – Cr(1) – Cl(1)	90.12(6)	O(1) – Cr(1) – O(3)	86.14(8)
O(1) – Cr(1) – N(1)	91.79(7)	O(1) – Cr(1) – N(2)	92.45(10)
N(2) – Cr(1) – Cl(1)	94.32(6)		

2.2.3 Copolymerization of CHO and CO₂

The copolymerization of CHO and CO₂ was carried out using complex **2.1** in the presence of DMAP, PPnCl or PPnN₃ at 60 °C and 40 bar CO₂. The results are summarized in Table 2-2. These conditions gave the best activity from previous work in the Kozak group.⁶⁸ The ¹H NMR spectrum (Figure 2-6) of the resulting product showed that PCHC was formed with a negligible amount of ether linkages and no cyclic carbonate was formed. The stereochemistry of produced polymers was atactic based on

the $^{13}\text{C}\{^1\text{H}\}$ NMR spectrum (Figure 2-7).

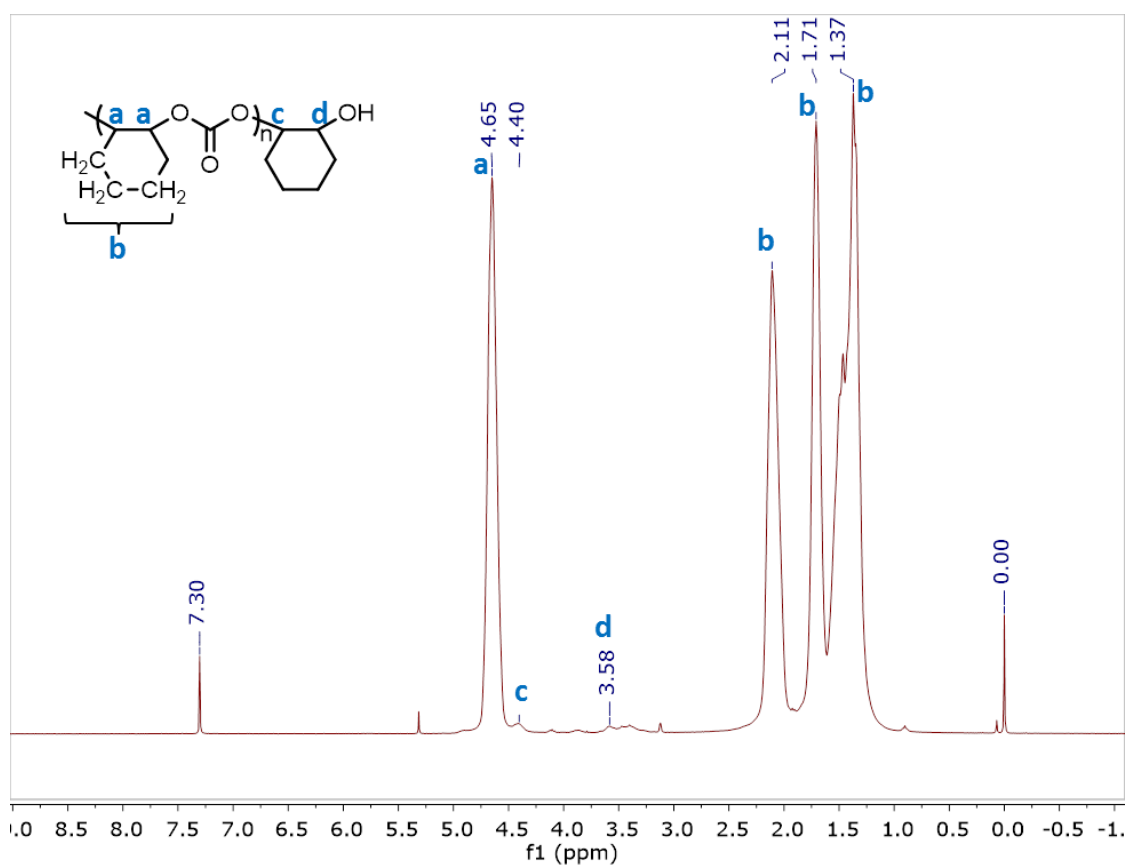


Figure 2-6. Representative ^1H NMR spectrum in CDCl_3 of the purified polycarbonate using PPNCI as cocatalyst (Table 2-2, entry 5).

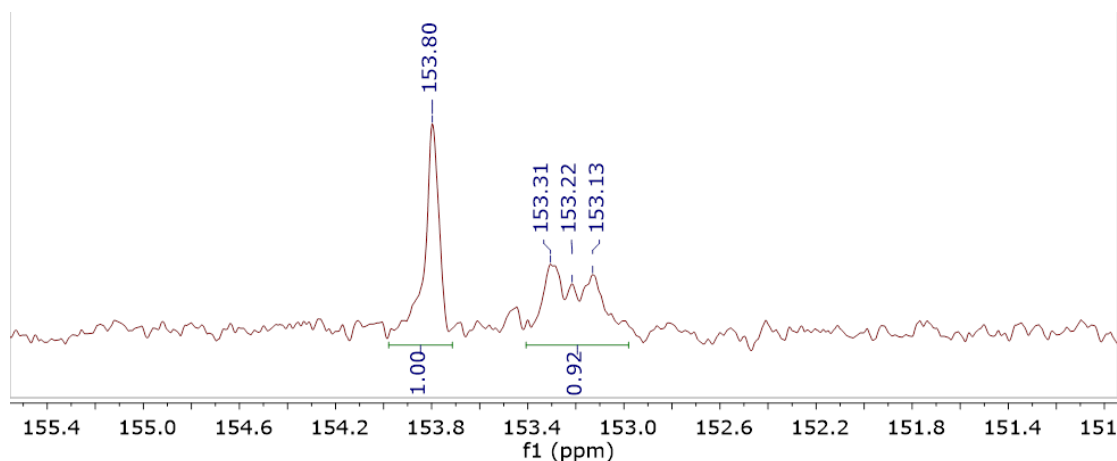
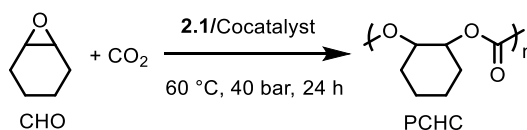


Figure 2-7. Representative carbonyl region of the ^{13}C NMR spectrum in CDCl_3 of PCHC (Table 2-2, entry 1).

Initial copolymerization reactions were carried out in a standard Parr 5500 series 100 mL stainless steel pressure vessel for 24 h to ensure a complete reaction. The conversion of CHO to PCHC obtained using **2.1** with DMAP, PPNCl or PPNN_3 as the cocatalyst was similar, ranging from 70% - 75% (Table 2-2, entries 1-3). To trace the formation of PCHC during the reaction, duplicate runs were performed in a 100 mL Parr 4560 mini reactor equipped with bottom-mounted Si-comp ATR probe (Table 2-2, entries 4-6). It is worth noting that this reaction vessel has the same volume but different dimensions to the Parr 5500 series, having a wider diameter, hence a larger surface area for exposure of the solution to CO_2 . Interestingly, the conversion of CHO to PCHC was increased by approximately 20%, likely due to the larger surface area (Table 2-2, entries 4-6 vs entries 1-3). Polymer molecular weights and dispersities were found to be unaffected by shape of

pressure vessel. Comparing the three co-catalysts utilized, there was no significant difference in conversions, molecular weights and dispersities obtained (entries 4-6). The molecular weights of the polymers were in the range of 13000 – 14000 g mol⁻¹. The dispersities were narrow with values between 1.08 and 1.12. Decreasing the catalyst loading resulted in an increasing molecular weight (entry 7), which was expected due to the higher number of CHO monomer per activated epoxide. The copolymerization activities of the related four chromium(III) amino-bis(phenolate) complexes (Figure 2-1, **2.2** – **2.5**) are shown in entries 8-11. Generally, complex **2.1** in the presence of DMAP, PPNCI or PPNN₃ showed higher conversions of CHO to polymer, higher molecular weights and narrower dispersities than these former reported complexes. In terms of initial copolymerization rate, **2.1** has exhibited a significantly higher rate than complexes **2.2** and **2.3** (entry 4 vs. entries 8 and 9).

Table 2-2. Results of copolymerization of CHO and CO₂ by complex **2.1**^a



Entry ^b	[Cr]:[CHO]:[Co-Cat.] molar ratio	Conv. (%) ^c	Yield (%) ^d	TON	Initial rate (abs×10 ⁴ /min) ^e	M _n ^f g mol ⁻¹	Đ ^f (M _w /M _n)
1	1:500:1(DMAP)	70	56	350	ND	10000	1.06
2	1:500:1(PPNCl)	75	64	374	ND	13000	1.11
3	1:500:1(PPNN ₃)	71	55	355	ND	11000	1.10
4	1:500:1(DMAP)	89	76	445	355	13000	1.10
5	1:500:1(PPNCl)	91	77	455	566	13000	1.08
6	1:500:1(PPNN ₃)	92	72	460	702	14000	1.12
7	1:1000:1(PPNCl)	91	78	910	201	35000	1.12
8 ^g	1(2.2):500:1(DMAP)	81	ND	400	29	13000	1.40
9 ^h	1(2.3):500:1(DMAP)	75	72	375	120	7100	1.36
10 ⁱ	1(2.4):500:1(DMAP)	68	58	340	ND	5700	1.48
11 ^j	1(2.5):500:1(DMAP)	12	ND	60	ND	ND	ND

^aReactions were carried out in neat CHO (5 mL) at 60 °C and 40 bar CO₂ for 24 h.

^bEntries 1-3 were run in a 100 mL stainless steel Parr autoclave with a diameter of 3.2 cm, entries 4-7 were run in a 100 mL stainless steel Parr autoclave with a diameter of 5.2 cm.

^cCalculated by ¹H NMR. ^dYield = (mass of polymer / molar mass of repeating unit) / moles of starting monomer. ^eSlope of absorbance vs. time curves calculated for the linear portion.

^fDetermined by triple detection GPC in THF, dn/dc= 0.0701 mL g⁻¹. ^gUsing catalyst **2.2** in Figure 2-1.^{75,76} ^hUsing catalyst **2.3**.⁷⁶ ⁱUsing catalyst **2.4**.⁷⁰ ^jUsing catalyst **2.5**.⁷⁶

The in situ infrared reaction profiles for the formation of PCHC using **2.1** with

different cocatalysts are shown in Figure 2-8. None of the reactions showed an induction period. The initial rates calculated from the slope of absorbance vs. time for the linear part showed that ionic cocatalysts were more efficient than DMAP, and PPNN₃ exhibited the fastest rate (Figure 2-9). This observation is consistent with a binary system of chromium salen complex with neutral/ionic cocatalyst reported by Darensbourg,⁴⁷ who showed that the anionic cocatalyst binds to form a well-characterized six-coordinate anionic species, proposed to be the active species for initiating copolymerization.⁷⁷ No induction period is observed in these ionic cocatalyzed reactions, suggesting that the formation of the active species is a fast process.

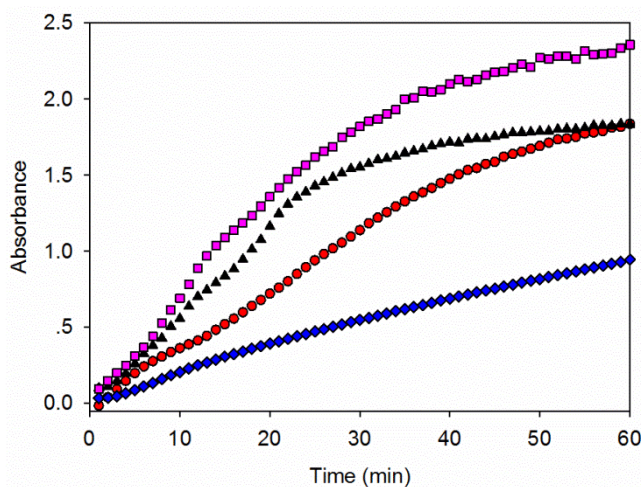


Figure 2-8. Time profiles of the absorbance at 1750 cm⁻¹ corresponding to the PCHC production by **2.1** and different cocatalysts (Table 2-2, entries 4-7): [Cr]:[CHO]:DMAP = 1:500:1, ●; [Cr]:[CHO]:PPNCl = 1:500:1, ▲; or [Cr]:[CHO]:PPNN₃ = 1:500:1, ■; [Cr]:[CHO]:PPNCl = 1:1000:1, ◆.

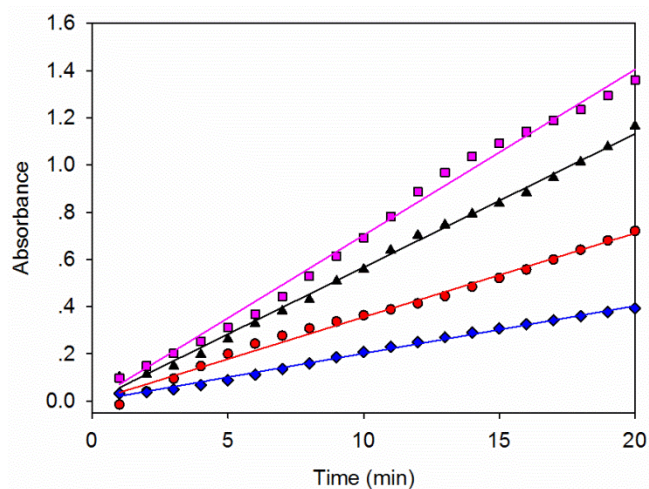
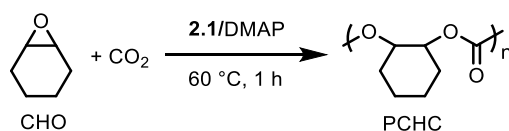


Figure 2-9. Plots of absorbance vs. time for the linear portion of polycarbonate formation for the data presented in Figure 2-8. Straight lines represent best fits of the data for [Cr]:[CHO]:DMAP = 1:500:1, ●, $y = 0.0355x$, $R^2 = 0.9909$; [Cr]:[CHO]:PPNCl = 1:500:1, ▲, $y = 0.0566x$, $R^2 = 0.9964$; [Cr]:[CHO]:PPNN₃ = 1:500:1, ■, $y = 0.0702x$, $R^2 = 0.9928$; [Cr]:[CHO]:PPNCl = 1:1000:1, ◆, $y = 0.0201x$, $R^2 = 0.9954$.

Copolymerization of CHO and CO₂ was further investigated at different CO₂ pressures. As shown in Table 2-3, the conversion increased with increasing CO₂ pressure. At the relatively low pressures of 12 bar CO₂, the carbonate linkages of the resulting polymer reached 92%, which increased to 98% when CO₂ pressure increased to 58 bar. Chromium salen and manganese porphyrin complexes have shown that CO₂ pressures as low as one atmosphere still produced copolymer with ~90% carbonate linkages.^{46,78} The molecular weight of the resulting polymer was found to slightly increase and a more narrow dispersity was obtained when higher CO₂ pressure was used. It is worth noting that the molecular weight of the polymer increased little with the reaction time from 1 h

to 24 h (Table 2-3, entry 4 vs. Table 2-2, entry 4), but conversion of CHO to PCHC continued to occur.

Table 2-3. Effect of CO₂ pressure on the copolymerization of CHO and CO₂^a



Entry ^a	CO ₂ pressure (bar)	Carbonate (%) ^b	Conv. (%) ^b	TOF (h ⁻¹) ^c	M _n ^d g mol ⁻¹	Đ (M _w /M _n) ^d
1	12	92	17	85	8400	1.25
2	20	95	28	140	10000	1.14
3	30	95	32	160	9400	1.08
4	40	94	33	165	11000	1.09
5 ^e	40	95	76 (4h)	95	13000	1.10
6	58	98	44	220	12000	1.06

^aAll copolymerization reactions were carried out in neat CHO (5 mL) at 60 °C for 1 h with 0.2 mol% catalyst loading and one equivalent DMAP per Cr. ^bDetermined by ¹H NMR. ^cTurnover frequency (TOF) is moles of repeating units produced per mol of Cr within 1 h. ^dDetermined by triple detection GPC in THF, dn/dc = 0.0701 mL g⁻¹. ^eReaction was run for 4 h.

2.2.4 Kinetic studies

Effect of temperature on the formation of PCHC was monitored by following the $\nu(\text{C}=\text{O})$ of polycarbonate at 1750 cm⁻¹ by in situ infrared spectroscopy wherein the temperature was successively increased and each temperature maintained for

approximately 20 min. Three-dimensional stack plots of the IR spectra and reaction profiles are shown in Figure 2-10. No PCHC was produced at room temperature ($\sim 25\text{ }^{\circ}\text{C}$), but increasing the temperature to $30\text{ }^{\circ}\text{C}$ the formation of PCHC could be observed at a very slow rate. The rate of PCHC formation was observed to increase further with increasing temperature. After approximately 90 minutes, the growth rate of the band at 1750 cm^{-1} began to slow either because of increasing viscosity of the solution or deposition of polymer on the ATR sensor (Figure 2-10, B). When the temperature increased to $85\text{ }^{\circ}\text{C}$, a 5-fold increase in initial reaction rate compared to the reaction at $60\text{ }^{\circ}\text{C}$ was obtained (Figure 2-11, A), however, the appearance of *trans*-cyclic carbonate was observed, which was identified by a new absorbance at 1825 cm^{-1} (Figure 2-11, B) and confirmed by ^1H NMR (Figure 2-12).^{79,80} The formation of cyclic cyclohexene carbonate at higher temperatures has been previously observed for Cr salen complexes.⁴⁴

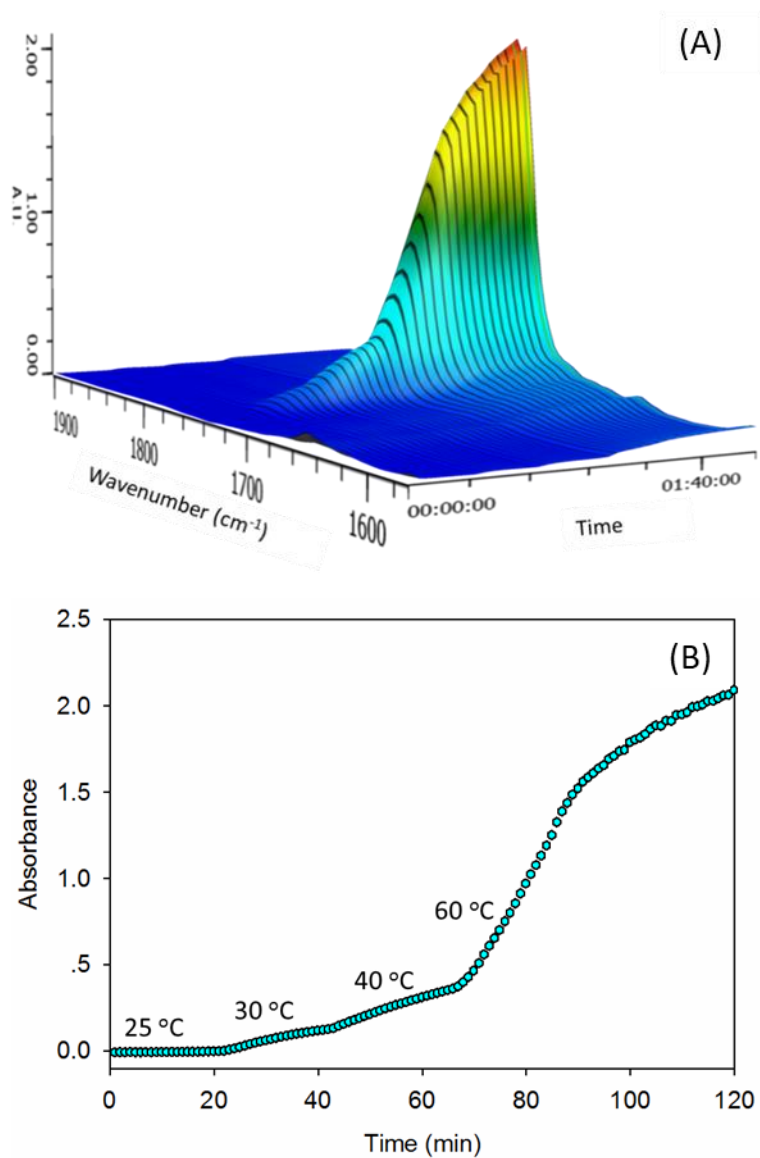


Figure 2-10. (A) Three-dimensional stack plot of IR spectra collected every 60 s during the reaction of CHO and CO_2 by the binary system of **2.1** and DMAP with a **2.1**:CHO:DMAP molar ratio of 1:500:1. (B) Time profile of the absorbance at 1750 cm^{-1} at different temperatures.

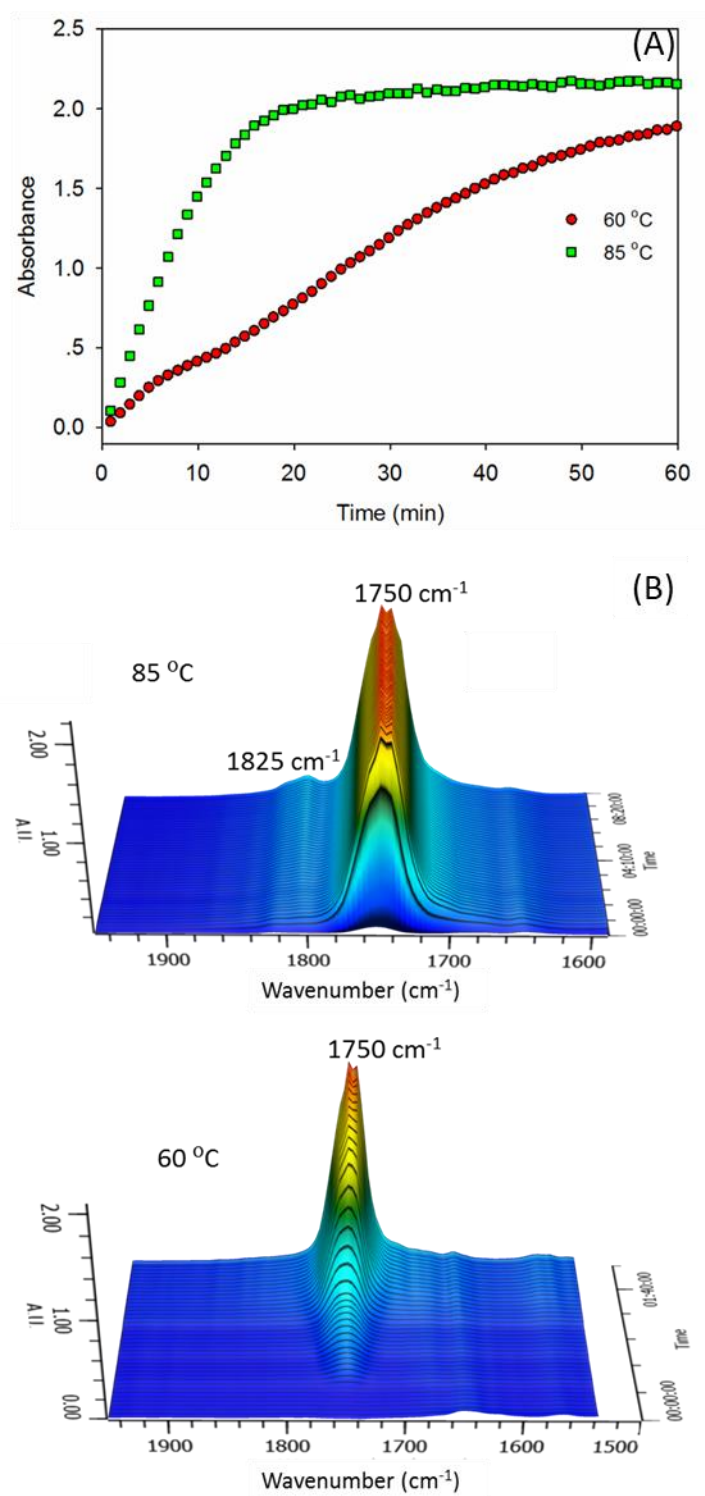


Figure 2-11. (A) Time profiles of the absorbance at 1750 cm^{-1} corresponding to the PCHC using DMAP as cocatalysts at $60\text{ }^{\circ}\text{C}$ and $85\text{ }^{\circ}\text{C}$. (B) Three-dimensional stack plots of the IR spectra.

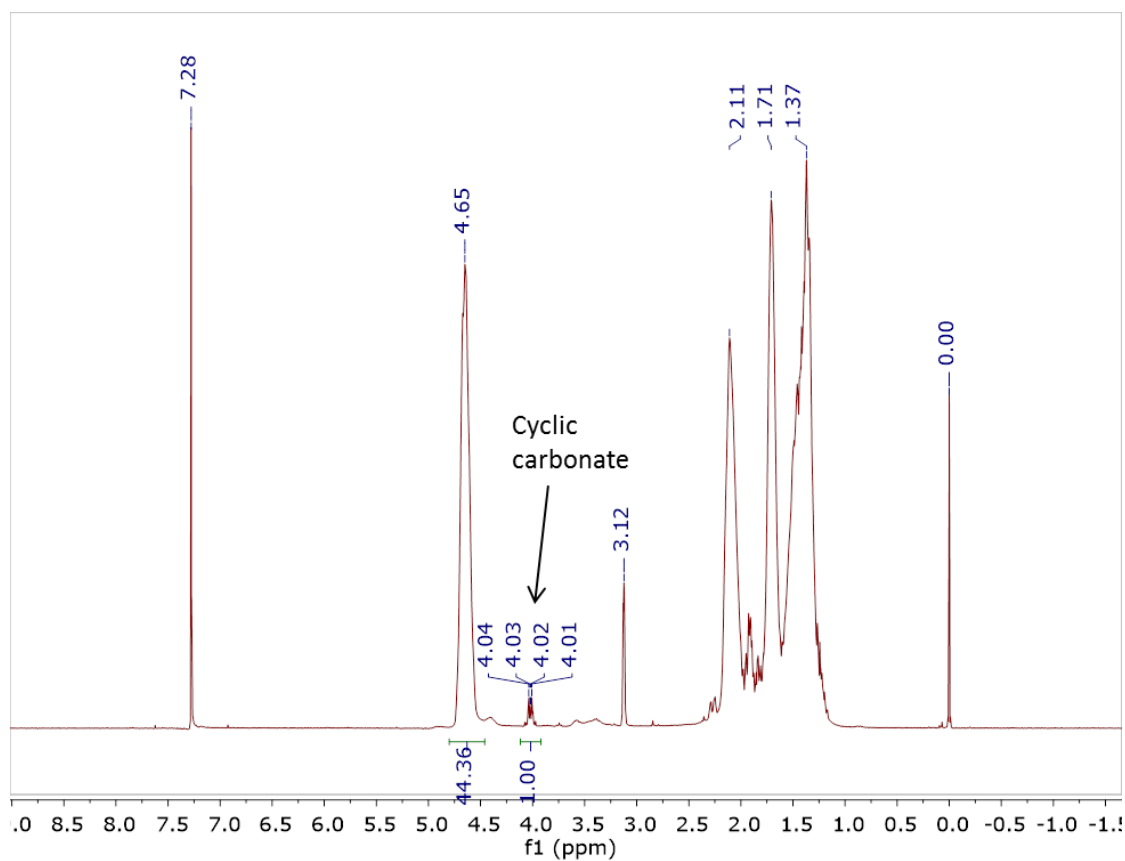


Figure 2-12. ^1H NMR spectrum in CDCl_3 of PCHC using DMAP as cocatalyst at 85°C .

The Arrhenius plot for PCHC formation by the **2.1**/DMAP system is shown in Figure 2-13. The activation barrier for PCHC formation was calculated to be $54 \pm 4 \text{ kJ mol}^{-1}$, which is similar to the values reported by Darensbourg (47 kJ mol^{-1})⁴⁴ and Lu (48 kJ mol^{-1})⁸¹ for Cr(III) salen and Co(III) salen complexes, respectively.

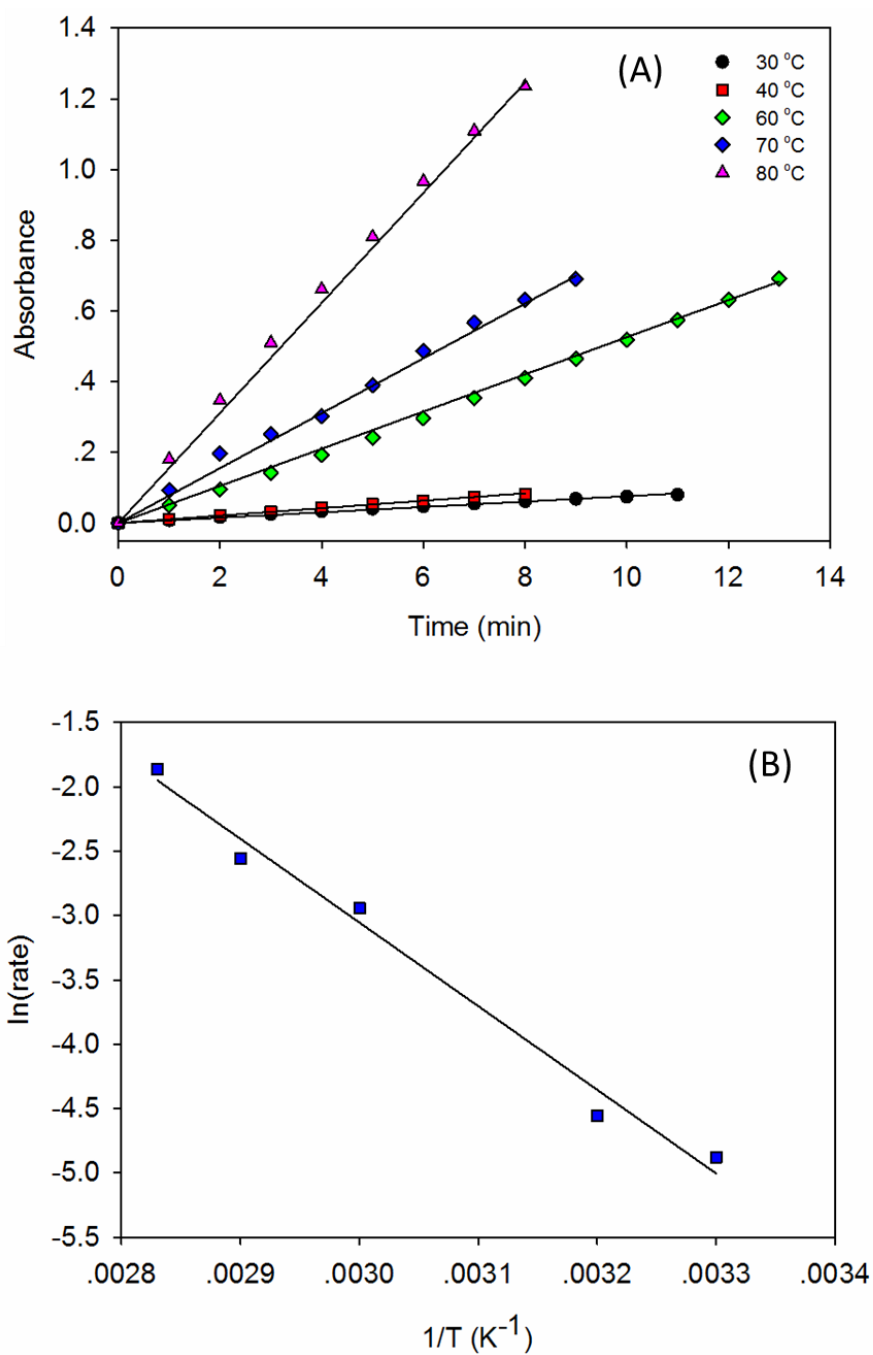


Figure 2-13. (A) Plots of absorbance vs. time for the linear portion of polycarbonate formation at various temperatures. 30 °C: $y = 0.0076x$, $R^2 = 0.9942$, 40 °C: $y = 0.0105x$, $R^2 = 0.9975$, 60 °C: $y = 0.0526x$, $R^2 = 0.9969$, 70 °C: $y = 0.0777x$, $R^2 = 0.9928$, 80 °C: $y = 0.1558x$, $R^2 = 0.9947$. (B) Arrhenius plot for the formation of PCHC. Straight line represents best fit with $y = -6503.5x + 16.4557$, $R^2 = 0.9858$.

2.2.5 End-group analysis

End-group analysis of the obtained polymers was carried out by MALDI-TOF MS to provide the insight into the initial CHO ring-opening step during the reaction. All the polymers obtained showed multiple series of ions separated with a repeating unit of m/z 142.1. The possible end-groups of the obtained polymers are shown in Figure 2-14.

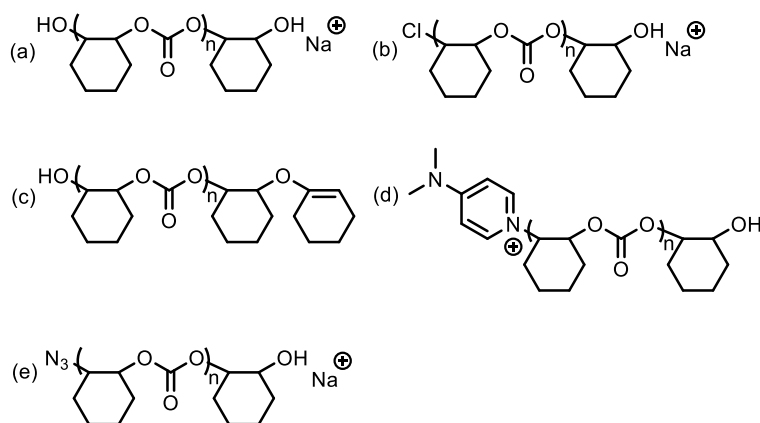


Figure 2-14. Series of chain end-groups observed in MALDI-TOF MS of the polymers produced by complex **2.1** with different cocatalysts.

The MALDI-TOF mass spectrum of the polymer produced by DMAP as the cocatalyst (Table 2-2, entry 4) is shown in Figure 2-15. The observed polymer chains in the high mass region correspond to the sodium ion containing polycarbonate $[35.5 (\text{Cl}) + 142.1n (\text{repeating cyclohexene carbonate}) + 99.1 (\text{C}_6\text{H}_{10}\text{OH})]\text{Na}^+$. This suggests the chloride (35.5 (Cl)) of Cr(III) complex initiated copolymerization by ring-opening of an epoxide monomer, and termination by protonolysis of the metal-alkoxide (99.1

(C₆H₁₀OH)) in methanol. At middle mass range (m/z 2000 to 4000), four series of copolymer chains were observed (Figure 2-16). Series (a) corresponds to the sodium ion containing polycarbonate having two hydroxyl end-groups [17.0 (OH) + 142.1n (repeating cyclohexene carbonate unit) + 99.1 (C₆H₁₀OH)]. Polycarbonate diols are typically observed due to adventitious moisture contamination causing chain transfer.⁵² Series (b) consists of the expected end-groups from chloride initiation and protonation of an alkoxide chain end (Cl⁻ and OH⁻). Series (c) corresponds to the presence of one hydroxyl end-group and an ether linkage with cyclohexenyl end-group [17.0 (OH) + 142.1n (repeating unit) + 180.0 (C₁₂H₂₀O)]. The ether linkage with cyclohexenyl end-group can be attributed to the elimination of HCl from the expected chloro-cyclohexanolate chromium species and chain transfer reaction.⁵⁷ Series (d) contains DMAP and hydroxyl end-groups [122.2 (DMAP) + 142.1n (repeating unit) + 99.1 (C₆H₁₀OH)], indicating DMAP can also initiate copolymerization by ring-opening of an epoxide monomer.

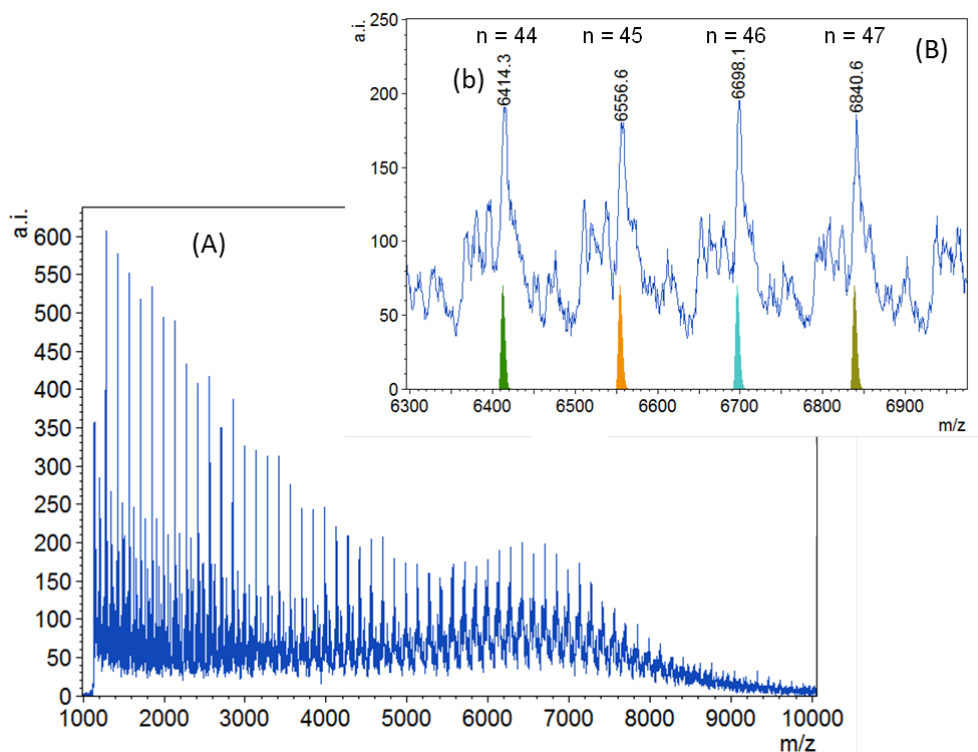


Figure 2-15. (A) MALDI-TOF mass spectrum of PCHC obtained using **2.1** and DMAP (Table 2-2, entry 4). (B) Higher mass region of the spectrum ($n = 44 - 47$) with the modeled polymer chain (b) illustrated in Figure 2-14.

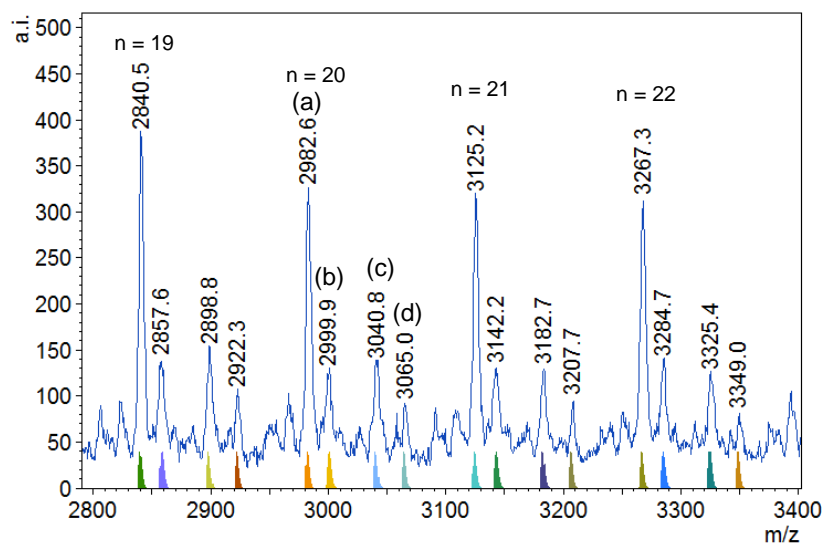


Figure 2-16. Lower mass region (2750 – 3350 m/z , $n = 19 - 22$) of the MALDI-TOF mass spectrum obtained using DMAP as cocatalyst.

When PPNCI was used (Table 2-2, entry 5), the MALDI-TOF mass spectrum of the resulting polymer showed the presence of chloride and hydroxyl end-groups (Figure 2-17), demonstrating that the chloride from **2.1** and/or PPNCI initiated the copolymerization reaction. In the low mass region series (a) was observed again (See appendix Figure B-2). When PPNN₃ was used, the MALDI-TOF mass spectrum showed the expected azide-initiated and hydroxyl-terminated polymer chains (Figure 2-18). Series (a) and (b) were also visible in the low mass region (See appendix Figure B-3). It is worth noting that MALDI-TOF MS showed the absence of ether linkages in polymers produced using PPNCI or PPNN₃ as the cocatalyst.

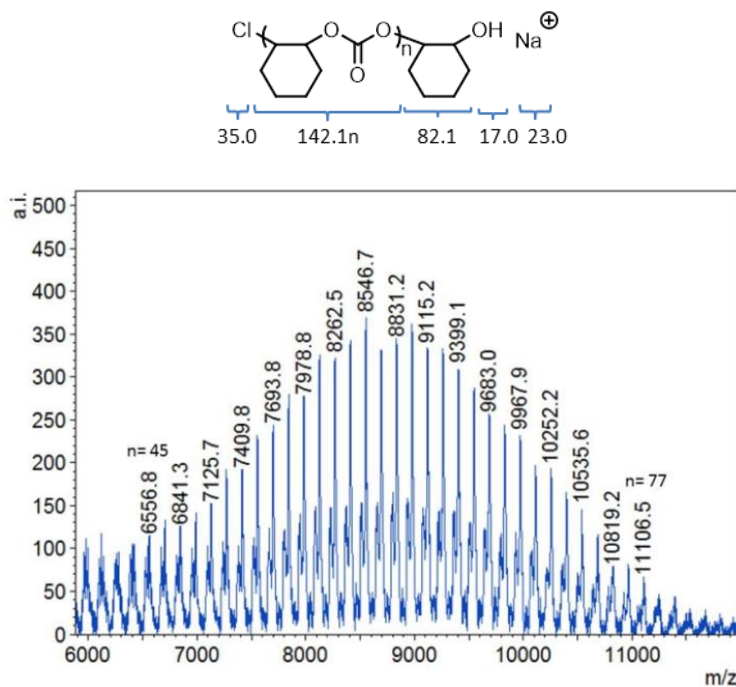


Figure 2-17. High mass region (m/z 6500 – 11100, $n = 45 - 77$) of the MALDI-TOF mass spectrum obtained using PPNCI as cocatalyst.

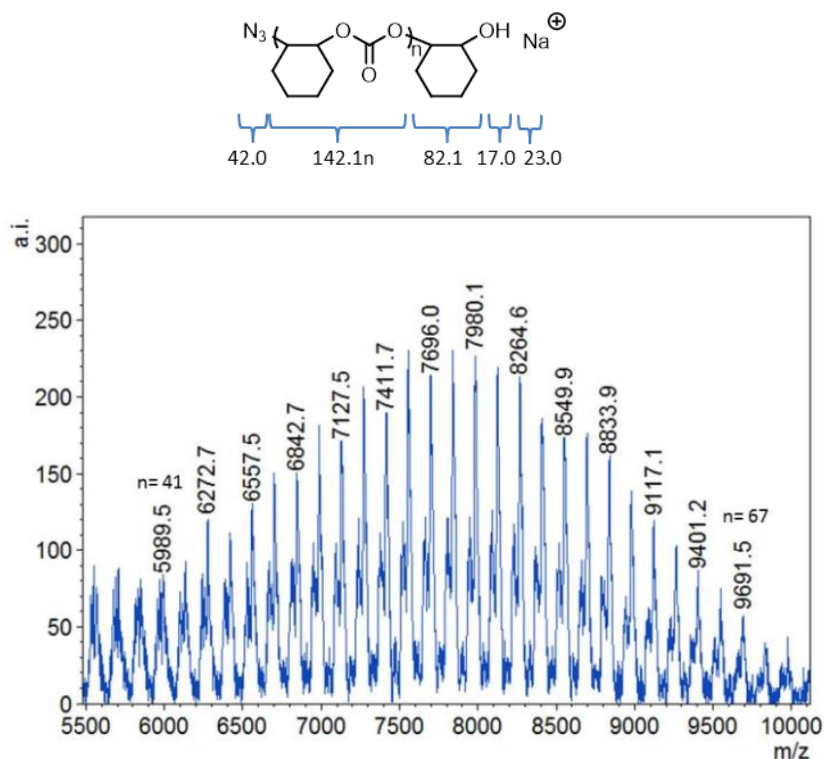


Figure 2-18. High mass region (m/z 5500 – 10000, $n = 41 - 67$) of the MALDI-TOF mass spectrum obtained using $PPNN_3$ as cocatalyst.

Thermal properties of the polymers were analyzed by thermal gravimetric analysis (TGA) and differential scanning calorimetry (DSC) measurements. The decomposition temperature at 50% weight loss (T_{50}) was found to range between 322 and 332 °C. The glass transition temperature (T_g) at the midpoint was found to range between 90 and 109 °C (See appendix Figure E-1 and Figure E-2). Similar weight loss and T_g values for PCHC have been reported by others.^{40, 82}

2.3 Conclusions

A new amino-bis(phenolate) chromium(III) complex, **2.1** bearing a *N,N*-dimethylaminoethyl pendant donor has been synthesized in high yield and characterized by MALDI-TOF mass spectrometry, elemental analysis, UV-Vis spectroscopy and X-ray diffraction. This complex combined with DMAP, PPNCI or PPNN₃ has shown improved activity over previously reported amino-bis(phenolate) chromium(III) complexes for the copolymerization of CHO and CO₂ to yield PCHC. Kinetic studies of the monometallic complex/DMAP system revealed the activation energy for polycarbonate formation to be 54 ± 4 kJ mol⁻¹. End-group analysis of the resulting polymers via MALDI-TOF MS revealed either chloride of the Cr(III) complex or the external nucleophile initiated the copolymerization reaction.

2.4 Experimental

2.4.1 General materials

Unless otherwise stated, all manipulations were performed under an atmosphere of dry, oxygen-free nitrogen by means of standard Schlenk techniques or using an MBraun Labmaster DP glove box. CrCl₃(THF)₃ was prepared by the standard method.⁸³ H₂[**L1**] was prepared by a modified literature procedure by using water instead of methanol as the reaction medium,⁸⁴ and dried over sodium sulfate in tetrahydrofuran. Anhydrous

tetrahydrofuran was distilled from sodium/benzophenone ketyl under nitrogen. Cyclohexene oxide was purchased from Aldrich and freshly distilled from CaH_2 under nitrogen. Dichloromethane was purified by an MBraun Manual Solvent Purification System. PPNCl was purchased from Alfa Aesar and used without further purification. PPNN_3 was prepared via previously reported method.⁸⁵

2.4.2 Instrumentation

MALDI-TOF MS was performed using an Applied Biosystems 4800 MALDI TOF/TOF Analyzer equipped with a reflectron, delayed ion extraction and high performance nitrogen laser (200 Hz operating at 355 nm). Samples of complexes were prepared in the glove box and sealed under nitrogen in a Ziploc® bag for transport to the instrument. Anthracene was used as the matrix for **2.1** and 2,5-dihydroxybenzoic acid (DHBA) was used as the matrix for the copolymers. Anthracene and **2.1** were each dissolved in toluene at concentrations of 10 mg mL^{-1} . The matrix and complex solutions were combined in a ratio of 1:1 as the final analyzed sample. DHBA was dissolved in THF at approximately 16 mg mL^{-1} and polymer was dissolved in THF at approximately 10 mg mL^{-1} . The matrix and polymer solutions were combined in a ratio of 4:1 as the final analyzed sample. $1 \text{ }\mu\text{L}$ aliquots of these samples were spotted on the MALDI plate and left to dry. Images of mass spectra were prepared using mMass™ software

(www.mmass.org).

Molecular weight determination of copolymer was performed on an Agilent Infinity HPLC instrument connected to a Wyatt Technologies triple detector system (light scattering, viscometry and refractive index) equipped with two Phenogel 10^3 \AA $300 \times 4.60 \text{ mm}$ columns with THF as eluent. Copolymer samples were prepared in THF at a concentration of 4 mg mL^{-1} and filtered through 0.2 \mu m syringe filters. The sample solution was then eluted at a flow rate of $0.30 \text{ mL} \cdot \text{min}^{-1}$. The values of dn/dc were calculated online (columns detached) assuming 100% mass recovery using the Astra 6 software package (Wyatt Technologies) giving dn/dc of PCHC = 0.0701 mL g^{-1} . This work was completed with the assistance of Hart Plommer.

^1H NMR and ^{13}C NMR spectra were in CDCl_3 recorded at 300 MHz. Elemental analysis was performed at Guelph Chemical Laboratories, Guelph, ON, Canada. In situ infrared experiments were performed using a 100 mL stainless steel reactor (Parr Instruments) equipped with a SiComp Sentinel probe connected to a ReactIR 15TM reaction analysis system. UV-vis spectroscopy was conducted on an Ocean Optics USB4000+ fiber optic spectrophotometer.

The glass transition (T_g) temperatures were measured using a Mettler Toledo DSC 1 STAR^e System equipped with a Julabo FT 100 immersion cooling system, using R1150 refrigerant in an EtOH bath with a working range of -100 to $+20 \text{ }^\circ\text{C}$. Samples were

weighed into 40 μL aluminum pans and subjected to two heating cycles from 0 to 180 $^{\circ}\text{C}$ at a rate of 10 $^{\circ}\text{C min}^{-1}$. The glass transition (T_g) temperatures of copolymers were determined from the second heating. Thermogravimetric analysis measurement was performed with a TA Instruments Q500. Samples were loaded onto a platinum pan and subjected to a dynamic high-resolution scan. Each sample was heated from room temperature to 400 $^{\circ}\text{C}$ at a heating rate of 10 $^{\circ}\text{C min}^{-1}$.

2.4.3 Synthesis of the amino-bis(phenolate) chromium complex

$\text{H}_2[\text{L1}]$ (3.50 g, 6.67 mmol) and sodium hydride (0.64 g, 26.67 mmol) were loaded into a Schlenk tube and cooled to -78 $^{\circ}\text{C}$. THF (50 mL) was added to give a white suspension, which was warmed to room temperature and further stirred for 2 h. This mixture was transferred via filter cannula to a suspension of $\text{CrCl}_3(\text{THF})_3$ (2.50 g, 6.67 mmol) in THF (50 mL) cooled to -78 $^{\circ}\text{C}$ to give a pink/purple mixture. The resulting mixture was warmed to room temperature and stirred overnight to give a purple solution. The solvent was removed under vacuum, and the residue extracted into toluene. The mixture was filtered through Celite, and the solvent was removed under vacuum. The residue was washed with pentane and dried to yield 4.33 g (95%) of purple powder. Crystals suitable for X-ray diffraction were obtained by slow evaporation of a solution of **2.1** in THF and hexamethyldisiloxane in a glove box under nitrogen or toluene at room

temperature exposed to air. Anal. Calcd for $C_{38}H_{62}ClCrN_2O_3$: C, 66.89; H, 9.16; N, 4.11. Found: C, 66.77; H, 8.89; N, 3.94. MS (MALDI-TOF) m/z (% ion): 609.3 (50, $[CrCl[L1]^+]$), 574.3 (100, $[Cr[L1]^+]$).

2.4.4 Copolymerization conditions

Reactions were carried out in neat CHO (4.85 g), which was added to the catalyst and the appropriate amount of co-catalyst in a glovebox. The reactant solution was added via a syringe to the pressure vessel, which was predried under vacuum at 80 °C. The autoclave was then charged with 40 bar of CO_2 and left to stir at 60 °C for 24 h. After the desired time, the autoclave was cooled in an ice bath and CO_2 vented in the fume hood. An aliquot was taken immediately after opening the reactor for the determination of conversion by 1H NMR. The contents of the reactor were extracted with CH_2Cl_2 and the polymer precipitated using cold methanol. For the ionic co-catalysts, catalyst and co-catalyst were dissolved in CH_2Cl_2 first and stirred for 15 min before solvent was removed, the resulting mixture was then dissolved in CHO.

2.5 References

- (1) Aresta, M. (Ed.), *Carbon Dioxide as Chemical Feedstock*; Wiley-VCH Verlag GmbH & Co. KGaA, **2010**.
- (2) Coates, G. W.; Moore, D. R. *Angew. Chem., Int. Ed.* **2004**, *43*, 6618.
- (3) Darensbourg, D. J. *Chem. Rev.* **2007**, *107*, 2388.
- (4) Darensbourg, D. J. *Inorg. Chem.* **2010**, *49*, 10765.
- (5) Kember, M. R.; Buchard, A.; Williams, C. K. *Chem. Commun.* **2011**, *47*, 141.
- (6) Klaus, S.; Lehenmeier, M. W.; Anderson, C. E.; Rieger, B. *Coord. Chem. Rev.* **2011**, *255*, 1460.
- (7) Lu, X.-B.; Darensbourg, D. J. *Chem. Soc. Rev.* **2012**, *41*, 1462.
- (8) Trott, G.; Saini, P. K.; Williams, C. K. *Philos. Trans. A Math Phys. Eng. Sci.* **2016**, *374*, 20150085/1.
- (9) Kember, M. R.; Williams, C. K. *J. Am. Chem. Soc.* **2012**, *134*, 15676.
- (10) Chapman, A. M.; Keyworth, C.; Kember, M. R.; Lennox, A. J. J.; Williams, C. K. *ACS Catal.* **2015**, *5*, 1581.
- (11) Darensbourg, D. J.; Billodeaux, D. R. *Inorg. Chem.* **2005**, *44*, 1433.
- (12) Ikpo, N.; Barbon, S. M.; Drover, M. W.; Dawe, L. N.; Kerton, F. M. *Organometallics* **2012**, *31*, 8145.
- (13) Chatterjee, C.; Chisholm, M. H. *Chem. Rec.* **2013**, *13*, 549.

- (14) Lee, B. Y.; Kwon, H. Y.; Lee, S. Y.; Na, S. J.; Han, S.-i.; Yun, H.; Lee, H.; Park, Y.-W. *J. Am. Chem. Soc.* **2005**, *127*, 3031.
- (15) Kember, M. R.; Knight, P. D.; Reung, P. T. R.; Williams, C. K. *Angew. Chem., Int. Ed.* **2009**, *48*, 931.
- (16) Qin, J.; Xu, B.; Zhang, Y.; Yuan, D.; Yao, Y. *Green Chem.* **2016**, *18*, 4270.
- (17) Kissling, S.; Altenbuchner, P. T.; Lehenmeier, M. W.; Herdtweck, E.; Deglmann, P.; Seemann, U. B.; Rieger, B. *Chem. Eur. J.* **2015**, *21*, 8148.
- (18) Rajendran, N. M.; Haleel, A.; Reddy, N. D. *Organometallics* **2014**, *33*, 217.
- (19) Klaus, S.; Lehenmeier, M. W.; Herdtweck, E.; Deglmann, P.; Ott, A. K.; Rieger, B. *J. Am. Chem. Soc.* **2011**, *133*, 13151.
- (20) Kember, M. R.; White, A. J. P.; Williams, C. K. *Inorg. Chem.* **2009**, *48*, 9535.
- (21) Darensbourg, D. J.; Holtcamp, M. W.; Struck, G. E.; Zimmer, M. S.; Niezgoda, S. A.; Rainey, P.; Robertson, J. B.; Draper, J. D.; Reibenspies, J. H. *J. Am. Chem. Soc.* **1999**, *121*, 107.
- (22) Darensbourg, D. J.; Wildeson, J. R.; Yarbrough, J. C.; Reibenspies, J. H. *J. Am. Chem. Soc.* **2000**, *122*, 12487.
- (23) Darensbourg, D. J.; Lewis, S. J.; Rodgers, J. L.; Yarbrough, J. C. *Inorg. Chem.* **2003**, *42*, 581.
- (24) Van Meerendonk, W. J.; Duchateau, R.; Koning, C. E.; Gruter, G.-J. M.

Macromolecules **2005**, *38*, 7306.

(25) Cheng, M.; Lobkovsky, E. B.; Coates, G. W. *J. Am. Chem. Soc.* **1998**, *120*, 11018.

(26) Moore, D. R.; Cheng, M.; Lobkovsky, E. B.; Coates, G. W. *Angew. Chem., Int. Ed.* **2002**, *41*, 2599.

(27) Lu, X.-B.; Shi, L.; Wang, Y.-M.; Zhang, R.; Zhang, Y.-J.; Peng, X.-J.; Zhang, Z.-C.; Li, B. *J. Am. Chem. Soc.* **2006**, *128*, 1664.

(28) Yoo, J.; Na, S. J.; Park, H. C.; Cyriac, A.; Lee, B. Y. *Dalton Trans.* **2010**, *39*, 2622.

(29) Nakano, K.; Hashimoto, S.; Nozaki, K. *Chem. Sci.* **2010**, *1*, 369.

(30) Wu, G.-P.; Wei, S.-H.; Ren, W.-M.; Lu, X.-B.; Xu, T.-Q.; Darensbourg, D. J. *J. Am. Chem. Soc.* **2011**, *133*, 15191.

(31) Anderson, C. E.; Vagin, S. I.; Xia, W.; Jin, H.; Rieger, B. *Macromolecules* **2012**, *45*, 6840.

(32) Saunders, L. N.; Ikpo, N.; Petten, C. F.; Das, U. K.; Dawe, L. N.; Kozak, C. M.; Kerton, F. M. *Catal. Commun.* **2012**, *18*, 165.

(33) Lu, X.-B.; Ren, W.-M.; Wu, G.-P. *Acc. Chem. Res.* **2012**, *45*, 1721.

(34) Reiter, M.; Altenbuchner, P. T.; Kissling, S.; Herdtweck, E.; Rieger, B. *Eur. J. Inorg. Chem.* **2015**, *2015*, 1766.

(35) Cohen, C. T.; Chu, T.; Coates, G. W. *J. Am. Chem. Soc.* **2005**, *127*, 10869.

(36) Liu, B.; Zhao, X.; Guo, H.; Gao, Y.; Yang, M.; Wang, X. *Polymer* **2009**, *50*, 5071.

- (37) Lu, X.-B.; Wang, Y. *Angew. Chem., Int. Ed.* **2004**, *43*, 3574.
- (38) Paddock, R. L.; Nguyen, S. T. *Macromolecules* **2005**, *38*, 6251.
- (39) Qin, Z.; Thomas, C. M.; Lee, S.; Coates, G. W. *Angew. Chem., Int. Ed.* **2003**, *42*, 5484.
- (40) Mang, S.; Cooper, A. I.; Colclough, M. E.; Chauhan, N.; Holmes, A. B. *Macromolecules* **2000**, *33*, 303.
- (41) Paddock, R. L.; Nguyen, S. T. *J. Am. Chem. Soc.* **2001**, *123*, 11498.
- (42) Darensbourg, D. J.; Yarbrough, J. C. *J. Am. Chem. Soc.* **2002**, *124*, 6335.
- (43) Eberhardt, R.; Allmendinger, M.; Rieger, B. *Macromol. Rapid Commun.* **2003**, *24*, 194.
- (44) Darensbourg, D. J.; Yarbrough, J. C.; Ortiz, C.; Fang, C. C. *J. Am. Chem. Soc.* **2003**, *125*, 7586.
- (45) Darensbourg, D. J.; Mackiewicz, R. M.; Rodgers, J. L.; Fang, C. C.; Billodeaux, D. R.; Reibenspies, J. H. *Inorg. Chem.* **2004**, *43*, 6024.
- (46) Darensbourg, D. J.; Mackiewicz, R. M.; Billodeaux, D. R. *Organometallics* **2005**, *24*, 144.
- (47) Darensbourg, D. J.; Mackiewicz, R. M. *J. Am. Chem. Soc.* **2005**, *127*, 14026.
- (48) Xu, X.; Wang, C.; Li, H.; Wang, Y.; Sun, W.; Shen, Z. *Polymer* **2007**, *48*, 3921.
- (49) Li, B.; Zhang, R.; Lu, X.-B. *Macromolecules* **2007**, *40*, 2303.

- (50) Li, B.; Wu, G.-P.; Ren, W.-M.; Wang, Y.-M.; Rao, D.-Y.; Lu, X.-B. *J. Polym. Sci. A Polym. Chem.* **2008**, *46*, 6102.
- (51) Darensbourg, D. J.; Ulusoy, M.; Karroonnirum, O.; Poland, R. R.; Reibenspies, J. H.; Cetinkaya, B. *Macromolecules* **2009**, *42*, 6992.
- (52) Nakano, K.; Nakamura, M.; Nozaki, K. *Macromolecules* **2009**, *42*, 6972.
- (53) Guo, L.; Wang, C.; Zhao, W.; Li, H.; Sun, W.; Shen, Z. *Dalton Trans.* **2009**, 5406.
- (54) Darensbourg, D. J.; Fitch, S. B. *Inorg. Chem.* **2009**, *48*, 8668.
- (55) Darensbourg, D. J.; Poland, R. R.; Strickland, A. L. *J. Polym. Sci. A Polym. Chem.* **2012**, *50*, 127.
- (56) Stamp, L. M.; Mang, S. A.; Holmes, A. B.; Knights, K. A.; de Miguel, Y. R.; McConvey, I. F. *Chem. Commun.* **2001**, 2502.
- (57) Buchard, A.; Kember, M. R.; Sandeman, K. G.; Williams, C. K. *Chem. Commun.* **2011**, *47*, 212.
- (58) Taherimehr, M.; Al-Amsyar, S. M.; Whiteoak, C. J.; Kleij, A. W.; Pescarmona, P. P. *Green Chem.* **2013**, *15*, 3083.
- (59) Buonerba, A.; De Nisi, A.; Grassi, A.; Milione, S.; Capacchione, C.; Vagin, S.; Rieger, B. *Catal. Sci. Technol.* **2015**, *5*, 118.
- (60) Decortes, A.; Haak, R. M.; Martin, C.; Belmonte, M. M.; Martin, E.; Benet-Buchholz, J.; Kleij, A. W. *Macromolecules* **2015**, *48*, 8197.

- (61) Nakano, K.; Kobayashi, K.; Nozaki, K. *J. Am. Chem. Soc.* **2011**, *133*, 10720.
- (62) Rao, D.-Y.; Li, B.; Zhang, R.; Wang, H.; Lu, X.-B. *Inorg. Chem.* **2009**, *48*, 2830.
- (63) Adhikari, D.; Nguyen, S. T.; Baik, M.-H. *Chem. Commun.* **2014**, *50*, 2676.
- (64) Xiao, Y.; Wang, Z.; Ding, K. *Macromolecules* **2006**, *39*, 128.
- (65) Luinstra, G. A.; Haas, G. R.; Molnar, F.; Bernhart, V.; Eberhardt, R.; Rieger, B. *Chem. Eur. J.* **2005**, *11*, 6298.
- (66) Chisholm, M. H.; Zhou, Z. *J. Am. Chem. Soc.* **2004**, *126*, 11030.
- (67) Cheng, M.; Moore, D. R.; Reczek, J. J.; Chamberlain, B. M.; Lobkovsky, E. B.; Coates, G. W. *J. Am. Chem. Soc.* **2001**, *123*, 8738.
- (68) Dean, R. K.; Dawe, L. N.; Kozak, C. M. *Inorg. Chem.* **2012**, *51*, 9095.
- (69) Dean, R. K.; Devaine-Pressing, K.; Dawe, L. N.; Kozak, C. M. *Dalton Trans.* **2013**, *42*, 9233.
- (70) Chen, H.; Dawe, L. N.; Kozak, C. M. *Catal. Sci. Tech.* **2014**, *4*, 1547.
- (71) Devaine-Pressing, K.; Dawe, L. N.; Kozak, C. M. *Polym. Chem.* **2015**, *6*, 6305.
- (72) Devaine-Pressing, K.; Kozak, C. M. *ChemSusChem* **2017**, *10*, 1266.
- (73) Kozak, C. M.; Woods, A. M.; Bottaro, C. S.; Devaine-Pressing, K.; Ni, K. *Faraday Discuss.* **2015**, *183*, 31.
- (74) Dean, R. K.; Granville, S. L.; Dawe, L. N.; Decken, A.; Hattenhauer, K. M.; Kozak, C. M. *Dalton Trans.* **2010**, *39*, 548.

- (75) Dean, R. K.; Dawe, L. N.; Kozak, C. M. *Inorg. Chem.* **2012**, *51*, 9095.
- (76) Devaine-Pressing, K.; Dawe, L. N.; Kozak, C. M. *Polym. Chem.* **2015**, *6*, 6305.
- (77) Darensbourg, D. J.; Moncada, A. I. *Inorg. Chem.* **2008**, *47*, 10000.
- (78) Sugimoto, H.; Ohshima, H.; Inoue, S. *J. Polym. Sci., Part A: Polym. Chem.* **2003**, *41*, 3549.
- (79) Darensbourg, D. J.; Lewis, S. J.; Rodgers, J. L.; Yarbrough, J. C. *Inorg. Chem.* **2003**, *42*, 581.
- (80) Buchard, A.; Kember, M. R.; Sandeman, K. G.; Williams, C. K. *Chem. Commun.* **2011**, *47*, 212.
- (81) Liu, J.; Ren, W.-M.; Liu, Y.; Lu, X.-B. *Macromolecules* **2013**, *46*, 1343.
- (82) Ren, W.-M.; Zhang, X.; Liu, Y.; Li, J.-F.; Wang, H.; Lu, X.-B. *Macromolecules* **2010**, *43*, 1396.
- (83) So, J. H.; Boudjouk, P. *Inorg. Chem.* **1990**, *29*, 1592.
- (84) Tshuva, E. Y.; Goldberg, I.; Kol, M.; Goldschmidt, Z. *Organometallics* **2001**, *20*, 3017.
- (85) Demadis, K. D.; Meyer, T. J.; White, P. S. *Inorg. Chem.* **1998**, *37*, 3610.

Co-Authorship Statement

The results in Chapter 3 and 4 are currently in the preparation for publication

Authors: Kaijie Ni, Valentine Paniez-Grave and Christopher M. Kozak

The first author (Kaijie Ni) contributed 90% of the content of the article as the main researcher including: performing the experiments, analyzing and collecting data, and writing the paper.

The co-author (Valentine Paniez-Grave) was an undergraduate student who worked one summer alongside the first author helping in the preparation of samples analyzed by MALDI-TOF MS and ESI-MS.

The corresponding author (Christopher M. Kozak), my supervisor, was the principal investigator of this research work. He suggested initial experiments, assisted with analyzing data and revised this manuscript

Chapter 3. Chromium(III) amino-bis(phenolate) complex as the catalyst for CO₂ and cyclohexene oxide copolymerization and initiation mechanism studies

3.1 Introduction

The initiation mechanism of CO₂/epoxide copolymerization by salen or salan complexes combined with cocatalysts has been widely studied.¹⁻⁷ The possible pathways (a detailed description was given in Chapter 1, Section 1.3.4) include a monometallic initiation or bimetallic initiation pathway (Figure 3-1). Monometallic initiation can occur by nucleophilic attack via an intermolecular or intramolecular pathway. Bimetallic initiation involves two active metal complexes wherein the six-coordinate species (derived from the addition of cocatalyst to the complex) may ring-open the epoxide that is coordinated to the other metal center via an intermolecular pathway. The nucleophile (Nu) from the cocatalyst and/or the ancillary ligand (X) in the complex can be observed as the end-groups in the resulting polymer by MALDI-TOF-MS, indicating that both the cocatalyst and ancillary ligand can ring-open the epoxide. However, whether the main pathway of the ring-opening step is initiated by the cocatalyst and/or the ancillary ligand in the complex still remains unclear.

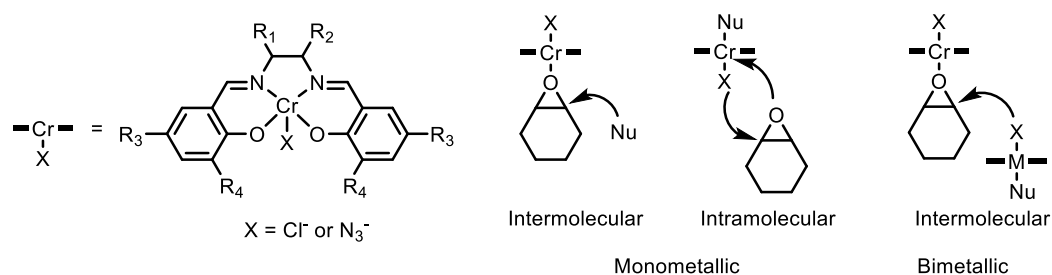


Figure 3-1. Possible initiation pathways for the salen complex and cocatalyst.

The Kozak group studied the amino-bis(phenolate) ligands incorporated with chromium, which in the presence of cocatalysts such as DMAP, PPNCI or PPNN₃ have demonstrated efficient catalytic activity towards the copolymerization of CO₂ and epoxide.⁸⁻¹⁰ Subsequently, MALDI-TOF MS was used to study the binding of DMAP to amino-bis(phenolate) chromium(III) chloride complexes.¹¹ The MALDI-TOF mass spectra suggests DMAP can coordinate to the chromium center forming a six coordinate species. It was also observed and demonstrated that the five-coordinate species resulting from loss of chloride or DMAP was the major peak in the mass spectra. Based on this observation, it was proposed that epoxide was activated by the five-coordinate species, followed by chloride or DMAP ring-opening via an intermolecular pathway as the main initiation step. More recently, the Kozak group has isolated the DMAP adduct of an amino-bis(phenolate) Cr(III) chloride complex that was characterized by single crystal X-ray diffraction.¹² This DMAP adduct alone or in combination with PPNCI

demonstrated efficient activity. In the latter case, DMAP was observed as the end-group in the high mass region of the MALDI-TOF mass spectrum. They proposed that DMAP dissociation in the presence of extra nucleophile most likely led to the ring-opening of epoxide via an intermolecular pathway. However, detailed studies on the role of the ionic cocatalyst in the amino-bis(phenolate) complexes for CO₂/epoxide copolymerization have not been carried out.

Interestingly, the Cr(III) amino-bis(phenolate) complex with a methoxy as the pendant donor group, **3.1** (Figure 3-2) in dichloromethane showed a color change from green to pink when PPnCl was added. In this chapter, spectroscopic studies of the reaction of **3.1** with PPnCl and **3.1** in the presence of PPnCl as the catalyst system for the copolymerization of CO₂ and CHO were reported. Other cocatalysts such as PPnN₃ and DMAP were also used for comparison.

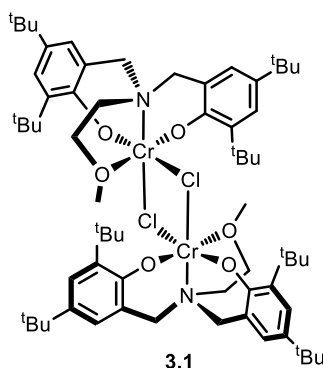
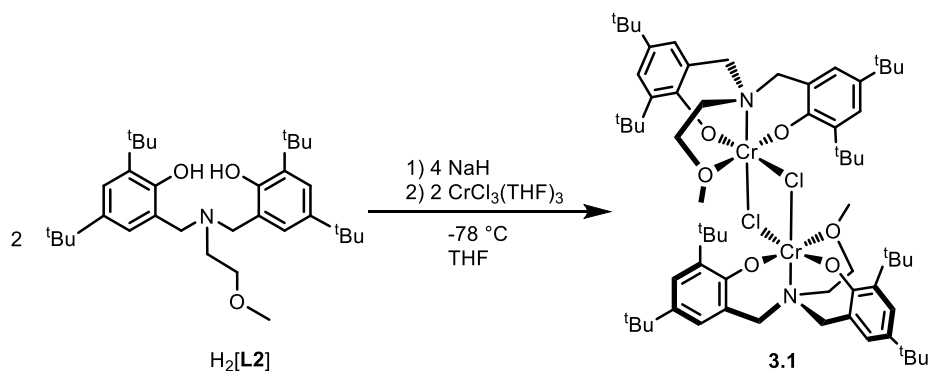


Figure 3-2. The dimeric structure of the Cr(III) amino-bis(phenolate) complex with a methoxy pendant donor group.

3.2 Results and discussion

3.2.1 Synthesis and characterization of Cr(III) complex 3.1

The amino-bis(phenolate) Cr(III) complex **3.1** was synthesized via the deprotonation of the proligand with sodium hydride in THF at $-78\text{ }^{\circ}\text{C}$, followed by reaction with $\text{CrCl}_3(\text{THF})_3$ in THF at $-78\text{ }^{\circ}\text{C}$ to give a green solid (Scheme 3-1). The paramagnetic complex was characterized by MALDI-TOF mass spectrometry, elemental analysis, UV-Vis spectroscopy and single crystal X-ray diffraction.



Scheme 3-1. Synthetic route to complex **3.1**.

The MALDI-TOF mass spectrum of complex **3.1** showed two peak at m/z 596 and 561, which correspond to the radical cation of $[\text{CrCl}[\text{L}2]]^{+\bullet}$ and the $[\text{Cr}[\text{L}2]]^+$ fragment resulting from a loss of a chloride ion (Figure 3-3). Two additional peaks were observed in the higher mass region at m/z 1194 and 1157 corresponding to the dimeric species

$[\text{CrCl}[\text{L2}]]_2^{+}$ and the fragment ion $[\text{Cr}_2\text{Cl}[\text{L2}]_2]^+$ after loss of one chloride ion loss. All the isotopic distribution patterns of the experimental ions were in good agreement with the theoretical representations. The Kozak group has previously observed similar ions of a related chloride-bridged bimetallic amino-bis(phenolate) Cr(III) chloride complex via MALDI-TOF MS.⁸

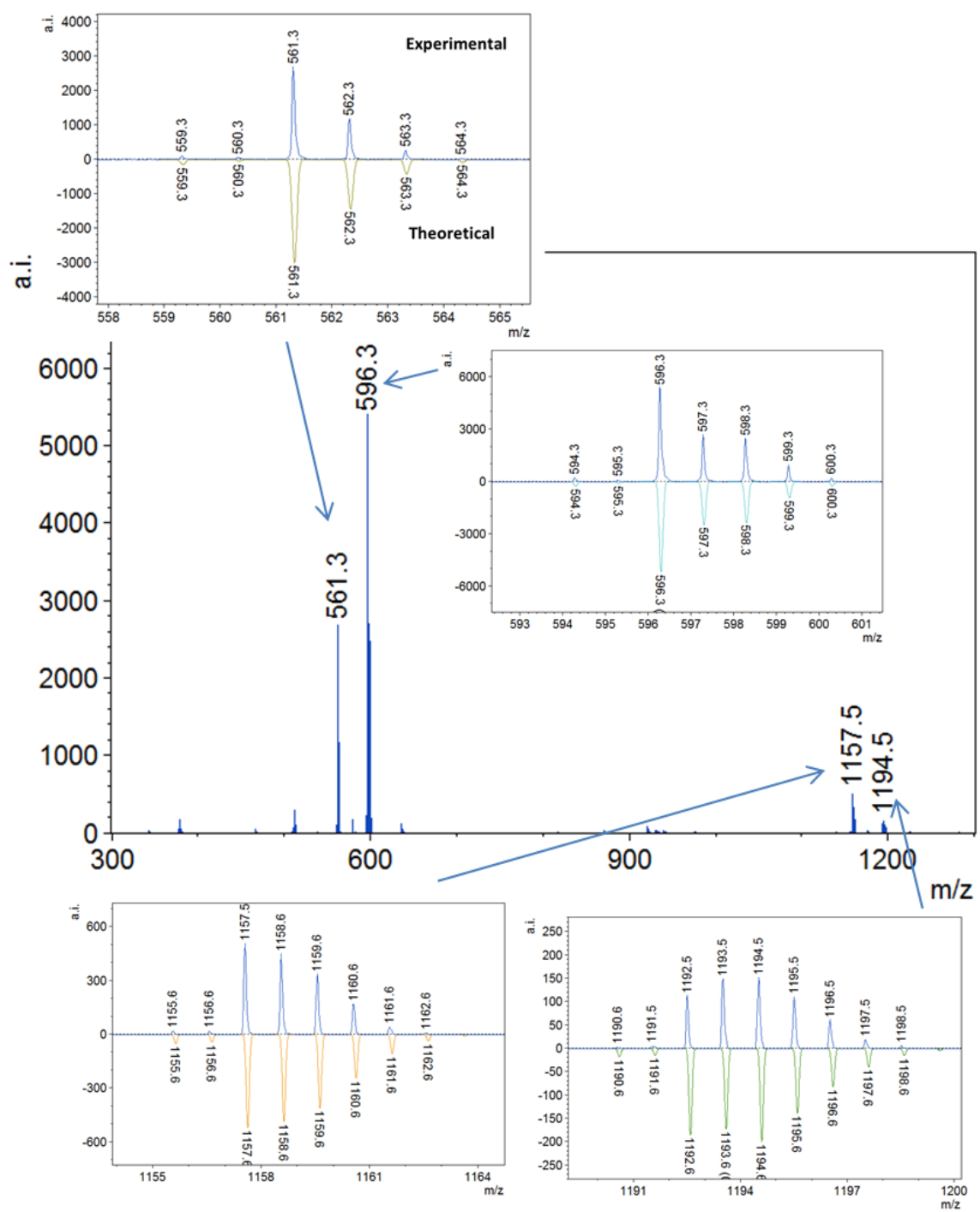


Figure 3-3. MALDI-TOF mass spectrum of complex **3.1** with isotopic patterns.

3.2.2 Crystal structure determination

Single crystals of **3.1** suitable for X-ray diffraction were obtained by slow evaporation of a toluene solution under nitrogen in the glovebox. The structure was found to be a chloride-bridged dimer (Figure 3-4). Selected bond distances and angles are listed in Table 3-1. The dimer of complex **3.1** exhibits distorted octahedral geometries in the two Cr centers. In each metal-ligand unit, the four coordination sites are occupied by the ligand system where the two phenolate oxygen atoms are *cis* to each other. The other two coordination sites are occupied by the two chloride ligands. One is *trans* to a phenolate oxygen and the other is *trans* to the amino donor. This geometry is identical to the previously reported X-ray structure of a related Cr(III) amino-bis(phenolate) complex with a pyridine as the pendant donor.⁸ The bond angle of Cr(1)–Cl(1)–Cr(1) is 97.26(2)°, slightly larger than the analog with pyridine pendant donor showing 95.66(3)°. The Cr–Cl distances are 2.4783(8) and 2.3922(8) (Å), respectively, which are slightly shorter than the observed bond distances in the pyridine pendant donor analogue (2.4431(8) and 2.4050(8) (Å)). These bond distances and angles lie within the ranges observed in other six-coordinate Cr(III) chloride-bridged species.¹³⁻¹⁵

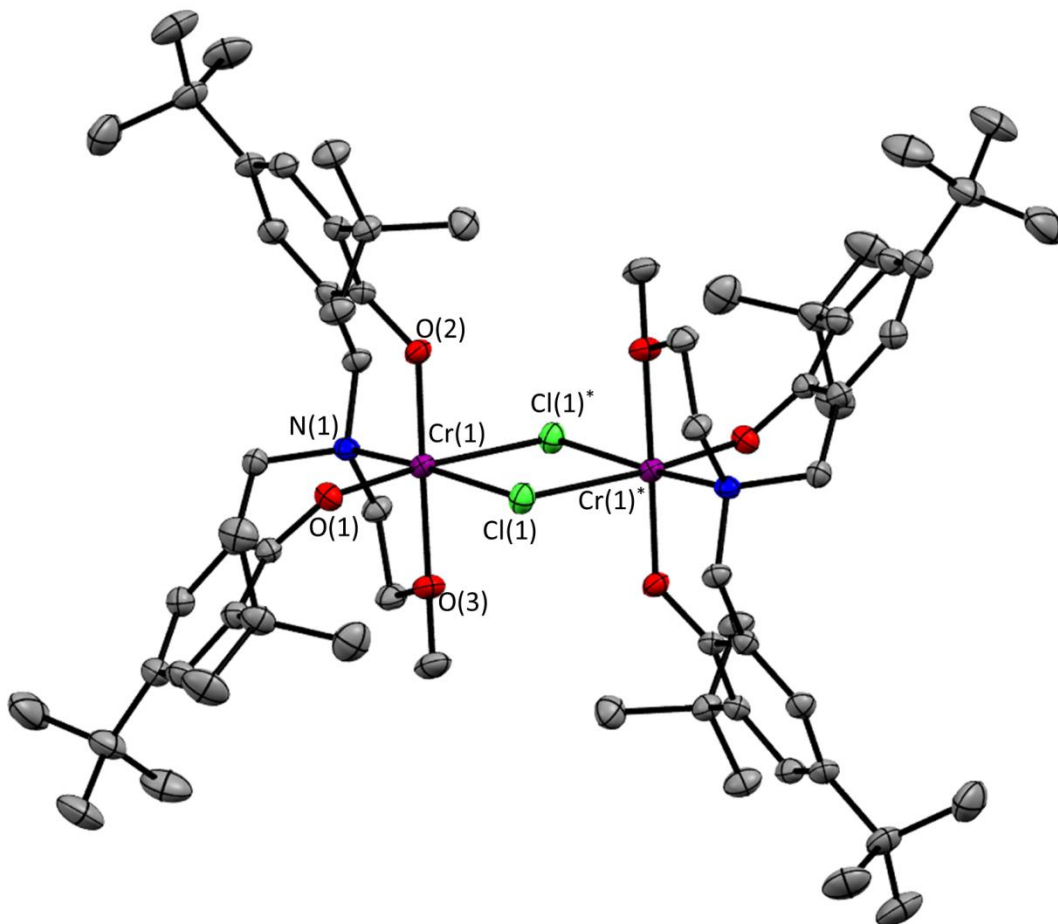


Figure 3-4. Molecular structure (ORTEP) and partial numbering scheme of complex **3.1**. Ellipsoids are drawn at 50% probability. Hydrogen atoms omitted for clarity. Symmetry operations used to generate equivalent atoms (*): $-x, -y, -y+1$.

Table 3-1. Selected bond distances (Å) and angles (°) for complex **3.1**

Bond lengths (Å)			
Cr(1)–Cl(1)*	2.4783(8)	Cr(1)–O(1)	1.9169(14)
Cr(1)–Cl(1)	2.3922(8)	Cr(1)–O(2)	1.8714(13)
Cr(1)–N(1)	2.0758(13)	Cr(1)–O(3)	2.0877(13)
Bond angles (°)			
O(1)–Cr(1)–N(1)	92.69(6)	O(2)–Cr(1)–Cl(1)*	89.33(5)
O(1)–Cr(1)–O(2)	94.16(6)	N(1)–Cr(1)–O(2)	92.89(5)
O(1)–Cr(1)–O(3)	91.97(6)	O(1)–Cr(1)–Cl(1)*	174.13(4)
O(3)–Cr(1)–Cl(1)	93.35(4)	N(1)–Cr(1)–Cl(1)	171.97(4)
O(2)–Cr(1)–O(3)	171.00(5)	Cl(1)–Cr(1)–Cl(1)*	82.74(2)
Cr(1)–Cl(1)–Cr(1)*	97.26(2)		

3.2.3 UV-Vis titration

Anionic cocatalysts have been shown to bind to salen Cr(III) complexes to form *trans*-six-coordinate anionic species which have been characterized by X-ray diffraction.¹⁶ The six-coordinate anionic species was proposed to be the active species for CO₂/CHO copolymerization catalyzed by the salen Cr(III) complex in the presence of ionic cocatalyst.¹ The MALDI-TOF mass spectrum of complex **3.1** and PPNCI dissolved in dichloromethane showed the peak at *m/z* 631 corresponding to the monometallic six-coordinate anionic species, [CrCl₂[L2]][−] (Figure 3-5), which demonstrated formation of

the six-coordinate species. Detailed studies of the reaction between complex **3.1** and PPNCI were carried out by UV-Vis spectroscopy. The titration of complex **3.1** with different amounts of PPNCI in dichloromethane showed that a new band at 537 nm grew commensurate with a decreasing band at 616 nm corresponding to complex **3.1** (Figure 3-6). The peak at 537 nm did not increase in intensity after the addition of two equivalents of PPNCI (per Cr). These observations suggest the dimer of **3.1** dissociates to form the six-coordinate anion in the presence of PPNCI (Scheme 3-2). The equilibrium constant for this reaction was calculated to be $1.6 \times 10^3 \text{ M}^{-1}$. The equilibrium constants for the reaction between PPNN₃ and porphyrin aluminum complexes have also been reported,¹⁷ which were estimated to be $1.6 \times 10^2 \text{ M}^{-1}$, 9.3 M^{-1} and 6.6 M^{-1} depending on the substituents on the porphyrin ligand system. The larger value shown by this amino-bis(phenolate) complex **3.1** suggests that the external nucleophile is more strongly bound to the metal center and is a result of both the different metal (Cr vs. Al) and the different ligand.

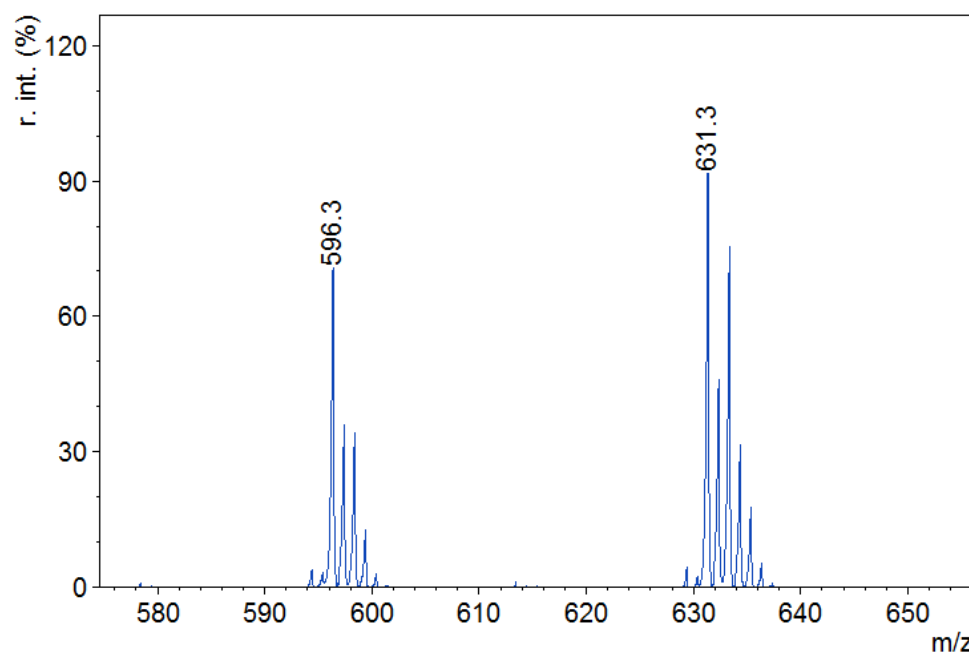


Figure 3-5. MALDI-TOF mass spectrum of the sample of complex **3.1** with PPNCI in negative mode.

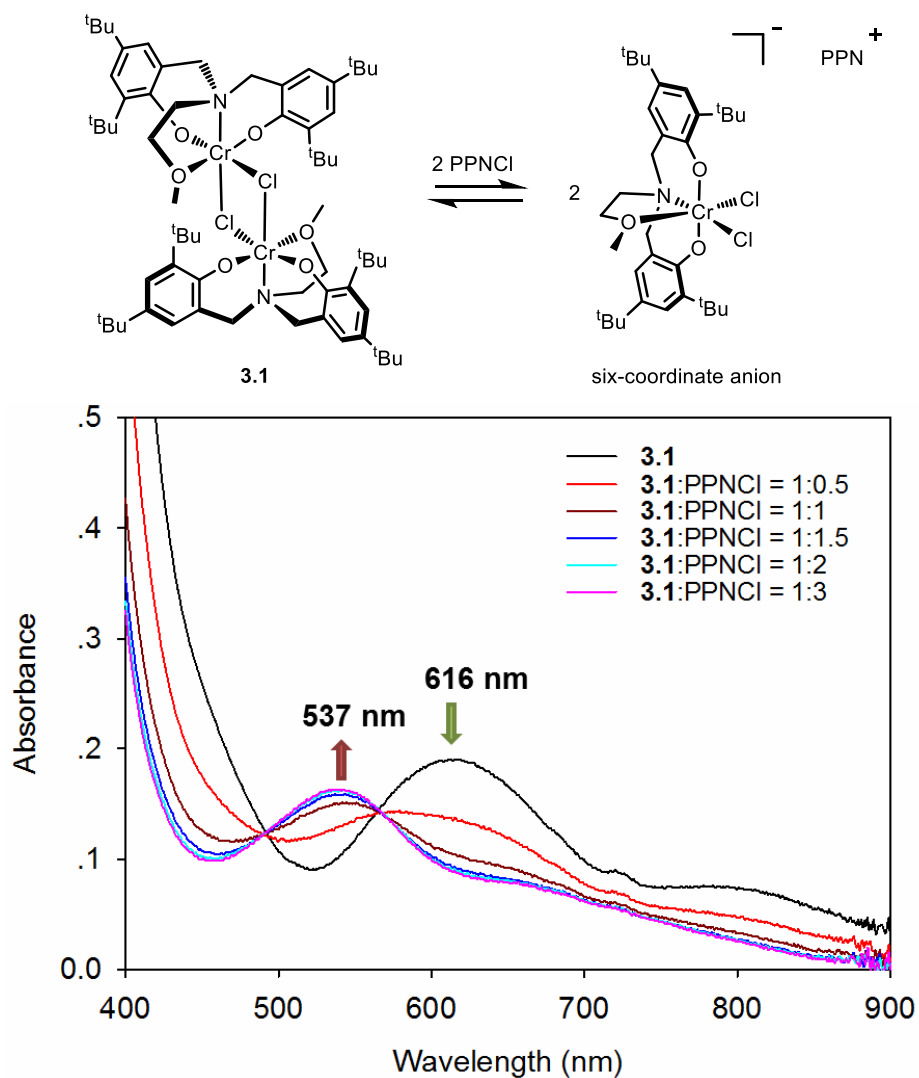


Figure 3-6. UV-Vis spectra of complex **3.1** with different ratios of PPNCI added.

The reaction of **3.1** with different amounts of CHO in dichloromethane was also monitored by UV-Vis spectroscopy (Figure 3-7). The band corresponding to **3.1** at 616 nm decreased with the addition of CHO and a new band at 481 nm started to grow. This indicates **3.1** probably reacts with CHO to generate a monometallic six-coordinate Cr(III) complex, CrCl(CHO)[L2] (Scheme 3-2). The equilibrium constant of the reaction was

estimated to be $8.5 \times 10^2 \text{ M}^{-1}$. Crystallographically authenticated structures of THF and oxetane adducts of the analogs of six-coordinate epoxide complexes, such as (salen)Cr(N₃)·THF and (salen)CrCl·oxetane, have been reported.^{16,18} The Kozak group also previously reported a THF adduct of a monometallic amino-bis(phenolate) Cr(III) complex.¹⁹

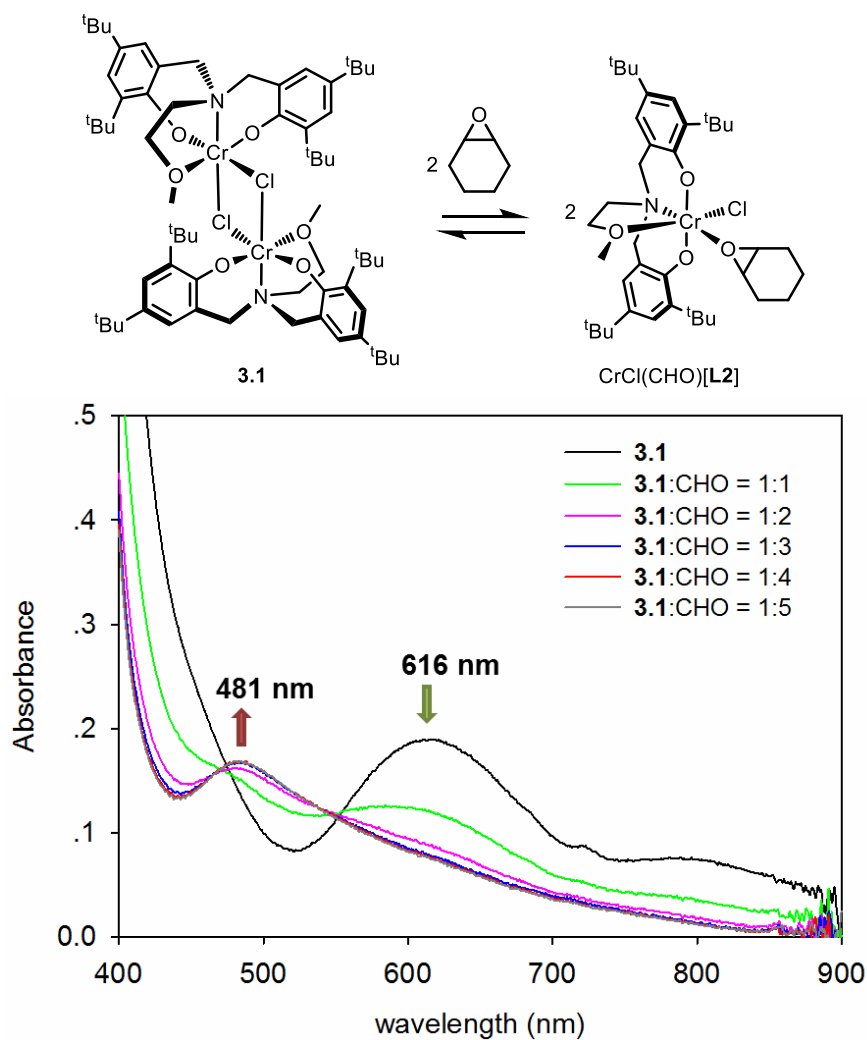
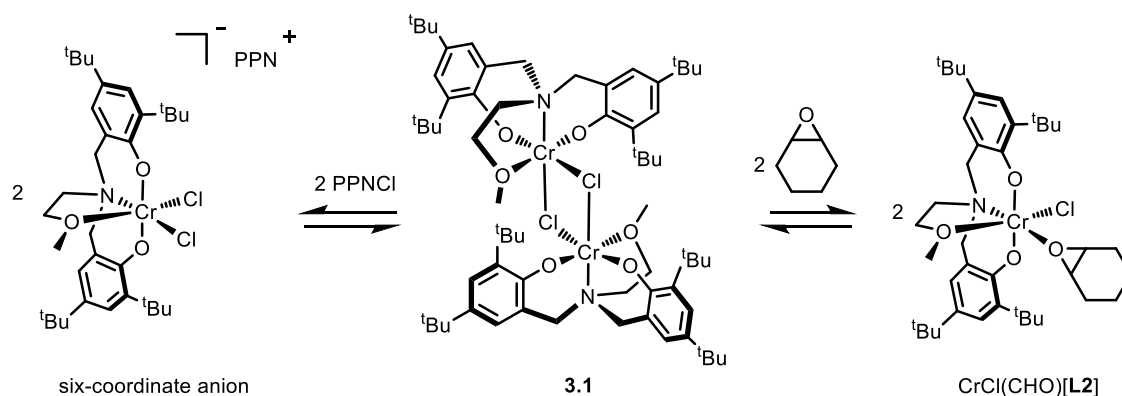


Figure 3-7. UV-Vis spectra of complex **3.1** with different amounts of CHO.



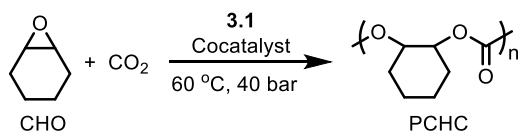
Scheme 3-2. Equilibrium reactions of **3.1** with PPNCl and CHO

3.2.4 Copolymerization of CHO and CO₂

Complex **3.1** combined with PPNCl was employed in the copolymerization of CHO and CO₂ at 60 °C and 40 bar CO₂ (Table 3-2, entries 1-6). The ¹H NMR spectrum (See appendix, Figure C-3) of the resulting product showed PCHC was formed with a negligible amount of ether linkages and no cyclic carbonate was produced. The stereochemistry of the produced polycarbonate was also atactic based on ¹³C NMR spectrum (See appendix, Figure C-4). The initial reactions were investigated with different PPNCl loadings, running for 24 h (Table 3-2, entries 1-4). The best results in terms of the conversion and molecular weight were obtained using one equivalent of PPNCl (per Cr), where 87% conversion was obtained and the molecular weight of resulting polymer reached 18.4 kg mol⁻¹ with a narrow dispersity of ~1.1 (Table 3-2, entry 1). The use of 0.5 equivalents of PPNCl showed a lower conversion (72%), but a higher molecular weight (Table 3-2, entry 2). Complex **3.1**

combined with two equivalents of PPNCI showed a high conversion (87%), however, the molecular weight of obtained polymer decreased and dispersity increased slightly (Table 3-2, entry 3). For related catalyst systems studied by the Kozak group it was consistently found that the polymer molecular weight decreased as the cocatalyst loading ratio was increased.⁸ Rieger and co-workers have also proposed that the growing polymer chain more easily dissociates from the metal center with a high cocatalyst loading, leading to polymer with a low molecular weight.⁴

Table 3-2. Results of the copolymerization of CO₂ and CHO by **3.1**



Entry ^a	Cocat	[Cr]:[CHO]:[Cocat.] (molar ratio)	Time (h)	Conv. (%) ^b	Yield (%) ^c	TON ^c	TOF ^d (h ⁻¹)	M_n^e (kg mol ⁻¹)	\bar{D}^e (M_w/M_n)
1	PPNCl	1:500:1	24	87	68	435	18	18.4	1.12
2	PPNCl	1:500:0.5	24	72	44	360	15	25.9	1.18
3	PPNCl	1:500:2	24	87	60	435	18	13.0	1.46
4	PPNCl	1:500:0	24	2	-	-	-	-	-
5	PPNCl	1:500:1	4	54	32	270	68	9.5	1.05
6	PPNCl	1:500:0.5	4	37	10	185	46	6.2	1.04
7	PPNN ₃	1:500:1	24	87	64	435	18	13.0	1.05
8	DMAP	1:500:1	24	86	51	430	18	20.6	1.05

^aCopolymerization reactions were carried out in neat CHO (5 mL) at 60 °C and 40 bar CO₂. ^bCalculated by ¹H NMR. ^cIsolated yield: mass polymer/expected mass polymer * 100%. ^cTurnover number (TON): moles of repeating units produced per mole of Cr present. ^dTurnover frequency (TOF): moles of repeating units produced per mol of Cr per hour. ^eDetermined by triple detection GPC in THF, dn/dc= 0.0701 mL g⁻¹.

The effect of PPNCl loading on reaction rate was monitored via in situ infrared spectroscopy by following the absorbance at 1750 cm⁻¹ corresponding to the carbonate region. Interestingly, the time profiles demonstrated that complex **3.1** in the presence of two equivalents of PPNCl exhibited the slowest reaction rate with a short induction period (Figure 3-8). This is contrary to the reports on salen Cr(III) complexes and anionic

cocatalysts, where the most efficient catalytic activity was obtained using two equivalents of anionic cocatalyst.¹ This observation, combined with the UV-Vis titration results where the concentration of the six-coordinate anionic species became maximized under two or more equivalents of PPnCl, suggest that the catalytically inactive six-coordinate anionic species is relatively stable during the polymerization. Dissociation of one chloride to produce a vacant site for CHO coordination maybe slow, thus causing an induction period and an overall slower reaction rate. It is worth noting that unlike salen Cr(III) complexes, the geometry of **3.1** directs the incoming nucleophile *cis* to the ancillary chloride ligand, thus forming the *cis*-six-coordinate anionic species. Indeed, a salan Cr(III) complex exhibiting *cis* geometry also showed a decrease in reaction rate when an additional equivalent of PPnN₃ was added.²⁰ When the reactions were stopped after 4 h, the conversion to polymer obtained using one equivalent of PPnCl was higher than that obtained using 0.5 equivalents of PPnCl (Table 3-2, entries 5 and 6), as a result of fewer initiated epoxide ring-opening steps. Polymer molecular weights were lower after 4 h when 0.5 equivalents of PPnCl was used, which can be attributed to a slower reaction rate due to the presence of less active species. When the reaction was run for 24 h, conversion to PCHC was slightly lower for 0.5 equivalents of PPnCl than one equivalent of PPnCl, but higher molecular weight polymer was obtained as expected due to the higher number of CHO monomers per activated epoxide.

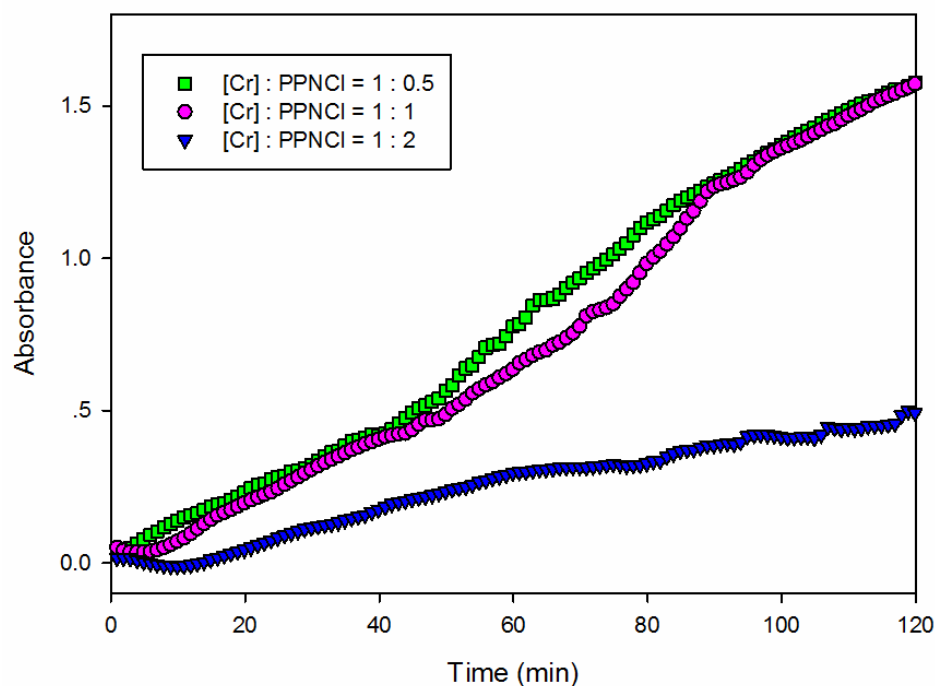


Figure 3-8. Time profiles of the absorbance at 1750 cm^{-1} corresponding to the PCHC obtained using different PPNCI to Cr ratios (Table 3-2, entries 1-3).

Other cocatalysts such as DMAP or PPNN_3 showed similar CHO conversion to PPNCI after 24 h, but the polymer obtained using DMAP as the cocatalyst exhibited the highest molecular weight (Table 3-2, entries 1, 7 and 8). Time profiles of the reactions showed complex **3.1** combined with DMAP exhibited a faster reaction rate than the ionic cocatalysts (Figure 3-9), but PPNN_3 or PPNCI with **3.1** showed similar reaction rates. It is worth noting that for **2.1** described in Chapter 2, the fastest rates were obtained using ionic cocatalyst. This different observation will be discussed in Chapter 4. The reaction exhibited a short induction period in the case of PPNN_3 , which may be a result of a more

complicated reaction equilibrium between complex **3.1** and PPNN₃. Specifically, the negative mode MALDI-TOF mass spectrum of the products obtained from a dichloromethane solution of **3.1** and PPNN₃ exhibited peaks at m/z 631, 638 and 645 which correspond to $[\text{CrCl}_2[\text{L2}]]^-$, $[\text{CrClN}_3[\text{L2}]]^-$ and $[\text{Cr}(\text{N}_3)_2[\text{L2}]]^-$ anions, respectively (Figure 3-10). Similarly Darensbourg reported three crystallographically characterized ionic species (i.e. $[(\text{salen})\text{CrCl}_2]^-$, $[(\text{salen})\text{CrClN}_3]^-$ and $[(\text{salen})\text{CrN}_3]^-$) from a solution of $(\text{salen})\text{CrCl}$ with one equivalent of PPNN₃.¹⁶

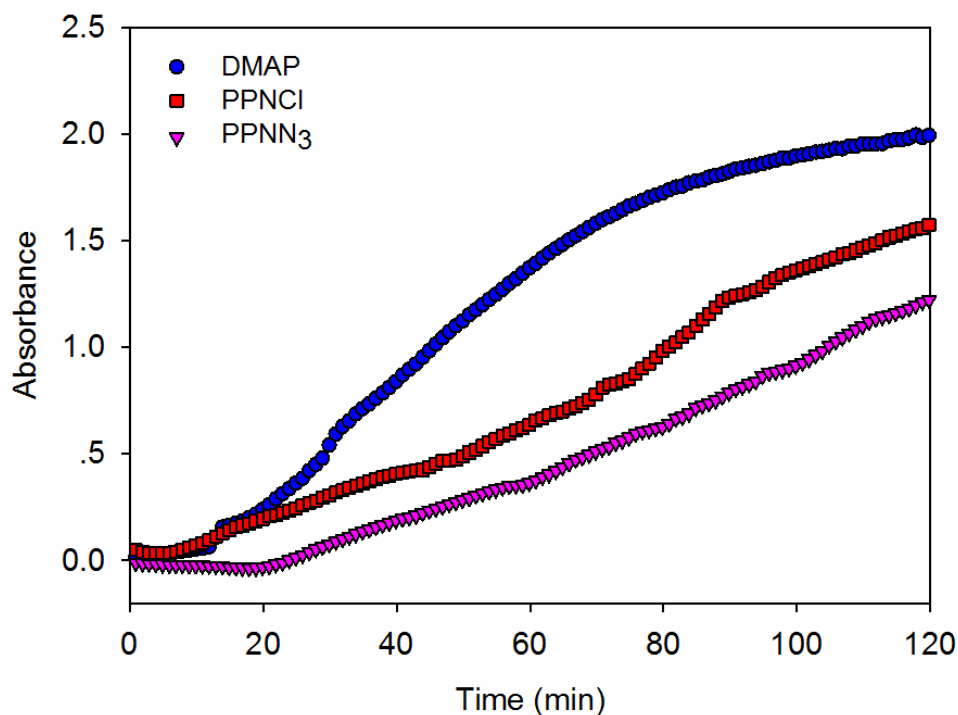


Figure 3-9. Time profiles of the absorbance at 1750 cm^{-1} corresponding to the PCHC obtained using different cocatalysts (Table 3-2, entries 1, 7 and 8).

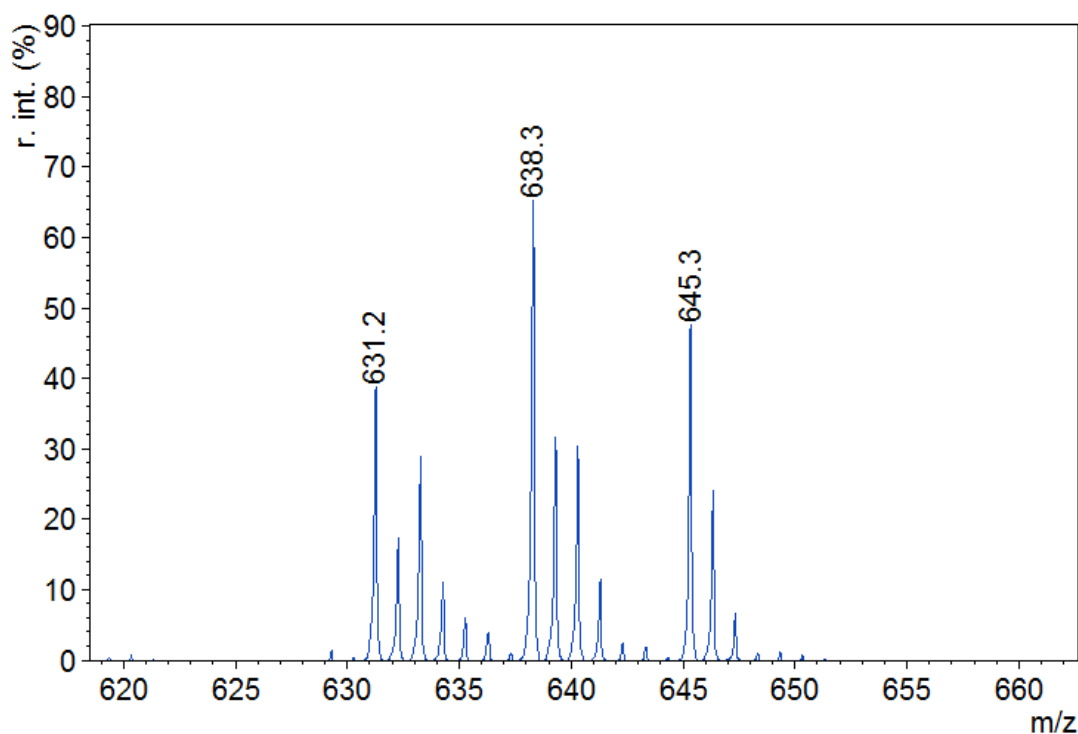


Figure 3-10. MALDI-TOF mass spectrum of the sample of complex **3.1** with PPNN₃ in negative mode.

3.2.5 End-group analysis

MALDI-TOF MS is useful for end-group analysis of the polycarbonates, thus providing insight into the mechanism of the copolymerization of CO₂ and CHO. The polymer produced with PPNNCl as the cocatalyst (Table 3-2, entry 1) showed two major polymer chains (Figure B-5). Two chloride end-groups were observed in the high mass region (Figure 3-11) which could result from chain transfer between the two growing polymer chains initiated by chloride.^{8,9} In the lower mass region, chloride and hydroxyl end-groups were observed, which are expected if the epoxide ring-opening is chloride

initiated and polymerization was terminated by hydrolysis in methanol (Figure 3-12).

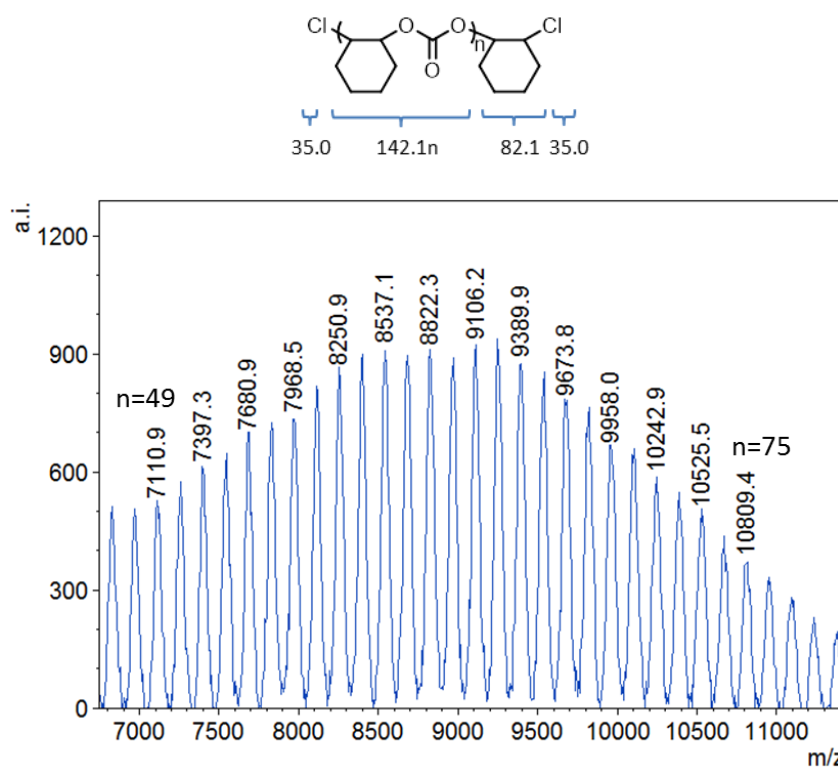


Figure 3-11. Higher mass region (m/z 7111 – 10809, $n = 49 - 75$) of the MALDI-TOF mass spectrum obtained using PPNC1 as cocatalyst (Table 3-2, entry 1).

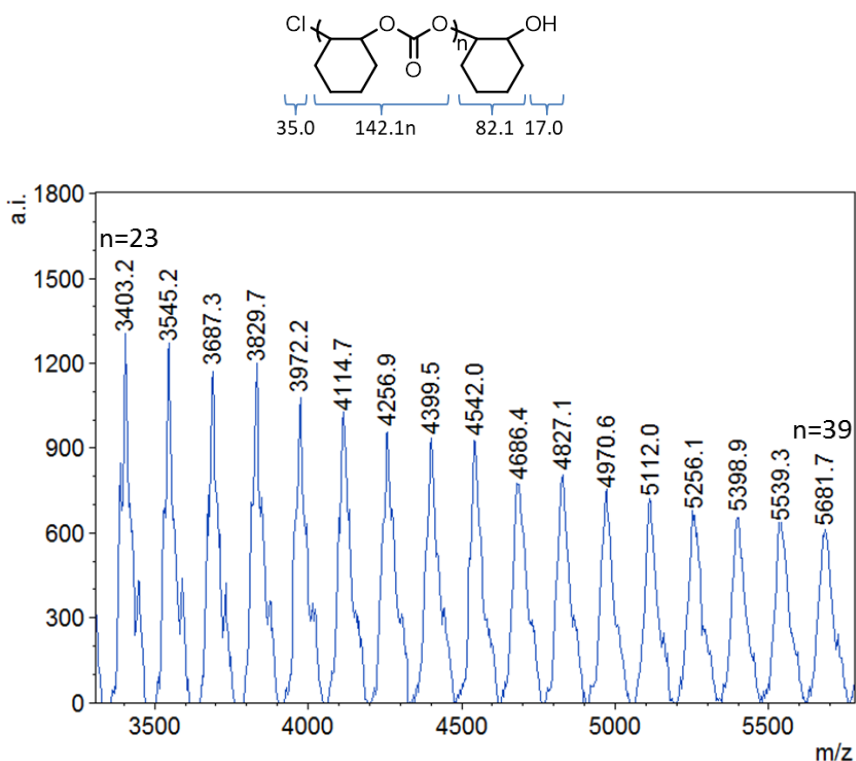


Figure 3-12. Lower mass region (m/z 3403 – 5682, $n = 23 - 39$) of the MALDI-TOF mass spectrum obtained using PPNCI as cocatalyst (Table 3-2, entry 1).

The polymer produced using PPNN_3 as the cocatalyst showed three major polymer chains in the low mass region (Figure 3-13). Series (a) corresponds to the chloride-initiated and hydroxyl group-terminated polymer chain with a K^+ ion. Series (b) represents two hydroxyl groups terminated with one ether linkage and a K^+ ion in the polymer chain, which can be attributed to the presence of adventitious moisture and/or cyclohexene diol causing chain transfer.^{21,22} Series (c) exhibiting the most intense peaks represents the doubly azide-terminated polymer chain with one ether linkage and a Li^+ ion, which could result from chain transfer between two growing polymer chains initiated by azide. The

peaks at high mass region were not identified due to the poor resolution.

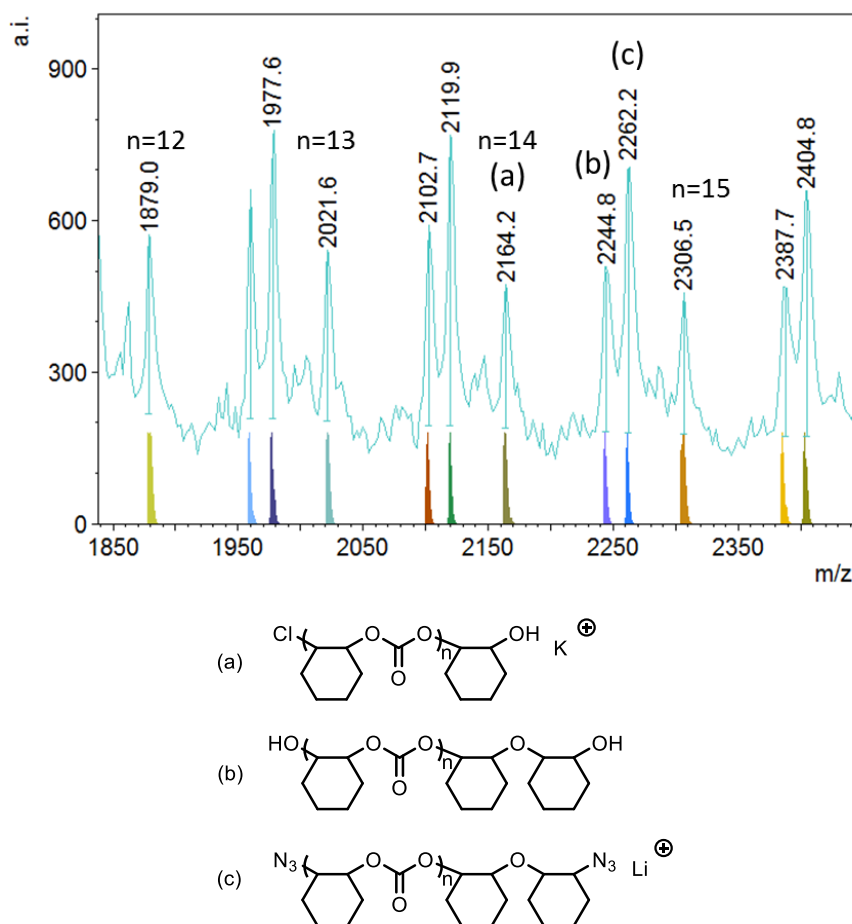


Figure 3-13. Low mass region (m/z 1879 – 2405, n = 12 – 15) of the MALDI-TOF mass spectrum obtained using PPNN₃ as cocatalyst (Table 3-2, entry 7).

When DMAP was used as the cocatalyst, the growing polymer chain was monitored by MALDI-TOF MS by taking aliquots of the reaction mixture at various intervals (Figure 3-14). It should be noted that in order to obtain aliquots, the reaction vessel needed to be depressurized and open to air, therefore the contents were exposed to oxygen and moisture.

The MALDI-TOF mass spectrum of the polymer obtained after 20 min showed only one polymer chain with DMAP and hydroxyl end-groups, indicating DMAP initiation (Figure 3-14, 20 min). The aliquot taken after a further 10 minutes showed the same end-groups and the peaks shifted to a higher molecular weight (Figure 3-14, 30 min) demonstrating that the DMAP-initiated polymerization is well controlled. After further 10 and 20 minutes the MALDI mass spectra of the polymers were identical (Figure 3-14, 40 and 60 min), implying catalysis has halted, possibly due to the sensitivity of the catalyst to moisture.

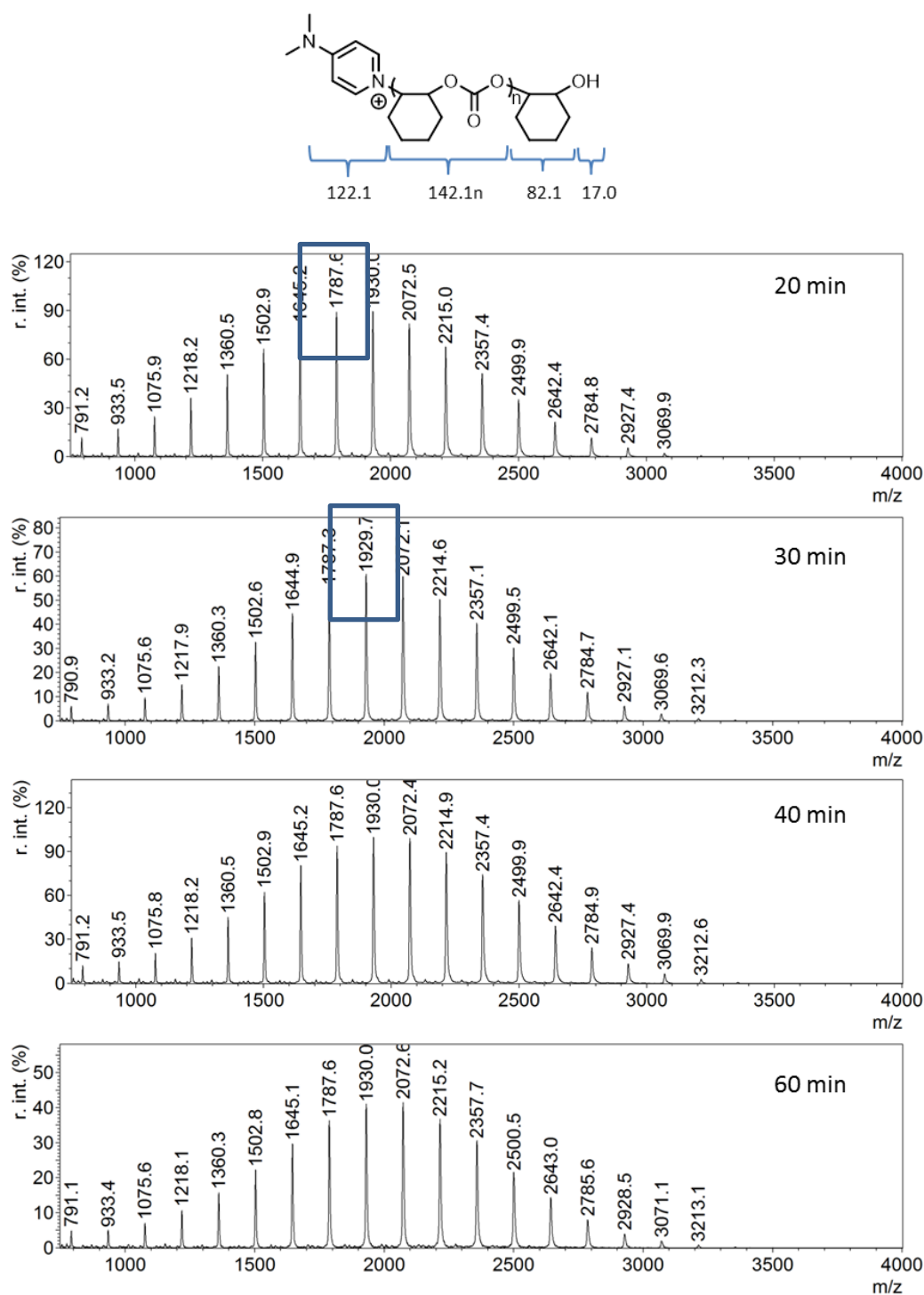


Figure 3-14. MALDI-TOF mass spectra of aliquots obtained at the specified times from the copolymerization of CHO and CO₂ by **3.1** and DMAP.

When the reaction was run for 24 h, the mass spectrum of the resulting polymer obtained by precipitation from methanol only, rather than the typical acidified methanol showed multiple polymer chains in the lower molecular weight region and one major polymer chain in the high molecular weight region (Figure 3-15). After detailed inspection of the end-groups in the low mass region four polymer chains were identified (Figure 3-16). Series (a) represents the polymer chain with two chloride termini and a K^+ ion, resulting from chain transfer between two polymer chains initiated by chloride. Series (b) contains the most intense peaks and corresponds to the presence of two hydroxyl end-groups with two ether linkages due to adventitious moisture and/or impurity of diol causing chain transfer reactions. Series (c) has only one ether linkage compared to series (b). Series (d) belongs to the polymer chain containing one ether linkage and a K^+ ion with hydroxyl and chloride termini. In the high mass region, the polymer chain with DMAP and cyclohexenyl end-groups was observed (Figure 3-17) and is consistent with DMAP initiation as shown in Figure 3-14. The cyclohexenyl end-group probably results from the elimination of HCl or H_2O from the expected chloro or hydroxyl-cyclohexanolate chromium species.^{23,24}

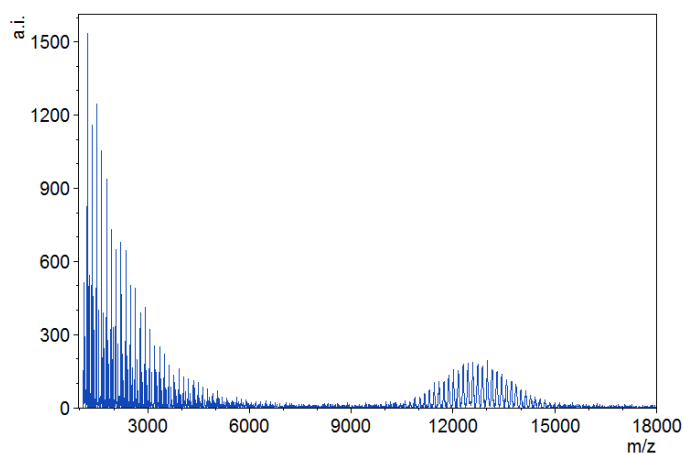


Figure 3-15. MALDI-TOF mass spectrum of the polymer produced using DMAP as cocatalyst (Table 3-2, entry 8).

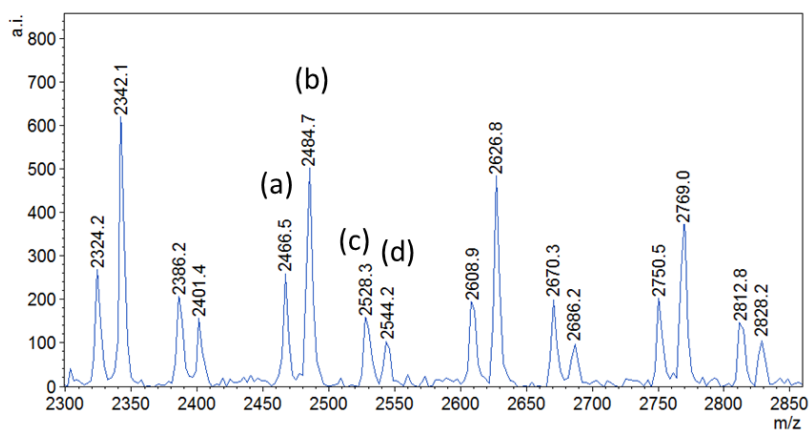
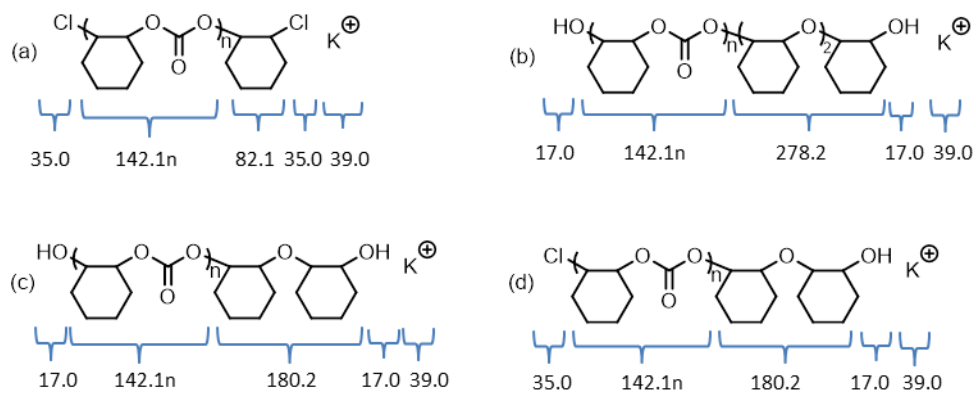


Figure 3-16. MALDI-TOF mass spectrum in the low molecular weight region of the polymer produced using DMAP as cocatalyst (Table 2, entry 8).

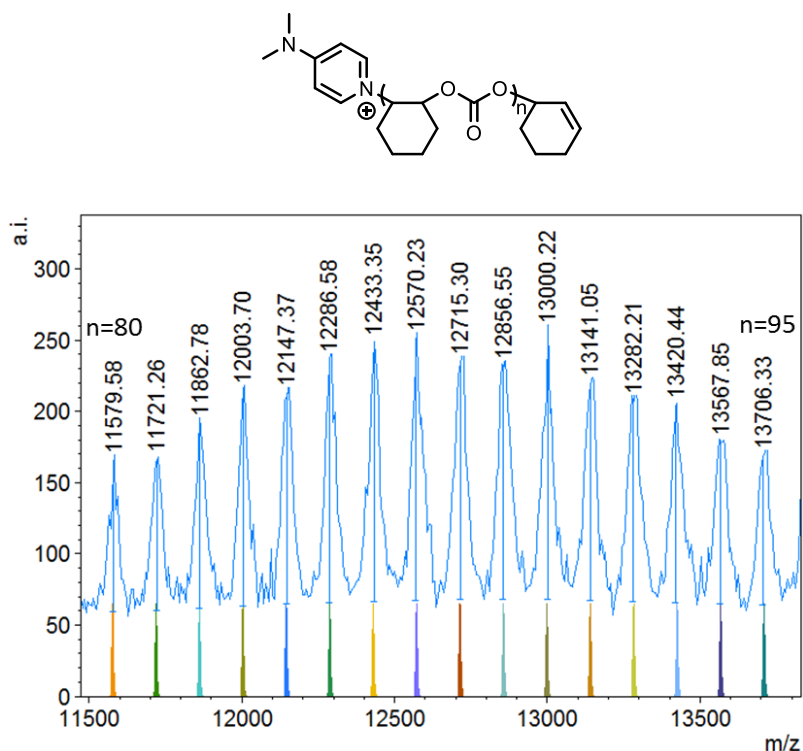
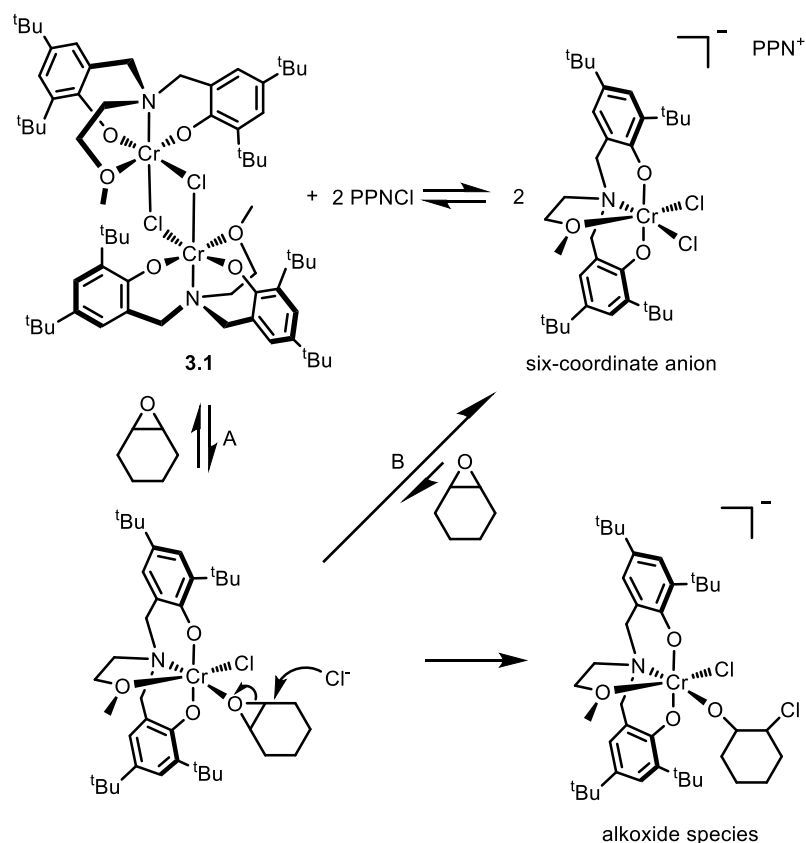


Figure 3-17. MALDI-TOF mass spectrum in the high molecular weight region of the polymer produced using DMAP as cocatalyst (Table 2, entry 8) and the modeled isotopic masses: $C_7H_{10}N_2(DMAP) + (C_7H_{10}O_3)_n$ (repeating unit) + C_6H_9 (cyclohexenyl), $n = 80 - 95$.

3.2.6 Mechanistic considerations

The presence of chloride end-groups in the polymer obtained using PPnCl as the cocatalyst clearly demonstrates the chloride ring-opens CHO. A detailed initiation step for CO_2/CHO copolymerization catalyzed by **3.1** and PPnCl is shown in Scheme 3-3. Initially, a preliminary equilibrium is established among **3.1**, PPnCl and the six-coordinate anionic species. When an excess (500 equivalents) of CHO is added, CHO can bind to **3.1**, subsequently ring-opened by the chloride ion from PPnCl via an intermolecular pathway

(Scheme 3-3, A). Since **3.1** in the absence of PPNCI did not exhibit activity (Table 3-2, entry 4), the ring-opening of CHO by chloride via an intramolecular way is not favored. Alternatively, CHO can also compete with the chloride of the six-coordinate anion to bind to Cr center, the substituted chloride then can ring-open the coordinated CHO (Scheme 3-3, B). When two equivalents of PPNCI was used, the preliminary equilibrium shifted to the right side, affording more inert six-coordinate anions, which resulted in a slower reaction rate and an induction period as shown in Figure 3-8.



Scheme 3-3. Proposed initiation mechanism in the presence of PPNCI as cocatalyst. (A) Major initiation pathway (B) Minor initiation pathway.

Complex **3.1** combined with DMAP exhibited a faster reaction rate than with the ionic cocatalyst, indicating initiation occurs by a different pathway. Lu and co-workers have proposed that the DMAP adduct of salen complex, [(salen)CrX(DMAP)] is the active species where both DMAP and X⁻ can ring-open the epoxide.³ The Kozak group previously proposed a cationic pathway for ring-opening of CHO by a Cr(III) amino-bis(phenolate) complex with DMAP in which the chloride of the Cr(III) complex was replaced by CHO and the dissociated chloride ring-open CHO via an intermolecular pathway.¹² The presence of DMAP end-groups in the MALDI-TOF mass spectra of the obtained polymers (Figure 3-17 and Figure 3-14), however, suggested that DMAP is the initiator. If the initiation mechanism in the case of **3.1** and DMAP also follows the cationic pathway, the ring-opening of CHO is most likely initiated by DMAP via an intramolecular pathway. Baik and Nguyen's computational studies of salenCr and DMAP catalysts for PO/CO₂ copolymerization also support DMAP initiation.² It is worth noting that end-group analysis of the polymer obtained after 24 h (Figure 3-16) demonstrated that the chloride is a possible initiating group, but this is only a minor pathway perhaps once DMAP concentration decreases over the course of the reaction since chloride end-group can only be observed in low mass region.

3.3 Conclusions

A new amino-bis(phenolate) chromium(III) complex bearing methoxy pendant groups **3.1** was synthesized in high yield and characterized by MALDI-TOF mass spectrometry, elemental analysis, UV-Vis spectroscopy and X-ray diffraction. Although this complex in the presence of PPNCl, PPNN₃ or DMAP did not show improved activity for the copolymerization of CHO and CO₂, the spectrophotometric titrations, combined with the copolymerization reaction monitored via React-IR suggested that the six-coordinate anion arising from the addition of ionic cocatalyst to complex **3.1** was kinetically inert for CHO/CO₂ copolymerization. End-group analysis of the polymer obtained by **3.1** with PPNCl, combined with the absence of reactivity without an ionic cocatalyst indicated that the major ring-opening step was most likely initiated by the anion from the cocatalyst via an intermolecular pathway.

3.4 Experimental

3.4.1 General materials

Unless otherwise stated, all manipulations were performed under an atmosphere of dry, oxygen-free nitrogen by means of standard Schlenk techniques or using an MBraun Labmaster DP glove box. CrCl₃(THF)₃ and PPNN₃ were prepared by the previously reported methods.^{25,26} H₂[**L2**] was prepared by a modified literature procedure by using

water instead of methanol as the reaction solvent,²⁷ and dried over sodium sulfate in tetrahydrofuran. Anhydrous THF was distilled from sodium/benzophenone ketyl under nitrogen. Cyclohexene oxide was purchased from Aldrich and freshly distilled from CaH₂ under nitrogen. Dichloromethane was purified by an MBraun Manual Solvent Purification System.

3.4.2 Instrumentation

MALDI-TOF MS was performed using an Applied Biosystems 4800 MALDI TOF/TOF Analyzer equipped with a reflectron, delayed ion extraction and high performance nitrogen laser (200 Hz operating at 355 nm). Complex samples were prepared in the glove box and sealed under nitrogen in a Ziploc® bag for transport to the instrument. Anthracene was used as the matrix for complexes **3.1**. 2,5-Dihydroxybenzoic acid (DHBA) was used as the matrix for the copolymers. Anthracene and complex were each dissolved in toluene at concentrations of 10 mg·mL⁻¹. The matrix and complex solutions were combined in a ratio of 1:1 as the analyzed sample. DHBA was dissolved in THF at approximately 16 mg·mL⁻¹ and polymer was dissolved in THF at approximately 10 mg·mL⁻¹. The matrix and polymer solutions were combined in a ratio of 3:1 as the analyzed sample. 1 µL aliquots of these samples were spotted on the MALDI plate and left to dry. Images of mass spectra were prepared using mMass™ software

(www.mmass.org).

Molecular weight determination of the obtained copolymers was performed by GPC on an Agilent Infinity HPLC instrument connected to a Wyatt Technologies triple detector system (light scattering, viscometry and refractive index) equipped with two Phenogel 10³ Å 300 × 4.60 mm columns with THF as eluent. Copolymer samples were prepared in THF at a concentration of 4 mg mL⁻¹ and filtered through syringe filters (0.2 µm). The sample solution was then eluted at a flow rate of 0.30 mL·min⁻¹. The values of dn/dc were calculated online (columns detached) assuming 100% mass recovery using the Astra 6 software package (Wyatt Technologies) giving dn/dc (poly(cyclohexene carbonate) = 0.0701 mL·g⁻¹).

¹H and ¹³C NMR spectra were recorded at 300 MHz and 75 MHz respectively on a Bruker Avance III spectrometer. CDCl₃ was used for NMR solvent which was purchased from Cambridge Isotope Laboratories. Elemental analysis was performed at Guelph Chemical Laboratories, Guelph, ON, Canada. In situ infrared experiments were performed on a ReactIR 15TM reaction analysis system with a SiComp Sentinel probe.

UV-Vis spectroscopy was conducted on a dual-beam Evolution 300 UV-Vis spectrophotometer equipped with a xenon lamp. Complex **3.1** (30 mg, 5.0 × 10⁻² mmol (per Cr)) was dissolved in 50 mL dichloromethane. Because the Cr(III) amino-bi(phenolate) complexes are air sensitive, a special cuvette was used in this

experiment (see Figure 3-18). The appropriate amount of PPnCl was successively added into **3.1** solution for analysis.



Figure 3-18. The special cuvette used for UV-Vis titration under inert atmosphere.

3.4.3 Synthesis of complex **3.1**

$\text{H}_2[\text{L2}]$ (2.00 g, 3.90 mmol) and sodium hydride (0.38 g, 15.60 mmol) in a Schlenk tube were cooled to $-78\text{ }^\circ\text{C}$ with a dry ice bath. THF ($\sim 50\text{ mL}$) was transferred to the mixture, which was then warmed to room temperature and further stirred for 2 h. The resulting suspension was transferred via filter cannula to a suspension of $\text{CrCl}_3(\text{THF})_3$ (2.50 g, 6.67 mmol) in THF ($\sim 50\text{ mL}$) at $-78\text{ }^\circ\text{C}$ to give a pink/purple mixture. The mixture was warmed to room temperature and stirred 18 h to give a dark purple solution. The solvent was removed under vacuum. The solid residue was extracted into toluene and filtered through a pad of Celite. As the complex is not very soluble in toluene, the extraction was repeated two times by addition of toluene into the remaining solid in the

pad containing Celite. Toluene was then removed under vacuum. The residue was washed with pentane and dried to yield 1.14 g (49%) of green powder. Crystals suitable for X-ray diffraction were obtained by slow evaporation of a solution of **3.1** in toluene at room temperature in a glovebox under nitrogen. Calculated (%) for $C_{66}H_{102}Cl_2Cr_2N_2O_6$: C, 66.37; H, 8.64; N, 2.35. Found (%): C, 66.13; H, 8.42; N, 2.62. MS (MALDI-TOF) m/z (% ion): 596.3 (100, $CrCl[L2]^+$), 561.3 (50, $Cr[L2]^+$), 1157.5 (9, $[Cr[L2]]_2Cl^+$) and 1194.5 (3, $[CrCl[L2]]_2^{++}$)

3.4.4 Copolymerization conditions

Complex **3.1** (59 mg, 4.9×10^{-2} mmol) and the appropriate amount of ionic cocatalyst were firstly dissolved in ~ 3 mL of dichloromethane and allowed to stir for 10 min before removal of solvent in vacuum. CHO (4.9 g, 49 mmol) was added to the residue and stirred for 10 min. The reactant solution/suspension was added via syringe to a stainless steel Parr autoclave, which was pre-dried under vacuum overnight at 80 °C. The autoclave was heated to 60 °C, then charged with 40 bar of CO_2 and left to stir. After the desired time the autoclave was cooled in an ice bath and vented in the fume hood. An aliquot for 1H NMR was taken immediately after opening for the determination of conversion. The copolymer was extracted with dichloromethane and precipitated out by adding cold methanol. The product was then dried through Schlenk line overnight. For

the reaction done in the presence of DMAP, complex **3.1** and DMAP were directly dissolved in CHO. The remaining procedure was followed in the same manner as described above.

3.5 References

- (1) Darensbourg, D. J.; Mackiewicz, R. M. *J. Am. Chem. Soc.* **2005**, *127*, 14026.
- (2) Adhikari, D.; Nguyen, S. T.; Baik, M.-H. *Chem. Commun.* **2014**, *50*, 2676.
- (3) Rao, D.-Y.; Li, B.; Zhang, R.; Wang, H.; Lu, X.-B. *Inorg. Chem.* **2009**, *48*, 2830.
- (4) Luinstra, G. A.; Haas, G. R.; Molnar, F.; Bernhart, V.; Eberhardt, R.; Rieger, B. *Chem. Eur. J.* **2005**, *11*, 6298.
- (5) Xiao, Y.; Wang, Z.; Ding, K. *Macromolecules* **2006**, *39*, 128.
- (6) Chisholm, M. H.; Zhou, Z. *J. Am. Chem. Soc.* **2004**, *126*, 11030.
- (7) Cheng, M.; Moore, D. R.; Reczek, J. J.; Chamberlain, B. M.; Lobkovsky, E. B.; Coates, G. W. *J. Am. Chem. Soc.* **2001**, *123*, 8738.
- (8) Dean, R. K.; Dawe, L. N.; Kozak, C. M. *Inorg. Chem.* **2012**, *51*, 9095.
- (9) Dean, R. K.; Devaine-Pressing, K.; Dawe, L. N.; Kozak, C. M. *Dalton Trans.* **2013**, *42*, 9233.
- (10) Chen, H.; Dawe, L. N.; Kozak, C. M. *Catal. Sci. Tech.* **2014**, *4*, 1547.
- (11) Kozak, C. M.; Woods, A. M.; Bottaro, C. S.; Devaine-Pressing, K.; Ni, K. *Farad. Discuss.* **2015**.
- (12) Devaine-Pressing, K.; Dawe, L. N.; Kozak, C. M. *Polym. Chem.* **2015**, *6*, 6305.
- (13) MacAdams, L. A.; Kim, W.-K.; Liable-Sands, L. M.; Guzei, I. A.; Rheingold, A. L.; Theopold, K. H. *Organometallics* **2002**, *21*, 952.

- (14) Wong, E. W. Y.; Das, A. K.; Katz, M. J.; Nishimura, Y.; Batchelor, R. J.; Onishi, M.; Leznoff, D. B. *Inorg. Chim. Acta* **2006**, *359*, 2826.
- (15) Gibson, V. C.; Newton, C.; Redshaw, C.; Solan, G. A.; White, A. J. P.; Williams, D. J. *Eur. J. Inorg. Chem.* **2001**, 1895.
- (16) Darensbourg, D. J.; Moncada, A. I. *Inorg. Chem.* **2008**, *47*, 10000.
- (17) Chatterjee, C.; Chisholm, M. H. *Inorg. Chem.* **2011**, *50*, 4481.
- (18) Darensbourg, D. J.; Mackiewicz, R. M.; Billodeaux, D. R. *Organometallics* **2005**, *24*, 144.
- (19) Dean, R. K.; Granville, S. L.; Dawe, L. N.; Decken, A.; Hattenhauer, K. M.; Kozak, C. M. *Dalton Trans.* **2010**, *39*, 548.
- (20) Darensbourg, D. J.; Ulusoy, M.; Karroonnirum, O.; Poland, R. R.; Reibenspies, J. H.; Cetinkaya, B. *Macromolecules* **2009**, *42*, 6992.
- (21) Nakano, K.; Nakamura, M.; Nozaki, K. *Macromolecules* **2009**, *42*, 6972.
- (22) Jutz, F.; Buchard, A.; Kember, M. R.; Fredriksen, S. B.; Williams, C. K. *J. Am. Chem. Soc.* **2011**, *133*, 17395.
- (23) Van Meerendonk, W. J.; Duchateau, R.; Koning, C. E.; Gruter, G.-J. M. *Macromolecules* **2005**, *38*, 7306.
- (24) Buchard, A.; Kember, M. R.; Sandeman, K. G.; Williams, C. K. *Chem. Commun.* **2011**, *47*, 212.

(25) So, J. H.; Boudjouk, P. *Inorg. Chem.* **1990**, *29*, 1592.

(26) Demadis, K. D.; Meyer, T. J.; White, P. S. *Inorg. Chem.* **1998**, *37*, 3610.

(27) Tshuva, E. Y.; Groysman, S.; Goldberg, I.; Kol, M.; Goldschmidt, Z.

Organometallics **2002**, *21*, 662.

Chapter 4. MALDI-TOF and ESI MS analysis studies of the binding of azide to amino-bis(phenolate) Cr(III) chloride complexes: Mechanistic understanding of catalytic CO₂/cyclohexene oxide copolymerization

4.1 Introduction

Mechanistic understanding of a catalyzed reaction is important for the design of highly efficient catalyst systems and several excellent mechanistic studies of CO₂/epoxide copolymerization have been reported.¹⁻³ Mass spectrometry (MS), is a useful tool for mechanistic studies since it affords insight into the molecular composition of transition metal complexes.⁴ Particularly, soft ionization MS such as ESI-MS^{5,6} and more recent MALDI-TOF MS^{7,8} have been widely used in mechanistic studies as they can keep weakly bound ligand intact in a complex ion. Chen and co-workers have employed electrospray tandem mass spectrometry to study the binding of propylene oxide (PO) to a series of salen complexes with different metals and discussed these results in terms of catalytic activities towards the copolymerization of PO with CO₂.⁹ ESI-MS has been used by Lu and co-workers to confirm intermediates in PO/CO₂ copolymerization by a single-site cobalt(III) salen catalyst.¹⁰ MALDI-TOF MS has also been used by Duchateau and co-workers to identify unexpected side reactions and chain transfer reactions for the zinc catalyzed copolymerization of cyclohexene oxide (CHO) and CO₂.^{11,12}

Darensbourg and co-workers have carried out elegant kinetic studies on the copolymerization of epoxide and CO₂ catalyzed by salenCr(III) complexes with Lewis bases where initiation was proposed to occur via a bimetallic process and propagation proceeded via a monometallic ring-opening of epoxide.¹³⁻¹⁶ Their studies also suggest the Lewis base coordinates to the Cr center trans to the growing polymer chain, thus labilizing the propagation alkoxide or carbonate ligand. However, these salen-based complexes conjugated with organic Lewis base typically exhibit induction periods.^{14,16} Recently, Lu and co-workers have used ESI-MS to study the binding of the organic Lewis base DMAP to salenCr(III) and salanCr(III) complexes in which they clearly demonstrated that salenCr(III) complexes readily bind two DMAP molecules, whereas salanCr(III) complexes preferentially bind only one DMAP.¹⁷ This difference in DMAP binding affinity was found to result in a significantly different catalytic activity for PO/CO₂ copolymerization. Specifically, salenCr(III)/DMAP exhibited a long induction period of up to 2 h, however, a very short or no induction period was observed for salanCr(III)/DMAP. It was proposed that DMAP dissociation from the bis-DMAP adduct was difficult, hindering formation of the active species. This was also thought to be the cause of the long induction period exhibited by salenCr(III)/DMAP.

In the Kozak group, amino-bis(phenolate) Cr(III) chloride complexes have been investigated for CO₂/epoxide copolymerization.¹⁸⁻²¹ In the presence of the neutral

co-catalyst DMAP, or the ionic nucleophiles chloride or azide paired with bulky bis(triphenylphosphoranylidene)ammonium cation, these Cr(III) complexes have shown promising activities towards epoxide/CO₂ copolymerization. The binding of DMAP to amino-bis(phenolate) Cr(III) chloride complexes with different pendant donor groups (Figure 4-1, **2.1**, **4.1-4.4**) was also studied via MALDI-TOF MS.²² The Cr(III) amino-bis(phenolate) complex containing a dimethylaminoethyl pendant group (**2.1**) prefers to bind one DMAP, while the other derivatives having methoxyethyl (**4.1**), tetrahydrofuran (**4.2**) or pyridyl pendant donor groups (**4.3** and **4.4**) readily bind two DMAP molecules. Similar to the observations of Lu and co-workers where slight differences in the electronic and steric properties of the two similar salen and salan-containing catalyst systems impact the resulting activity for CO₂/epoxide copolymerization, this difference in affinity for DMAP binding in Cr(III) amino-bis(phenolate) complexes resulting from the nature of pendant donor group was also found to influence their catalytic activity for this reaction. Specifically, the amino-bis(phenolate) Cr(III) chloride complex with the dimethylaminoethyl donor group (**2.1**) exhibits higher catalytic activity than the other derivatives studied. These observations, therefore, warranted further investigations.

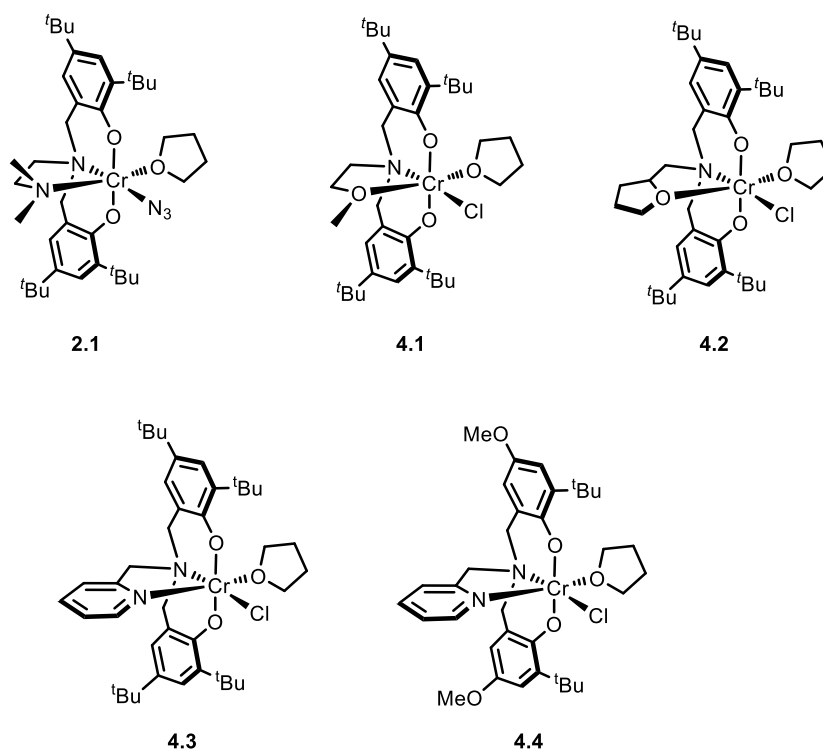


Figure 4-1. Chromium(III) complexes with different pendant donor groups.

In this chapter, the binding of the ionic cocatalyst, PPNN₃, to the amino-bis(phenolate) Cr(III) chloride complexes was studied because of the smaller steric demand of azide compared to DMAP as well as their anticipated electronic differences. Both MALDI-TOF MS and ESI-MS were used to study the binding of azide to the amino-bis(phenolate) Cr(III) chloride complexes (Figure 4-2) wherein the dimethylaminoethyl (**2.1**) and methoxyethyl (**3.1**) pendant donor groups were employed since they exhibit significant difference in steric and electronic properties. The ring-opening step of epoxide was also examined by ESI-MS and MALDI-TOF MS. These investigations, combined with kinetic studies by

infrared spectroscopy, provided some mechanistic insight into the copolymerization of CO₂ and CHO catalyzed by amino-bis(phenolate) Cr(III) chloride complexes and PPNN₃.

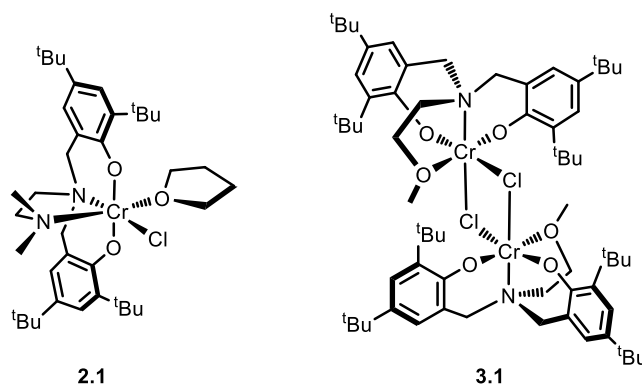


Figure 4-2. Amino-bis(phenolate) Cr(III) chloride complexes **2.1** and **3.1**.

4.2 Results and discussion

4.2.1 Binding of azide to amino-bis(phenolate) Cr(III) chloride complexes

MALDI-TOF MS was used to study the binding of azide to **2.1** and **3.1** by preparing dichloromethane solutions of each complex with the anthracene matrix and varying ratios of PPNN₃. These solutions were spotted on the MALDI plate within a nitrogen-filled glove box and mass spectra were collected in negative mode. The ions observed are shown in Figure 4-3 and the mass spectra obtained using varying amounts of PPNN₃ are shown in Figure 4-4. The spectrum of **3.1** in the presence of 0.5 equivalents of PPNN₃ exhibited three new species at m/z 603, 638 and 645, which correspond to $[\mathbf{L2CrN_3}]^{\bullet-}$ (**F3**), $[\mathbf{L2CrClN_3}]^{\bullet-}$

(**F5**) and $[\text{L2Cr}(\text{N}_3)_2]^-$ (**F6**), respectively. Similarly, the mass spectra of **2.1**, combined with varying amounts of PPNN₃ also showed three ions at m/z 616, 651 and 658 representing $[\text{L1CrN}_3]^-$ (**F3**), $[\text{L1CrClN}_3]^-$ (**F5**) and $[\text{L1Cr}(\text{N}_3)_2]^-$ (**F6**), respectively. These observations demonstrated replacement of chloride in amino-bis(phenolate) Cr(III) chloride complexes by azide occurred in both **2.1** and **3.1**. (salen)CrCl in combination with PPNN₃ has also been reported to form the three ions, $[(\text{salen})\text{CrCl}_2]^-$, $[(\text{salen})\text{Cr}(\text{N}_3)\text{Cl}]^-$, and $[(\text{salen})\text{Cr}(\text{N}_3)_2]^-$, which were characterized by ESI-MS and X-ray diffraction.²³ It is important to note when the molar ratio of PPNN₃ to **3.1** (per Cr) was 1 to 1, the bis-azide species, $[\text{L2Cr}(\text{N}_3)_2]^-$ (**F6**) at m/z 645 became the base peak (Figure 4-4). However, in the case of **2.1**/PPNN₃ the bis-azide species of $[\text{L1Cr}(\text{N}_3)_2]^-$ (**F6**) ion at m/z 658 required 2 equivalents of PPNN₃ to become the base peak (Figure 4-4). Since the conditions of the preparation of these analyte mixtures and the instrumental conditions used to collect the mass spectra are identical, this observation suggests complex **3.1** in the presence of PPNN₃ forms bis-azide species more easily than complex **2.1**. Additionally, a striking difference in the relative abundance of the five-coordinate species $[\text{LCrCl}]^-$ (**F2**) between **3.1**/PPNN₃ and **2.1**/PPNN₃ was also observed (Figure 4-5). The relative abundance of the five-coordinate ion (**F2**) in the **3.1**/PPNN₃ mixture dramatically decreased with increasing proportion of PPNN₃, while the relative abundance of **F2** in the **2.1**/PPNN₃ mixture was resistant to decrease, and still showed more than 60% even in the presence of 10

equivalents of PPNN₃. This significantly different trend in the relative abundance of **F2** ion clearly demonstrates in the presence of PPNN₃ complex **2.1** can generate much more five-coordinate species (**F2**) than complex **3.1**.

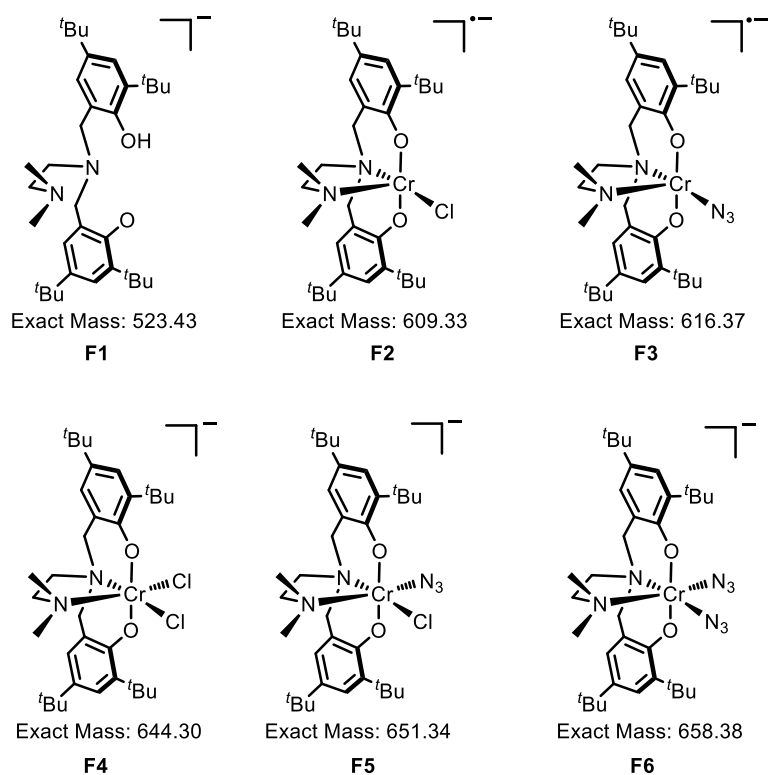
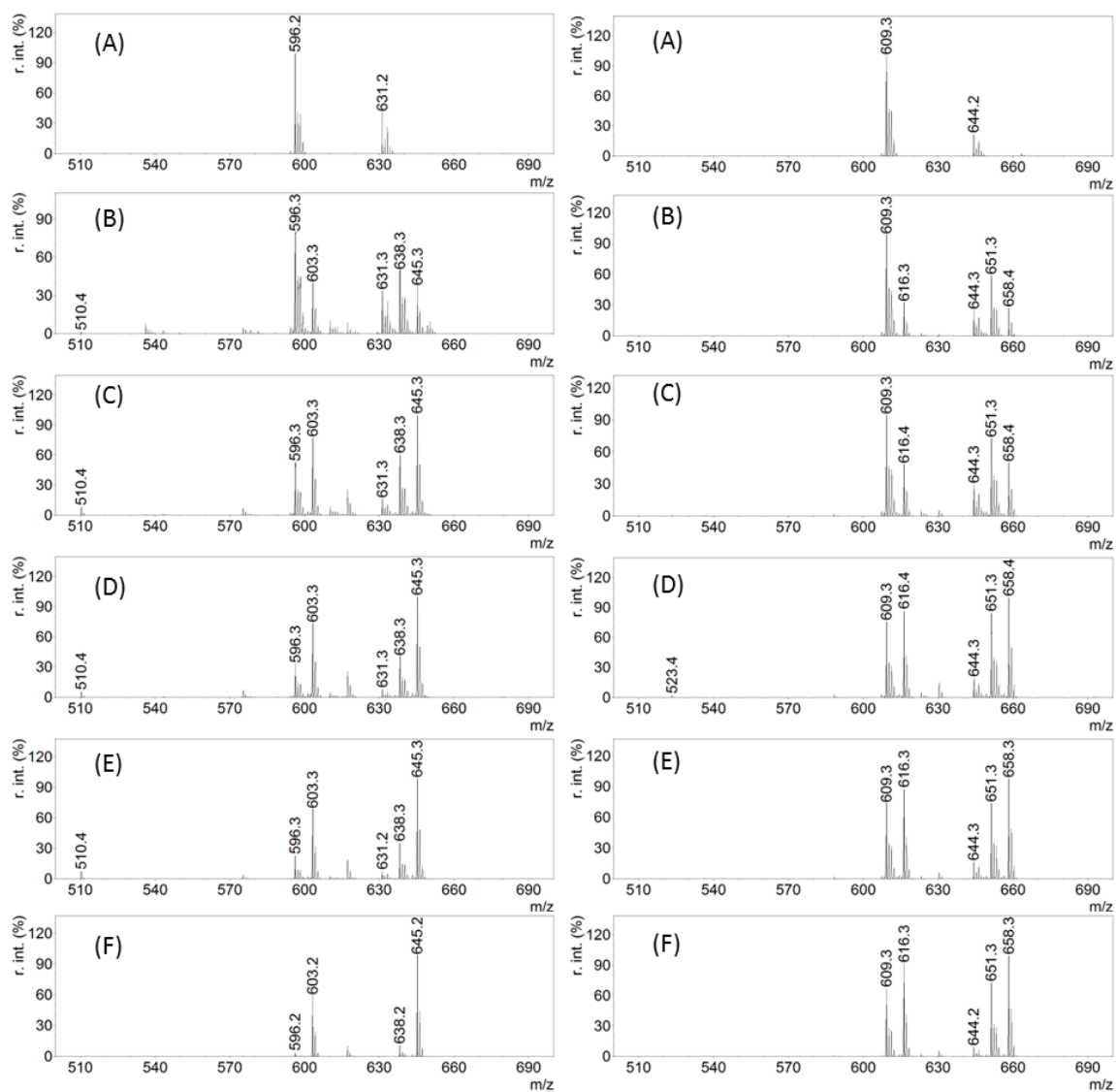


Figure 4-3. Anions and radical anions observed in the MALDI-TOF mass spectra of **2.1** with added PPNN₃. The corresponding ions of **3.1** are represented by the analogous structures shown for F1–F6.



3.1/PPNN₃

2.1/PPNN₃

Figure 4-4. MALDI-TOF mass spectra of different molar ratios of **3.1**/PPNN₃ and **2.1**/PPNN₃. (A) 1:0, (B) 1:0.5, (C) 1:1, (D) 1:2, (E) 1:4, and (F) 1:10.

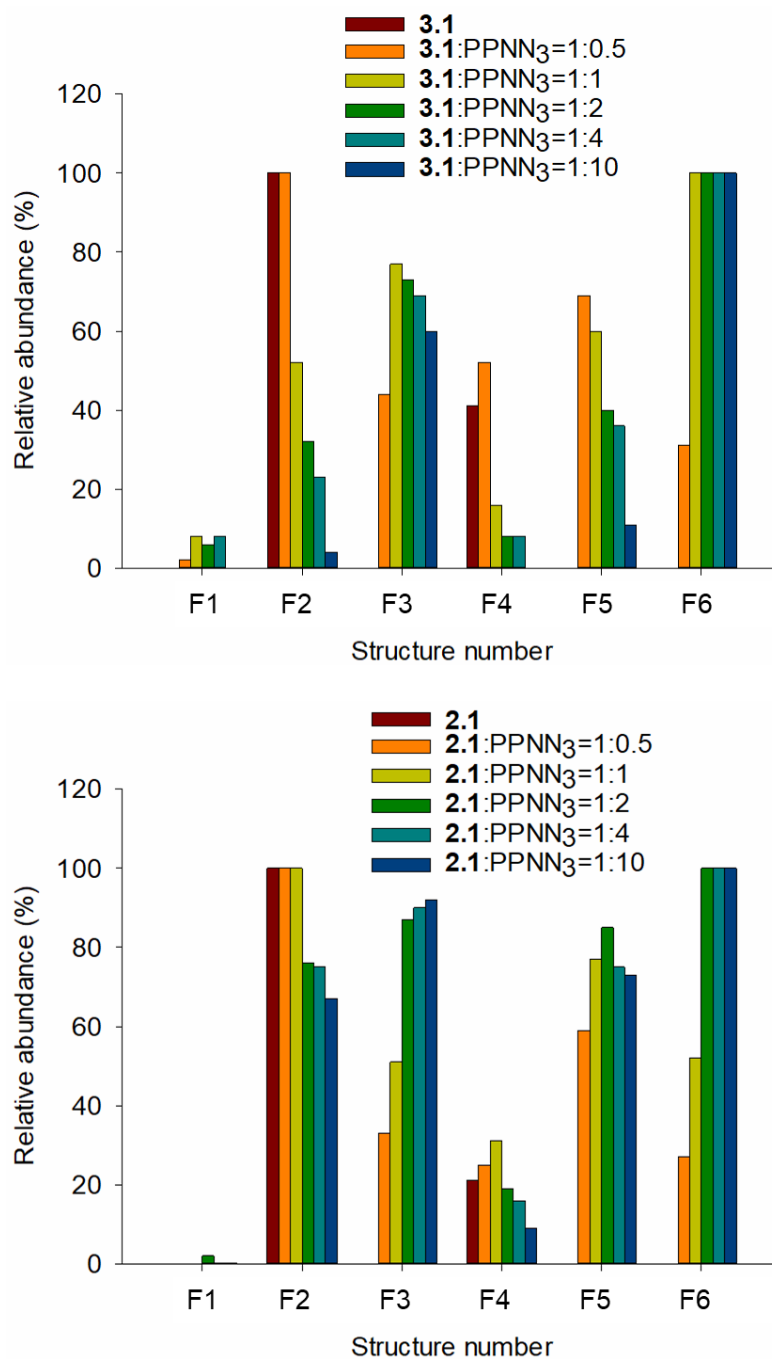


Figure 4-5. Comparison of relative abundance of ions observed by MALDI-TOF MS for complexes **3.1** (top) and **2.1** (bottom) with varying amounts of PPNN₃ as shown. Relative abundance is given in % and structure numbers F1–F6 correspond to ions shown in Figure 4-3.

Acetonitrile solutions of PPNN₃ with **3.1** and **2.1** in various ratios were further studied using ESI-MS. The negative mode ESI mass spectra of different ratios of **3.1**/PPNN₃ and **2.1**/PPNN₃ are illustrated in Figure 4-6 and a comparison of the relative abundance of the observed ions is shown in Figure 4-7. It is worth noting that unlike the studies by MALDI-TOF MS, ESI-MS spectra showed that the relative abundance of unmetallated ligand ion of [LH]⁻ (**F1**) was not negligible. Specifically, a significant abundance of unmetallated ligand ion were observed in the case of **3.1**/PPNN₃ (Figure 4-7). This may suggest the ligand with methoxy pendant donor is more weakly coordinated to Cr than that with dimethyl amine pendant donor, which is consistent with our previous observation by MALDI-TOF MS.²² When 0.5 equivalents of PPNN₃ was added to **3.1**, the spectrum showed (Figure 4-6, left) three new peaks at *m/z* 510, 638, and 645, which correspond to [L2H]⁻ (**F1**), [L2CrClN₃]⁻ (**F5**) and [L2Cr(N₃)₂]⁻ (**F6**), respectively. When the ratio of **3.1** to PPNN₃ was 1 to 1 (Figure 4-6, left), the bis-azide species of [L2Cr(N₃)₂]⁻ (**F6**) at *m/z* 645 became the most abundant. In contrast, when 0.5 equivalents of PPNN₃ were added to **2.1**, (Figure 4-6, right) the bis-azide species (**F6**) at *m/z* 658 was negligible and only became the most abundant ion in the presence of 2 equivalents of PPNN₃ (Figure 4-6, right). These observations also suggest complex **3.1** more easily binds two azide ligands than complex **2.1**, which is consistent with the observation by MALDI-TOF MS as discussed above.

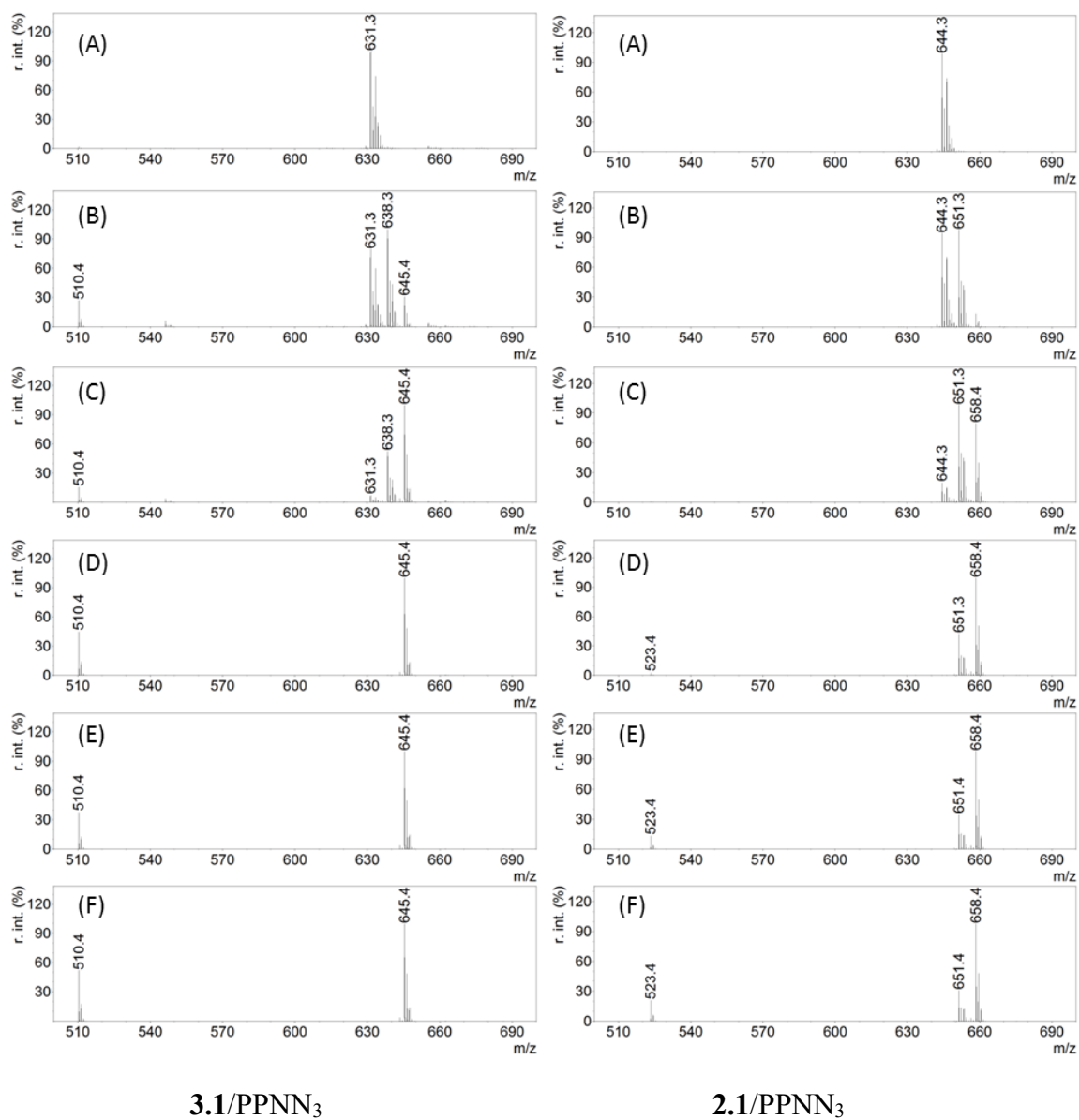


Figure 4-6. Negative mode ESI mass spectra of mixtures of **3.1**/PPNN₃ (left) and **2.1**/PPNN₃ (right) in the following molar ratios: (A) 1:0, (B) 1:0.5, (C) 1:1, (D) 1:2, (E) 1:4, and (F) 1:10.

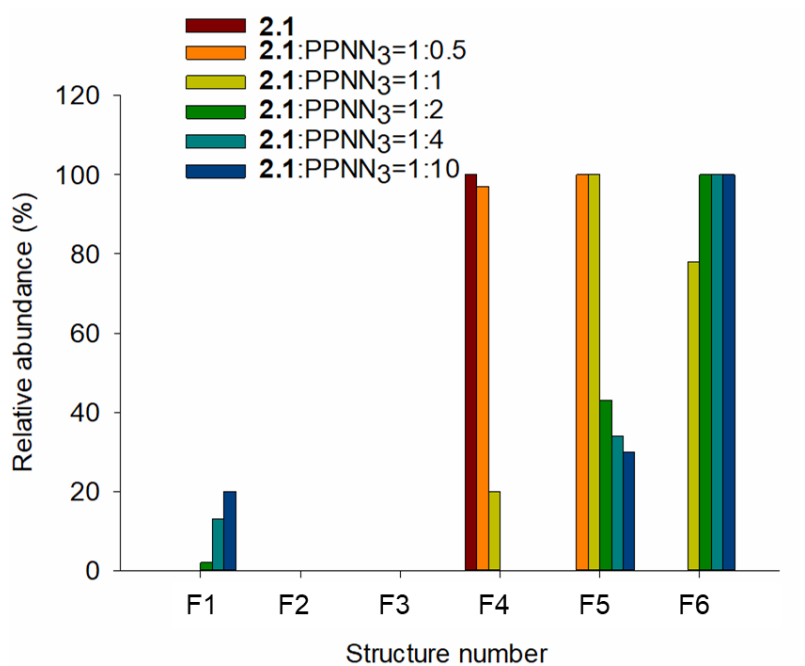
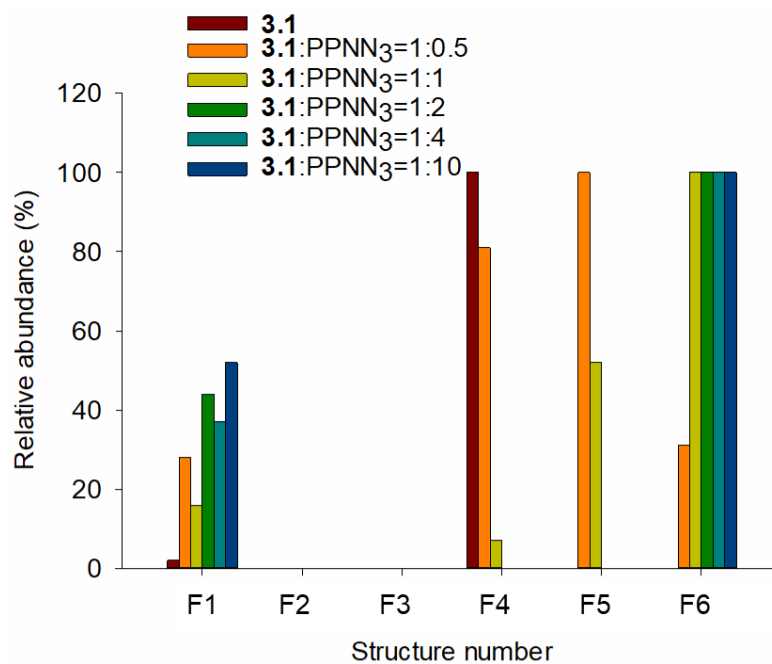


Figure 4-7. Comparison of relative abundance of ions observed by ESI-MS for complexes **3.1** (top) and **2.1** (bottom) with varying amounts of PPNN₃ as shown. Relative abundance is given in % and structure numbers F1–F6 correspond to ions shown in Figure 4-3.

4.2.2 Ring-opening steps examined by ESI-MS

End-group analysis of the polymer by MALDI-TOF or ESI MS is the most common method to identify the initiating species, particularly if the bond formed is stable to cleavage by hydrolysis.²⁴⁻²⁸ Darensbourg and co-workers also monitored the initial ring-opening step by analyzing the solution of CHO/(salen)CrCl/*n*-Bu₄NN₃ with infrared spectroscopy.²³ After addition of a 100-fold excess of CHO to the catalyst system, an organic azide infrared band at 2100 cm⁻¹ was observed and increased in intensity with time at ambient temperature, demonstrating azide-initiated ring-opening of CHO. To investigate the initial ring-opening species of our catalyst system, a mixture of **2.1**/PPNN₃/CHO in a ratio of 1:1:20 was studied by negative ion mode ESI-MS. The ESI mass spectrum observed for the mixture of **2.1**/PPNN₃/CHO showed a major peak at *m/z* 651 corresponding to [L1CrClN₃]⁻ (Figure 4-8). Interestingly, three new species at *m/z* 742, 749 and 756 with relatively low abundance were also observed, which correspond to the alkoxide-containing anions [L1CrCl(C₆H₁₀O)Cl]⁻, [L1CrCl(C₆H₁₀O)N₃]⁻ and [L1CrN₃(C₆H₁₀O)N₃]⁻, respectively (Figure 4-8). These three observed ions confirmed both the chloride from the Cr(III) complex and the azide from PPNN₃ can ring-open CHO, which is also consistent with the observed MALDI-TOF mass spectrum of the polymer obtained by **2.1** and PPNN₃, which showed chloride or azide occurred as the end group (Figure 4-9). In the case of the ion [L1CrCl(C₆H₁₀O)N₃]⁻ at *m/z* 749, either chloride or

azide may be the nucleophile responsible for epoxide ring-opening, which explains why this species was more abundant than the other alkoxide species.

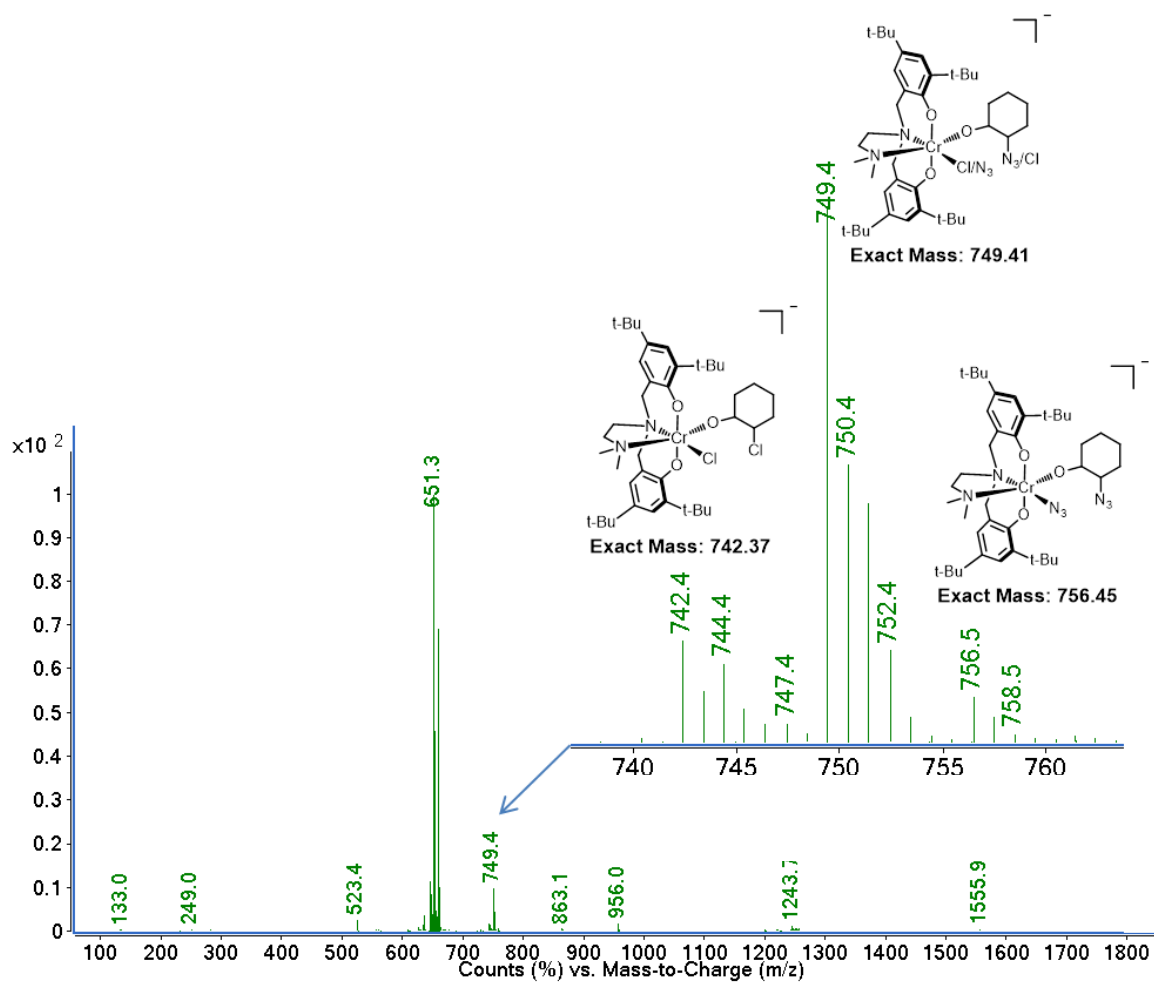


Figure 4-8. ESI mass spectra of the mixture of **2.1**/PPNN₃/CHO in a ratio of 1:1:20.

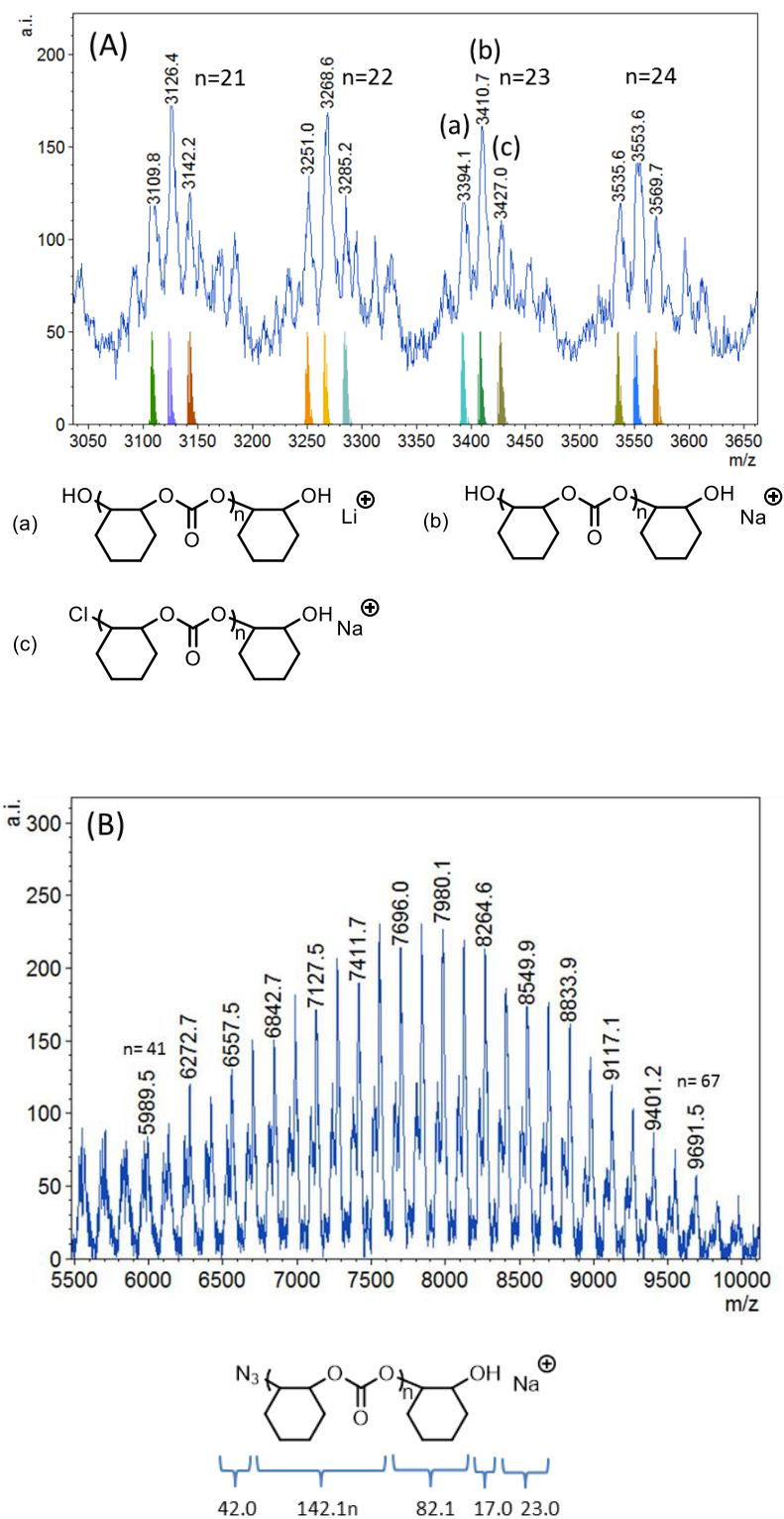


Figure 4-9. Magnified sections of MALDI-TOF mass spectrum for the polymer by **2.1** and PPNN₃. (A) Low mass ($n = 21 - 24$) and (B) high mass regions ($n = 41 - 67$).

4.2.3 Propagating species observed by MALDI-TOF MS

Lu and co-workers observed the propagating polymer species having DMAP as the end-group at various intervals in the copolymerization of PO and CO₂ catalyzed by salenCr(III)NO₃/DMAP or salanCr(III)NO₃/DMAP using ESI-MS, which clearly demonstrated initiation by DMAP.¹⁷ Aliquots of the substrate of the copolymerization of CHO and CO₂ by **2.1** with DMAP or PPNN₃ were also taken at various intervals and analyzed by MALDI-TOF MS. The resulting mass spectra are illustrated in Figure 4-10, Figure 4-11 and Figure 4-12. The mass spectrum of the polymer obtained after 20 min showed only one polymer chain with DMAP end-group (Figure 4-10). The polymer chain propagation over time was observed with a shift of the envelope of peaks to higher *m/z*. This observed propagation process clearly demonstrated DMAP initiation. This observation is consistent with the result described in Chapter 3 where propagation polymer chain obtained by **3.1** and DMAP also showed DMAP end-group. Furthermore, the MALDI-TOF mass spectrum of the aliquot obtained after 60 min showed that new polymer chains at low mass region occurred (Figure 4-10). The magnified low mass region is illustrated in Figure 4-11, where the most intense peak series corresponds to the polymer chain (a) containing DMAP end-group, suggesting DMAP initiation. Interestingly, polymer chain (b) containing chloride end-group was also observed, which clearly indicated that chloride also acts as an initiator as the reaction proceeds.

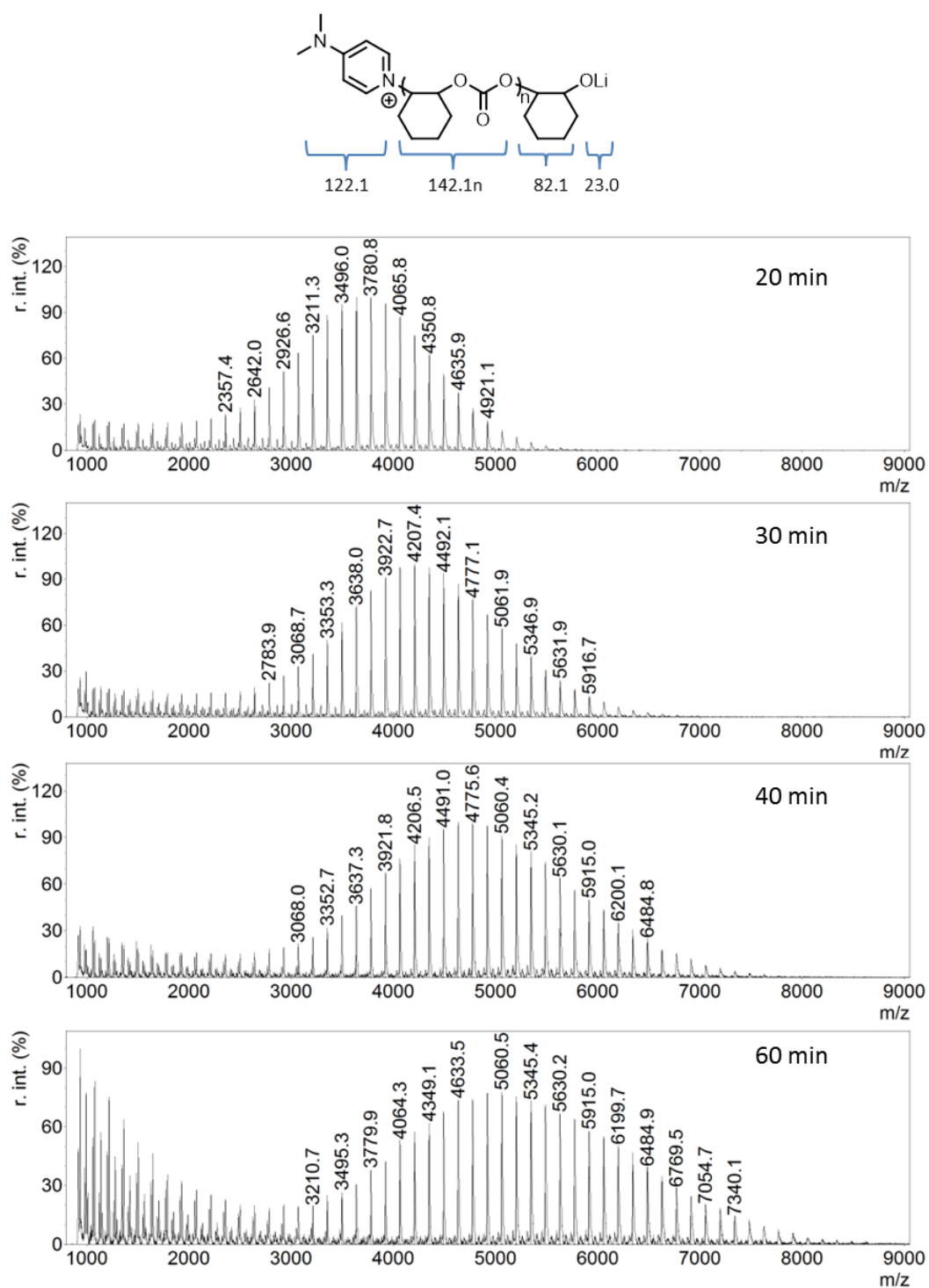


Figure 4-10. MALDI-TOF mass spectra of aliquots obtained at the specified times from the copolymerization of CHO and CO₂ by **2.1** and DMAP.

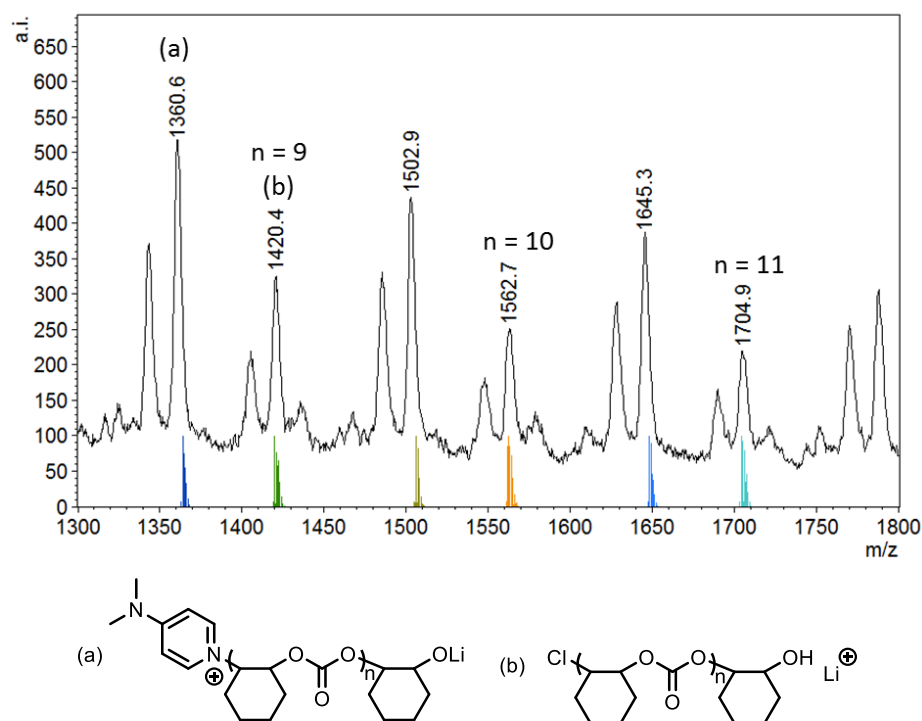


Figure 4-11. MALDI-TOF mass spectrum in the low mass region of aliquot obtained after 60 min shown in Figure 4-10. Modeled isotopic masses for polymers (a and b) are shown below the experimental spectrum.

Similarly in the case of PPNN₃ as a cocatalyst, the mass spectrum showed one polymer chain with azide and hydroxyl end-groups (Figure 4-12). Again, the envelope of polymer peaks moved to the higher *m/z* region with time demonstrating propagation, but showed relatively poor resolution compared to the mass spectra obtained using DMAP as a cocatalyst. This observation provided the evidence that added azide most likely plays the main role in the ring-opening of CHO in the binary catalyst system of amino bis(phenolate) Cr(III) chloride complexes and PPNN₃.

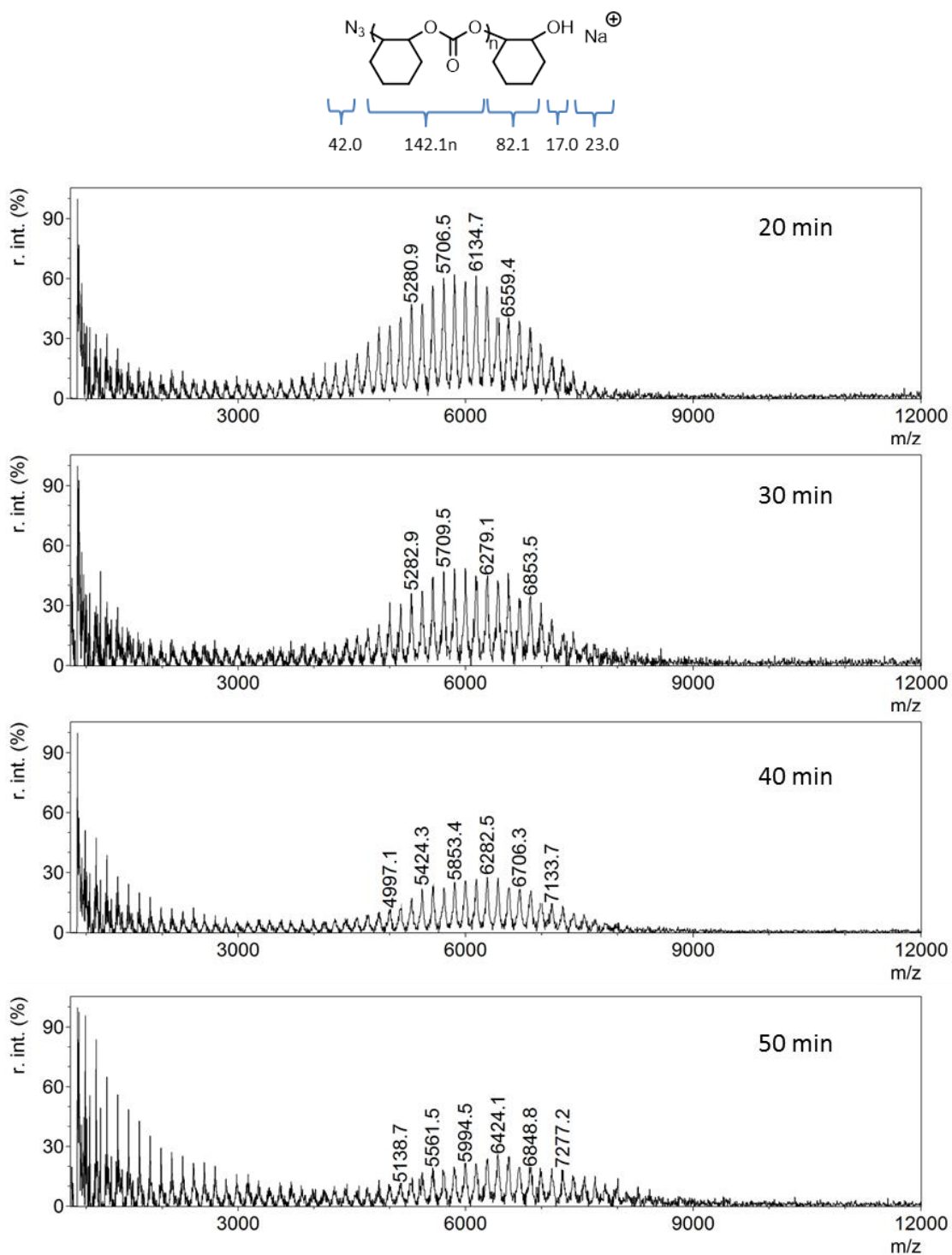


Figure 4-12. MALDI-TOF mass spectra of the aliquots obtained from the copolymerization of CHO and CO₂ by complex **2.1** and PPNN₃ at various intervals.

4.2.4 Mechanistic understanding

The mechanism of epoxide/ CO_2 copolymerization catalyzed by salen complexes and anions coupled with PPN^+ or tetraalkylammonium cation has been well studied.^{29,30} Darensbourg and co-workers proposed the six-coordinate metal anion derived from addition of ionic cocatalyst to salen complex is the active species, which is responsible for epoxide binding and concomitant ring-opening of epoxide by the displaced nucleophile. Due to the fast formation of this six-coordinate metal anion, the most striking feature of using ionic cocatalysts in the salen complex system is the lack of an induction period. To investigate the mechanistic aspects of the binary catalyst system of amino bis(phenolate) Cr(III) chloride complexes and PPNN_3 , kinetic studies of the CHO/CO_2 copolymerization by **3.1** or **2.1** in the presence of 1 equivalent of PPNN_3 were carried out by infrared spectroscopy. The resulting time profiles of the copolymerization reactions are illustrated in Figure 4-13 and show remarkably different rates of catalytic activity for the two metal complexes. **3.1**/ PPNN_3 exhibited a slow growth of the polycarbonate band at 1750 cm^{-1} following a 20 min induction period whereas **2.1**/ PPNN_3 showed a significantly faster rate of polycarbonate formation and no prolonged induction period. This notable difference in the catalytic activities, combined with the mass spectrometric studies of azide binding to **3.1** and **2.1**, provided some mechanistic information concerning epoxide/ CO_2 copolymerization by amino bis(phenolate) Cr(III) chloride complexes and PPNN_3 .

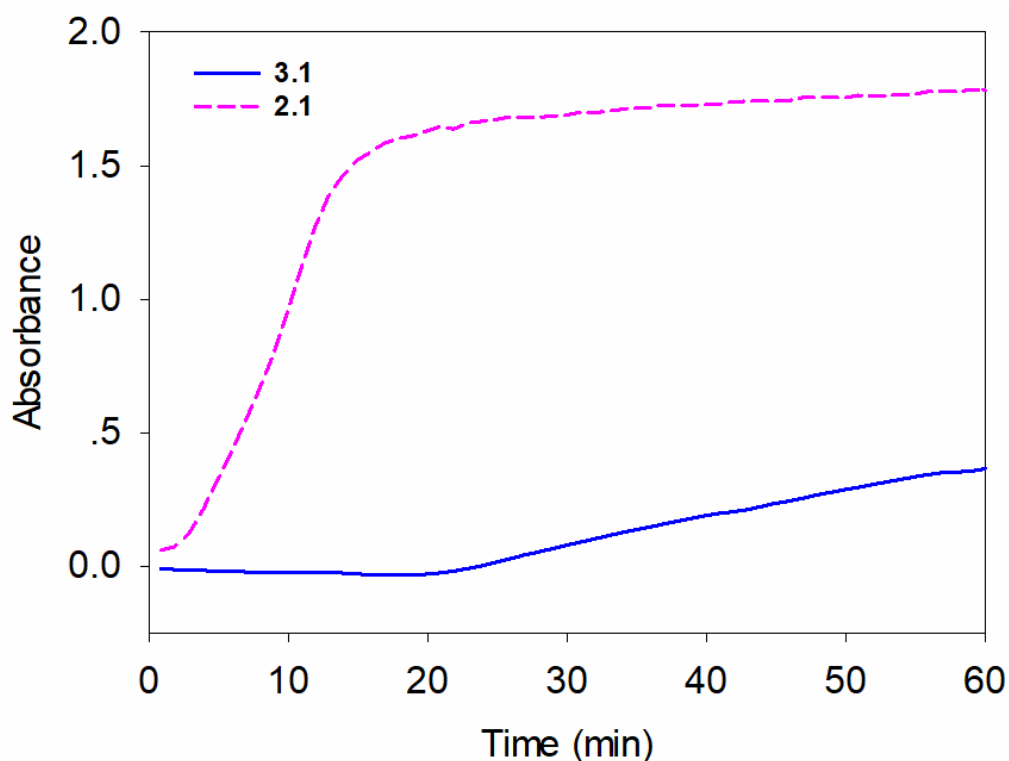
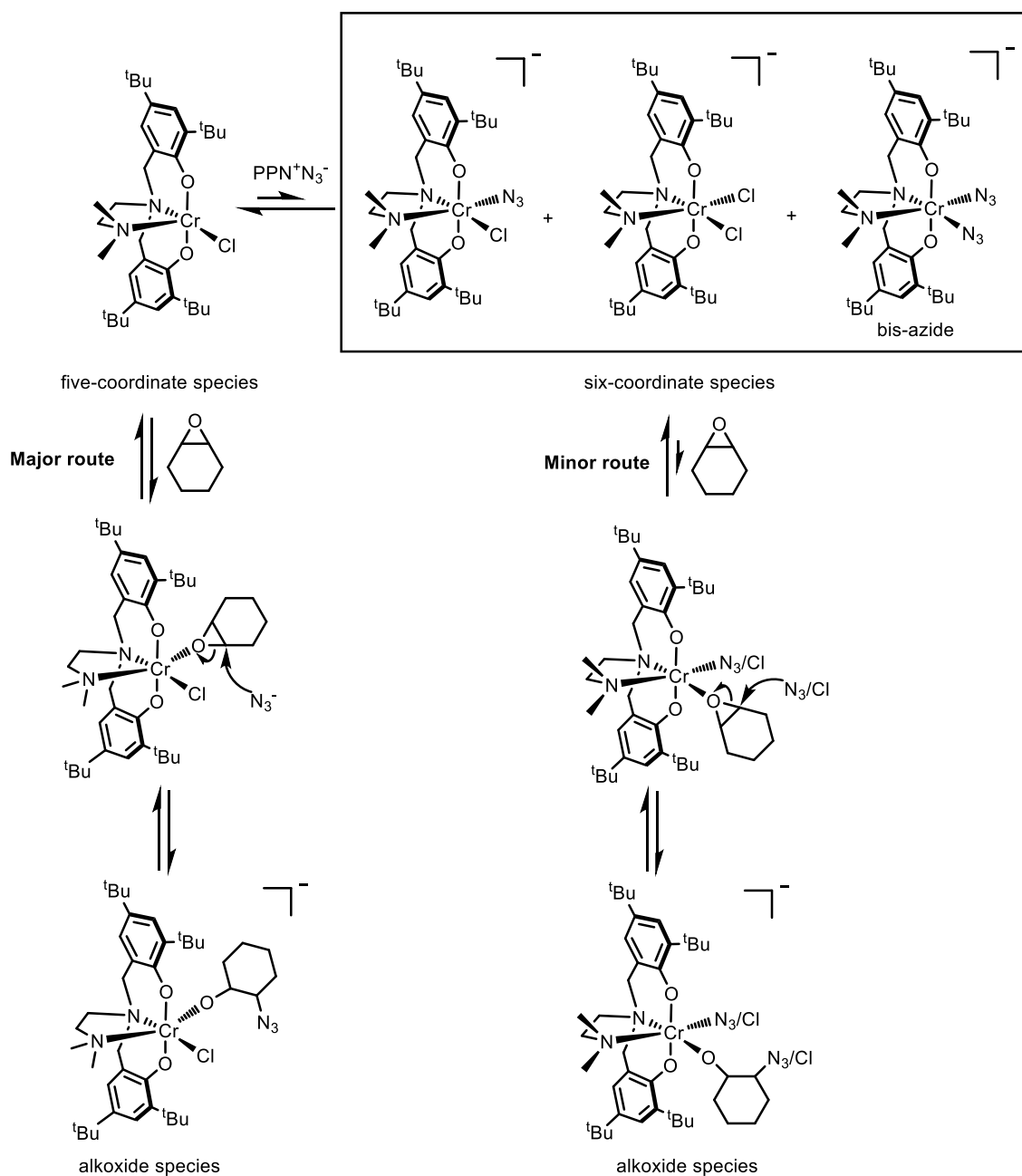


Figure 4-13. Time profiles of the absorbance at 1750 cm^{-1} corresponding to PCHC obtained using complexes **3.1** (solid blue line) and **2.1** (dashed pink line) in the presence of 1 equivalent of PPNN_3 .

Four possible species can be present and establish an equilibrium in the binary system of amino bis(phenolate) Cr(III) chloride complexes and PPNN_3 in which the five-coordinate species plus a “free azide” is likely the active species, which provides the main pathway for the initiation reaction (Scheme 4-1). Specifically, epoxide coordinates to the five-coordinate species, followed by the “free azide” performing epoxide ring-opening, which leads to azide as the end-group (Scheme 4-1). This proposed initiation is also consistent with the observed propagating species terminated with azide group at various

intervals by MALDI-TOF MS (Figure 4-12). On the other hand, these six-coordinate anions, especially the bis-azide anion, most likely hinder the reaction in which epoxide competes with the coordinated chloride and/or azide to bind to the chromium center (Scheme 4-1). Only if the epoxide successfully replaces the coordinated chloride or azide, can ring-opening of the epoxide occur. This process likely provides a minor initiation pathway and results in the presence of chloride as the end-group, as observed in the low m/z region of MALDI-TOF mass spectrum (Figure 4-9). Similarly, the complex of salanCr(III)Cl in combination with PPNN_3 has shown a decreased activity towards CHO/ CO_2 copolymerization from changing 1 equivalent of PPNN_3 to 2 equivalents of PPNN_3 .³¹ This observation is consistent with the mechanism proposed here.



Scheme 4-1. Proposed initiation pathways for the copolymerization of CHO and CO₂ by 2.1 and PPNN₃.

It is worth noting that the study of the binding of azide to amino-bis(phenolate) Cr(III) chloride complexes is comparable to the previous study of the binding of DMAP to

amino-bis(phenolate) Cr(III) chloride complexes in the Kozak group.²² Firstly due to the lower steric effect of the pendant donor in **3.1**, both the bis-azide and bis-DMAP species were observed. However, in the case of **2.1**, which contains a more sterically hindering pendant donor, only the bis-azide complex was observed and the bis-DMAP complex was not. That can be attributed to azide being smaller than DMAP. This comparison demonstrated that both the steric effects of the pendant donor group in the Cr(III) complex and cocatalyst can influence the binding of cocatalyst to the Cr(III) complexes. Secondly, a significant difference between azide and DMAP binding to **3.1** was observed. Specifically, the five-coordinate [LCrCl] species, which was proposed to be the active species for epoxide binding did not decrease in abundance in these mass spectrometry, even with the addition of excess DMAP.²² In contrast the abundance of the five-coordinate species [LCrCl] (**F2**) dramatically decreased with the addition of PPNN₃ (Figure 4-5). This difference can be attributed to the smaller steric size of azide, making it more capable of coordinating to the Cr center of **3.1** to form inert six-coordinate species. This is a possible explanation why **3.1**/PPNN₃ or PPNNCl showed lower activity than **3.1**/DMAP described in Chapter 3.

It is also important to note that the dimethylaminoethyl pendant donor group in **2.1** not only favors the formation of five-coordinate species due to a larger steric effect, but it also increases electron density at chromium more than the methoxyethyl pendant group in

3.1. Similar enhanced catalytic activity by salen complexes has been observed by increasing the electron density at the metal center through introducing more electron donating substituents.³²

4.3 Conclusions

The negative mode MALDI-TOF and ESI mass spectra of amino-bis(phenolate) Cr(III) chloride complexes in the presence of azide demonstrated that the binding behavior of azide to the chromium center is influenced by the nature of the pendant donor group. Complex **3.1** with a methoxyethyl pendant arm showed a higher abundance of bis-azide-containing ions using both ionization methods and generated a much lower abundance of five-coordinate ions than **2.1** possessing the dimethylaminoethyl pendant donor. This different behavior in the binding of azide is coincident with a striking difference in the catalytic activities of **2.1** and **3.1** for the copolymerization of CHO and CO₂. In the presence of 1 equivalent of PPNN₃, **3.1** exhibited a slow reaction rate with an induction period, whereas **2.1** showed a much faster reaction rate and no induction period observed. The observed propagating polymer chains at various times in CHO/CO₂ copolymerization by **2.1** and PPNN₃ by MALDI-TOF MS indicated azide initiation wherein the five-coordinate species plus a free azide is most likely the active species initiating the reaction.

4.4 Experimental

4.4.1 General materials

All manipulations were performed under atmosphere of dry, oxygen-free nitrogen by means of standard Schlenk techniques or using an MBraun Labmaster DP glove box. Anhydrous dichloromethane was obtained by purification using an MBraun Manual Solvent Purification System. Acetonitrile was purchased from Fisher Scientific and dried over 4 Å molecular sieves. Cyclohexene oxide was purchased from Aldrich and freshly distilled from CaH_2 under nitrogen. PPNN_3 was prepared followed a previously procedure.³³ Complexes **2.1** and **3.1** were prepared via the previously reported methods in Chapter 2 and 3.

4.4.2 MALDI-TOF MS experimental

MALDI-TOF MS was performed using an Applied Biosystems 4800 MALDI TOF/TOF Analyzer equipped with a reflectron, delayed ion extraction and high performance nitrogen laser (200 Hz operating at 355 nm). Chromium complex samples were prepared in the glove box and sealed under nitrogen in a Ziploc© bag for transport to the instrument. For chromium complex samples, reflectron mode was used and anthracene was used as the matrix. For polymer samples, linear mode was used and 2,5-dihydroxybenzoic acid (DHBA) was used as the matrix. 1 μL aliquots of these

samples were spotted on the MALDI plate and left to dry. Images of mass spectra were prepared using mMassTM software (www.mmass.org).

The solution of complex **3.1** (6.0 mg, 1.0×10^{-5} mol (per Cr)) and anthracene (6.0 mg, 3.3×10^{-5} mol) was prepared in 1.2 mL of dichloromethane. Appropriate amounts (3.0 mg, 3.0 mg, 5.8 mg, 11.6 mg, 34.8 mg) of PPNN₃ were added into the solution in sequence and allowed to stir for 5 min, giving the analytes with different ratios of complex **3.1** (per Cr) to PPNN₃ (1:0.5, 1:1, 1:2, 1:4, 1:10). Sample preparations of complex **2.1** and PPNN₃ followed the same procedure. Laser intensity of 4526 and reflectron mode were used in the experiments

Aliquots taken from the copolymerization reactions catalyzed by **2.1** in combination with DMAP or PPNN₃ at different intervals were dissolved in THF at approximately 10 mg mL⁻¹. DHBA was dissolved in THF at approximately 16 mg mL⁻¹. The polymer and matrix solutions were combined in a volume ratio of 1:3. Laser intensity of 5406 and mid linear mode were applied in the experiments.

4.4.3 ESI-MS experimental

ESI-MS was performed using an Agilent 6230 TOF LC/MS. The ESI capillary voltage was maintained at 3500 V. All the mass spectra were recorded using MassHunter workstation software (version B.06.00).

The solutions of complex **3.1** (3.0 mg, 5.0×10^{-6} mol (per Cr)) were made in 3.0 mL of acetonitrile. A stock solution of 58.4 mg of PPNN₃ in 2 mL of acetonitrile was prepared. Appropriate volumes (50 μ L, 100 μ L, 200 μ L, 400 μ L, 1000 μ L) of PPNN₃ solution was added into the complex **3.1** solutions and stirred for 5 min, giving the molar ratios of complex **3.1** (per Cr) to PPNN₃: 1:0.5, 1:1, 1:2, 1:4, 1:10. The resulting solutions were diluted with acetonitrile to a concentration of 0.75 mg mL⁻¹. The sample preparations of complex **2.1** and PPNN₃ followed the same procedure.

The solutions of complex **2.1** (3.0 mg, 4.5×10^{-6} mol) and PPNN₃ (2.6 mg, 4.5×10^{-6} mol) were made in 4 mL of acetonitrile. Appropriate amounts (8.8 μ L, 13.2 μ L, 26.4 μ L, 52.8 μ L) of CHO were added into the solutions and stirred for 5 min, giving the analytes with different ratios among **2.1**, PPNN₃ and CHO (1:1:20, 1:1:30, 1:1:60, 1:1:120).

4.5 References

- (1) Chisholm, M. H.; Zhou, Z. *J. Am. Chem. Soc.* **2004**, *126*, 11030.
- (2) Cheng, M.; Moore, D. R.; Reczek, J. J.; Chamberlain, B. M.; Lobkovsky, E. B.; Coates, G. W. *J. Am. Chem. Soc.* **2001**, *123*, 8738.
- (3) Xiao, Y.; Wang, Z.; Ding, K. *Macromolecules* **2006**, *39*, 128.
- (4) Ingram, A. J.; Boeser, C. L.; Zare, R. N. *Chem. Sci.* **2016**, *7*, 39.
- (5) Chen, P. *Angew. Chem., Int. Ed.* **2003**, *42*, 2832.
- (6) Yunker, L. P. E.; Stoddard, R. L.; McIndoe, J. S. *J. Mass Spectrom.* **2014**, *49*, 1.
- (7) Wyatt, M. F. *J. Mass Spectrom.* **2011**, *46*, 712.
- (8) Bailey, G. A.; Fogg, D. E. *ACS Catal.* **2016**, *6*, 4962.
- (9) Chen, P.; Chisholm, M. H.; Gallucci, J. C.; Zhang, X.; Zhou, Z. *Inorg. Chem.* **2005**, *44*, 2588.
- (10) Ren, W.-M.; Liu, Z.-W.; Wen, Y.-Q.; Zhang, R.; Lu, X.-B. *J. Am. Chem. Soc.* **2009**, *131*, 11509.
- (11) Van Meerendonk, W. J.; Duchateau, R.; Koning, C. E.; Gruter, G.-J. M. *Macromolecules* **2005**, *38*, 7306.
- (12) Duchateau, R.; van Meerendonk, W. J.; Yajjou, L.; Staal, B. B. P.; Koning, C. E.; Gruter, G.-J. M. *Macromolecules* **2006**, *39*, 7900.
- (13) Darensbourg, D. J.; Yarbrough, J. C. *J. Am. Chem. Soc.* **2002**, *124*, 6335.

- (14) Darensbourg, D. J.; Phelps, A. L. *Inorg. Chem.* **2005**, *44*, 4622.
- (15) Darensbourg, D. J.; Yeung, A. D. *Polym. Chem.* **2015**, *6*, 1103.
- (16) Darensbourg, D. J.; Yarbrough, J. C.; Ortiz, C.; Fang, C. C. *J. Am. Chem. Soc.* **2003**, *125*, 7586.
- (17) Rao, D.-Y.; Li, B.; Zhang, R.; Wang, H.; Lu, X.-B. *Inorg. Chem.* **2009**, *48*, 2830.
- (18) Dean, R. K.; Devaine-Pressing, K.; Dawe, L. N.; Kozak, C. M. *Dalton Trans.* **2013**, *42*, 9233.
- (19) Dean, R. K.; Dawe, L. N.; Kozak, C. M. *Inorg. Chem.* **2012**, *51*, 9095.
- (20) Chen, H.; Dawe, L. N.; Kozak, C. M. *Catal. Sci. Tech* **2014**, *4*, 1547.
- (21) Devaine-Pressing, K.; Dawe, L. N.; Kozak, C. M. *Polym. Chem.* **2015**, *6*, 6305.
- (22) Kozak, C. M.; Woods, A. M.; Bottaro, C. S.; Devaine-Pressing, K.; Ni, K. *Farad. Discuss.* **2015**.
- (23) Darensbourg, D. J.; Moncada, A. I. *Inorg. Chem.* **2008**, *47*, 10000.
- (24) Kember, M. R.; Jutz, F.; Buchard, A.; White, A. J. P.; Williams, C. K. *Chem. Sci.* **2012**, *3*, 1245.
- (25) Reiter, M.; Altenbuchner, P. T.; Kissling, S.; Herdtweck, E.; Rieger, B. *Eur. J. Inorg. Chem.* **2015**, *2015*, 1766.
- (26) Nakano, K.; Nakamura, M.; Nozaki, K. *Macromolecules* **2009**, *42*, 6972.
- (27) Lu, X.-B.; Shi, L.; Wang, Y.-M.; Zhang, R.; Zhang, Y.-J.; Peng, X.-J.; Zhang, Z.-C.;

Li, B. *J. Am. Chem. Soc.* **2006**, *128*, 1664.

(28) Li, B.; Zhang, R.; Lu, X.-B. *Macromolecules* **2007**, *40*, 2303.

(29) Darensbourg, D. J.; Mackiewicz, R. M. *J. Am. Chem. Soc.* **2005**, *127*, 14026.

(30) Darensbourg, D. J. *Chem. Rev.* **2007**, *107*, 2388.

(31) Darensbourg, D. J.; Ulusoy, M.; Karroonnirum, O.; Poland, R. R.; Reibenspies, J. H.; Cetinkaya, B. *Macromolecules* **2009**, *42*, 6992.

(32) Darensbourg, D. J.; Mackiewicz, R. M.; Rodgers, J. L.; Fang, C. C.; Billodeaux, D. R.; Reibenspies, J. H. *Inorg. Chem.* **2004**, *43*, 6024.

(33) Demadis, K. D.; Meyer, T. J.; White, P. S. *Inorg. Chem.* **1998**, *37*, 3610.

Co-authorship statement

Chapter 5: Synthesis of polycarbonate diols and their polylactide tri-block copolymers

This chapter is currently in the preparation for publication.

Authors: Kaijie Ni and Christopher M. Kozak

The first author (Kaijie Ni) contributed 90% of the content of the article as the main researcher including: performing the experiments, analyzing and collecting data, and writing the paper.

The corresponding author (Christopher M. Kozak), my supervisor, was the principal investigator of this research work. He suggested initial experiments, assisted with analyzing data and revised this manuscript.

Chapter 5. Synthesis of polycarbonate diols and their polylactide tri-block copolymers

5.1 Introduction

There is a need to find alternatives to petroleum-derived plastics with those that can incorporate significant amounts of renewably sourced materials as well as be less pernicious to the environment and human health. Various biomass-derived polymers are being commercially applied, most notably poly(lactide), PLA; poly(hydroxyl alkanoates) and cellulosic/starch derivatives. Because PLA is a biocompatible, biodegradable and renewable polymer, it has received significant interest in both academic and industrial research over recent years.¹⁻³ Various catalysts have been developed for the ring-opening polymerization (ROP) of lactide to produce PLA with controlled molecular weight and low dispersity.⁴⁻⁷ Another process that utilizes an abundant, inexpensive and non-toxic carbon source is the production of carbonates from CO₂, such as the coupling or copolymerization of CO₂ with epoxides as discussed in Chapter 1.

The preparation of new materials incorporating CO₂-based copolymers with other monomers to give multi-block polymers is a valuable and challenging goal for future research and development. There have been two strategies reported to date for the synthesis of block co-polymers of polycarbonates obtained from CO₂ and epoxides and other

monomers.^{8,9} One involves the use of monomers such as cyclic acid anhydrides along with epoxides and CO₂. This route relies upon the rate of CO₂ incorporation to be slower than that of anhydride/epoxide copolymerization to give polyester-block-polycarbonate polymers. This has the advantage of being a one-pot terpolymerization of the three monomers and several catalyst systems have demonstrated the ability to perform this reaction.¹⁰⁻¹² Its disadvantage, however, is that it is rather limited in that only cyclic anhydrides are suitable. Other monomers such as lactide,¹³ lactone¹⁴ or maleic anhydride¹⁵ give random structures with typically broad molecular weight distributions and ether linkages when copolymerized with epoxides and CO₂. A second strategy that has recently been exploited is the use of a polymer with terminal initiating sites that can be used as chain-transfer agents. By preparing polycarbonates with hydroxyl-functionalized end-groups, these diols can be used as macroinitiators for polymerization of a third monomer such as cyclic esters.^{16,17} A further promising application of polycarbonate diols is in the production of polyurethane foams.¹⁸ Although polycarbonate diols have been observed by MALDI-TOF MS of polymer products obtained by CO₂/epoxide copolymerization by various catalytic systems, selective formation of di-hydroxyl end-capped chains has required using hydrolysable sites. Darensbourg and Williams have shown that using trifluoroacetate-containing (TFA) metal complexes leads to TFA-polycarbonate-OH polymers, which upon hydrolysis or in presence of adventitious

water yield polycarbonate diols.^{16,17}

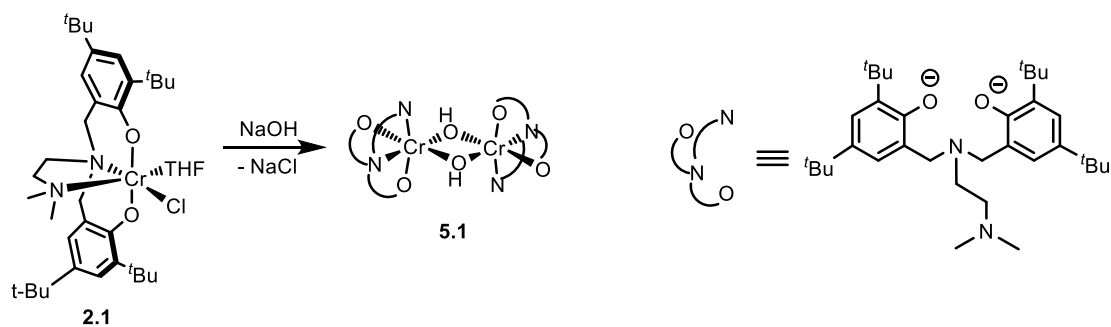
In this chapter, the use of an efficient polymerization catalyst system to produce hydroxyl-terminated polycarbonate from CHO and CO₂ independent of using hydrolysable sites was described. The resultant hydroxyl-terminated polycarbonates served as macroinitiators for the ring-opening polymerization of *rac*-lactide in the presence of DBU to generate the tri-block copolymer.

5.2 Results and discussion

5.2.1 Synthesis and characterization

Kozak's group previously reported a Cr(III) diamino-bis(phenolate) catalyst, which showed efficient activity for converting CHO and CO₂ to polycarbonate in the presence of various cocatalysts.¹⁹ MALDI-TOF mass spectra of the produced polycarbonates showed multiple end-groups occurring, which is not suitable for preparation of well-defined block copolymers. New chromium complex of **5.1** bearing a hydroxide ancillary ligand was prepared to produce polycarbonate with strictly hydroxyl-terminated end-groups. **5.1** was synthesized via salt metathesis reaction of **2.1** with sodium hydroxide under nitrogen in tetrahydrofuran, affording a green solid in 64% yield (Scheme 5-1). **5.1** was characterized by MALDI-TOF MS and combustion analysis. The MALDI-TOF mass spectrum of **5.1** showed peaks at *m/z* 614.4 and 591.4 corresponding to the [CrOH[L1] + Na]⁺ cation and

the $[\text{CrOH}[\text{L1}]]^+$ cation (Figure 5-1). The other observed peak at m/z 654.4 can be assigned to the $[\text{CrOH}[\text{L1}] + \text{NaOH} + \text{Na}]^+$ cation due to the contamination by NaOH. The peak at m/z 609 corresponding to $[\text{CrCl}[\text{L1}]]^{+*}$ was not observed, indicating complete replacement of the chloride by the hydroxide. Combustion analysis of **5.1** consistently showed contamination by NaOH.



Scheme 5-1. Synthetic route to complex **5.1**.

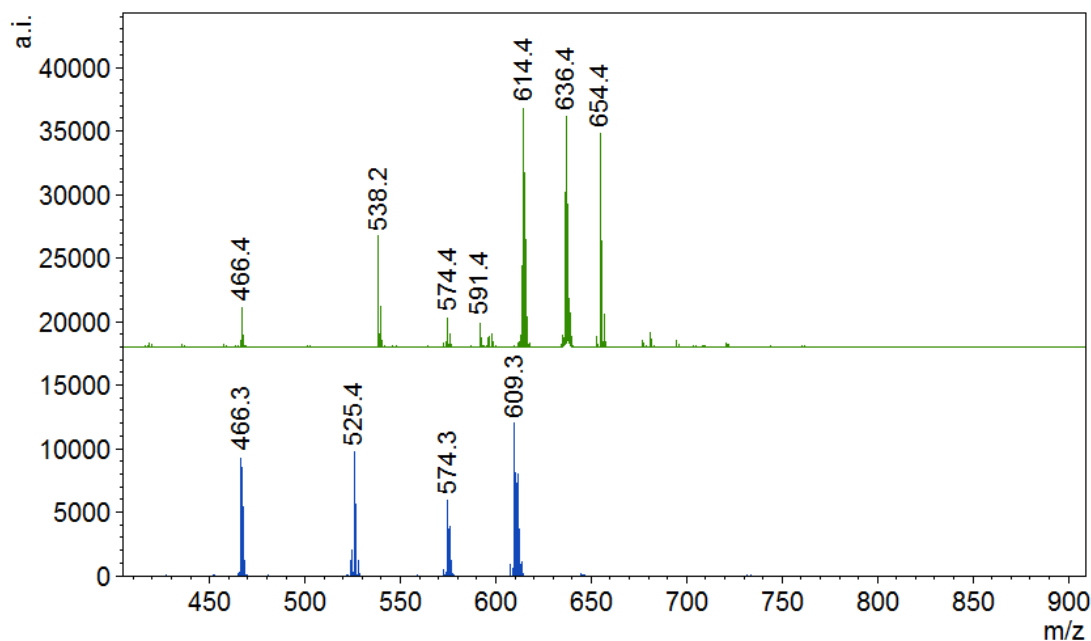


Figure 5-1. MALDI-TOF mass spectra of **2.1** (blue, bottom) and **5.1** (green, top).

5.2.2 Single crystal structure determination

Single crystals were obtained from a solution of **5.1** in HMDSO and THF. Interestingly, the crystal structure showed that a trimethylsilyloxy group coordinated to the chromium centre, affording a new complex **5.2** (Figure 5-2). The single crystal structure is shown in Figure A-1. Si-O bond cleavage reactions in HMDSO have been reported in the literature.²⁰⁻²³ The investigation of the effect of strong base on HMDSO by Tatlock and Rochow has shown that in the presence of hydroxide ion a pentavalent silicon intermediate would be formed (Scheme 5-2).²⁴ The following reaction then proceeds either by cleavage of the Si-O bond or Si-C bond. During the process of single

crystals of **5.1** growing in HMDSO and THF, the cleavage of Si-O bond of HMDSO likely occurred due to the contamination of NaOH in **5.1**, which resulted in the new complex of **5.2**.

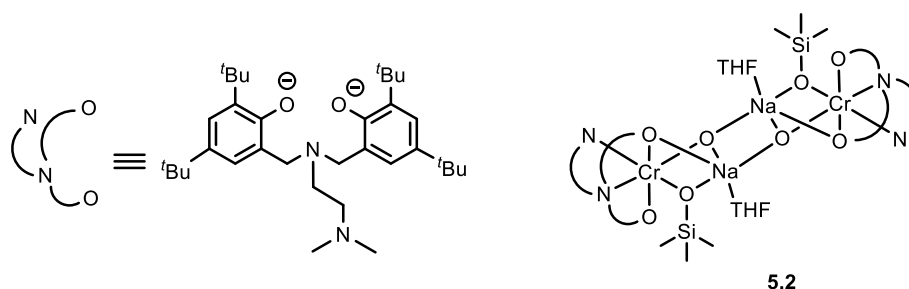
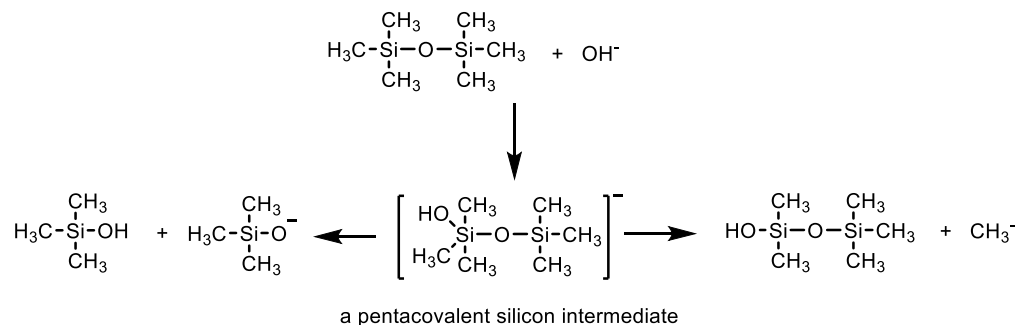


Figure 5-2. The structure of **5.2**.



Scheme 5-2. The proposed mechanism of the reaction of HMDSO with a hydroxide ion.

Although single crystals of the hydroxide-bridged dimer, **5.1** suitable for X-ray diffraction analysis were not obtained, single crystals of a related hydroxide-bridged dimer **5.3** with a methoxyl group as the pendant donor were obtained (Figure 5-3). The structure possesses an inversion center within the Cr₂O₂ rhomboid and the two Cr(III) centers exhibit

distorted octahedral geometries. The related hydroxide-bridged dimer containing a pyridine group as the pendant donor has also been found in the Kozak group as a product upon quenching the polymerization reaction mixture.²⁵ Darensbourg's group also isolated related hydroxide-bridged dimeric Cr(III) complexes possessing salen and acacen (*N,N'*-bis(*t*-butylacetylacetone)-1,2-ethylenediamine) ligands.²⁶ The Cr(1)–O(7)–Cr(2) and Cr(1)–O(8)–Cr(2) angles in **5.3** are 99.99(18)° and 98.19(18)°, which are close to the corresponding angles typically reported for other hydroxide-bridged Cr(III) dimers. The hydroxides are orientated *cis* to the oxygen on the pendant methoxy group. The Cr(1)–OH bond distances are asymmetric at 1.976(4) and 2.070(4) Å, whereas Cr(2)–OH bond distances are more symmetric with distances of 2.051(4) and 2.011(4) Å. These lengths are within the range values reported for five or six-coordinate Cr(III) hydroxide-bridged species in literature.

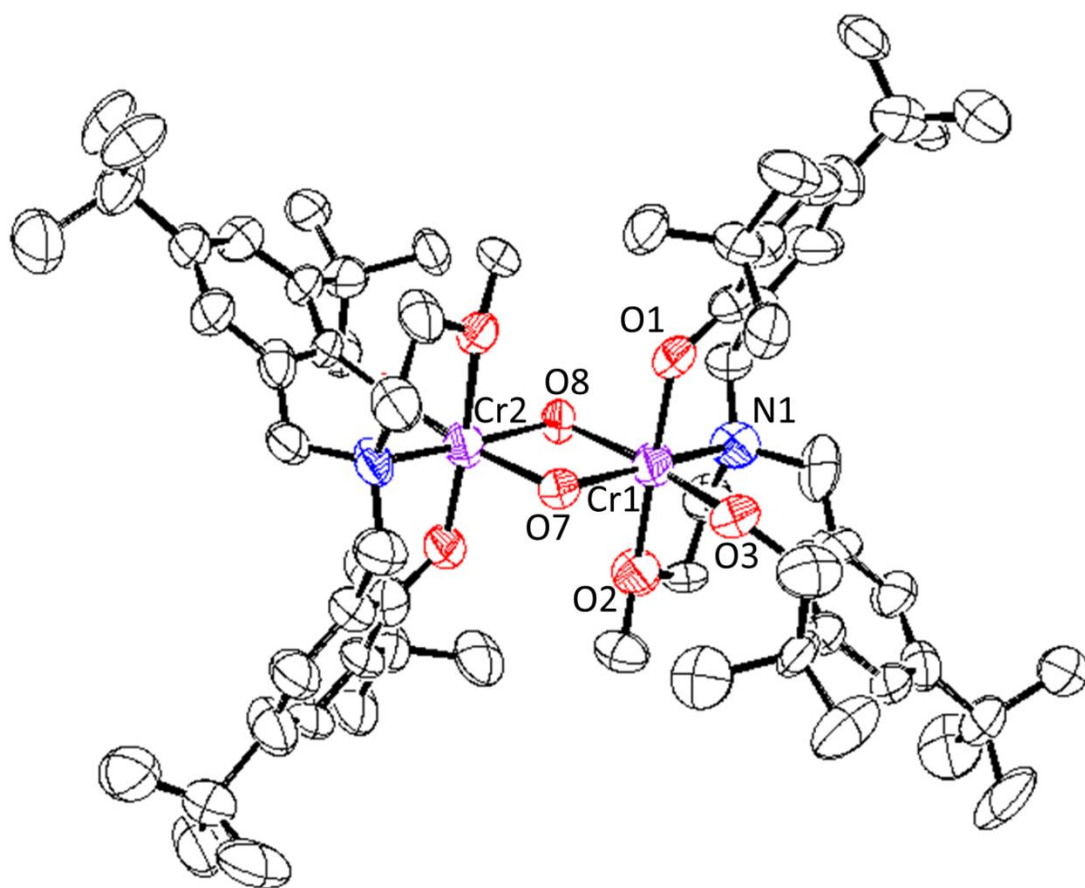


Figure 5-3. Molecular structure (ORTEP) and partial numbering scheme of complex **5.3**. Ellipsoids are drawn at 50% probability. Hydrogen atoms omitted for clarity.

Table 5-1. Selected bond distances (Å) and angles (°) of **5.3**.

Bond lengths (Å)			
Cr(1) – O(1)	1.908(5)	Cr(1) – O(2)	2.065(6)
Cr(1) – O(3)	1.902(4)	Cr(1) – N(1)	2.076(5)
Cr(1) – O(7)	1.976(4)	Cr(1) – O(8)	2.070(4)
Bond angles (°)			
O(2) – Cr(1) – O(3)	90.3(2)	O(2) – Cr(1) – N(1)	82.1(2)
O(2) – Cr(1) – O(1)	173.33(18)	O(2) – Cr(1) – O(7)	92.44(19)
O(7) – Cr(1) – O(8)	81.09(16)	O(7) – Cr(2) – O(8)	80.73(16)
N(1) – Cr(1) – O(8)	92.27(18)	N(1) – Cr(1) – O(1)	91.6(2)
N(1) – Cr(1) – O(3)	92.26(19)	O(1) – Cr(1) – O(8)	92.30(19)
O(1) – Cr(1) – O(3)	92.1(2)	Cr(1) – O(7) – Cr(2)	99.99(18)
Cr(1) – O(8) – Cr(2)	98.19(18)		

Another hydroxide-bridged complex was obtained by slow evaporation of a saturated toluene solution of **2.1**, which due to the presence of water led to the formation of **2.6** (See chapter 2). Similar single crystals of the hydroxide-bridged dimers have been isolated by recrystallization of the amino-bis(phenolate) Cr(III) complexes in air.²⁷ The single crystal structure of **2.6** is shown in Figure 5-4, and selected bond distances (Å) and angles (°) are shown in Table 5-2. It is worth noting that the bridged OH⁻ and the H⁺ (H(3A)) show reversible binding ability in **2.6**, which has been discussed in Chapter 2, Section 2.2.1. In each metal-ligand unit of the bimetallic complex, the Cr(III) ion center exhibits a distorted

octahedral geometry where the two phenolate-oxygen atoms maintain *trans* orientation and the chloride ligand resides *trans* to the amino donor. The selected bond distances and angles are within the range of the typical values for bimetallic Cr(III) complexes bearing single hydroxide-bridged ligand.²⁸ Due to hydrogen bonding between the hydrogen atom H(3A) and the other phenolate-oxygen atom O(2), the bond distances between the Cr(III) center and phenolate-oxygen atoms at each metal-ligand unit are not symmetrical. For example, Cr(1)–O(1) is 1.886(3) Å while Cr(1)–O(2) is 2.046(2) Å. For the other metal-ligand unit, Cr(2)–O(3) is 2.034(3) Å while Cr(2)–O(4) is 1.879(3) Å.

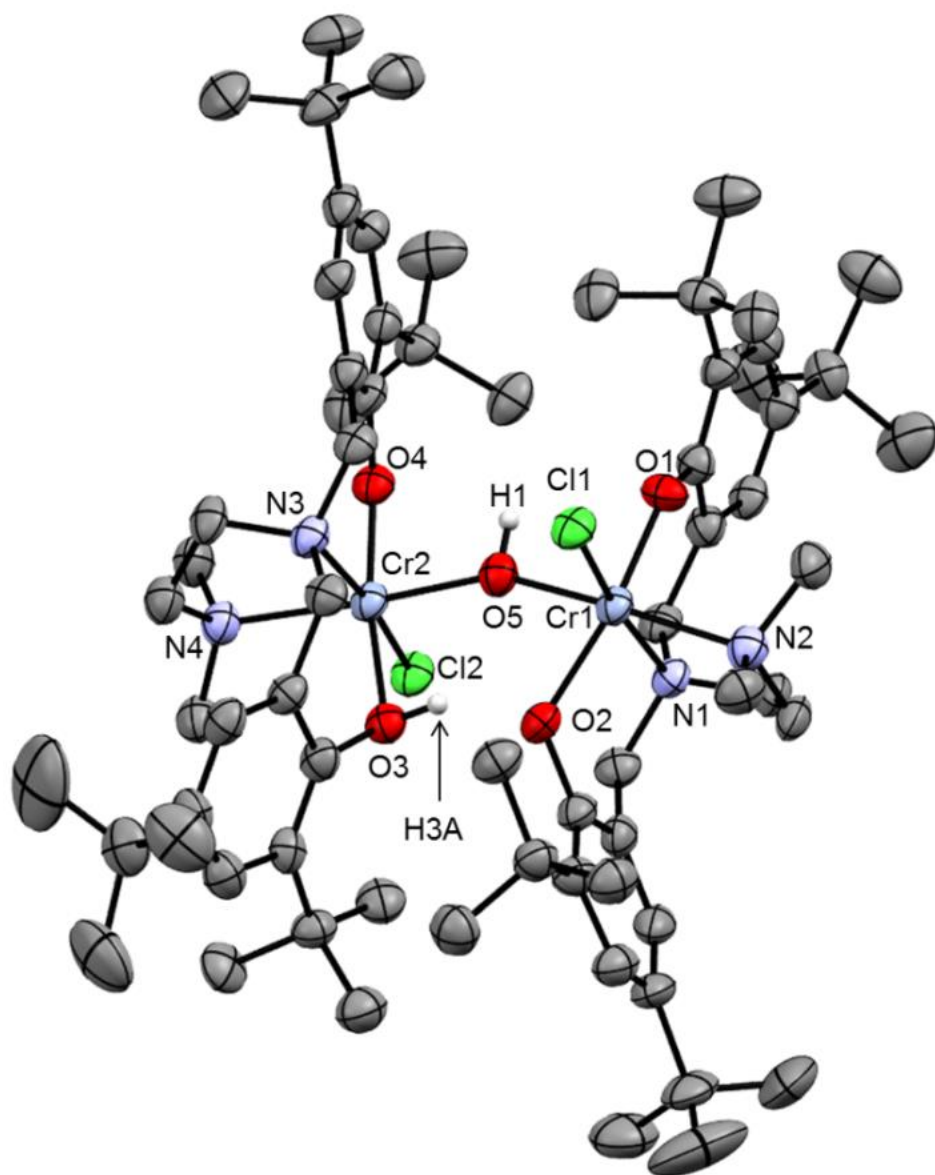


Figure 5-4. Molecular structure (ORTEP) and partial numbering scheme of **2.6**. Ellipsoids are drawn at 50% probability. Hydrogen atoms other than H(1) and H(3A) are omitted for clarity.

Table 5-2. Selected bond distances (Å) and angles (°) of complex **2.6**.

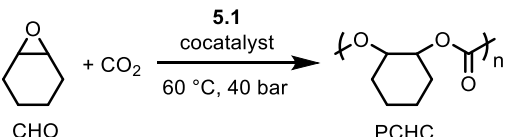
Bond lengths (Å)			
Cr(1) – Cl(1)	2.3466(12)	Cr(1) – O(1)	1.886(3)
Cr(1) – O(2)	2.046(2)	Cr(1) – O(5)	1.984(2)
Cr(1) – N(1)	2.117(3)	Cr(1) – N(2)	2.189(3)
Cr(2) – Cl(2)	2.3575(12)	Cr(2) – O(3)	2.034(3)
Cr(2) – O(4)	1.879(3)	Cr(2) – O(5)	1.972(2)
Cr(2) – N(3)	2.109(3)	Cr(2) – N(4)	2.200(3)
Bond angles (°)			
Cr(1) – O(5) – Cr(2)	152.21(14)	Cl(1) – Cr(1) – O(1)	89.07(9)
Cl(1) – Cr(1) – O(2)	91.42(8)	Cl(1) – Cr(1) – O(5)	96.38(9)
Cl(1) – Cr(1) – N(1)	171.76(8)	Cl(1) – Cr(1) – N(2)	89.75(10)
O(1) – Cr(1) – O(2)	170.88(10)	O(1) – Cr(1) – O(5)	87.02(11)
O(1) – Cr(1) – N(1)	89.82(12)	O(1) – Cr(1) – N(2)	92.92(11)
O(2) – Cr(1) – O(5)	83.87(10)	O(2) – Cr(1) – N(1)	90.97(12)
O(2) – Cr(1) – N(2)	96.18(11)	O(5) – Cr(1) – N(1)	91.72(11)
O(5) – Cr(1) – N(2)	173.87(13)	N(1) – Cr(1) – N(2)	82.15(12)

5.2.3 Copolymerization of CHO and CO₂

Complex **5.1** was used as the catalyst for the copolymerization of CHO and CO₂ under 40 bar CO₂ and 60 °C to produce PCHC. These conditions gave the best activity from the previous work using Cr(III) diamino-bis(phenolate) catalyst in the Kozak group.¹⁹ First, complex **5.1** was tested for the reaction in the absence of cocatalyst, which resulted in a

very low epoxide conversion as expected (Table 5-3, entry 1). Based on previous work concerning Cr(III) diamino-bis(phenolate) catalysts, copolymerization of epoxides and CO₂ typically requires an additional nucleophilic cocatalyst such as Cl⁻ or N₃⁻ paired with very bulky cation, such as PPN⁺ or DMAP.^{19,29,30}

Table 5-3. Copolymerization of CHO and CO₂ catalyzed by **5.1**^a



CHO + CO₂ $\xrightarrow[60\text{ }^{\circ}\text{C}, 40\text{ bar}]{\text{5.1 cocatalyst}}$ PCHC

Entry	[Cr]:[CHO]: [Cocat.]	Cocat.	Conv. ^b (%)	TON ^c	<i>M_n</i> ^d (g mol ⁻¹)	<i>D</i> ^d (<i>M_w</i> / <i>M_n</i>)	T _g (°C)	T _d (°C)
1	1:500:0	---	6	30	4800	1.09	---	---
2	1:500:1	PPNCl	89	445	27000	1.19	104	284
3	1:500:1	Ph ₂ P(O)NPPH ₃	84	420	28500	1.13	110	302
4	1:500:1	Bu ₄ NOH	88	440	6300	1.10	79	254

^a Copolymerization reactions were carried out in neat CHO at 60 °C and 40 bar CO₂ for 24 h. ^b Calculated by ¹H NMR. ^c Turnover number (TON): moles of repeating units produced per mole of Cr present. ^d Determined by triple detection GPC in THF using a dn/dc value of 0.0701 mL g⁻¹.

When PPNCl was used as cocatalyst, complex **5.1** can efficiently produce polycarbonate exhibiting a number-averaged molecular weight of 27000 g mol⁻¹ with a narrow dispersity (Table 5-3, entry 2). MALDI-TOF MS analysis of the polymer (Figure

5-5), however, showed four different polymer chains including (a) dihydroxyl terminated polymer with an ether linkage, (b) chloride and hydroxyl-group terminated polymer with an ether linkage, (c) dichloride terminated polymer with an ether linkage, and (d) chloride and hydroxyl terminated polymer. Series (a) is the expected polymer chain if polymerization is initiated by the hydroxide from complex **5.1** and terminated by hydrolysis. However, the two hydroxyl end-groups could also possibly result from water contamination causing chain transfer,^{25,31} which could also lead to the formation of the ether linkage, but contamination by cyclohexene diol or double insertion of two epoxide units without CO₂ incorporation are also possible.³⁰ The appearance of chloride as one of the end-groups in the produced PCHC demonstrates the chloride from PPnCl could also initiate the epoxide ring-opening step. Thus in order to strictly obtain di-hydroxyl-group terminated polymer, replacement of the chloride in PPnCl with hydroxide was attempted.

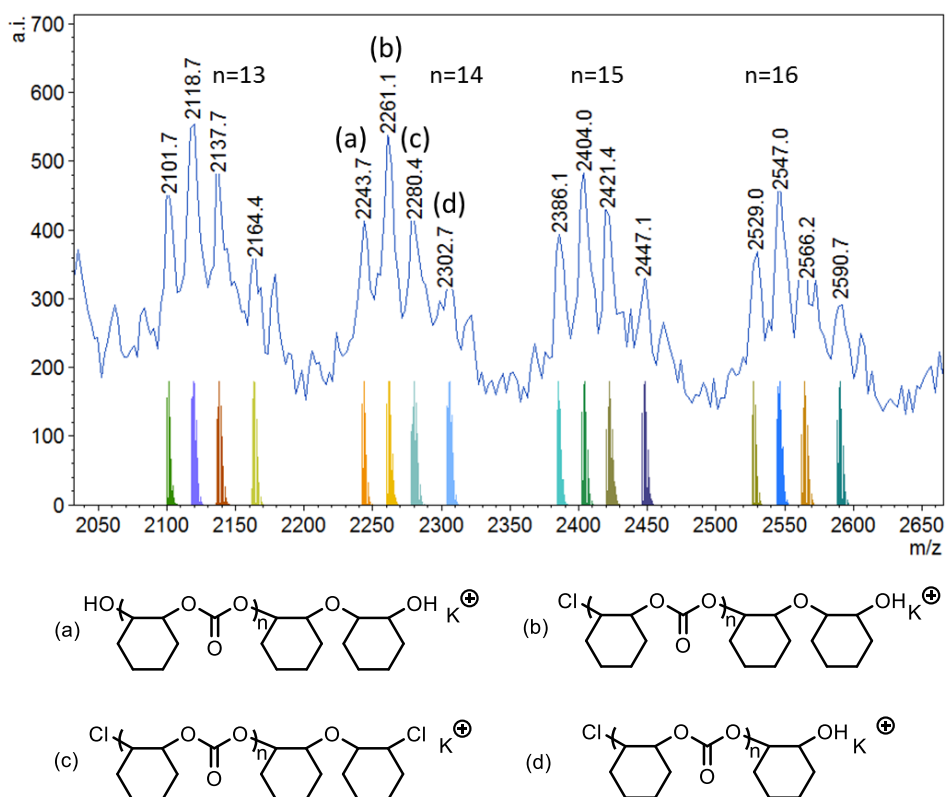


Figure 5-5. Magnified section of MALDI-TOF mass spectrum of PCHC ($n = 13\text{--}16$) obtained using **5.1** and PPNCI (Table 5-3, entry 2). Modeled isotopic masses for polymers (a–d) containing different end-groups are shown below the experimental spectrum.

Sodium hydroxide was attempted to react with PPNCI to produce PPNOH. However, the ^{31}P NMR spectrum of the isolated product showed two phosphorus resonances at 13.23 and 14.35 ppm, identical to the resonances observed for the commercially obtained diphenylphosphonimidotriphenylphosphorane, $\text{Ph}_2\text{P}(\text{O})\text{NPPh}_3$ (Figure 5-6). The crystal structure of $\text{Ph}_2\text{P}(\text{O})\text{NPPh}_3$ obtained from the reaction of PPNCI with NaOMe in methanol has been reported.³²

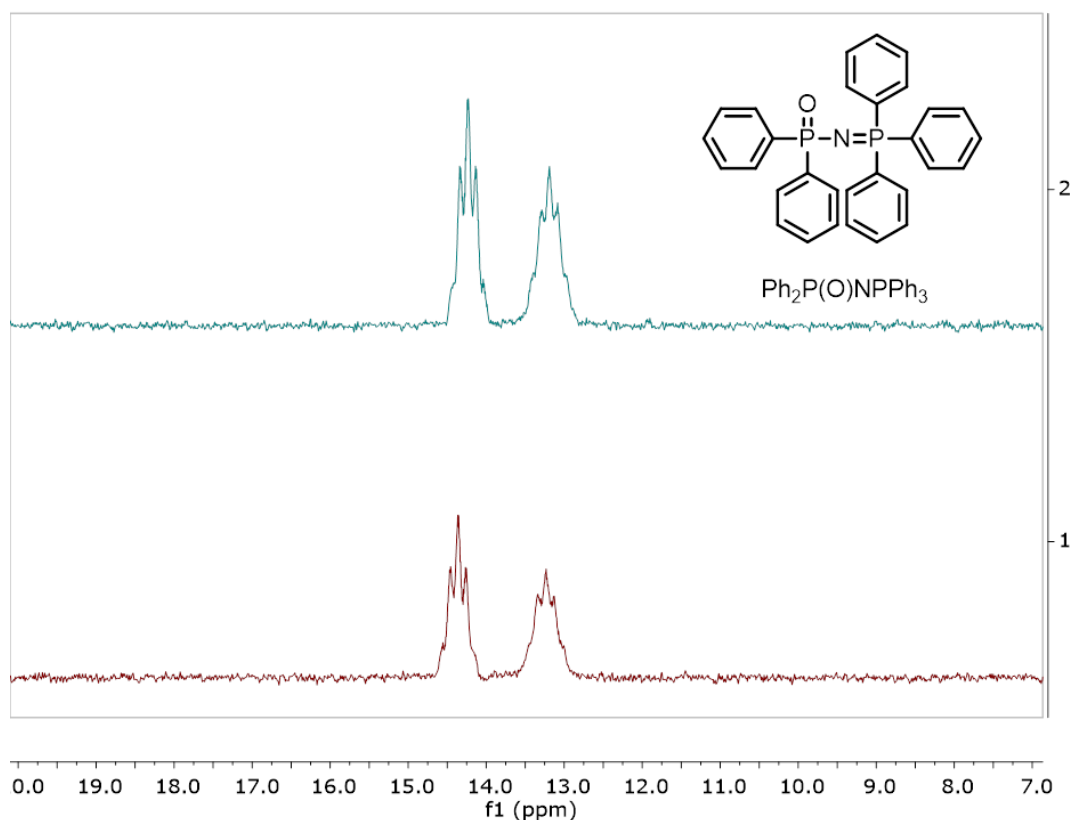


Figure 5-6. ^{31}P NMR spectra in CDCl_3 of commercial $\text{Ph}_2\text{P}(\text{O})\text{NPPh}_3$ (red, bottom) and $\text{Ph}_2\text{P}(\text{O})\text{NPPh}_3$ obtained from the reaction of PPNCl and NaOH (blue, top).

Interestingly, the combination of complex **5.1** with $\text{Ph}_2\text{P}(\text{O})\text{NPPh}_3$ can also efficiently convert CHO and CO_2 to PCHC with a similar molecular weight and narrow dispersity compared to that produced using **5.1** and PPNCl (Table 5-3, entry 2 and 3). The MALDI-TOF mass spectrum of this polymer precipitated from methanol showed multiple series of signals separated by a repeating unit of m/z 142 (See appendix Figure B-6). A closer inspection of these repeating units showed three identifiable ions (Figure 5-7). Ion series (a) and (c) correspond to the expected polycarbonate diols possessing K^+ ions. The

only difference is ion series (a) contains one ether linkage, $[17 \text{ (OH)} + 142n \text{ (repeating cyclohexene carbonate unit)} + 180 \text{ (C}_{12}\text{H}_{20}\text{O)} + 17 \text{ (OH)}]$. Dominant ion series (b) corresponds to the presence of $\text{Ph}_2\text{P(O)NPPh}_3$ and hydroxyl as the end-groups, $[17 \text{ (OH)} + 142n \text{ (repeating cyclohexene carbonate unit)} + 82 \text{ (C}_6\text{H}_{10}) + 477 \text{ (Ph}_2\text{P(O)NPPh}_3)]$ possessing Na^+ ions.

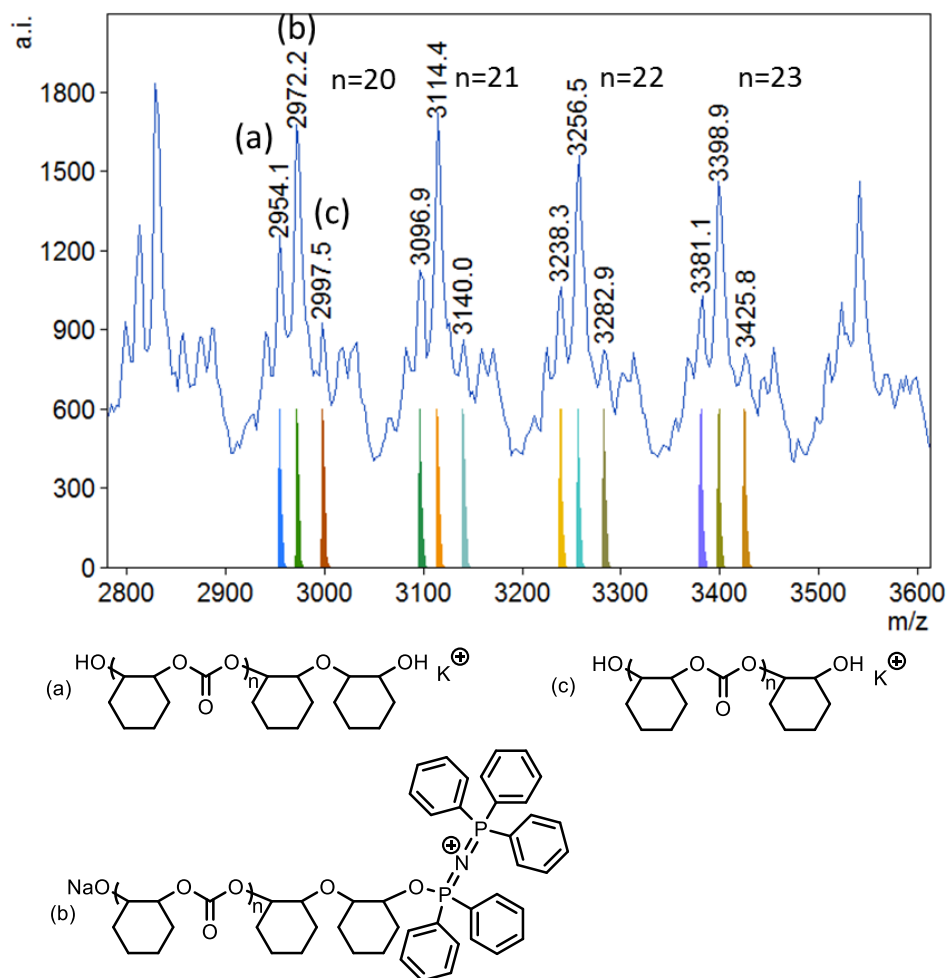


Figure 5-7. Magnified section of MALDI-TOF mass spectrum of PCHC obtained using **5.1** and $\text{Ph}_2\text{P(O)NPPh}_3$ (Table 5-3, entry 3). Modeled isotopic masses for polymers (a–c) containing different end-groups are shown below the experimental spectrum.

However, the ^{31}P NMR spectrum of the resulting polymer did not show any phosphorus resonances (See appendix Figure C-6,7), which is not consistent with the end-group analysis via MALDI-TOF MS. One possible reason for the absence of phosphorus signals is the high molecular weight of the polymer leading to the resulting phosphorus concentration being too low to be detected. Therefore, the copolymerization of CHO and CO₂ by **5.2** and Ph₂P(O)NPh₃ was run for 2 h to decrease the molecular weight of the resulting polymer. The GPC traces of the resulting polymer vs. the polymer obtained after 24 h clearly demonstrated that the polymer obtained after 2 h had a lower molecular weight (Figure 5-8). $^{31}\text{P}\{^1\text{H}\}$ NMR spectrum of the resulting purified polymer clearly showed two peaks at 29.71 and 20.57 ppm, corresponding to the Ph₂P(O)NPh₃ end-group in the polymer chain (Figure 5-10). Unlike the TFA-polycarbonate-OH polymers,^{16,17} the Ph₂P(O)NPh₃-polycarbonate-OH polymer likely could not be hydrolysed in the presence of adventitious water during the reaction or terminated by hydrolysis in methanol to afford polycarbonate diol.

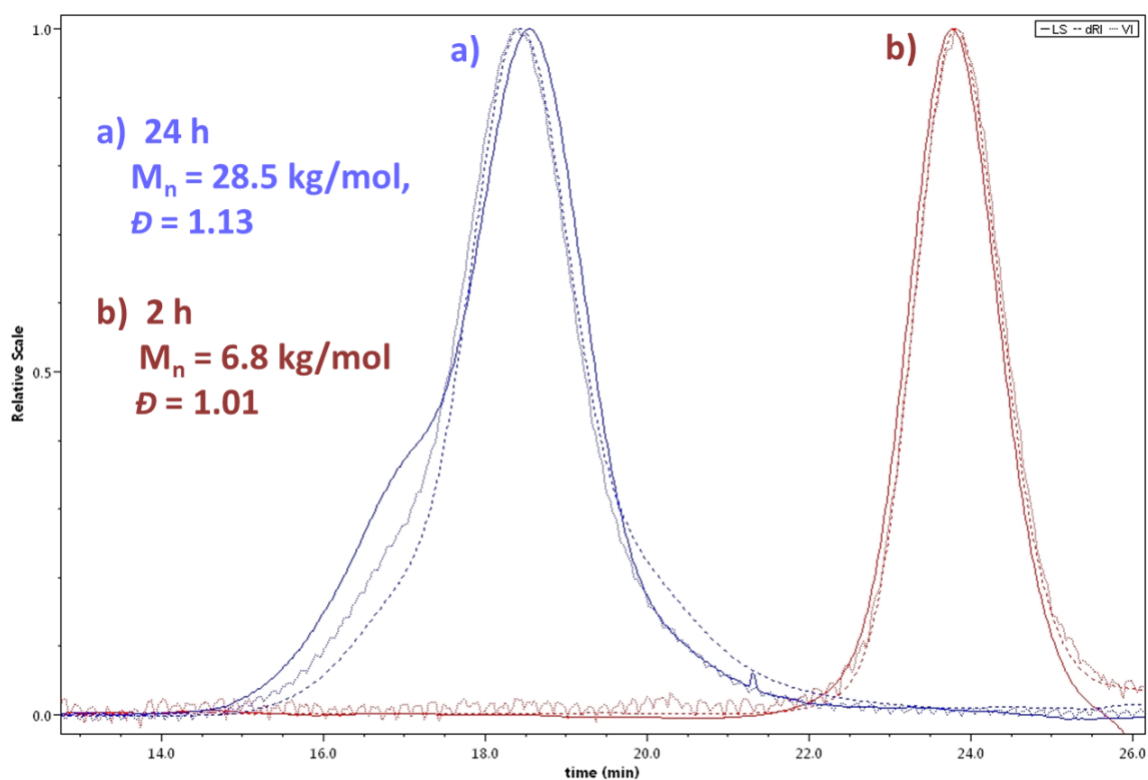


Figure 5-8. GPC traces determined by triple detection of the polymers obtained from CHO/CO₂ copolymerization by **5.1** and Ph₂P(O)NPPPh₃ with different reaction times (a) 24 h (b) 2 h.

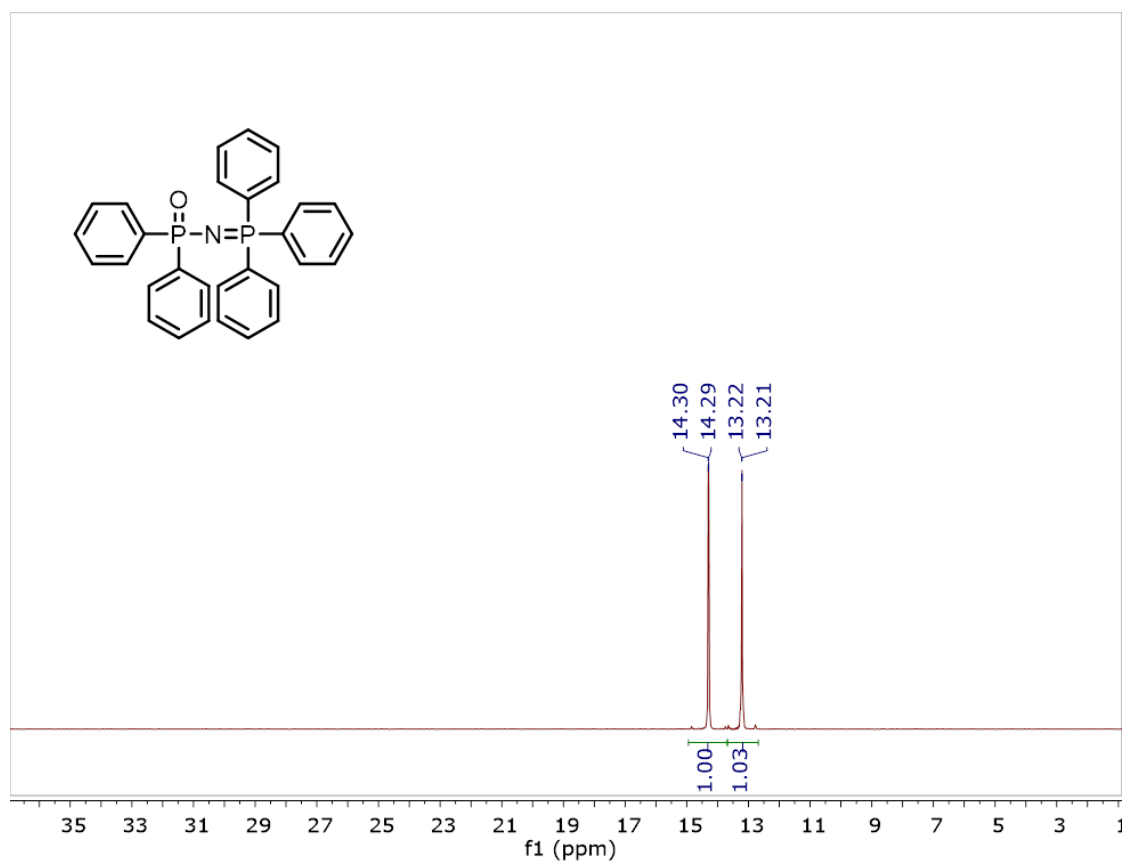


Figure 5-9. $^{31}\text{P}\{^1\text{H}\}$ NMR spectrum of $\text{Ph}_2\text{P}(\text{O})\text{NPh}_3$ in CDCl_3 .

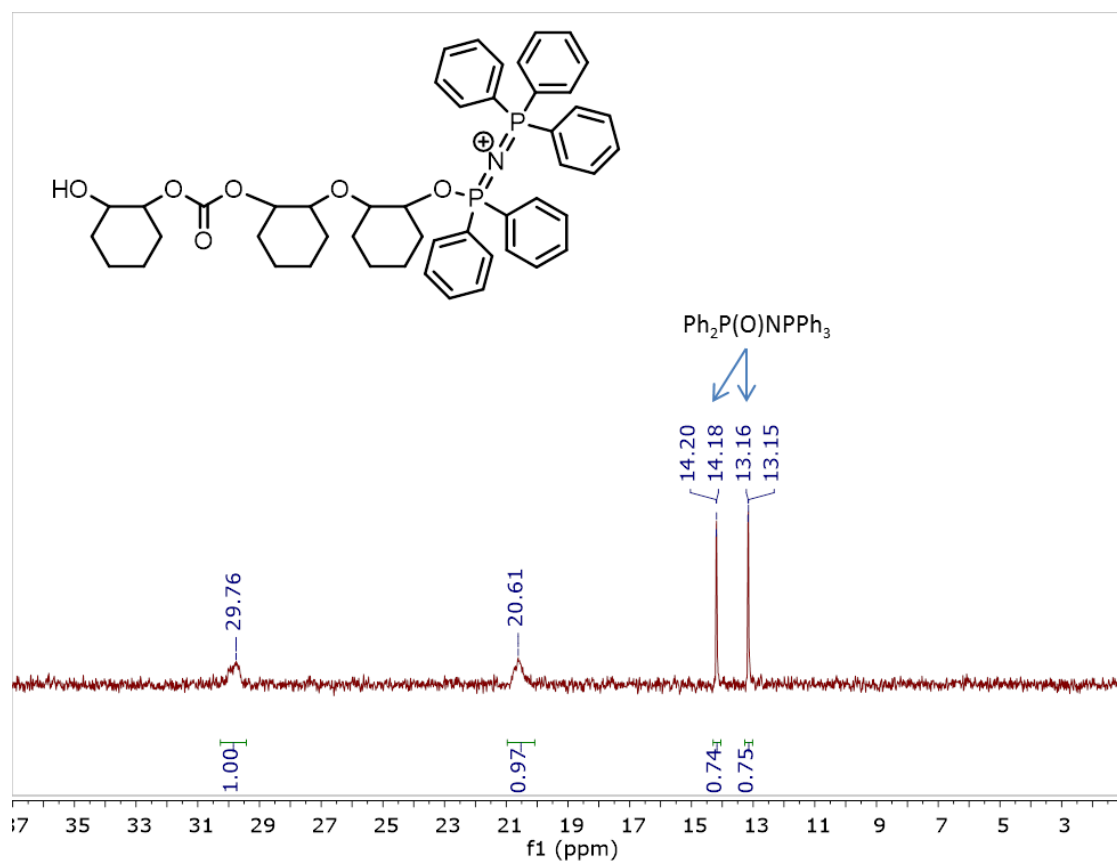


Figure 5-10. ^{31}P $\{^1\text{H}\}$ NMR spectrum in CDCl_3 of the purified polymer obtained from CHO/ CO_2 copolymerization by **5.1** and $\text{Ph}_2\text{P}(\text{O})\text{NPPH}_3$ for 2 h.

Next, tetra(*n*-butyl)ammonium hydroxide (Bu_4NOH) was tested for its ability to produce polycarbonate diol. Because isolation of pure Bu_4NOH can induce a Hofmann elimination forming of Bu_3N and 1-butene, a methanol solution of Bu_4NOH was used as cocatalyst for the copolymerization reaction (Table 5-3, entry 4). The produced PCHC showed a good conversion but a lower number-averaged molecular weight ($M_n = 6300 \text{ g mol}^{-1}$) than that produced using PPNCl or $\text{Ph}_2\text{P}(\text{O})\text{NPPH}_3$ as cocatalyst, likely due to chain transfer reactions by the presence of water and methanol.^{33,34} The MALDI-TOF mass

spectrum of this PCHC showed a single series of polymer chains corresponding to the expected polycarbonate diol, but with ether linkages, $[17 \text{ (OH)} + 142n \text{ (repeating cyclohexene carbonate unit)} + 5 \times 98 \text{ (C}_6\text{H}_{10}\text{O)} + 82 \text{ (C}_6\text{H}_{10}) + 17 \text{ (OH)}]$ (Figure 5-11), wherein the hydroxide from **5.1** or Bu₄NOH initiated the polymerization and terminated by hydrolysis. The ¹H NMR spectrum of the resulting polymer also showed a peak at *ca.* 3.4 ppm, which corresponds to the ether linkages (Figure 5-12).

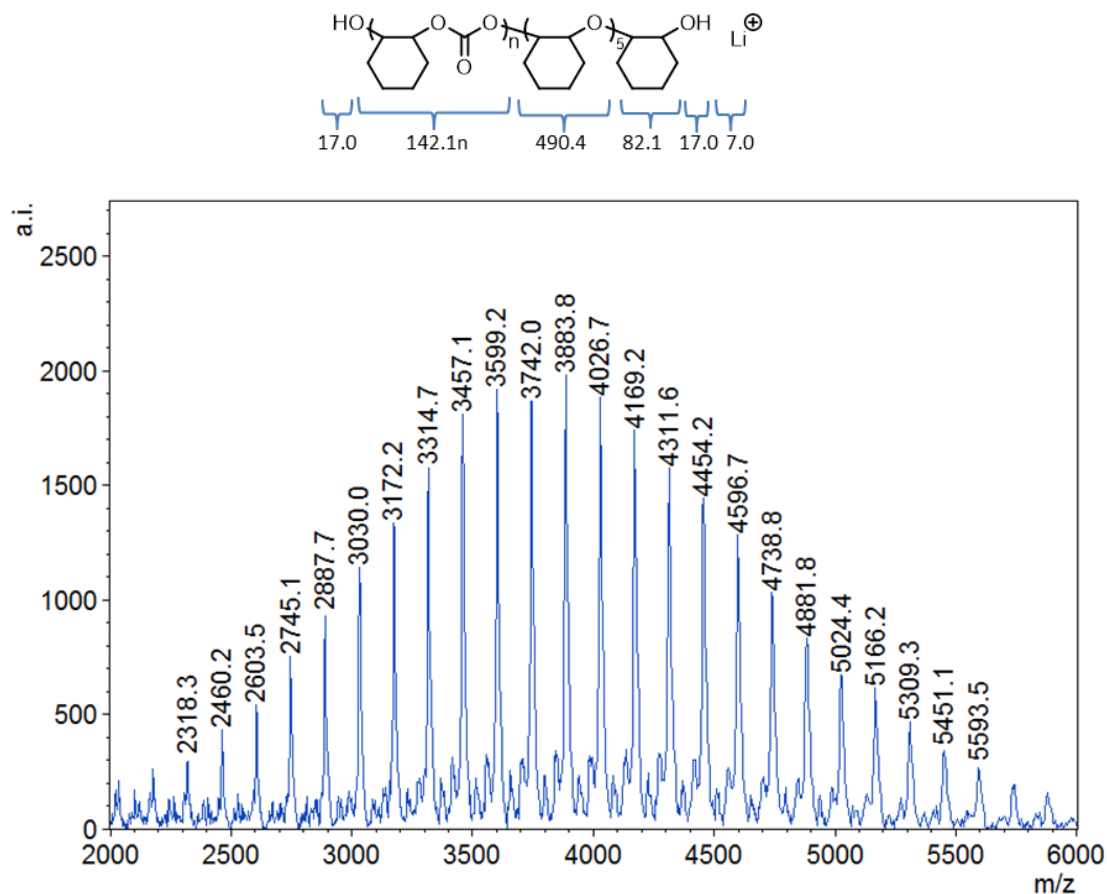


Figure 5-11. MALDI-TOF mass spectrum of polycarbonate diol produced using Bu₄NOH as cocatalyst according to the conditions in Table 5-3, entry 4.

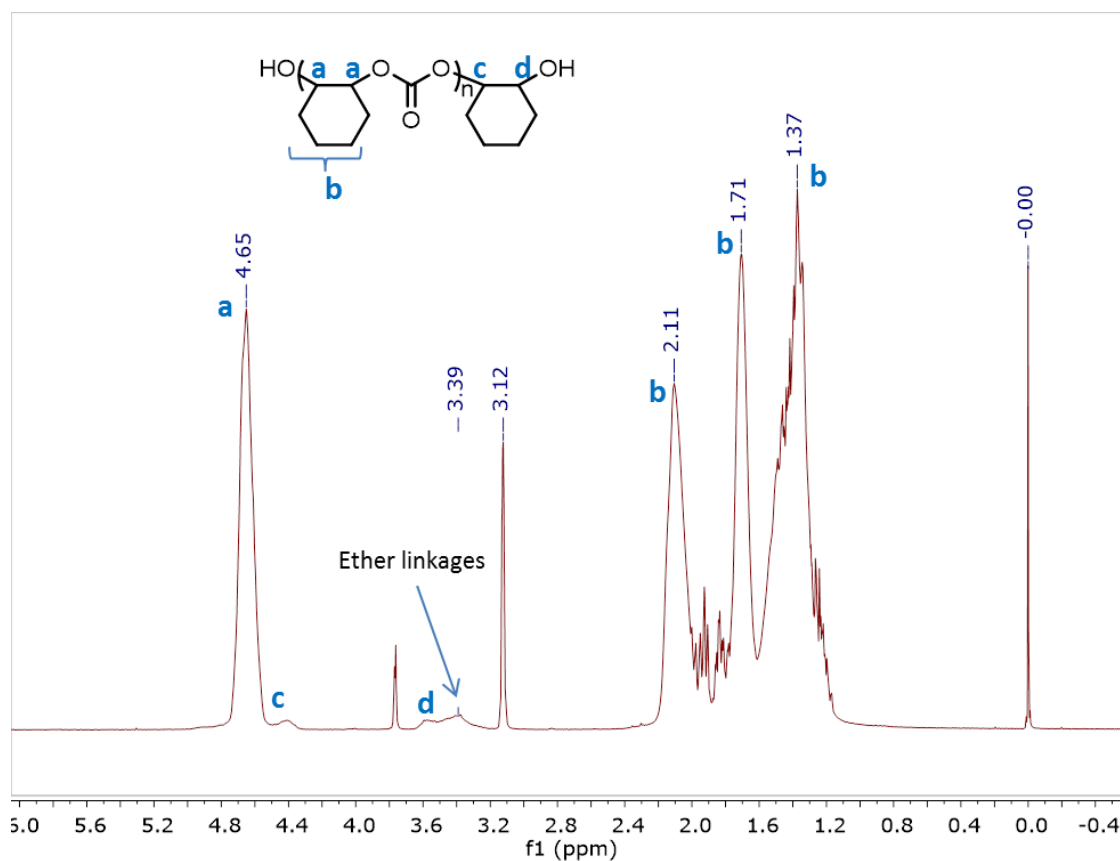


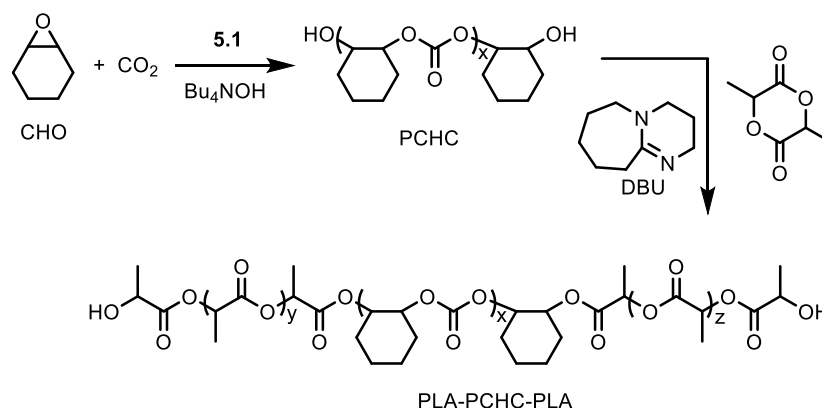
Figure 5-12. ^1H NMR spectrum of the polymer produced using Bu_4NOH as cocatalyst according to the conditions in Table 5-3, entry 4.

The thermal properties of the produced PCHCs were analyzed using differential scanning calorimetry (DSC) and thermal gravimetric analysis (TGA). The midpoint glass transition temperatures of PCHC with $M_n = 27000 \text{ g mol}^{-1}$ and $M_n = 28500$ were measured to be 104°C and 110°C , which are close to the reported value of 116°C .³⁵ For the lower molecular weight polycarbonate diol ($M_n = 6300 \text{ g mol}^{-1}$), a lower midpoint glass transition temperature of 79°C was observed, which can be attributed to the presence of multiple ether linkages.³⁶ The onset of decomposition temperatures of the produced PCHCs were

found to be between 254 °C and 284 °C, which are close to those reported values between 253 °C and 275 °C by Darensbourg and co-workers.⁹ It is worth noting that the polycarbonate with a $\text{Ph}_2\text{P}(\text{O})\text{NPPH}_3$ end-group exhibited a higher decomposition temperature of 302 °C. This suggests that varying end-groups of polycarbonate polymers can have a significant effect on their thermal properties and is a route to polycarbonate-modification that should be explored further in the future.

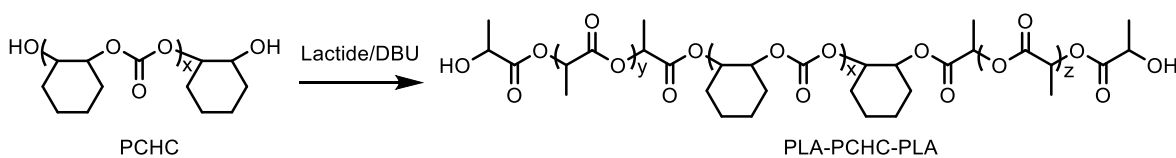
5.2.4 Block copolymerization of PCHC and lactide

The di-hydroxyl terminated PCHC ($M_n = 6300 \text{ g mol}^{-1}$) obtained by using **5.1** with Bu_4NOH was used for the ring-opening polymerization of *rac*-lactide in the presence of 1,8-Diazabicyclo[5.4.0]undec-7-ene (DBU) to produce tri-block copolymer (Scheme 5-3). The PCHC with shorter polymer chain ($M_n = 6300 \text{ g mol}^{-1}$) was extended with 87 and 44 equiv. of *rac*-lactide (Table 5-4).



Scheme 5-3. Copolymerization of CHO and CO₂ and subsequent block copolymerization with *rac*-lactide.

Table 5-4. The result of tri-block copolymerization from PCHC and *rac*-lactide



Entry	M _n	T _g	T _d	[PCHC]:[LA]	Conv. ^b	M _n ^c	Đ ^c	M _n ^d	T _g	T _d
	PCHC ^a	(°C)	(°C)	(molar ratio)	(%)	PLA-PCHC-PLA	(M _w /M _n)	PLA-PCHC-PLA	(°C)	(°C)
	(g mol ⁻¹)					(g mol ⁻¹)		(Calc) g mol ⁻¹		
1	6300	79	254	1:87	98	14000	1.05	18000	56	313
2	6300	79	254	1:44	97	11000	1.04	12000	71	311

^a Determined by triple detection GPC in THF (dn/dc = 0.0701 mL g⁻¹). ^b Conversion determined by ¹H NMR. ^c Determined by triple detection GPC in THF (dn/dc = 0.0497 mL g⁻¹). ^d Determined from the sum of experimentally determined M_n (GPC) for PCHC and the expected M_n for the PLA blocks calculated from the conversion of lactide.

The ¹H NMR spectrum of the resulting product showed a tri-block copolymer was obtained (Figure 5-13). The resonances at 4.6 ppm and 5.2 ppm (a and b) were assigned to

PCHC and PLA chains, respectively. The resonances assigned to the terminal PCHC methine protons (Figure 5-12, c and d) were not observed in the tri-block copolymer, which was likely attributed to the deshielding by the adjacent ester group leading to them being masked by the polymer chain resonances (a).¹⁷ Two resonances at 4.3 ppm were observed, which can be assigned to the methine protons within the linking PCHC-lactide unit (c) and the methine protons in the terminal lactide unit (d). Similar resonances were also observed in tri-block copolymer (PLA-X-PLA) obtained from using poly(ethylene glycol)s as macroinitiators by ¹H NMR.³⁷

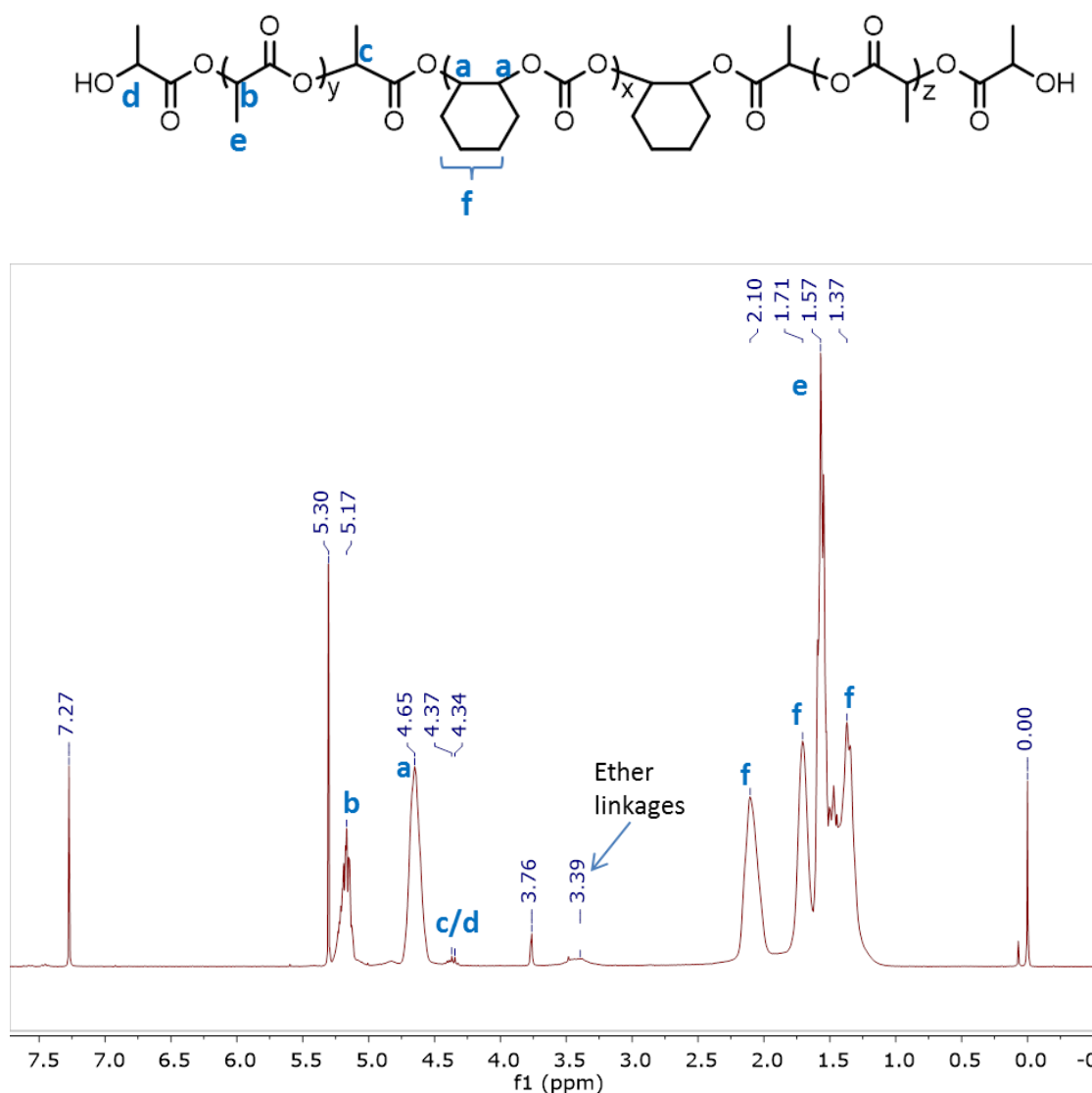


Figure 5-13. ^1H NMR spectrum in CDCl_3 of PLA-PCHC-PLA (Table 5-4, entry 1). Resonances at 3.4 ppm and 5.3 ppm in spectrum correspond to ether linkages (omitted in the above structure for clarify) and CH_2Cl_2 , respectively.

The number-average molecular weights (M_n) of the resulting tri-block copolymers determined by triple-detection GPC in THF were in reasonable agreement with the values for the calculated M_n . It is worth noting that dn/dc values is generally not suitable for

tri-block copolymer using triple detection. However, an exception to this case is that tri-block copolymers with narrow dispersities can be assumed to be close to the true molar mass, which makes it suitable for triple detection.³⁸ In our case, the resulting tri-block copolymers exhibited very narrow dispersities. The GPC traces of the PCHC and the resultant PLA-PCHC-PLA tri-block copolymer obtained using the conditions in Table 5-4 are showed in Figure 5-14. It is apparent that the resulting copolymer showed an increasing molecular weight and a very narrow dispersity, demonstrating successful chain extension from the two hydroxyl end-groups of the PCHC. In addition, using different loadings of *rac*-LA showed an increase in the molecular weight of the resulting copolymer consistent with the amount of *rac*-lactide used (Figure 5-14). It is worth noting that the GPC trace of the polycarbonate diol (peak a) showed slight bimodality, most likely due to the chain transfer reactions resulting from cyclohexane diol (formed in the presence of methanol from Bu₄NOH) causing the presence of multiple ether linkages.

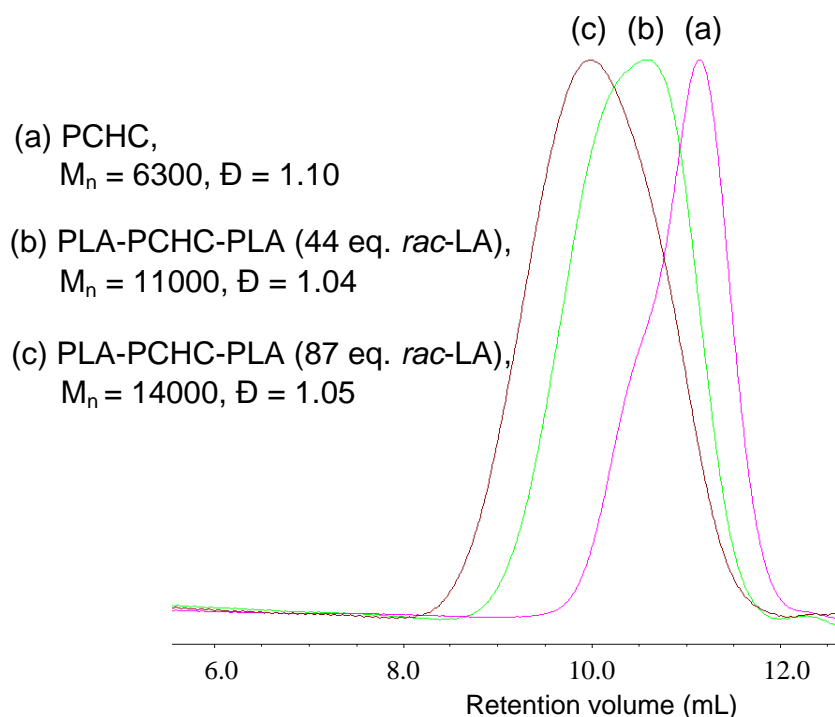


Figure 5-14. GPC traces of PCHC and PLA-PCHC-PLA from RI detector using THF as eluent (Table 5-4, entries 1 and 2).

The glass transition temperatures of the resulting tri-block copolymers were expected to decrease because of the presence of PLA blocks (Figure 5-15).³⁹ Herein a decreasing glass transition temperature of the tri-block copolymer was observed with an increase in *rac*-lactide incorporation (Table 5-4, entries 1 and 2). The onset decomposition temperatures of the tri-block copolymers (Table 5-4, entries 1 and 2) were found to increase, ranging between 307 °C and 313 °C (Figure 5-16).

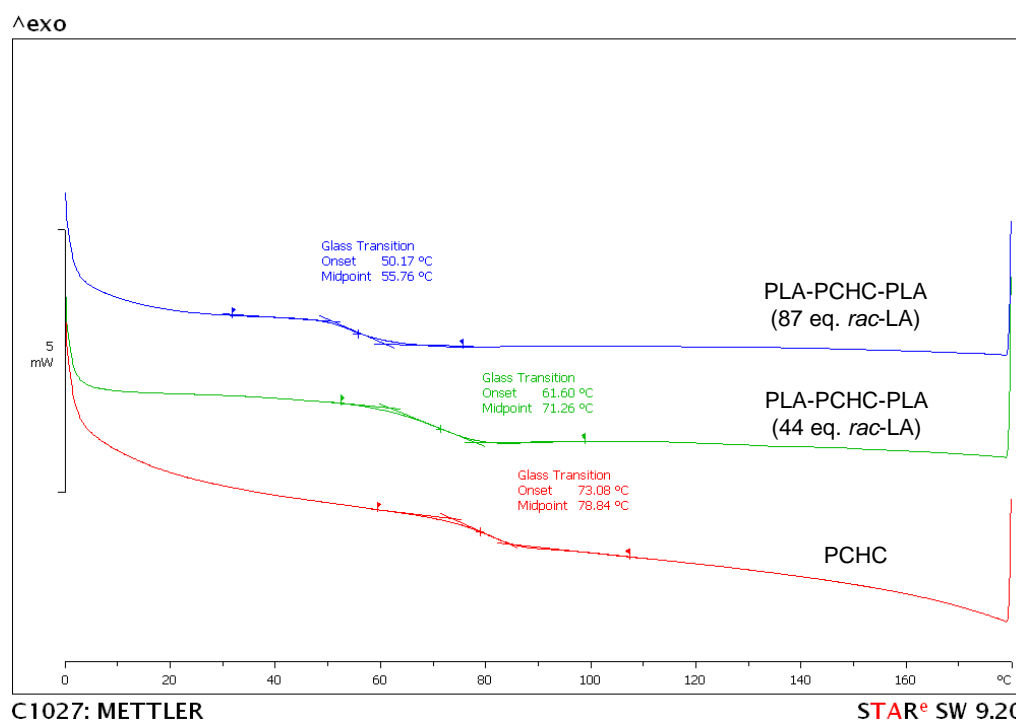


Figure 5-15. DSC second heating curves of PCHC and PLA-PCHC-PLA (Table 5-4, entries 1 and 2).

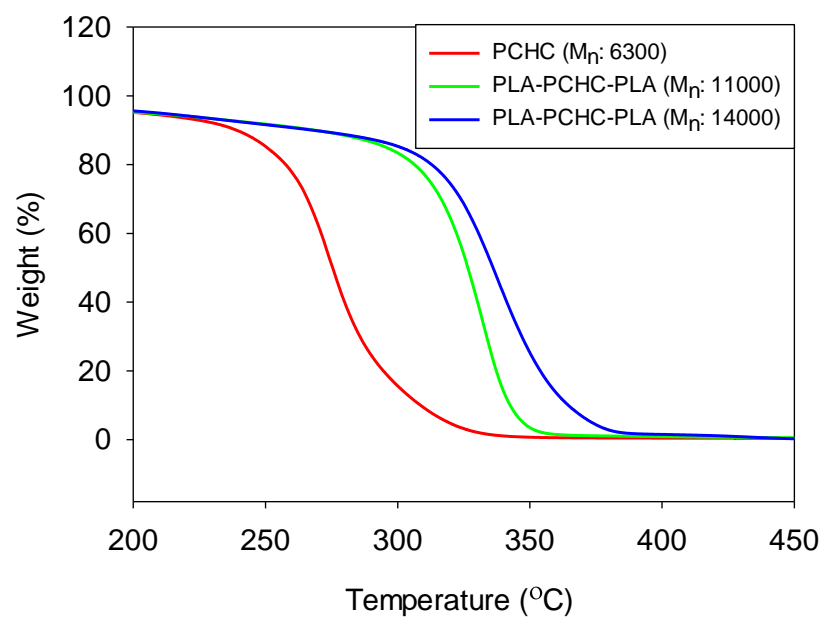


Figure 5-16. TGA curves of PCHC and PLA-PCHC-PLA (Table 5-4, entries 1 and 2).

Block copolymerization was also monitored using in situ infrared spectroscopy. Figure 5-17 showed the three-dimensional plot of the ring-opening polymerization of *rac*-lactide initiated by PCHC in the presence of DBU. From the infrared spectra, it is apparent that addition of DBU to the solution of lactide and PCHC caused a decrease in the *rac*-lactide carbonyl absorption at 1772 cm^{-1} commensurate with an increase in the carbonyl absorption of tri-block copolymer at 1757 cm^{-1} .

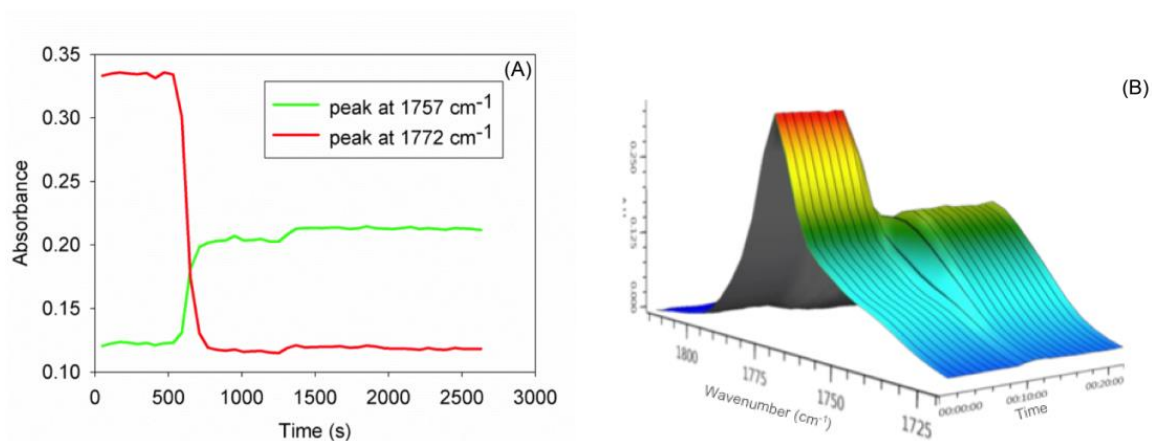


Figure 5-17. (A) Reaction profile and (B) resulting three-dimensional plot of IR spectra. The absorptions at 1772 and 1757 cm^{-1} arise from the carbonyl groups from *rac*-lactide and the resulting PLA of the tri-block copolymer, respectively. DBU added at $t = 10$ min.

5.3 Conclusions

Amino-bis(phenolate) chromium hydroxide complex in combination with different cocatalysts such as PPNCl, $\text{Ph}_2\text{P}(\text{O})\text{NPPH}_3$ or Bu_4NOH can efficiently convert of CHO to PCHC. The use of Bu_4NOH as a cocatalyst can copolymerize CHO with CO_2 to give

di-hydroxyl terminated PCHC in a controlled and systematic fashion. The di-hydroxyl terminated PCHC can be used as a macroinitiator in the ring-opening polymerization of *rac*-lactide, using DBU as a co-initiator. Near-quantitative conversion of *rac*-lactide was achieved to give ABA tri-block copolymers. The new copolymers were characterized by NMR spectroscopy, GPC, DSC and TGA analysis and represent potentially useful materials based on renewable feedstocks.

5.4 Experimental

5.4.1 General materials

Unless otherwise stated, all manipulations were performed under an atmosphere of dry, oxygen-free nitrogen by means of Schlenk techniques or using an MBraun Labmaster DP glove box. Anhydrous THF was distilled from sodium/benzophenone ketyl under nitrogen. CHO was purchased from Aldrich and freshly distilled from CaH₂ under nitrogen. CH₂Cl₂ was purified by an MBraun Manual Solvent Purification System. DBU was purchased from Aldrich, dried over CaH₂, and distilled under reduced pressure. PPNCl and NaOH were purchased from Alfa Aesar or Caledon, and used without further purification. *rac*-Lactide was purchased from Aldrich or Alfa Aesar and dried over Na₂SO₄ in THF, recrystallized and stored under an inert atmosphere prior to use. Bu₄NOH solution in MeOH was purchased from Alfa Aesar and used without further purification.

5.4.2 Instrumentation

MALDI-TOF MS was performed using an Applied Biosystems 4800 MALDI TOF/TOF Analyzer equipped with a reflectron, delayed ion extraction and high performance nitrogen laser (200 Hz operating at 355 nm). Samples of **2.1** and **5.1** were prepared in the glove box and sealed under nitrogen in a Ziploc© bag for transport to the instrument. Anthracene was used as the matrix for complexes **2.1** and **5.1**, and 2,5-dihydroxybenzoic acid (DHBA) was used as the matrix for the copolymers. Anthracene and complex were each dissolved in toluene at concentrations of 10 mg·mL⁻¹. The matrix and complex solutions were combined in a 1:1 ratio as the analyzed sample. DHBA was dissolved in THF at approximately 16 mg·mL⁻¹ and polymer was dissolved in THF at approximately 10 mg mL⁻¹. The matrix and polymer solutions were combined in a 4:1 ratio as the analyzed sample. 1 µL aliquots of these samples were spotted on the MALDI plate and left to dry. Images of mass spectra were prepared using mMass™ software (www.mmass.org).

Molecular weight determination of copolymer was performed on an Agilent Infinity HPLC instrument connected to a Wyatt Technologies triple detector system (multi angle light scattering (MALS), viscometry and refractive index) equipped with two Phenogel 10³ Å 300 × 4.60 mm columns with THF as eluent. Copolymer samples were prepared in THF at a concentration of 4 mg mL⁻¹ and filtered through syringe filters (0.2 µm). The

sample solution was then eluted at a flow rate of $0.30 \text{ mL} \cdot \text{min}^{-1}$. The values of dn/dc were calculated online (columns detached) assuming 100% mass recovery using the Astra 6 software package (Wyatt Technologies) giving dn/dc (poly(cyclohexene carbonate) = $0.0701 \text{ mL} \cdot \text{g}^{-1}$ and dn/dc (tri-block copolymer) = $0.0497 \text{ mL} \cdot \text{g}^{-1}$. This work was completed by the assist of Hart Plommer.

^1H NMR spectra were recorded at 300 MHz in CDCl_3 . ^{31}P NMR spectra were recorded at 300 MHz in CDCl_3 or 600 MHz. Elemental analysis was performed at Saint Mary's University, Halifax, Nova Scotia, Canada. Infrared spectra were obtained on a Bruker Alpha FTIR spectrometer. In situ IR experiments were performed with a Mettler Toledo ReactIR 15TM reaction analysis system with a SiComp Sentinel probe coupled to a 100 mL Parr stainless steel pressure vessel.

The glass transition (T_g) temperatures were measured using a Mettler Toledo DSC 1 STAR^c System equipped with a Julabo FT 100 immersion cooling system, using R1150 refrigerant in an EtOH bath with a working range of -100 to $+20$ °C. Samples were weighed into 40 μL aluminum pans and subjected to two heating cycles from 0 to 180 °C at a rate of 10 °C min^{-1} . T_g of copolymers were determined from the second heating. Thermogravimetric analysis measurement was performed with a TA Instruments Q500. Samples were loaded onto a platinum pan and subjected to a dynamic high-resolution scan. Each sample was heated from room temperature to 450 °C at a heating rate of

10 °C min⁻¹.

5.4.3 Synthesis of complex 5.1 and Ph₂P(O)NPh₃

Complex **2.1** (1.00 g, 1.46 mmol) and sodium hydroxide (0.29 g, 7.30 mmol) were placed in a Schlenk tube. THF (20 mL) was added and stirred for 2 days giving a green suspension. Filtration of the mixture via cannula gave a green solution, which upon removal of solvent under vacuum gave a green solid. The residue was extracted into toluene, filtered through Celite and the solvent was removed under vacuum. The product was dried to yield 0.55 g (64%) of green crystalline solid. Anal. Calcd for C₃₄H₅₅CrN₂O₃·1.65NaOH: C, 62.08; H, 8.68; N, 4.26. Found: C, 62.46; H, 9.04; N, 3.87. MS (MALDI-TOF) m/z (% ion): 654.4 (72, [CrOH[L]+NaOH+Na⁺]), 614.4 (80, [CrOH[L]Na⁺]), 591.4 (10, [CrOH[L]⁺]), 574.4 (10, [Cr[L]⁺]).

PPNCl (2.00 g, 3.48 mmol) was dissolved in 1 mL methanol and chilled to below 10 °C using an ice bath. NaOH (0.18 g, 4.50 mmol) was dissolved in 3 mL methanol. The resulting NaOH solution was added into PPNCl solution dropwise and stirred for 3 h. Precipitate was observed after ~20 min. The resulting mixture was filtered and solvent removed yielding a light-yellow oil. MeCN/Et₂O was used for recrystallization. Yield: 0.7 g (42%). ³¹P NMR (ppm, CDCl₃): 13.23, 14.35. Other spectroscopic characterization was as previously reported.⁴⁰

5.4.4 Copolymerization conditions.

5.1 (67 mg, 0.10 mmol) and $\text{Ph}_2\text{P}(\text{O})\text{NPPH}_3$ (47 mg, 0.10 mmol) were combined in 3 mL of CH_2Cl_2 and allowed to stir for 10 min before removal of solvent under vacuum. **CHO** (5.0 g, 50 mmol) was added to the residue and stirred for 10 min. The reactant solution was added via syringe to a stainless steel Parr autoclave, which was pre-dried under vacuum overnight at 80 °C. The autoclave was heated to 60 °C, then charged with 40 bar of CO_2 and left to stir for 24 h. After the desired time the autoclave was cooled in an ice bath and vented in the fume hood. An aliquot for ^1H NMR was taken immediately after opening for the determination of conversion. The copolymer was extracted with CH_2Cl_2 and precipitated using cold methanol. The product was then dried at 80 °C in a vacuum oven overnight. For reactions done in the presence of Bu_4NOH , **5.1** was first dissolved in **CHO** followed by addition of the resulting green solution to Bu_4NOH (40% w/w in methanol) and stirring for 5 min. The remaining procedure was followed in the same manner as described above.

5.4.5 Block copolymerization conditions.

Poly(cyclohexene carbonate) (Table 5-3, entry 4) (0.50 g) and the required amount of *rac*-lactide were dissolved in 4 mL CH_2Cl_2 . After 5 min, DBU (0.085 g, 0.56 mmol) dissolved in 1 mL CH_2Cl_2 was added and stirred overnight at 40 °C in an ampule. The

solvent was pumped off to give a crude polymer. The crude polymer was dissolved in CH_2Cl_2 and benzoic acid as per the method of Darensbourg,³ then precipitated from cold methanol. The purified colorless polymer was dried at 80 °C in a vacuum oven overnight.

5.5 References

- (1) Stanford, M. J.; Dove, A. P. *Chem. Soc. Rev.* **2010**, *39*, 486.
- (2) Dove, A. P. *Chem. Commun.* **2008**, *48*, 6446.
- (3) Martin, R. T.; Camargo, L. P.; Miller, S. A. *Green Chem.* **2014**, *16*, 1768.
- (4) Chamberlain, B. M.; Cheng, M.; Moore, D. R.; Ovitt, T. M.; Lobkovsky, E. B.; Coates, G. W. *J. Am. Chem. Soc.* **2001**, *123*, 3229.
- (5) Lian, B.; Thomas, C. M.; Casagrande, O. L., Jr.; Lehmann, C. W.; Roisnel, T.; Carpentier, J.-F. *Inorg. Chem.* **2007**, *46*, 328.
- (6) Breyfogle, L. E.; Williams, C. K.; Young, V. G., Jr.; Hillmyer, M. A.; Tolman, W. B. *Dalton Trans.* **2006**, 928.
- (7) Saunders, L. N.; Dawe, L. N.; Kozak, C. M. *J. Organomet. Chem.* **2014**, *749*, 34.
- (8) Kim, J. G.; Cowman, C. D.; LaPointe, A. M.; Wiesner, U.; Coates, G. W. *Macromolecules* **2011**, *44*, 1110.
- (9) Darensbourg, D. J.; Ulusoy, M.; Karroonnirum, O.; Poland, R. R.; Reibenspies, J. H.; Cetinkaya, B. *Macromolecules* **2009**, *42*, 6992.
- (10) Jeske, R. C.; Rowley, J. M.; Coates, G. W. *Angew. Chem., Int. Ed.* **2008**, *47*, 6041.
- (11) Huijser, S.; HosseiniNejad, E.; Sablong, R. I.; Jong, C. d.; Koning, C. E.; Duchateau, R. *Macromolecules* **2011**, *44*, 1132.
- (12) Darensbourg, D. J.; Poland, R. R.; Escobedo, C. *Macromolecules* **2012**, *45*, 2242.

- (13) Kröger, M.; Folli, C.; Walter, O.; Döring, M. *Adv. Synth. Catal.* **2006**, *348*, 1908.
- (14) Hwang, Y.; Jung, J.; Ree, M.; Kim, H. *Macromolecules* **2003**, *36*, 8210.
- (15) Liu, Y.; Huang, K.; Peng, D.; Wu, H. *Polymer* **2006**, *47*, 8453.
- (16) Darensbourg, D. J.; Wu, G. P. *Angew. Chem., Int. Ed.* **2013**, *52*, 10602.
- (17) Kember, M. R.; Copley, J.; Buchard, A.; Williams, C. K. *Polym. Chem.* **2012**, *3*, 1196.
- (18) Langanke, J.; Wolf, A.; Hofmann, J.; Bohm, K.; Subhani, M. A.; Muller, T. E.; Leitner, W.; Gurtler, C. *Green Chem.* **2014**, *16*, 1865.
- (19) Dean, R. K.; Dawe, L. N.; Kozak, C. M. *Inorg. Chem.* **2012**, *51*, 9095.
- (20) Jenkins, L. S.; Willey, G. R. *J. Chem. Soc., Dalton Trans.* **1979**, 1697.
- (21) Cowley, A. H.; Fairbrother, F.; Scott, N. *J. Chem. Soc.* **1959**, 717.
- (22) Emeleus, H. J.; Onyszchuk, M. *J. Chem. Soc.* **1958**, 604.
- (23) Cypriak, M.; Apeloig, Y. *Organometallics* **2002**, *21*, 2165.
- (24) Tatlock, W. S.; Rochow, E. G. *J. Am. Chem. Soc.* **1950**, *72*, 528.
- (25) Dean, R. K.; Devaine-Pressing, K.; Dawe, L. N.; Kozak, C. M. *Dalton Trans.* **2013**, *42*, 9233.
- (26) Darensbourg, D. J.; Frantz, E. B.; Andreatta, J. R. *Inorganica Chimica Acta* **2007**, *360*, 523.
- (27) Dean, R. K.; Granville, S. L.; Dawe, L. N.; Decken, A.; Hattenhauer, K. M.; Kozak, C. M. *Dalton Trans.* **2010**, *39*, 548.

- (28) Andersen, N. H.; Dossing, A.; Molgaard, A. *Inorg. Chem.* **2003**, *42*, 6050.
- (29) Devaine-Pressing, K.; Dawe, L. N.; Kozak, C. M. *Polym. Chem.* **2015**, *6*, 6305.
- (30) Kember, M. R.; Jutz, F.; Buchard, A.; White, A. J. P.; Williams, C. K. *Chem. Sci.* **2012**, *3*, 1245.
- (31) Nakano, K.; Nakamura, M.; Nozaki, K. *Macromolecules* **2009**, *42*, 6972.
- (32) Darensbourg, D. J.; Pala, M.; Rheingold, A. L. *Inorg. Chem.* **1986**, *25*, 125.
- (33) Kember, M. R.; Buchard, A.; Williams, C. K. *Chem. Commun.* **2011**, *47*, 141.
- (34) Jutz, F.; Buchard, A.; Kember, M. R.; Fredriksen, S. B.; Williams, C. K. *J. Am. Chem. Soc.* **2011**, *133*, 17395.
- (35) Koning, C.; Wildeson, J.; Parton, R.; Plum, B.; Steeman, P.; Darensbourg, D. J. *Polymer* **2001**, *42*, 3995.
- (36) Mang, S.; Cooper, A. I.; Colclough, M. E.; Chauhan, N.; Holmes, A. B. *Macromolecules* **2000**, *33*, 303.
- (37) Kricheldorf, H. R.; Rost, S.; Wutz, C.; Domb, A. *Macromolecules* **2005**, *38*, 7018.
- (38) Gores, F.; Kilz, P. *ACS Symp. Ser.* **1993**, *521*, 122.
- (39) Albertsson, A.-C.; Varma, I. K. *Biomacromolecules* **2003**, *4*, 1466.
- (40) Yilmaz, O.; Aslan, F.; Ozturk, A. I.; Vanli, N. S.; Kirbag, S.; Arslan, M. *Bioorg. Chem.* **2002**, *30*, 303.

Chapter 6. Attempted synthesis of derivatives of Cr(III)

amino-bis(phenolate) complexes

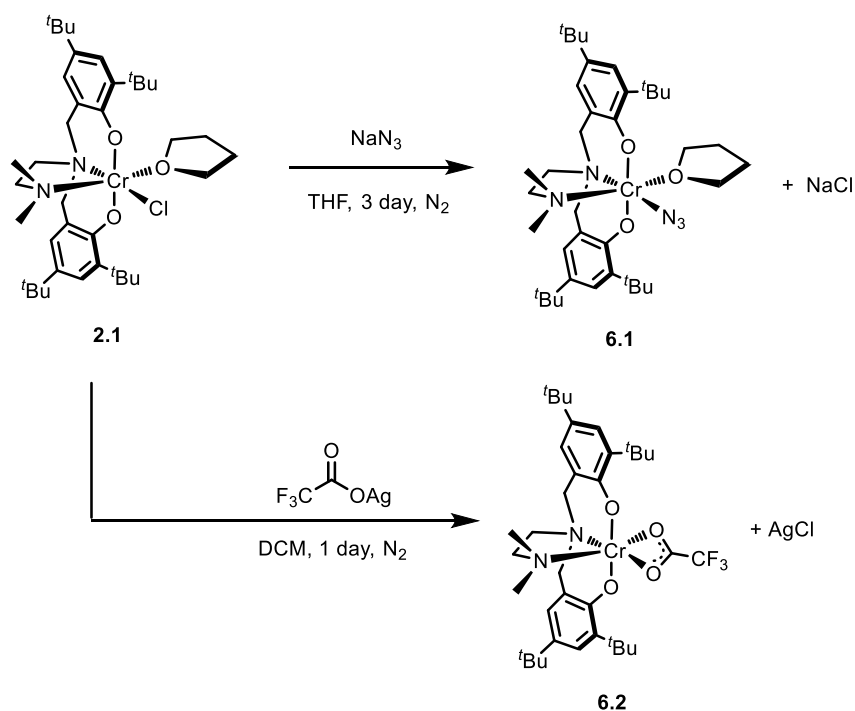
6.1 Introduction

Complex **2.1** has been found to show higher catalytic activity for CO₂/epoxide copolymerization than the previously reported Cr(III) amono-bis(phenolate) complexes as described in Chapter 2. This chapter included attempted synthesis of the derivatives of complex **2.1** to explore more active catalysts. However, only preliminary results were obtained due to the insufficient time of my PhD. Two new Cr(III) complexes were prepared and characterized by MALDI-TOF MS and elemental analysis. The purpose of this chapter was to provide a starting point for the future researchers in the group who may further explore Cr(III) amino-bis(phenolate) complexes with the goal of increasing catalytic activity and polymerization control.

6.2 Preparation and characterization of new Cr(III) complexes **6.1** and **6.2**

Complex **6.1** was prepared via reaction of **2.1** with sodium azide in THF at room temperature to produce a dark crystalline solid in a 29% yield (Scheme 6-1). MALDI-TOF mass spectrum of **6.1** showed the peaks at *m/z* 574, 616 and 639 corresponding to the [CrL]⁺, [CrN₃L]⁺ and [CrN₃L]Na⁺ ions, respectively (Figure 6-1).

The isotopic distributions of experimental peaks were in good agreement with the calculated model peaks. The peak at m/z 609 corresponding to $[\text{CrClL}]^{*+}$ was absent, indicating chloride was completely replaced with azide. Combustion analysis of **6.1** consistently showed contamination by NaCl.



Scheme 6-1. Preparation of derivatives of Cr(III) amino-bis(phenolate) complexes **6.1** and **6.2**.

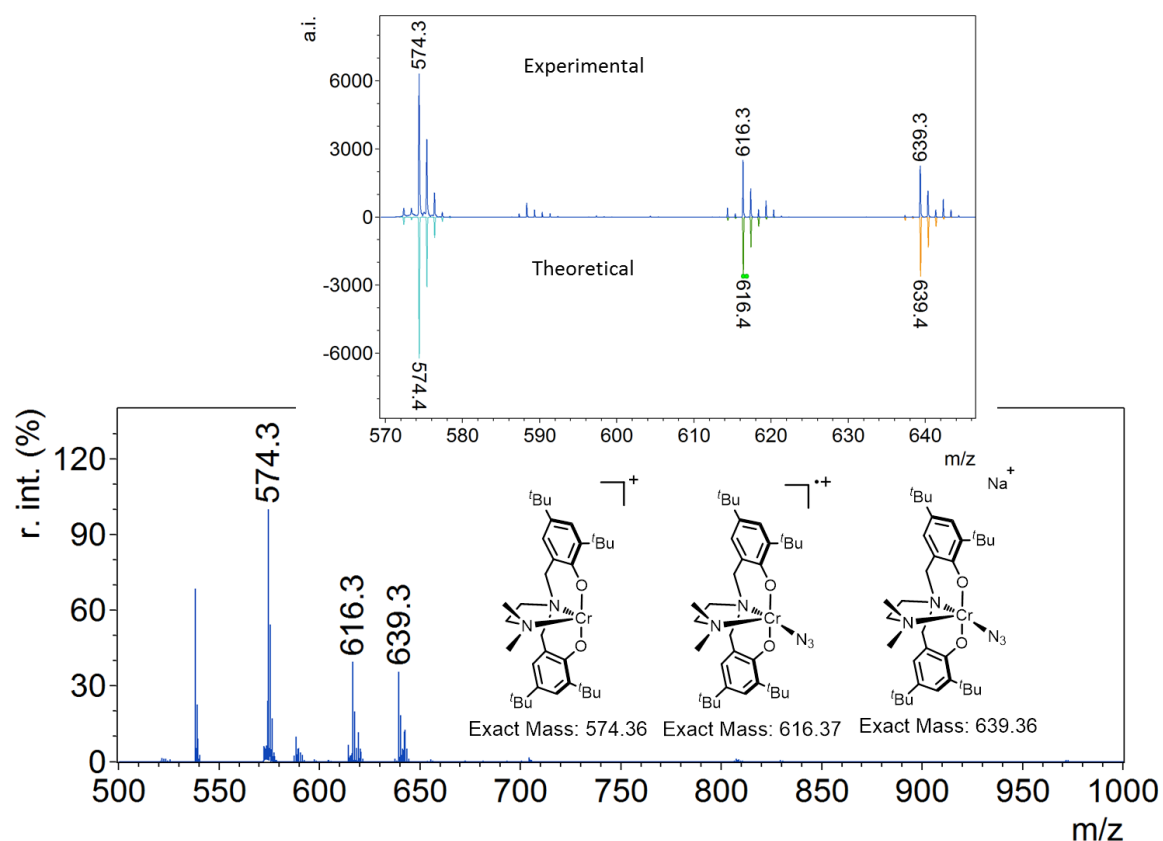


Figure 6-1. MALDI-TOF mass spectrum of **6.1** and the isotopic distributions of the model peaks.

Complex **6.2** was prepared via reaction of **2.1** with silver trifluoroacetate in DCM at room temperature to produce a dark orange solid in 50% yield (Scheme 6-1, B). MALDI-TOF mass spectrum of **6.2** showed the most intense peak at m/z 687 corresponding to $[CrLCF_3COO]^+$ ion. The peak at m/z 574 represented for the $[CrL]^+$ ion. The peak at m/z 609 corresponding to $[CrClL]^+$ was also absent, indicating chloride was completely replaced with trifluoroacetate.

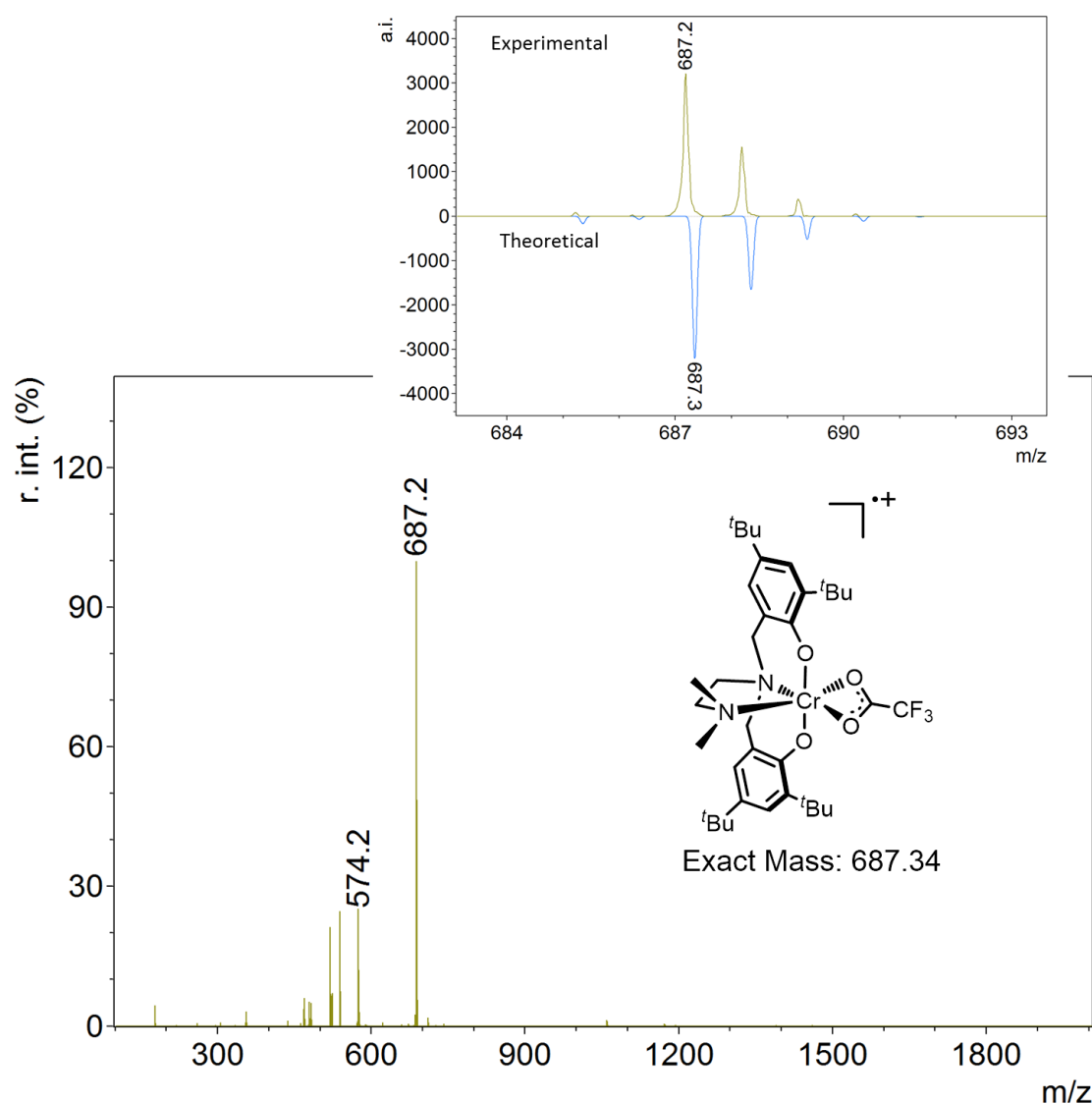


Figure 6-2. MALDI-TOF mass spectrum of **6.2** and the isotopic distribution of the model peaks.

6.3 Experimental

6.3.1 General experimental conditions

All manipulations were performed under an atmosphere of dry, oxygen-free nitrogen by means of Schlenk techniques or using an MBraun Labmaster DP glove box.

Anhydrous THF was distilled from sodium/benzophenone ketyl under nitrogen. DCM was purified by an MBraun Manual Solvent Purification System. Sodium azide was purchased from J.T.Baker Chemical Co. and silver trifluoroacetate was purchased from Alfa Aesar.

6.3.2 MALDI-TOF MS

MALDI-TOF MS was performed using an Applied Biosystems 4800 MALDI TOF/TOF Analyzer equipped with a reflectron, delayed ion extraction and high performance nitrogen laser (200 Hz operating at 355 nm). Samples of **6.1** and **6.2** were prepared in the glove box and sealed under nitrogen in a Ziploc© bag for transport to the instrument. Anthracene was used as the matrix for samples **6.1** and **6.2**. Anthracene and complex were each dissolved in toluene at concentrations of 10 mg mL⁻¹. The matrix and complex solutions were combined in a 1:1 ratio. 1 µL aliquots of these samples were spotted on the MALDI plate and left to dry. Images of mass spectra were prepared using mMass™ software (www.mmass.org).

6.3.3 Preparation of complex 6.1

2.1 (0.52 g, 0.76 mmol) was dissolved in THF (20 mL) in a Schlenk flask to produce a purple solution. Sodium azide (0.25 g, 0.76 mmol) was added into the solution. The

resulting mixture was stirred for 3 days to produce a dark purple suspension. THF was then removed under vacuum, giving a dark solid. The solid was extracted into toluene and filtered through a pad of celite. Toluene was removed under vacuum to give a dark solid in the yield of 0.15 g (29%). Anal. Calcd for $C_{38}H_{61}CrN_5O_3 \cdot 0.35NaCl$: C, 64.43; H, 8.68; N, 9.89. Found: C, 64.13, H, 8.72, N, 10.06. MS (MALDI-TOF) m/z (% ion): 639.3 (35, $[CrN_3L]Na^+$), 616.3 (40, $[CrN_3L]^{++}$), 574.3 (100, $[CrL]^+$).

6.3.4 Preparation of complex 6.2

2.1 (0.80 g, 1.17 mmol) was dissolved in DCM (20 mL) in a Schlenk flask to produce a purple solution. Silver trifluoroacetate (0.26 g, 1.17 mmol) was added into the solution. The flask was then wrapped by aluminum foil. The resulting suspension was stirred for 24 h, giving a dark orange suspension. Filtration of the mixture through a pad of celite gave a dark orange solution, which upon removal of DCM under vacuum gave a dark orange solid in a yield of 0.38 g (50%). MS (MALDI-TOF) m/z (% ion): 687.2 (100, $[CrLCF_3COO]^{++}$), 574.2 (30, $[CrL]^+$).

Chapter 7. Future work and conclusions

7.1 Ideas for the future work

As shown in Chapter 4, the key factor for the design of highly active Cr(III) amino-bis(phenolate) catalysts is to increase the steric effect of their pendant donor groups. Future work can be devoted to the modification of **2.1** to increase the steric effect of the pendant donor group. For example, the pendant donor group, dimethylaminoethyl of **2.1** can be replaced with diethylaminoethyl through synthesizing the new amino-bis(phenol) ligand, **7.1** (Figure 7-1). In addition, Chapter 4 mentioned that in the binary catalyst system the steric effect of the external nucleophile can also influence the catalytic activity, especially when the Cr(III) complex containing a pendant donor group with a small steric effect such as **3.1**. Therefore, besides using chloride or azide paired with PPN⁺ as the ionic cocatalysts, other nucleophiles such as 2,4-dinitrophenoxide and trifluoroacetate paired with PPN⁺, are worth trying.

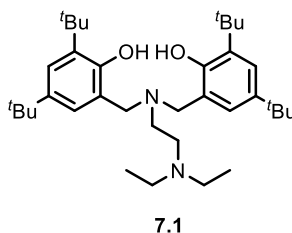


Figure 7-1. The new amino-bis(phenol) ligands worth being synthesized for the future work.

The preliminary results described in Chapter 6 provided a starting point to make the derivatives of Cr(III) amino-bis(phenolate) complexes which may show high activities. Salen catalyst containing 2,4-dinitrophenolate ligand has shown excellent activity and selectivity for CO₂/PO copolymerization at extremely mild temperature and CO₂ pressure (25 °C and 20 bar).¹ Therefore, it is worth trying to substitute the chloride of **2.1** to 2,4-dinitrophenolate through salt metathesis reaction described in Chapter 6. It is also worth preparing **6.1** and **6.2** again and growing crystals to support their structures, especially **6.2**. Because **6.2** potentially allows the incoming epoxide to bind to the Cr center through opening one side of the chelating group (trifluoroacetate), and the remaining acetate group could ring-open the activated epoxide if it is labile enough.

As reviewed in Chapter 1, recent advanced catalyst design has focused on bifunctional complexes which avoid the use of cocatalyst. A typical strategy to make bifunctional complexes is to introduce a cationic group on the ligand to balance the anion co-initiator. For example, Bun Yeoul Lee introduced quaternary ammonium groups on the phenol groups of salen ligand through ligand synthesis design.^{2,3} In the Kozak group, design and synthesis of bifunctional Cr(III) amino-bis(phenoate) complexes have not started. Future work can attempt to synthesize new amine-bis(phenol) ligands such as **7.2** (Figure 7-2) by referring Bun Yeoul Lee's ligand synthesis design.³ It is worth noting that the salt metathesis route of making Cr(III) complexes described in this thesis (Chapter 2

and 3) is not applicable for the preparation of bifunctional Cr(III) complex by the ligand **7.2**. Because the quaternary ammonium group of the new ligand **7.2** can react with NaH. Alternatively, CrCl₂ can be attempted to react with **7.2**, followed oxidation by air to make the bifunctional Cr(III) complex.⁴

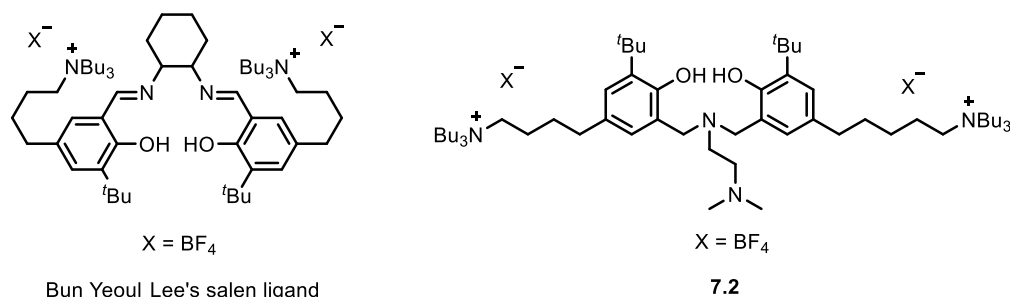


Figure 7-2. Bun Yeoul Lee's salen ligand³ and the proposed amino-bis(phenol) ligand

In terms of the modification of the physical properties of CO₂-based polymer, other epoxides, especially containing functional groups such as vinyl cyclohexene oxide can be screened to react with CO₂ by **2.1**. Because the functional group on the polycarbonate permits further functionalized, thus potentially producing more diverse CO₂-based polymers.⁵ As reviewed in Chapter 1, terpolymerization is another method to produce new CO₂-based polymer, however, such a reaction by Cr(III) amino-bis(phenolate) complexes has not been tested. For a starting point, terpolymerization of CHO and PO with CO₂ by **2.1** is worth trying since **2.1** has shown excellent activity and selectivity for CO₂/CHO copolymerization. Furthermore, the Ph₂P(O)NPh₃-polycarbonate-OH

polymer described in Chapter 5 may potentially be useful to form AB diblocks. Other researchers have primarily explored ABA block copolymers prepared from diols.

7.2 Conclusions

Due to the various applications of polycarbonates, it is of great interest that their manufacturing process starts from more environmentally starting materials. In addition, utilization of CO₂ as a chemical feedstock is receiving much attention due to the many advantages. Therefore, incorporation of CO₂ into polycarbonates has become an important and active area of research. Chapter 1 presented a literature review on this research area. Copolymerization of CO₂ and epoxides to afford polycarbonates by transition metal catalysts such as salen based ligand system coordinated with Cr⁶⁻¹⁵ or Co¹⁶⁻²¹ has shown excellent progress in terms of high reaction rate, selective polycarbonate formation, polymer molecular weight control and narrow dispersity. However, these successes by the current catalysts are generally only applied to a limited range of epoxides such CHO and PO. Further catalyst development is still required. In this thesis, research efforts have been made to synthesize new Cr(III) amino-bis(phenolate) complexes as the catalysts for CO₂/epoxide copolymerization and understand the mechanism for this reaction by the new family of catalysts. Tri-block copolymerization was also performed in an effort to produce more diverse CO₂-based copolymer.

Chapter 2 described the synthesis and characterization of a new Cr(III) amino-bis(phenolate) complex, **2.1** bearing a *N,N*-dimethylaminoethyl pendant donor. **2.1** combined with DMAP, PPNCI or PPNN₃ showed higher catalytic activity than the previously reported Cr(III) amino-bis(phenolate) complexes in the Kozak group. Kinetic studies of the catalyst system of **2.1**/DMAP revealed the activation energy for polycarbonate formation to be 54 ± 4 kJ/mol. End-group analysis of the resulting polymers via MALDI-TOF MS indicated either chloride of the Cr(III) complex or the external nucleophile initiates the copolymerization reaction.

Chapter 3 presented another new Cr(III) amino-bis(phenolate) catalyst, **3.1**. Although **3.1** only showed moderate activity for CO₂/CHO copolymerization, **3.1** solution in DCM was found to perform a color change from green to pink upon addition of PPNCI, which permits spectroscopic studies. The spectrophotometric titrations combined with monitoring the copolymerization reaction by React-IR demonstrated that the six-coordinate anionic species arising from the addition of ionic cocatalyst to **3.1** hinders the copolymerization reaction. In addition, end-group analysis of the polymers via MALDI-TOF MS indicates that when using DMAP as the cocatalyst, the main pathway of the ring-opening step is most likely initiated by DMAP.

In an effort to better understand the mechanism of CO₂/epoxide copolymerization by Cr(III) amino-bis(phenolate) complexes, the investigation of the binding of azide to **2.1**

and **3.1** were conducted by negative mode ESI-MS and MALDI-TOF MS in Chapter 4. The spectrometry results demonstrated that the binding behavior of azide to the chromium center is influenced by the nature of the pendant donor group in Cr(III) amino-bis(phenolate) complexes where **3.1** is much easier to bind two azides to form a bis-azide anion than **2.1**. This different behavior in the binding of azide is coincident with a striking difference in the catalytic activities of **2.1** and **3.1** for the copolymerization of CHO and CO₂. In the presence of 1 equivalent of PPNN₃, **3.1** exhibited a slow reaction rate with an induction period, whereas **2.1** showed a much faster reaction rate and no induction period observed. These results suggest the key of improving the catalytic activities is to increase the steric effect on the pendant donor group to prevent the formation of the inert six-coordinated anion. The observed propagating polymer chains at various times in CHO/CO₂ copolymerization via MALDI-TOF MS also indicate DMAP plays the main role in the initiation of the copolymerization reaction. As the reaction proceeded the concentration of DMAP decreased and the chloride of the Cr(III) complex also ring-opened the epoxide. Furthermore, Chapter 4 also elucidated the steric effect of the cocatalyst can influence the catalytic activity, especially when the Cr(III) complex containing a pendant donor group with a small steric effect.

Chapter 5 presented the synthesis of a new complex **5.1** and modification of PPNCI in an effort to produce a well-defined polycarbonate diol. Interestingly, the reaction of

PPNCl with sodium hydroxide led to an unexpected product, $\text{Ph}_2\text{P}(\text{O})\text{NPPh}_3$. **5.1** along with $\text{Ph}_2\text{P}(\text{O})\text{NPPh}_3$ can efficiently produce $\text{Ph}_2\text{P}(\text{O})\text{NPPh}_3$ -polycarbonate-OH polymer, which could not be hydrolysed in the presence of adventitious water during the reaction or terminated by hydrolysis in methanol to afford a polycarbonate diol. **5.1** in the presence of Bu_4NOH as the cocatalyst was found to efficiently copolymerize CHO with CO_2 to give polycarbonate diol in a controlled and systematic fashion. The produced polycarbonate diol was used as a macroinitiator for the ring-opening polymerization of *rac*-lactide, using DBU as a co-initiator. Near-quantitative conversion of *rac*-lactide is achieved to give ABA tri-block copolymer. The new copolymers were characterized by NMR spectroscopy, GPC, DSC and TGA analysis and represent potentially useful materials based on renewable feedstocks.

Lastly Chapter 6 described the attempt of synthesis of the derivatives of **2.1** in order to explore more highly active Cr(III) complexes. However, only preliminary results were obtained to date due to the insufficient time during my PhD. This chapter can be used as a starting point to synthesize derivatives of Cr(III) amino-bis(phenolate) complexes.

In summary, new Cr(III) amino-bis(phenolate) complexes have been synthesized and **2.1** in the presence of DMAP, PPNCl or PPNN_3 shows excellent catalytic activity for CO_2 /CHO copolymerization. Mechanistic studies indicate the key of designing highly efficient Cr(III) amino-bis(phenolate) catalysts is to increase the steric effect on the

pendant donor group. End-group analysis data and the propagating polymer chains observed via MALDI-TOF MS suggest that for the catalyst system of Cr(III) complex and DMAP, DMAP plays the main role in the initiation. Chloride from the Cr(III) complex can also ring-open the epoxide after the concentration of DMAP was decreased. The catalyst system of **5.1**/Bu₄NOH was able to produce controlled polycarbonate diol, which can be used for the polymerization of *rac*-lactide in the presence of DBU. The produced tri-block copolymer exhibited a decreased glass transition temperature and an increased decomposition temperature compared to the original polycarbonate.

Overall, this thesis has shown that mass spectrometric methods are extremely useful in determining possible reaction intermediates and in the identification of polycarbonate end-groups of relevance to understanding the mechanism of such reactions. Further, Cr(III) complexes of amino-phenolate ligands show varying activity with ligand structure and more of such species could be explored in the future with the goal of increasing catalytic activity and polymerization control.

7.3 References

- (1) Lu, X.-B.; Wang, Y. *Angew. Chem., Int. Ed.* **2004**, *43*, 3574.
- (2) Noh, E. K.; Na, S. J.; S, S.; Kim, S.-W.; Lee, B. Y. *J. Am. Chem. Soc.* **2007**, *129*, 8082.
- (3) Min, S. S. J. K.; Seong, J. E.; Na, S. J.; Lee, B. Y. *Angew. Chem., Int. Ed.* **2008**, *47*, 7306.
- (4) Dean, R. K (2012). *Multimetallic Lithium and Chromium Complexes of Amine-bis(phenolate) Ligands as Polymerization Catalysts* (Chapter 4, Ph.D. thesis), Memorial University.
- (5) Darensbourg, D. J.; Tsai, F.-T. *Macromolecules* **2014**, *47*, 3806.
- (6) Paddock, R. L.; Nguyen, S. T. *J. Am. Chem. Soc.* **2001**, *123*, 11498.
- (7) Darensbourg, D. J.; Yarbrough, J. C. *J. Am. Chem. Soc.* **2002**, *124*, 6335.
- (8) Darensbourg, D. J.; Yarbrough, J. C.; Ortiz, C.; Fang, C. C. *J. Am. Chem. Soc.* **2003**, *125*, 7586.
- (9) Eberhardt, R.; Allmendinger, M.; Rieger, B. *Macromol. Rapid Commun.* **2003**, *24*, 194.
- (10) Darensbourg, D. J.; Mackiewicz, R. M.; Rodgers, J. L.; Fang, C. C.; Billodeaux, D. R.; Reibenspies, J. H. *Inorg. Chem.* **2004**, *43*, 6024.
- (11) Darensbourg, D. J.; Mackiewicz, R. M. *J. Am. Chem. Soc.* **2005**, *127*, 14026.
- (12) Darensbourg, D. J.; Mackiewicz, R. M.; Billodeaux, D. R. *Organometallics* **2005**, *24*,

144.

(13) Li, B.; Wu, G.-P.; Ren, W.-M.; Wang, Y.-M.; Rao, D.-Y.; Lu, X.-B. *J. Polym. Sci., Part A: Polym. Chem.* **2008**, *46*, 6102.

(14) Nakano, K.; Nakamura, M.; Nozaki, K. *Macromolecules* **2009**, *42*, 6972.

(15) Guo, L.; Wang, C.; Zhao, W.; Li, H.; Sun, W.; Shen, Z. *Dalton Trans.* **2009**, 5406.

(16) Cohen, C. T.; Chu, T.; Coates, G. W. *J. Am. Chem. Soc.* **2005**, *127*, 10869.

(17) Liu, B.; Zhao, X.; Guo, H.; Gao, Y.; Yang, M.; Wang, X. *Polymer* **2009**, *50*, 5071.

(18) Lu, X.-B.; Wang, Y. *Angew. Chem., Int. Ed.* **2004**, *43*, 3574.

(19) Paddock, R. L.; Nguyen, S. T. *Macromolecules* **2005**, *38*, 6251.

(20) Qin, Z.; Thomas, C. M.; Lee, S.; Coates, G. W. *Angew. Chem., Int. Ed.* **2003**, *42*, 5484.

(21) Lu, X.-B.; Shi, L.; Wang, Y.-M.; Zhang, R.; Zhang, Y.-J.; Peng, X.-J.; Zhang, Z.-C.; Li, B. *J. Am. Chem. Soc.* **2006**, *128*, 1664.

Appendix A: Crystallographic and structure refinement data

Table A-1. Crystal data and structure refinement for **2.1** and **2.6**

Compound	2.1	2.6
Chemical formula	C ₃₈ H ₆₂ ClCrN ₂ O ₃	C _{85.50} H ₁₃₀ Cr ₂ N ₄ O ₅ Cl ₂
Formula weight	682.34	1468.84
Temperature/K	158	163
Crystal system	Triclinic	Triclinic
Space group	P-1 (#2)	P-1 (#2)
a/Å	10.1830(18)	15.947(3)
b/Å	16.615(3)	20.439(3)
c/Å	30.271(5)	31.205(6)
α /°	90.233(3)	72.448(9)
β /°	94.364(3)	81.063(9)
γ /°	91.025(3)	70.016(8)
Volume/Å ³	5105.8(16)	9098(3)
Z	4	4
D_c /g cm ⁻³	0.888	1.072
Radiation type	MoK α	MoK α
μ (MoK α)/mm ⁻¹	0.303	0.344
F(000)	1476.0	3172
Reflections measured	46302	80744
Unique reflections	19271	37268
R_{int}	0.0443	0.0659
R_I (all)	0.0759	0.1265
$wR(F_2)$ (all)	0.2290	0.3130
R_I ($I > 2 \sigma(I)$) ^a	0.0685	0.0939
$wR(F_2)$ ($I > 2 \sigma(I)$) ^b	0.2182	0.2705
Goodness of fit on F^2	1.062	1.034

Table A-2. Crystal data and structure refinement for **3.1** and **5.3**

Compound	3.1	5.3
Chemical formula	$\text{C}_{80}\text{H}_{118}\text{Cl}_2\text{Cr}_2\text{N}_2\text{O}_6$	$\text{C}_{87}\text{H}_{128}\text{Cr}_2\text{N}_2\text{O}_8$
Formula weight	1378.72	1433.97
Temperature/K	163	153
Crystal system	Triclinic	Monoclinic
Space group	P-1 (#2)	P2 ₁ /c (#14)
<i>a</i> /Å	9.662(3)	17.364(9)
<i>b</i> /Å	12.342(5)	17.177(8)
<i>c</i> /Å	16.717(6)	30.360(16)
α°	88.743(8)	90
β°	76.335(8)	110.4580(10)
γ°	84.594(8)	90
Volume/Å ³	1928.4(12)	8484(7)
<i>Z</i>	1	4
<i>D_c</i> /g cm ⁻³	1.187	1.121
Radiation type	MoK α	MoK α
μ (MoK α)/mm ⁻¹	0.402	0.308
<i>F</i> (000)	742	3096
Reflections measured	16005	14786
Unique reflections	7866	6471
<i>R_{int}</i>	0.0364	0.0000
<i>R_I</i> (all)	0.0446	0.1801
<i>wR</i> (<i>F</i> ₂) (all)	0.1125	0.3504
<i>R_I</i> (<i>I</i> > 2 σ (<i>I</i>)) ^a	0.0414	0.1284
<i>wR</i> (<i>F</i> ₂) (<i>I</i> > 2 σ (<i>I</i>)) ^b	0.1092	0.3199
Goodness of fit on <i>F</i> ²	1.040	1.407

Table A-3. Crystal data and structure refinement for **5.2** and **7**.

Compound	5.2	7
Chemical formula	C ₈₂ H ₁₄₂ Cr ₂ N ₄ Na ₂ O ₁₀ Si ₂	C ₄₀ H ₆₃ ClCrN ₃ O ₂
Formula weight	1550.15	705.38
Temperature/K	163	148(2)
Crystal system	Monoclinic	Triclinic
Space group	C2/c	P-1
a/Å	36.56(2)	11.873(5)
b/Å	10.636(6)	17.233(8)
c/Å	30.075(17)	20.453(8)
α /°	90	85.563(12)
β /°	121.551(6)	74.140(10)
γ /°	90	89.156(13)
Volume/Å ³	9967(10)	4013(3)
Z	4	4
D_c /g cm ⁻³	1.033	1.167
Radiation type	MoK α	MoK α
μ (MoK α)/mm ⁻¹	0.299	0.387
F(000)	3360.0	1524.0
Reflections measured	53113	24319
Unique reflections	9427	13549
R_{int}	0.1129	0.0605
R_I (all)	0.0944	0.1577
$wR(F_2)$ (all)	0.2700	0.3927
R_I (I > 2 σ (I)) ^a	0.0863	0.1472
$wR(F_2)$ (I > 2 σ (I)) ^b	0.2546	0.3870
Goodness of fit on F^2	1.046	1.036

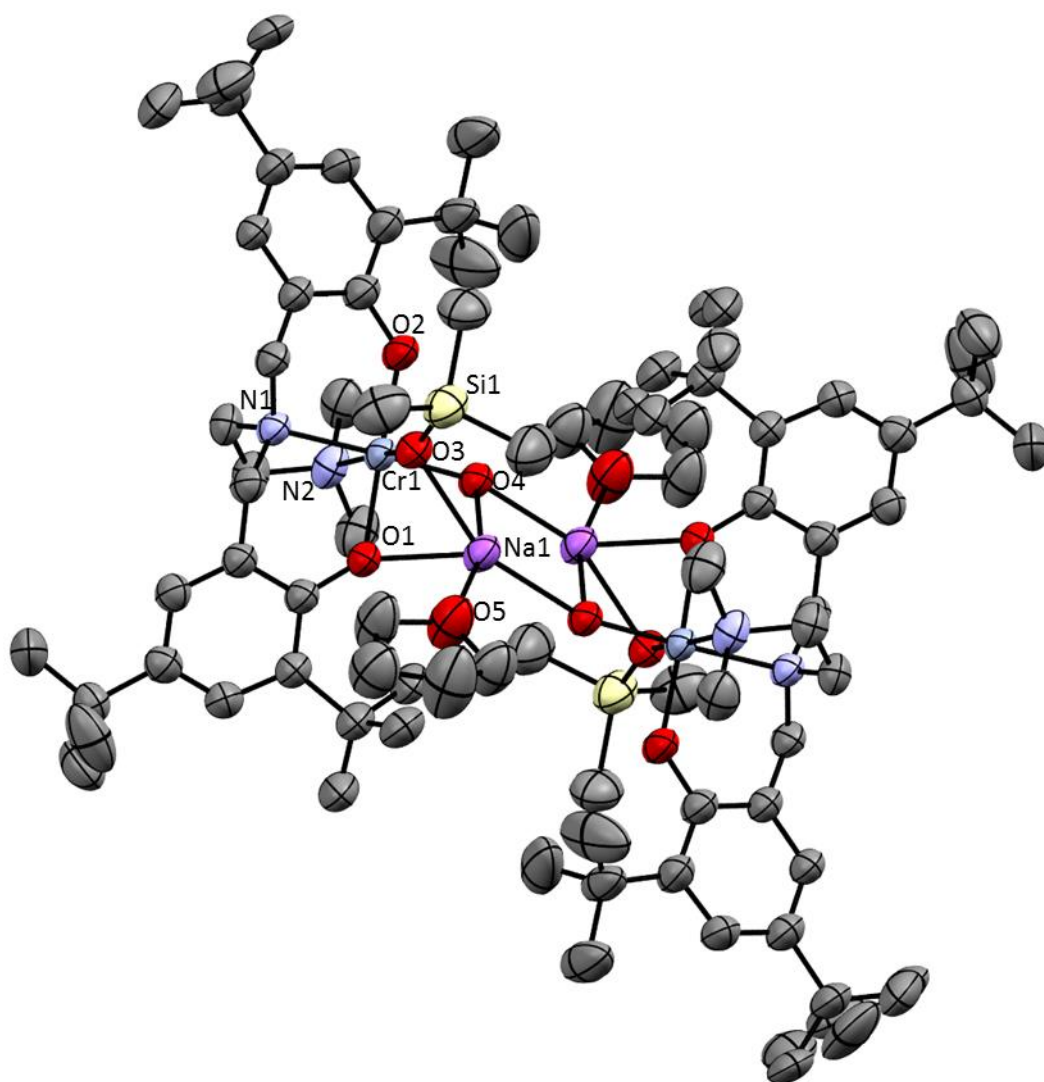


Figure A-1. Molecular structure (ORTEP) and partial numbering scheme of **5.2** (single crystals obtained from a solution of **5.1** in hexamethyldisiloxane (HMDSO) and toluene). Ellipsoids are drawn at 50% probability. Hydrogen atoms omitted for clarity.

Table A-4. Selected bond distances (Å) and angles (°) of **5.2**

Bond lengths (Å)			
Cr(1) – O(1)	1.990(3)	Si(1) – O(3)	1.579(3)
Cr(1) – O(2)	1.941(3)	Na(1) – O(4)	2.351(3)
Cr(1) – O(3)	1.943(2)	Na(1) – O(5)	2.375(4)
Cr(1) – O(4)	1.955(2)	Na(1) – O(1)	2.407(3)
Cr(1) – N(1)	2.107(3)	Na(1) – O(3)	2.350(4)
Cr(1) – N(2)	2.176(3)		
Bond angles (°)			
O(1) – Cr(1) – N(1)	91.90(9)	O(2) – Cr(1) – N(2)	91.59(13)
O(1) – Cr(1) – N(2)	88.64(11)	O(3) – Cr(1) – O(1)	86.52(10)
O(2) – Cr(1) – O(1)	177.77(8)	O(3) – Cr(1) – O(4)	93.18(10)
O(2) – Cr(1) – O(3)	93.47(12)	O(3) – Cr(1) – N(1)	92.39(10)
O(2) – Cr(1) – O(4)	90.31(9)	O(3) – Cr(1) – N(2)	172.27(11)
O(2) – Cr(1) – N(1)	90.33(9)	O(4) – Cr(1) – O(1)	87.46(9)
O(4) – Cr(1) – N(1)	174.35(10)	O(4) – Cr(1) – N(2)	92.63(10)
N(1) – Cr(1) – N(2)	81.74(10)	O(4) – Na(1) – O(5)	98.6(1)
O(4) – Na(1) – O(1)	126.8(1)	O(4) – Na(1) – O(3)	156.1(1)
O(5) – Na(1) – O(1)	95.3(1)	O(5) – Na(1) – O(3)	97.2(1)
O(5) – Na(1) – O(4)	163.2(1)	O(1) – Na(1) – O(3)	69.02(9)
Cr(1) – O(1) – Na(1)	83.28(9)	Cr(1) – O(3) – Si(1)	151.1(2)
Cr(1) – O(3) – Na(1)	85.8(1)	Si(1) – O(3) – Na(1)	112.7(1)
Cr(1) – O(4) – Na(1)	163.3(1)	Cr(1) – O(4) – Na(1)	83.55(9)

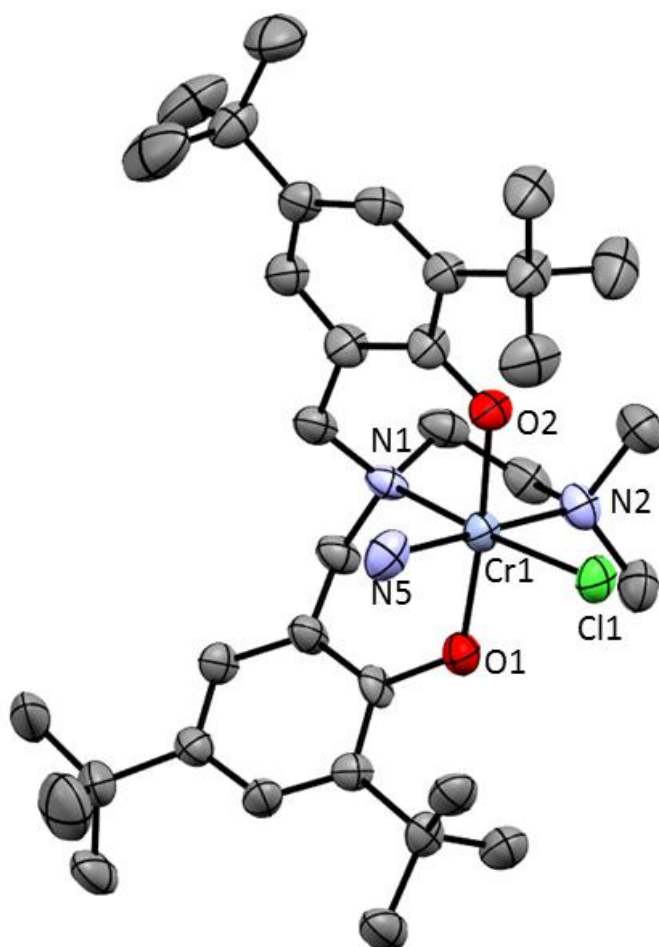


Figure A-2. Molecular structure (ORTEP) and partial numbering scheme of **7** (single crystals obtained from a solution of **2.1** in hexamethyldisilazane (HMDS) and toluene. Ellipsoids are drawn at 50% probability. Hydrogen atoms omitted for clarity.

Table A-5. Selected bond distances (Å) and angles (°) of **7**

Bond lengths (Å)			
Cr(1) – Cl(1)	2.349(3)	Cr(1) – N(5)	2.094(8)
Cr(1) – O(1)	1.953(6)	Cr(1) – N(1)	2.111(7)
Cr(1) – O(2)	1.909(6)	Cr(1) – N(2)	2.139(8)
Bond angles (°)			
O(1) – Cr(1) – N(2)	90.5(3)	O(2) – Cr(1) – N(2)	91.7(3)
O(2) – Cr(1) – Cl(1)	91.25(19)	N(5) – Cr(1) – N(1)	95.9(3)
O(2) – Cr(1) – O(1)	175.0(3)	N(1) – Cr(1) – Cl(1)	175.3(2)
O(2) – Cr(1) – N(5)	87.7(3)	N(2) – Cr(1) – Cl(1)	90.7(2)
O(2) – Cr(1) – N(1)	86.9(3)	N(5) – Cr(1) – N(2)	178.9(3)
N(5) – Cr(1) – Cl(1)	88.4(2)	N(1) – Cr(1) – N(2)	84.9(3)

Appendix B: MALDI-TOF Mass spectra of complexes and polymers

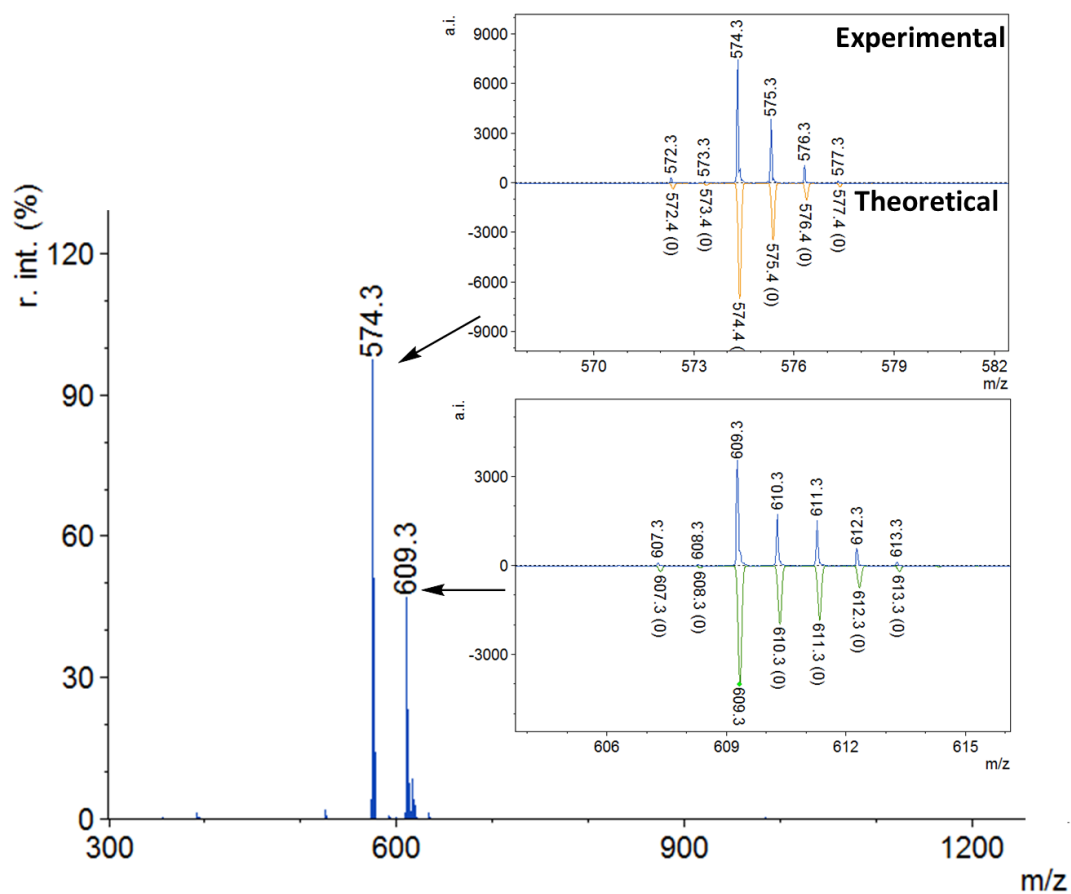


Figure B-1. MALDI-TOF mass spectrum of complex **2.1**.

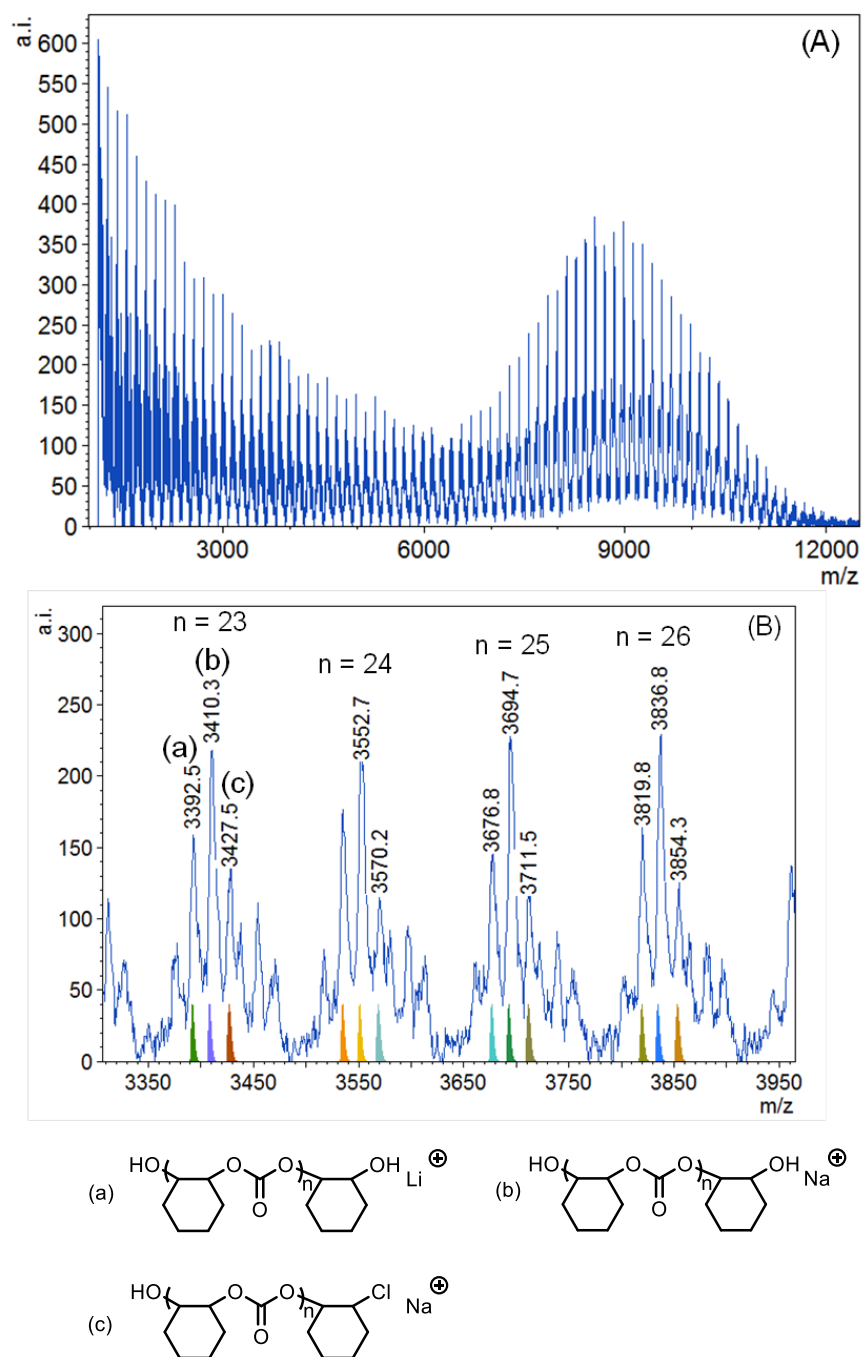


Figure B-2. (A) MALDI-TOF mass spectrum of PCHC obtained using **2.1** and PPNCI. (B) Magnified low mass region of the spectrum ($n = 23 - 26$) with modeled polymer chains.

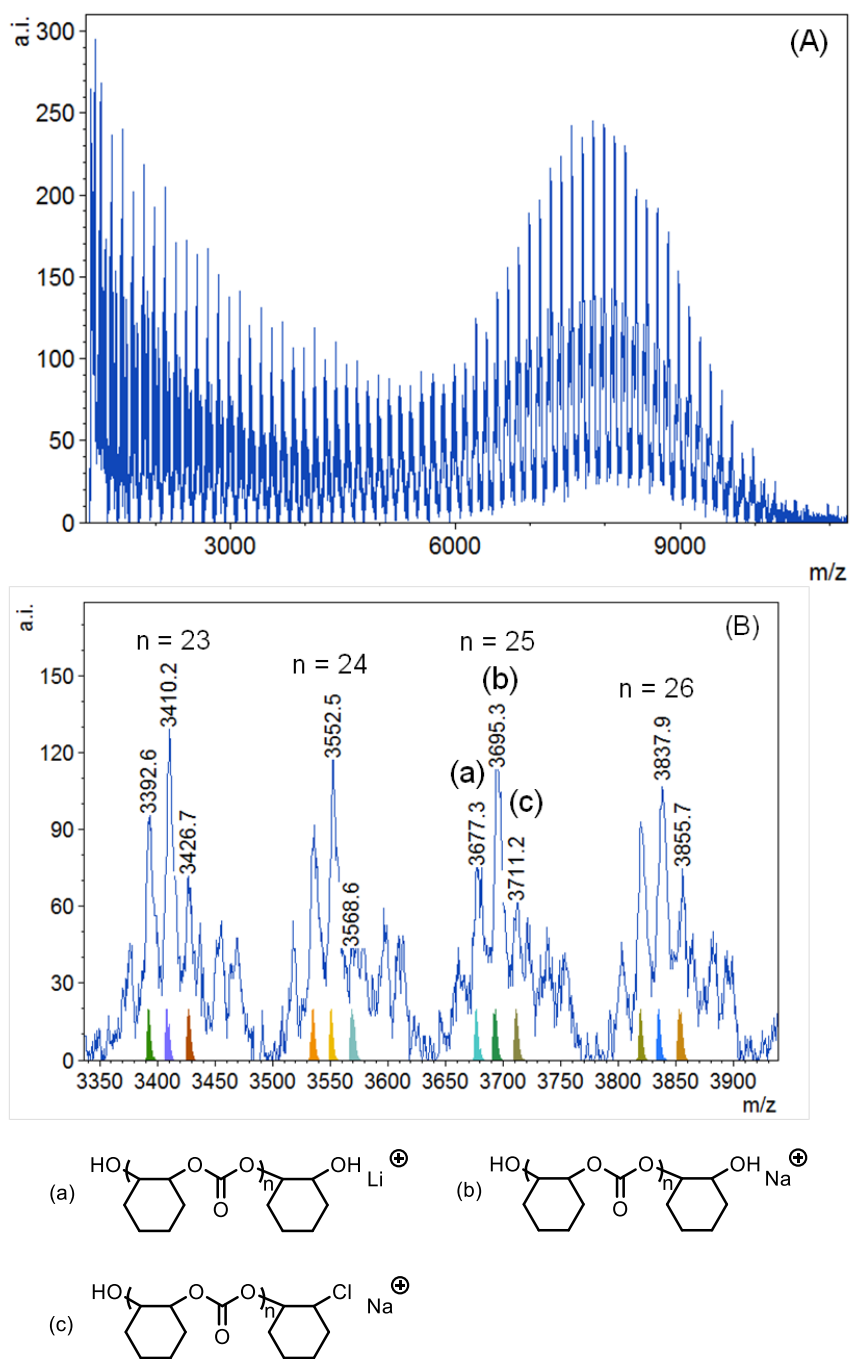


Figure B-3. (A) MALDI-TOF mass spectrum of PCHC obtained using **2.1** and PPNN₃. (B) Magnified low mass region of the spectrum (n = 23 – 26) with modeled polymer chains.

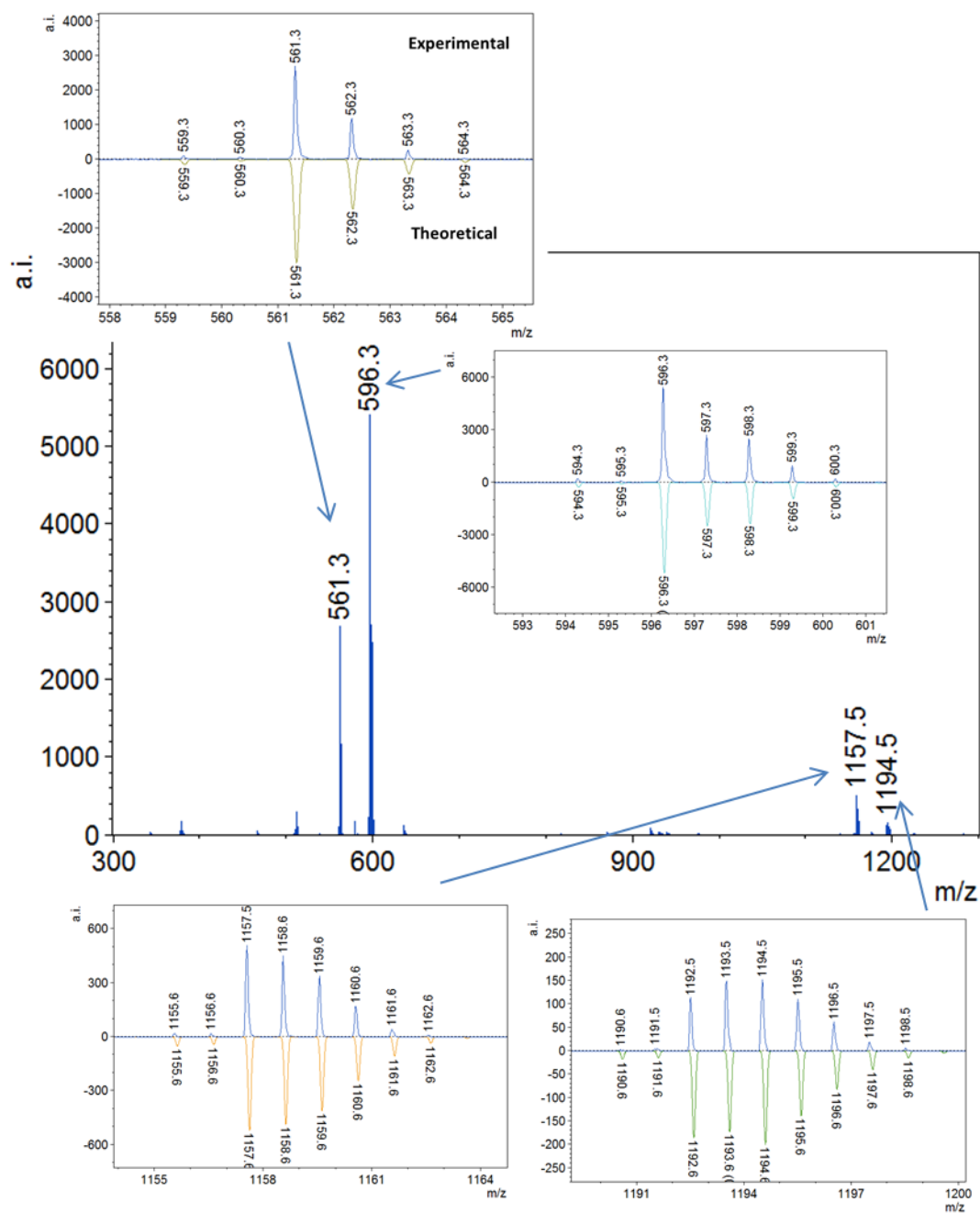


Figure B-4. MALDI-TOF mass spectrum of complex **3.1** with isotopic patterns.

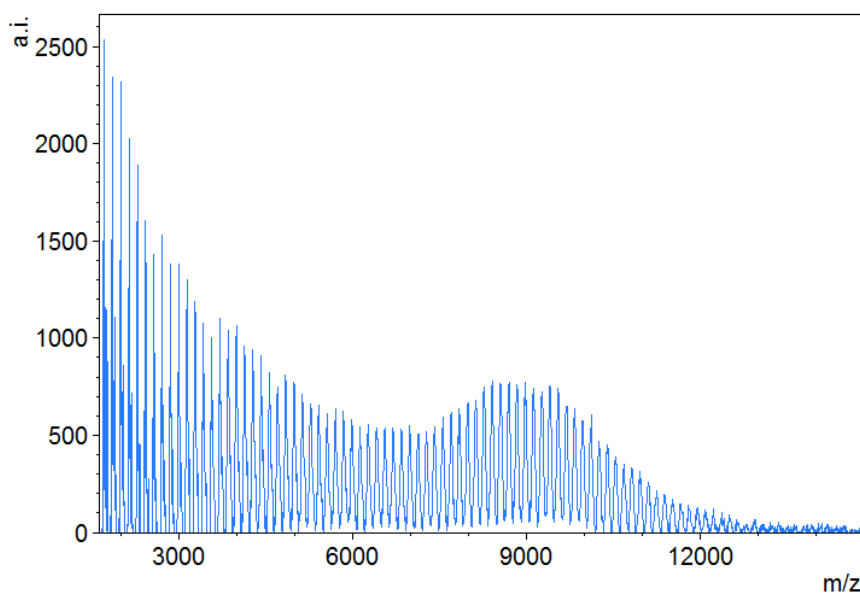


Figure B-5. The MALDI-TOF mass spectrum of polymer obtained using **3.1** and PPNCI (Table 3-2, entry 1)

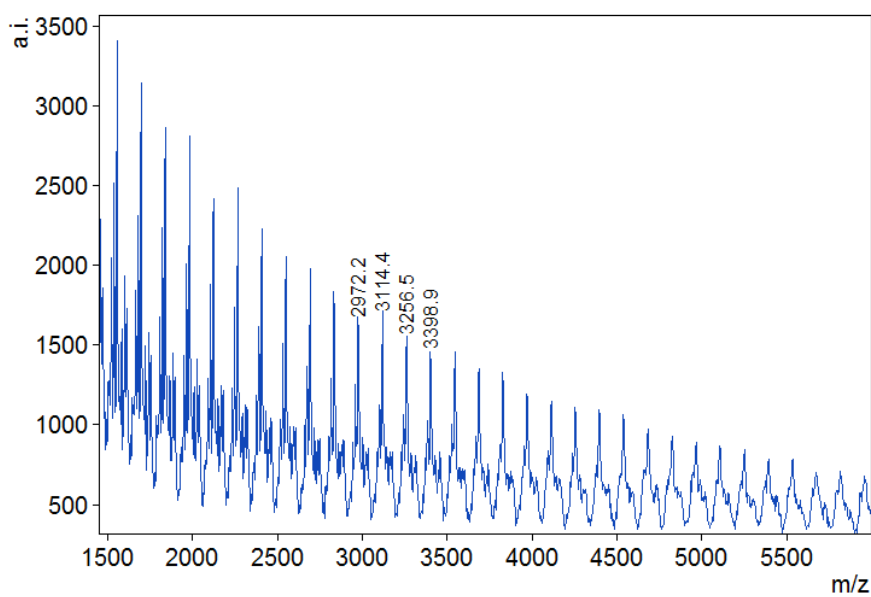


Figure B-6. MALDI-TOF mass spectrum of PCHC using $\text{Ph}_2\text{P}(\text{O})\text{NPh}_3$ as cocatalyst precipitated from methanol (Table 5-3, entry 3).

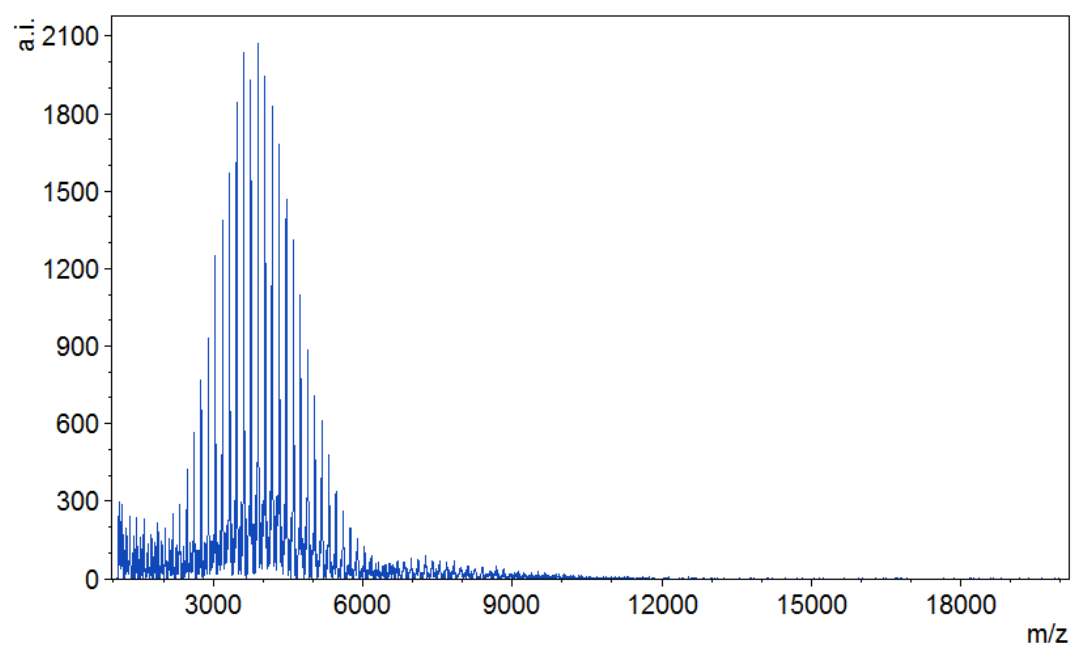


Figure B-7. MALDI-TOF mass spectrum of PCHC using Bu₄NOH as cocatalyst precipitated from methanol (Table 5-3, entry 4).

Appendix C: ^1H NMR, ^{13}C and ^{31}P NMR Spectra

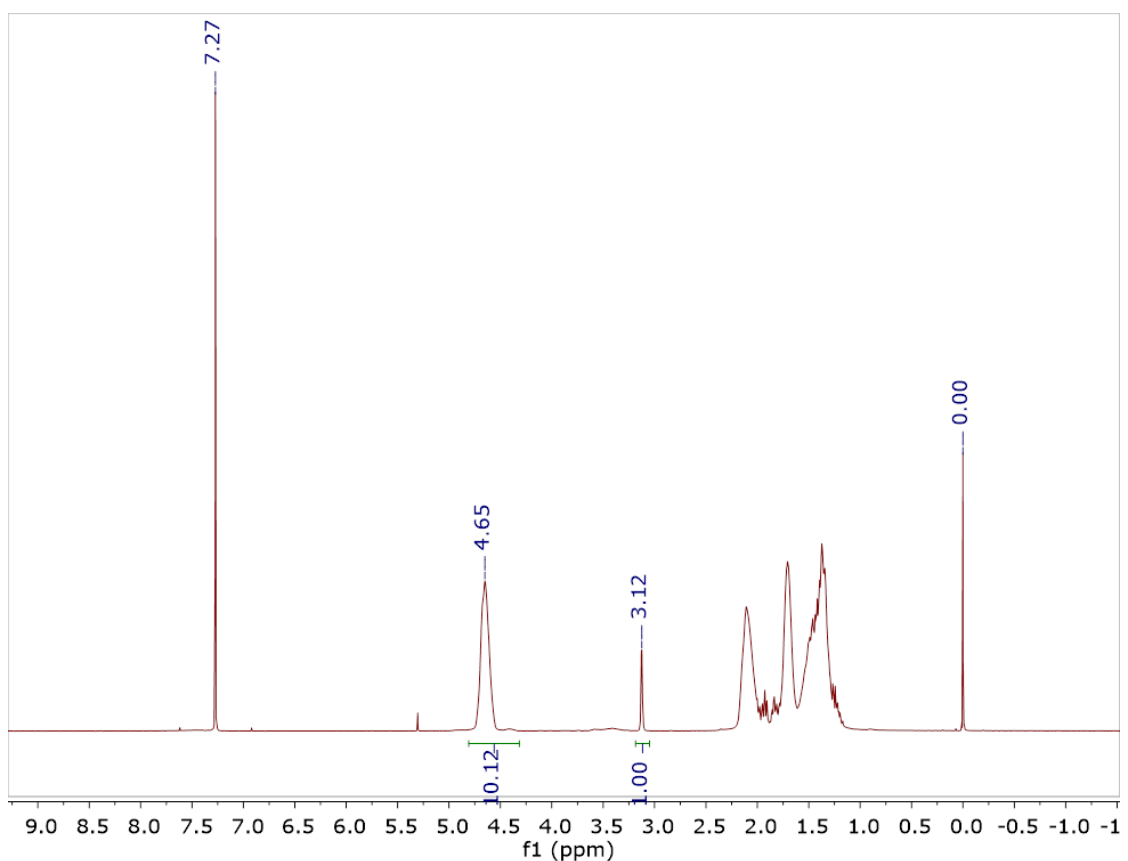


Figure C-1. Representative ^1H NMR spectrum in CDCl_3 of the aliquot taken right after polymerization (Table 2-2, entry 5). % Conversion calculation = polymer peak integration (10.06 at 4.65 ppm) divided by the sum of the polymer (10.06 at 4.65 ppm) and monomer (1.00 at 3.12 ppm) peak integrations.

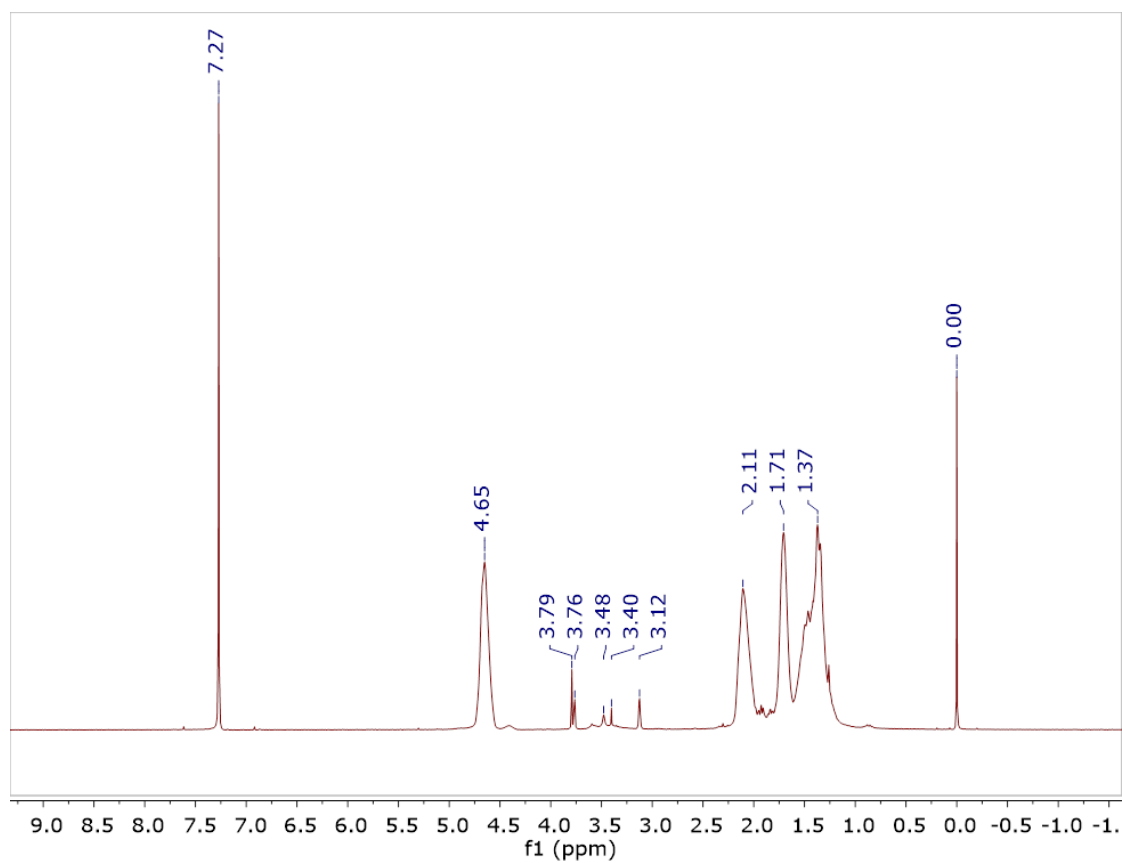


Figure C-2. ^1H NMR spectrum in CDCl_3 of PCHC (Table 2-2, entry 1) in the solution layer.

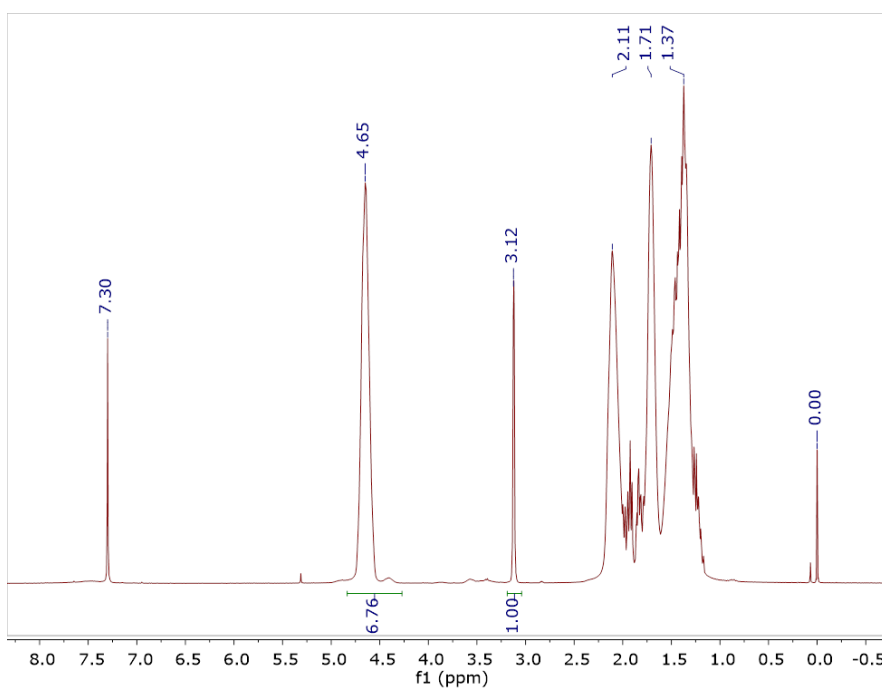


Figure C-3. ^1H NMR spectrum of raw polycarbonate obtained by **3.1** and PPNC1 (Table 3-2, entry 1). The conversion % = polycarbonate peak integration (6.66 at 4.65 ppm) divided by the sum of the polycarbonate integration (6.66 at 4.65 ppm) and CHO peak integration (1.00 at 3.12 ppm).

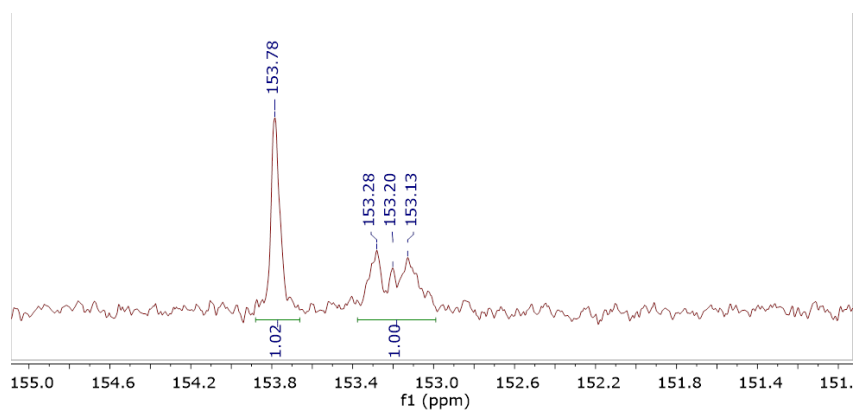


Figure C-4. $^{13}\text{C}\{^1\text{H}\}$ NMR spectrum of a representative polycarbonate obtained by **3.1** and PPNC1 (Table 3-2, entry 1) showing the presence of both isotactic and syndiotactic isomers.

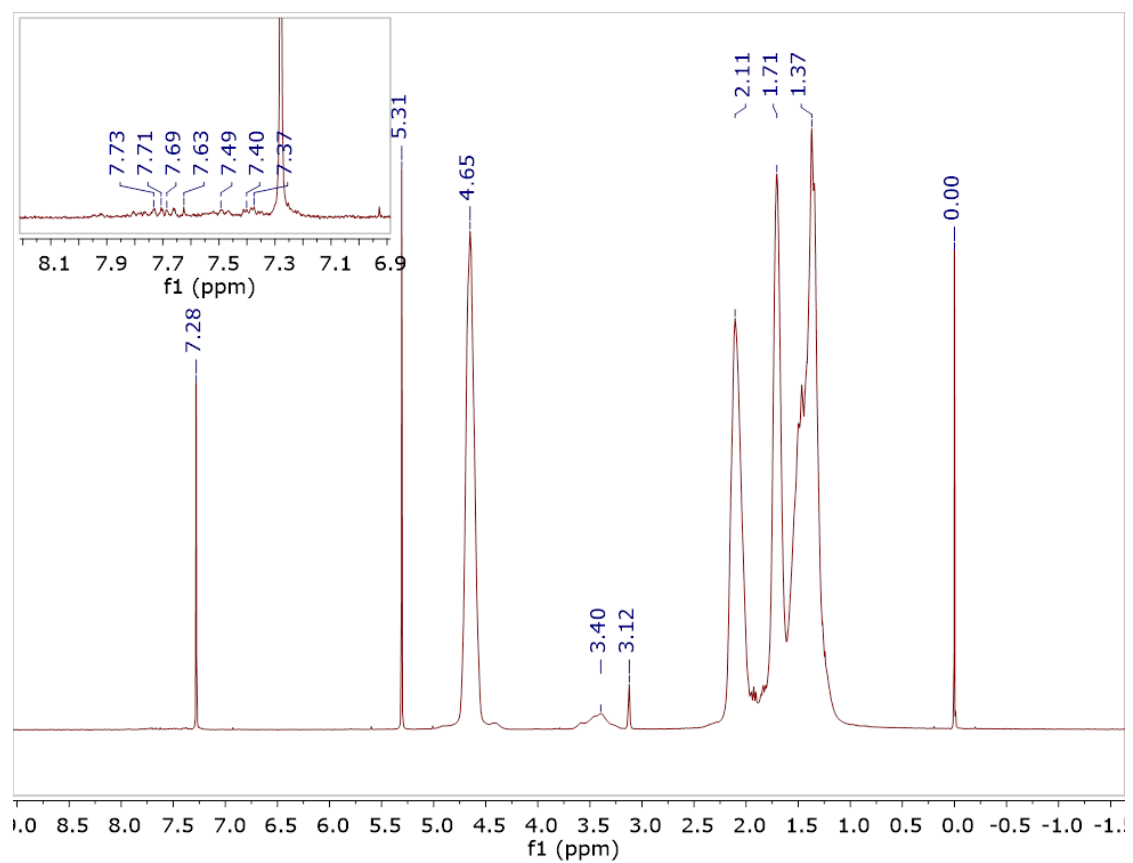


Figure C-5. ^1H NMR spectrum in CDCl_3 of polycarbonate obtained by **5.1** and $\text{Ph}_2\text{P}(\text{O})\text{NPPH}_3$ (Table 5-3, entry 3)

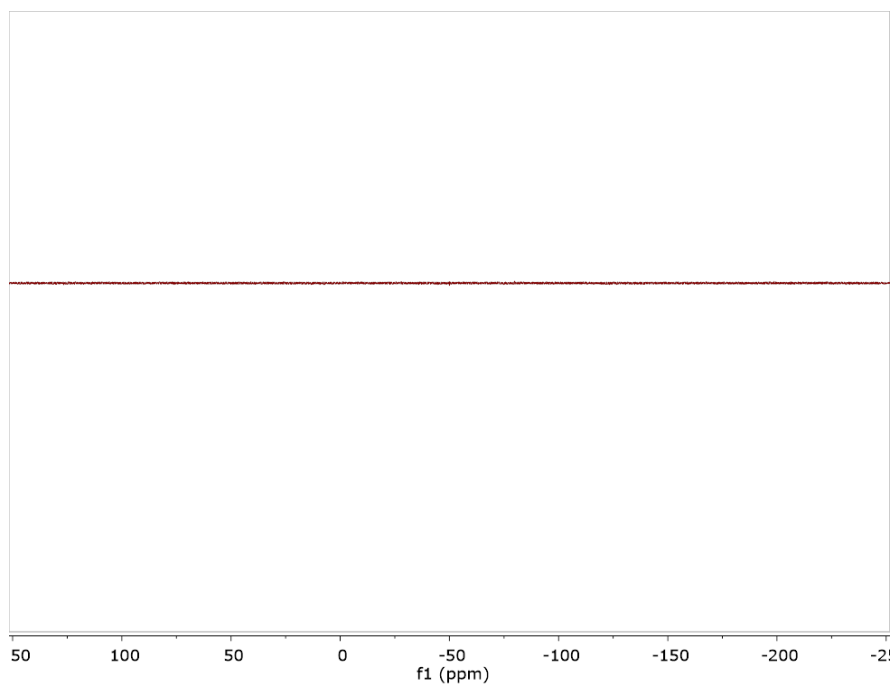


Figure C-6. ^{31}P NMR spectrum in acetone- d_6 of polycarbonate obtained by **5.1** and $\text{Ph}_2\text{P}(\text{O})\text{NPPH}_3$ (Table 5-3, entry 3)

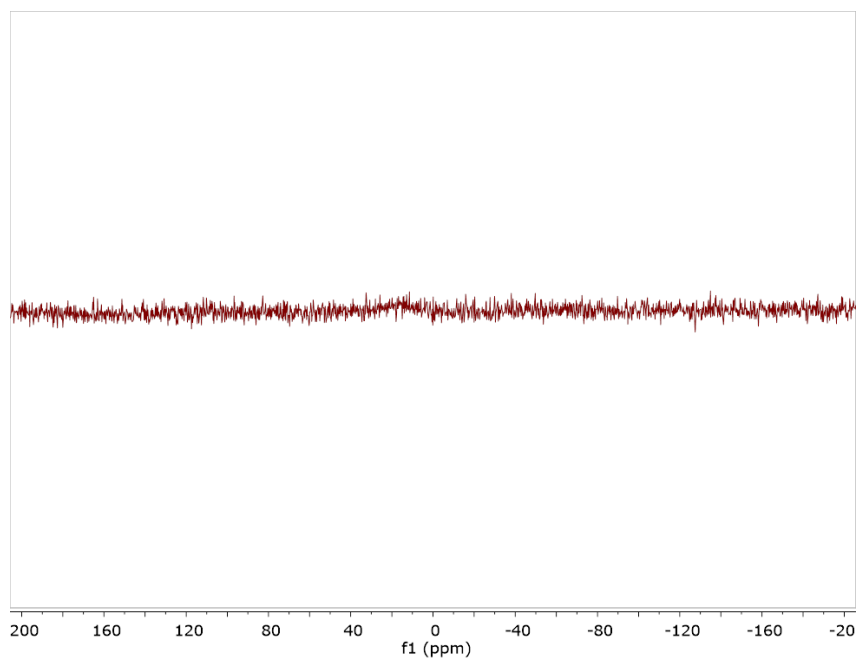


Figure C-7. ^{31}P NMR spectrum in solid state of polycarbonate obtained by **5.1** and $\text{Ph}_2\text{P}(\text{O})\text{NPPH}_3$ (Table 5-3, entry 3)

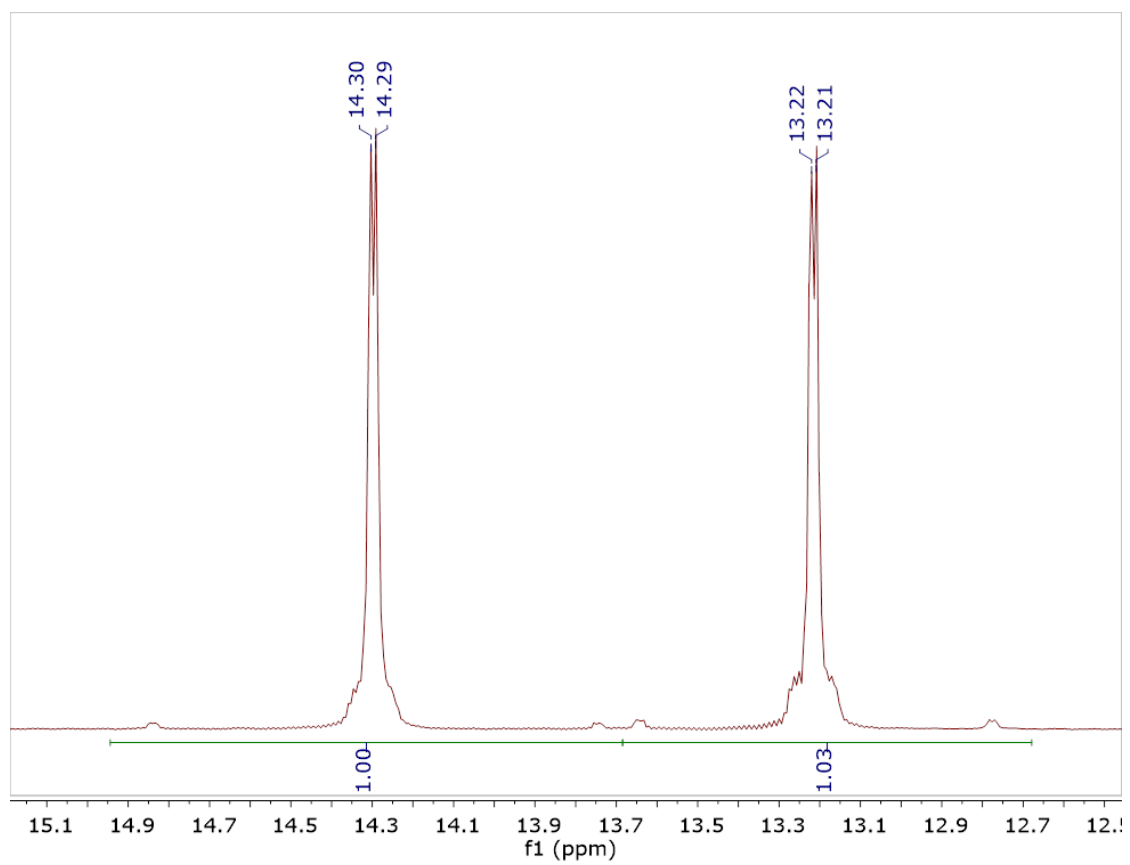


Figure C-8. $^{31}\text{P}\{^1\text{H}\}$ NMR of commercial $\text{Ph}_2\text{P}(\text{O})\text{NPh}_3$.

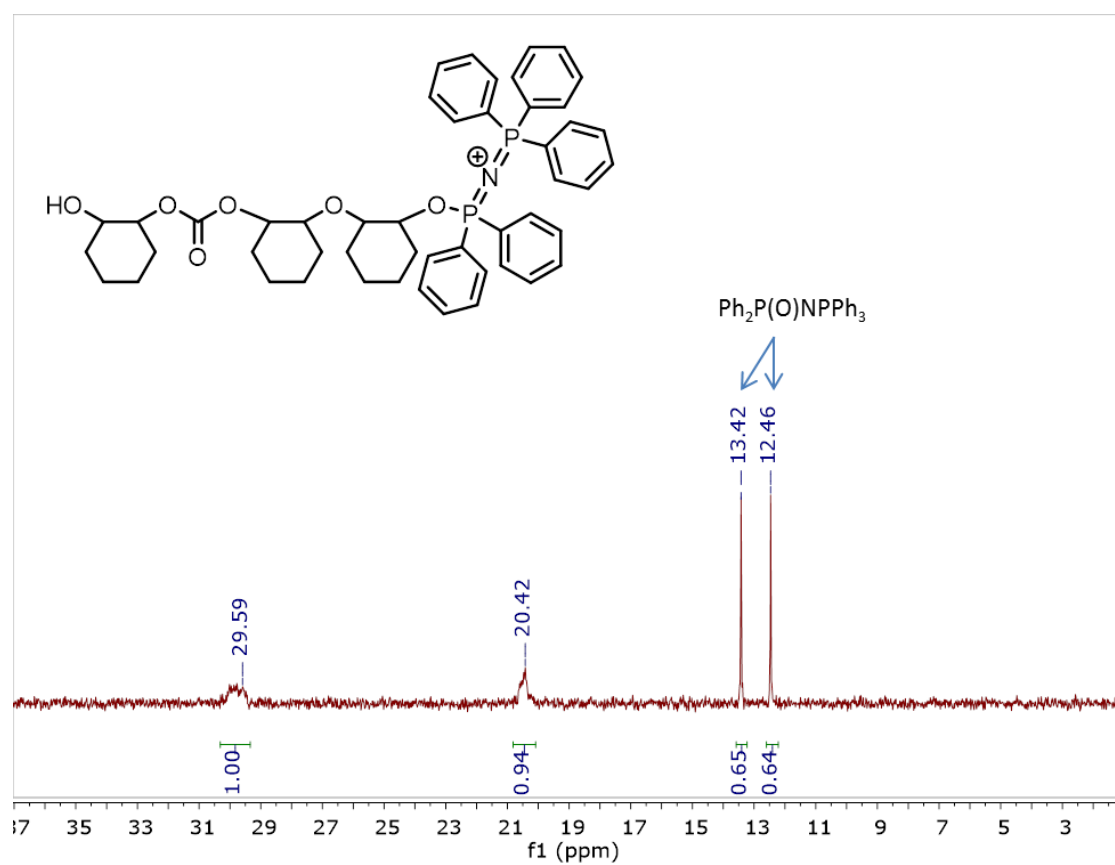


Figure C-9. $^{31}\text{P}\{^1\text{H}\}$ NMR spectrum in deuterated acetone of the purified polymer obtained from CHO/CO₂ copolymerization by **5.1** and $\text{Ph}_2\text{P}(\text{O})\text{NPPH}_3$ for 2 h.

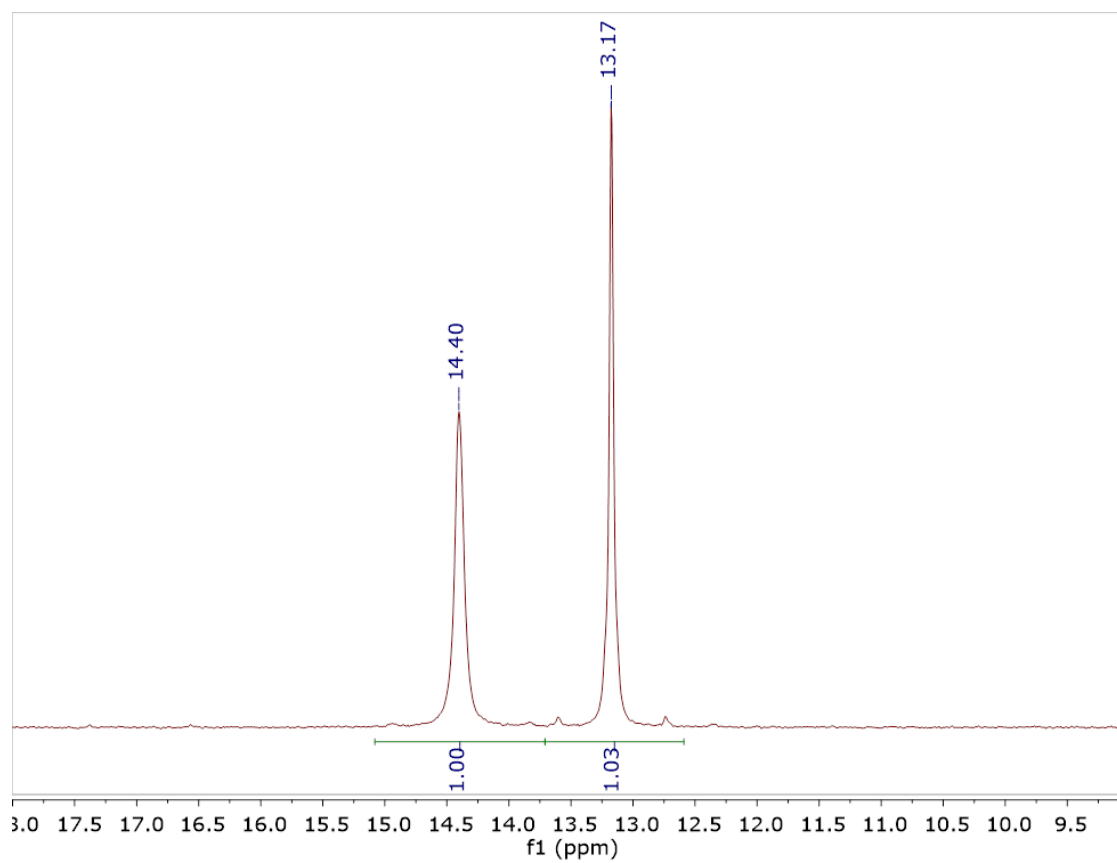


Figure C-10. $^{31}\text{P}\{^1\text{H}\}$ NMR spectrum in dichloromethane- d of the mixture of **5.1** and $\text{Ph}_2\text{P}(\text{O})\text{NPPH}_3$.

Appendix D: UV-Vis Spectra and photos

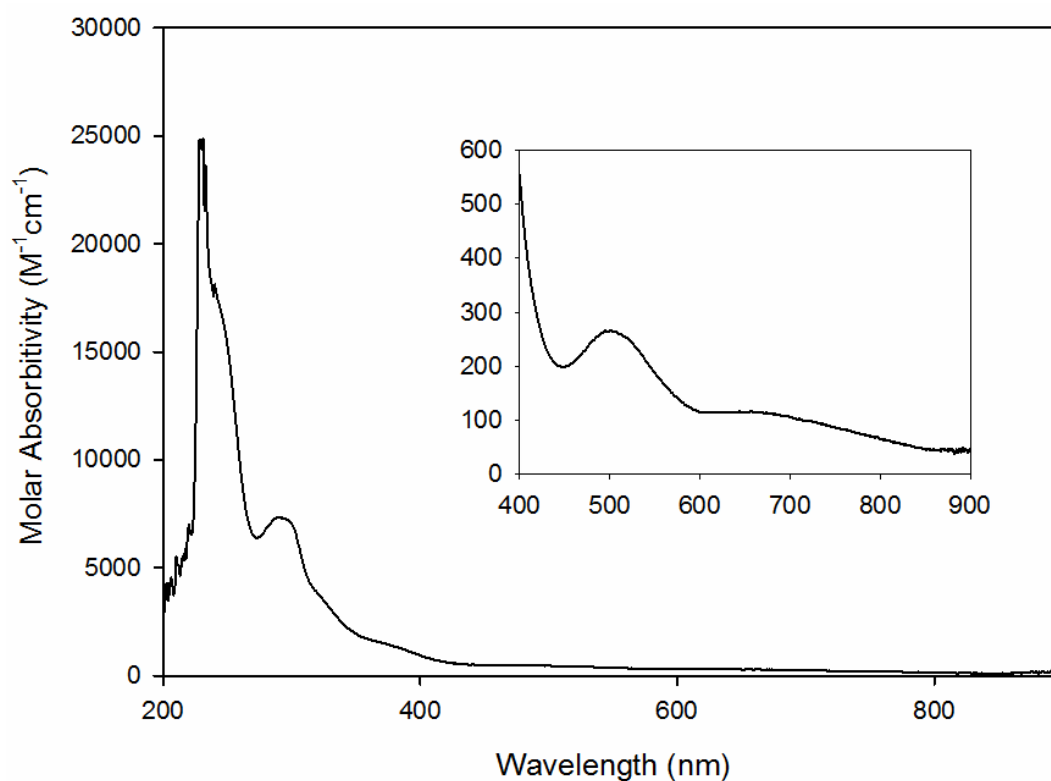


Figure D-1. UV-Vis absorption spectrum of complex **2.1** at concentration of 10^{-4} mol L^{-1} in dichloromethane.

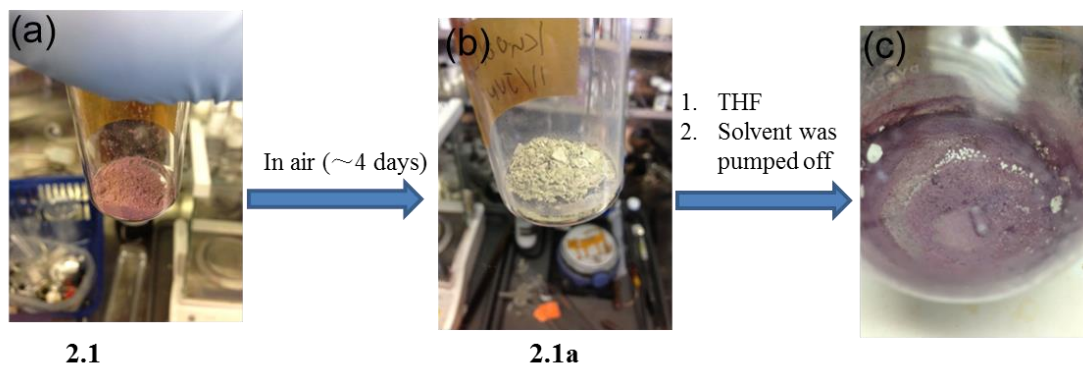


Figure D-2. Photos of (a) complex **2.1** (b) complex **2.2** (c) recovered complex **2.1**.

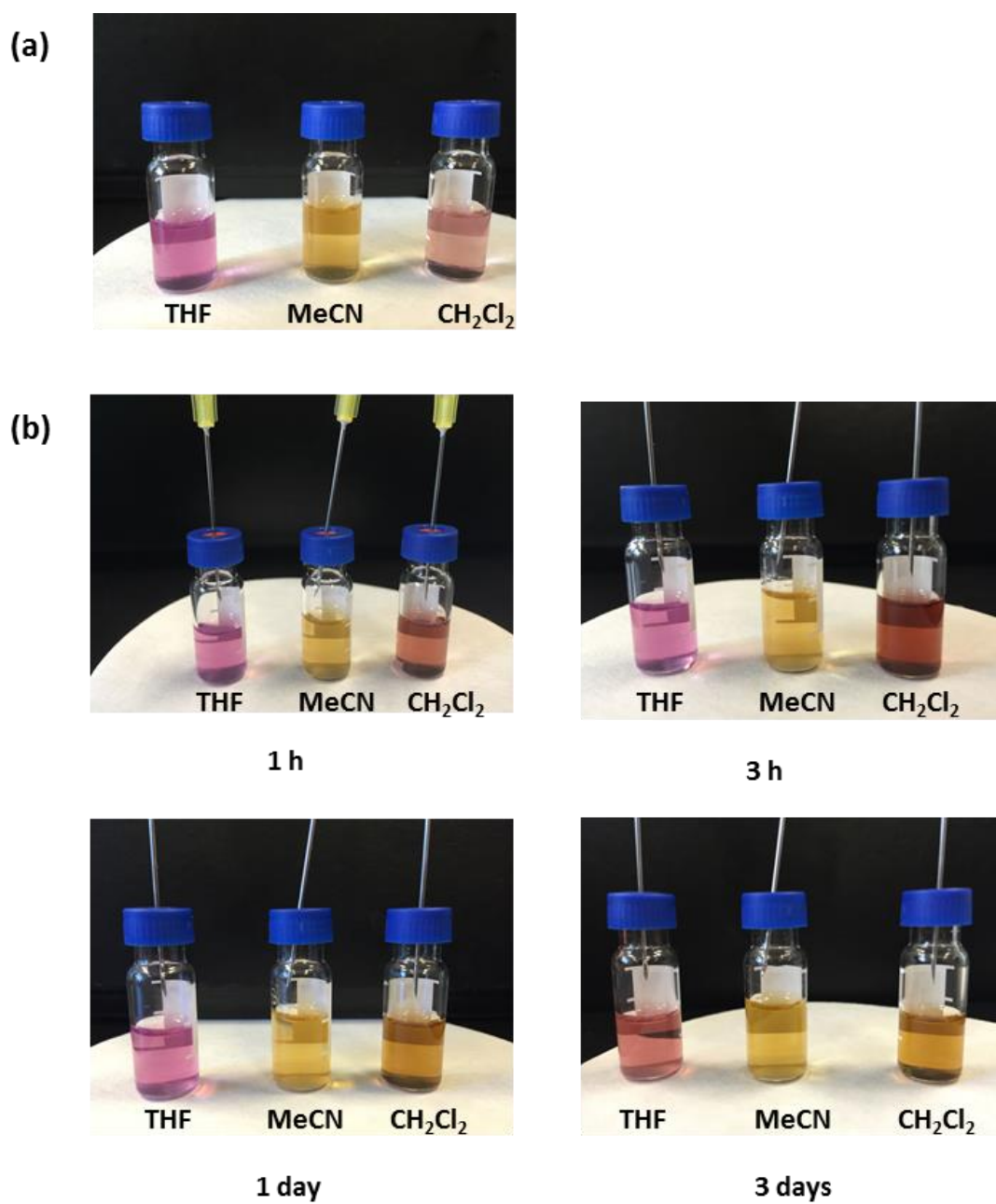
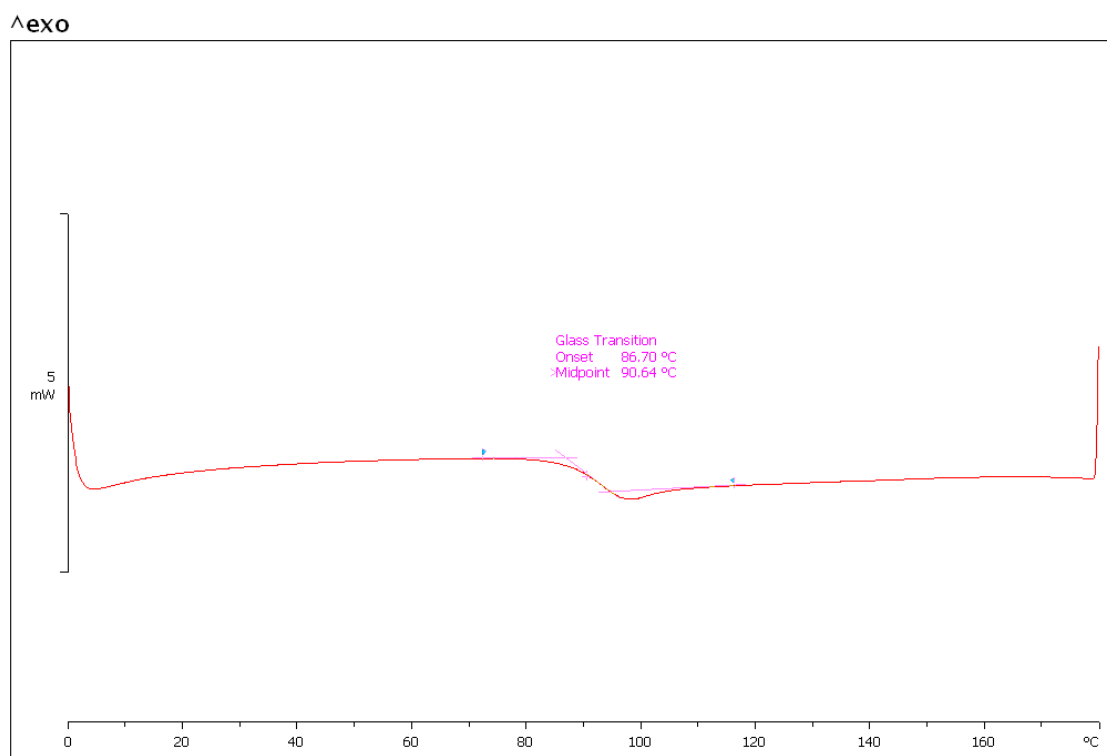


Figure D-3. (a) Complex **2.1** dissolved in THF, MeCN and CH₂Cl₂. (b) The solution of **2.1** was exposed to air for 1 h, 3 h, 1 day and 3 days.

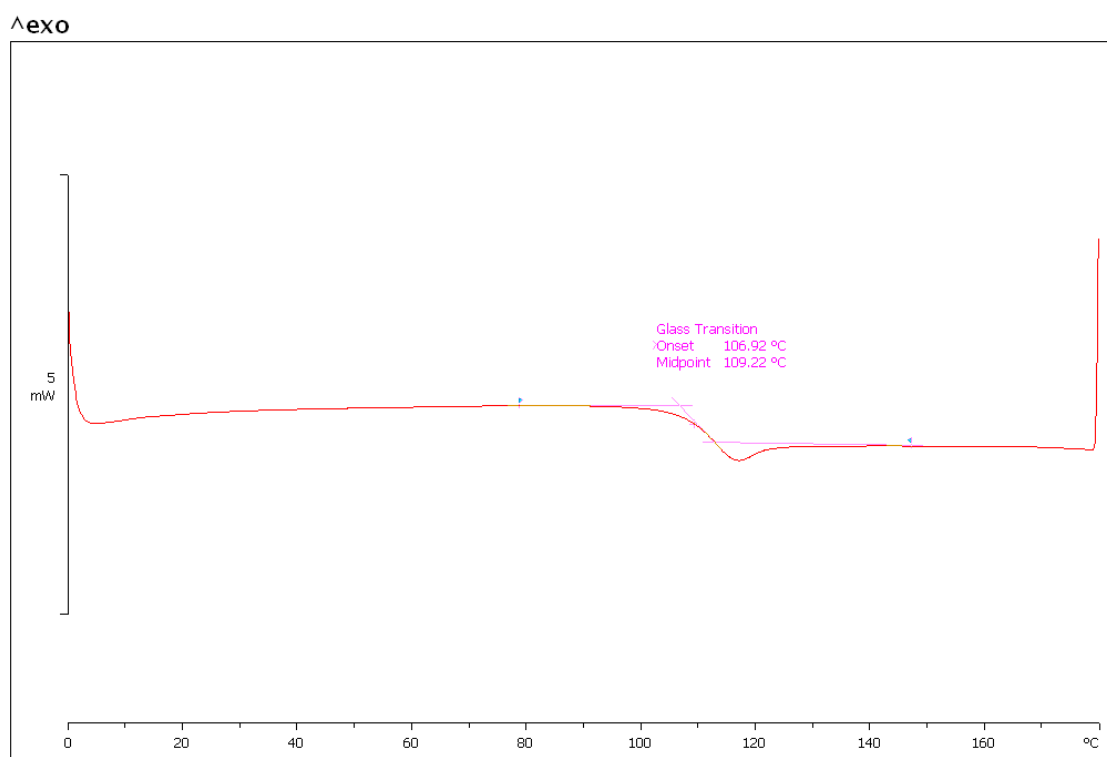
Appendix E: DSC and TGA diagrams of polymers



C1027: METTLER

STAR^e SW 9.20

Figure E-1. Representative DSC second heating curve of polymer produced using DMAP as cocatalyst.



C1027: METTLER

STAR^e SW 9.20

Figure E-2. Representative DSC second heating curve of polymer produced using PPNN₃ as cocatalyst.

Sample: kn003polymer
Size: 16.1420 mg
Method: Ramp

TGA

File: \\...\\data\\TGA\\kn\\KN003POLYMER
Operator: Ehab
Run Date: 15-May-2015 10:31
Instrument: TGA Q500 V20.10 Build 36

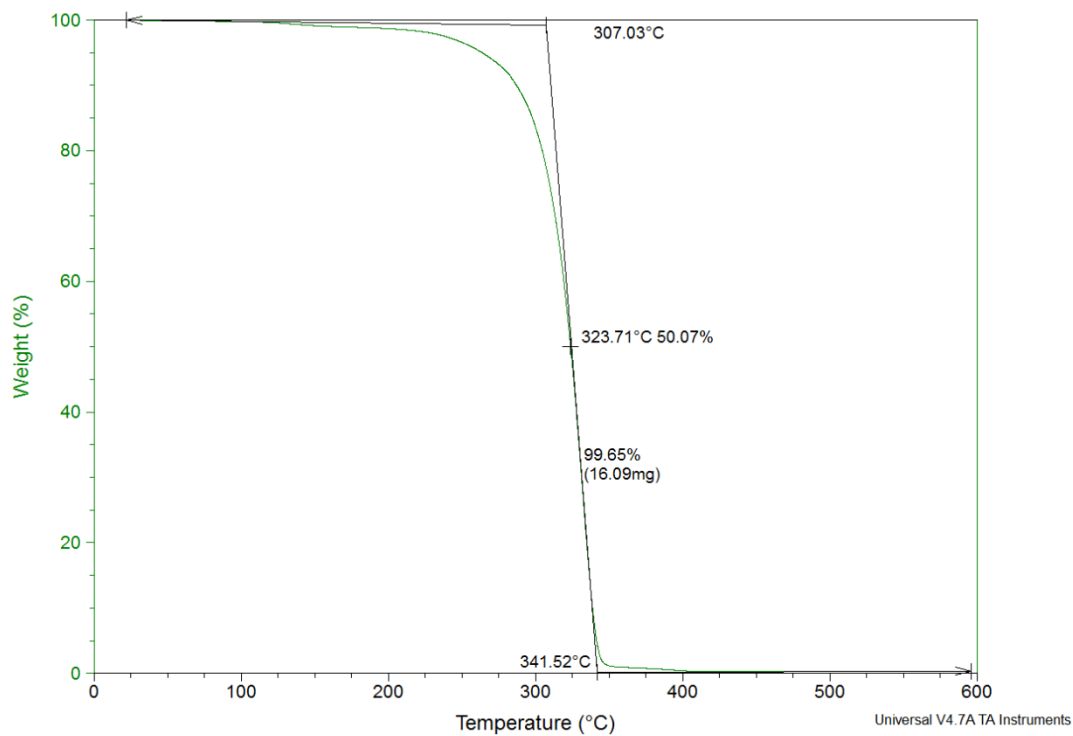
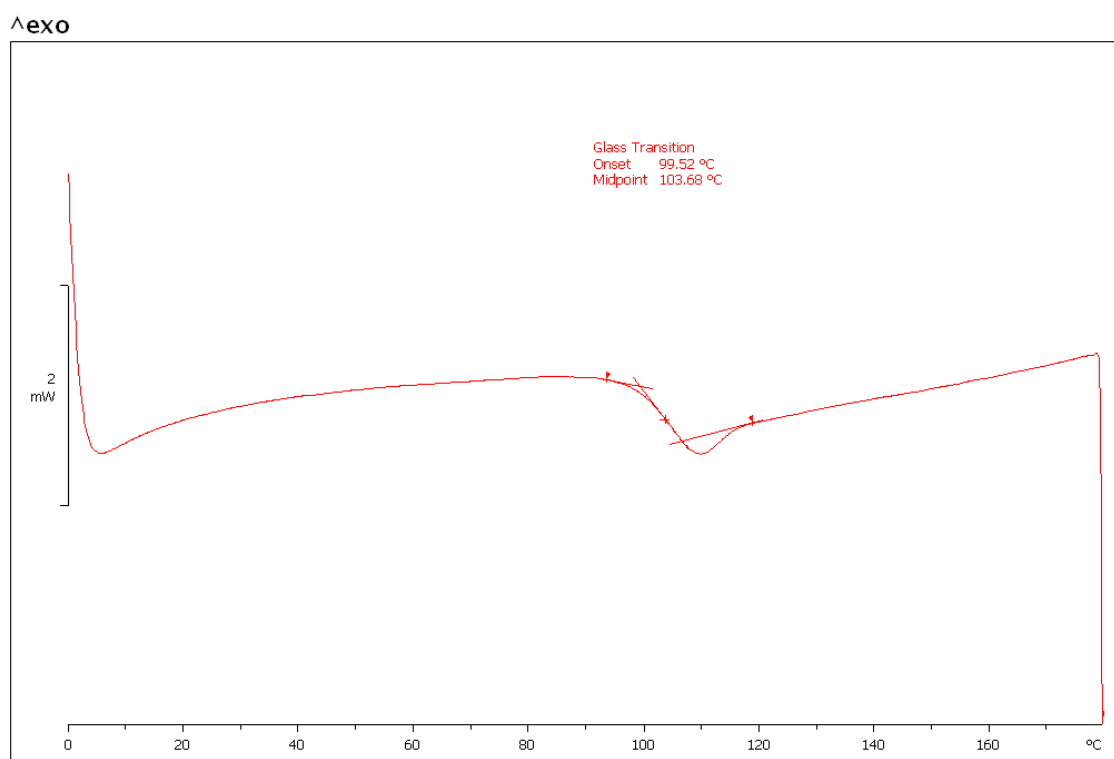


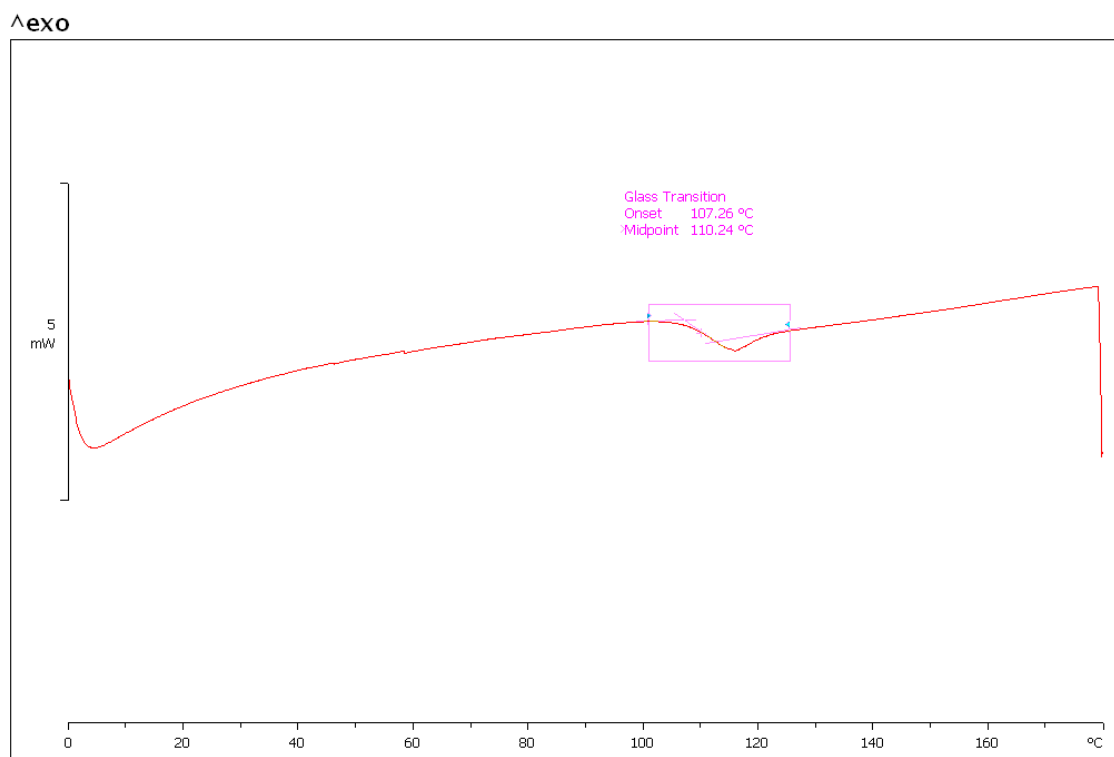
Figure E-3. Representative TGA curve of polymer produced using PPNN_3 as cocatalyst at a heating rate of $10\text{ }^\circ\text{C min}^{-1}$.



C1027: METTLER

STAR^e SW 9.20

Figure E-4. DSC second heating curves of polycarbonate obtained by **5.1** and PPNCI (Table 5-3, entry 2).



C1027: METTLER

STAR^e SW 9.20

Figure E-5. DSC second heating curves of polycarbonate obtained by **5.1** and $\text{Ph}_2\text{P}(\text{O})\text{NPPH}_3$ (Table 5-3, entry 3).

Sample: KN001CrOH PPNCI
Size: 30.3950 mg
Method: Ramp
Comment: kn001CrOH PPNCI JULY 08 2016

TGA

File: Z:\TGA\kn\KN001CrOH PPNCI.001
Operator: Amanda Parsons
Run Date: 08-Jul-2016 11:35
Instrument: TGA Q500 V20.13 Build 39

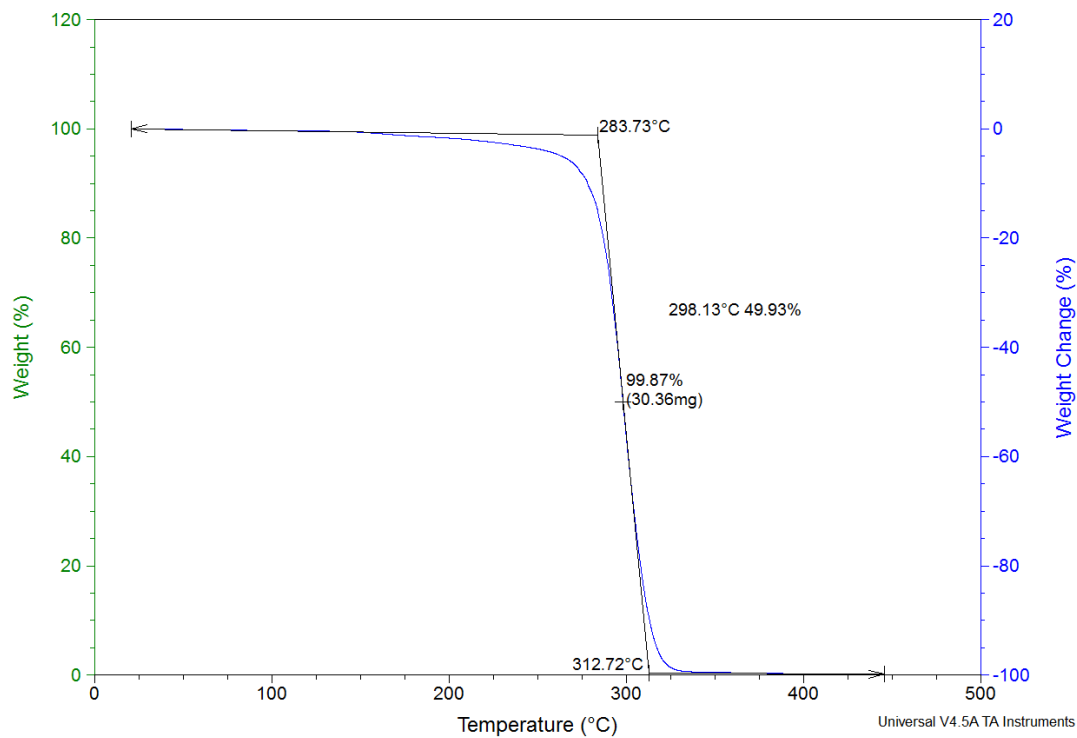


Figure E-6. TGA curve of PCHC at a heating rate of 10 °C min⁻¹ (Table 5-3, entry 2).

Sample: KN001CrOH PPNO
Size: 25.8570 mg
Method: Ramp
Comment: kn001CrOH PPNO JULY 08 2016

TGA

File: Z:\TGA\kn\KN001CrOH PPNO
Operator: Amanda Parsons
Run Date: 08-Jul-2016 13:03
Instrument: TGA Q500 V20.13 Build 39

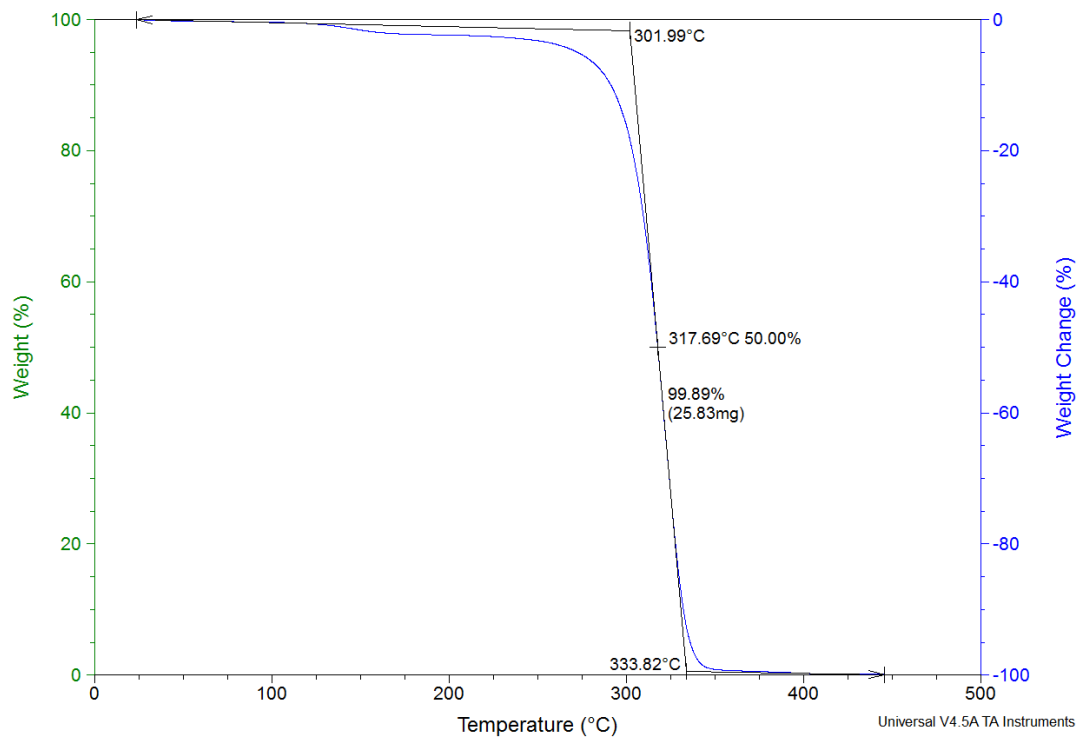


Figure E-7. TGA curve of PCHC at a heating rate of 10 °C min⁻¹ (Table 5-3, entry 3).

Appendix G: Copyright



RightsLink®

Home

Create Account

Help



ACS Publications
Most Trusted. Most Cited. Most Read.

Title:

Binding of 4-(N,N-dimethylamino)pyridine to Salen- and Salan-Cr(III) Cations: A Mechanistic Understanding on the Difference in Their Catalytic Activity for CO₂/Epoxide Copolymerization

Author: Dun-Yan Rao, Bo Li, Rong Zhang, et al

Publication: Inorganic Chemistry

Publisher: American Chemical Society

Date: Apr 1, 2009

Copyright © 2009, American Chemical Society

LOGIN

If you're a [copyright.com](#) user, you can login to RightsLink using your copyright.com credentials. Already a [RightsLink](#) user or want to [learn more?](#)

PERMISSION/LICENSE IS GRANTED FOR YOUR ORDER AT NO CHARGE

This type of permission/license, instead of the standard Terms & Conditions, is sent to you because no fee is being charged for your order. Please note the following: